UMONS
University of Mons

Faculté
des Sciences

# Analytical and numerical investigation of the two-photon spontaneous emission process near plasmonic nanostructures

**Smeets Steve**

Thesis presented in fulfillment of the requirements for the degree of Doctor of Science

**Thesis supervisors**

Prof. Bjorn Maes

Dr. Gilles Rosolen

**University of Mons**
**Faculty of Sciences**
**Micro- and Nanophotonic Materials Group**

**Academic year**

2024-2025

**Supervisors**


| | |
|---|---|
| Prof. Bjorn Maes | Micro- and Nanophotonic Materials Group, University of Mons |
| Dr. Gilles Rosolen | Micro- and Nanophotonic Materials Group, University of Mons |


**Jury members**

| | |
|---|---|
| Prof. Karolina Słowik | Faculty of Physics, Nicolaus Copernicus University in Toruń, Poland |
| Prof. Yves Caudano | Research Unit Lasers and Spectroscopies, University of Namur |
| Prof. Michel Voué | Physics of Materials and Optics Unit, University of Mons |
| Prof. Jérôme Cornil | Laboratory for Chemistry of Novel Materials, University of Mons |


University of Mons
Faculty of Sciences

Micro- and Nanophotonic Materials Group
Place du Parc 20
7000 Mons
Belgium

Tel.: +32-65/37.33.85
https://web.umons.ac.be/mmnp



This thesis was carried out in the context of a doctoral fellowship from the Fonds de la Recherche scientifique - FNRS under the Research Project No T.0166.20

# Acknowledgements

First, I would like to express my sincere gratitude to my supervisors Prof. Bjorn Maes and Dr. Gilles Rosolen for giving me the opportunity to perform a PhD thesis on a fascinating subject, encompassing both theoretical and numerical work. Their invaluable guidance and our regular meetings were crucial in ensuring the smooth progress of the research. In particular, I would like to express my deepest thanks to Gilles for the countless times that I went to see him in his office, for his availability and efficiency in answering my questions about theory, literature and COMSOL. I also thank them for allowing me to set up a small computing cluster, on the appreciated guidance of Dr. Colin van Dyck, allowing me to deepen my knowledge on this subject. Furthermore, I'm grateful to them for allowing me to continue working with them for an additional 11 months.

I would also like to thank Prof. Jérôme Cornil and Prof. Michel Voué for their interesting questions during the annual meetings of the support committee, as well as the members of the Jury for the time devoted to reading this thesis.

My thanks also go to my friends and colleagues. The warm ambience in the right-hand corridor on the second floor of B4. The card games between PhD students at the university restaurant. Thomas for all the interesting discussions in our office. Colin for introducing me to the joys of cycling and for the morning breaks. Bertrand, Mhamad, Alice and Thomas for the great time spent at conferences.

Je tiens également à remercier ma maman pour son soutien incommensurable qu'elle m'a toujours voué, pour avoir pris soins de mes petits chats lors de mes conférences à l'étranger et pour m'avoir permis de réaliser des études universitaires dans les meilleures conditions possibles. Enfin, un merci tout particulier à ma copine d'avoir toujours cru en moi quant à la réalisation de cette thèse, pour m'avoir accompagné lors de la conférence à Naples et pour la réalisation de l'illustration de couverture.

# Summary

The electric dipole approximation is prevalent in the field of light-matter interaction. However, in nanophotonic structures sustaining highly confined fields, the approximation no longer holds and higher-order processes can become significant. Among them, two-photon spontaneous emission (TPSE) is a second-order process that involves the simultaneous emission of two photons from a quantum emitter and is a promising alternative to conventional entangled photon pair sources for quantum applications. However, the study of advanced nanostructures for TPSE is hampered by a lack of efficient numerical and theoretical methods.

First, we develop a general framework that calculates the two-photon emission rate enhancement of a quantum emitter near an arbitrarily shaped nanostructure. The framework is based on the classical computation of Purcell factors in classical electromagnetic simulations and we consider the interaction up to the electric quadrupolar order. For a hydrogen atom near a plasmonic silver nanodisk, we demonstrate a substantial enhancement in the photon-pair emission rates by 5 and 11 orders of magnitude for the two-electric dipole (2ED) and two-electric quadrupole (2EQ) transitions, respectively. Second, our framework also includes the quantum interferences between the multipolar transitions of TPSE, which has never been studied before. For a hydrogen atom near a plasmonic graphene nanotriangle, we calculate the interference between the 2ED and 2EQ transitions, which can increase the total transition rate by more than 65%. Third, we do a first step towards the design of innovative two-photon nanoantennas. We exploit dipolar and quadrupolar modes on one or two silver nanorods to emit photons of different frequencies in separate directions.

In conclusion, we developed a powerful framework based on the classical computation of Purcell factors to design nanoantennas for TPSE that can be exploited for various quantum applications. It can be used for arbitrarily shaped nanostructures to optimize the efficiency and directionality, amongst others.

# Contents

Chapter 1

# Introduction

At first glance, the simultaneous emission of two photons by an atom might not seem significantly different from the emission of a single photon: the energy released by the transition is simply shared between two quanta instead of one. However, the deeper we delve into this process of two-photon spontaneous emission, the more we realize that it is far more complex. Because it momentarily and intriguingly challenges the laws of conservation of energy, it is a fascinating example of the oddities of quantum mechanics. What makes it even more interesting is that the spontaneous emission occurs through interaction with the vacuum modes of the electromagnetic field, allowing it to be strongly enhanced and controlled by designing a nanophotonic structure that shapes the surrounding field. The complex nature of the two-photon spontaneous emission process not only deepens our understanding of quantum phenomena, but also holds significant promise for the quantum technologies of tomorrow.

## 1.1 Context

In the early 1930s, Maria Göppert-Mayer predicted that quantum emitters could decay by simultaneously emitting two photons [1], a process termed now two-photon spontaneous emission (TPSE). This second-order process in perturbation theory [2] determines the mean lifetime of the $2s$ state of hydrogen [3], since single-photon transitions are forbidden from this state. Over the past century, numerous theoretical studies have been conducted, particularly to calculate the two-photon decay rate of hydrogenic atoms [3–5], to explain the origin of the continuous spectra observed in nebulae [4], and to understand the role of TPSE in the dynamics of cosmological hydrogen recombination [6–8]. It was not until 1975 that the first experimental measurement of a two-photon emission rate, in hydrogen, was carried out [9]. Since then, TPSE has been investigated in a variety of systems beyond hydrogen, including atoms [10, 11], molecules [12], semiconductors [13–16], and quantum dots [17–19]. Notably, the first observations of TPSE from semiconductors and quantum dots took place around the year 2010 [14, 17].

Nowadays, the exploitation and the control of the TPSE process is of great interest as it promises several applications [20–23], such as the conception of broadband absorbers and light emitters. In particular, TPSE is a promising alternative to the commonly used spontaneous parametric down conversion (SPDC) process to generate entangled photons pairs [13]. In SPDC, a high intensity laser source shines a non-linear crystal to generate two photons of lower energy [24]. In comparison, TPSE is theoretically more efficient [13], more flexible for designing sources with given output wavelengths [11], and could be used to fabricate integrated two-photon sources.

Despite the interest in controlling this process, TPSE typically occurs 8 to 10 orders of magnitude

slower than the competing spontaneous emission of a single photon [22], but such limitations can be overcome by shaping the surrounding electromagnetic field. Indeed, since the work of Purcell [25], it is known that the spontaneous emission rate of an emitter is not only an intrinsic property of the emitter itself but also depends on its environment: this is the Purcell effect. Since the last decade, TPSE enjoys a renewed interest [21, 22, 26, 27] due to the recent advancements in the field of plasmonics. Plasmonic nanostructures can confine the light at the nanoscale in the form of localized surface plasmons [22], which are resonances between the incident electric field and the collective oscillations of the conduction electrons at a metallic interface. Such confinement results in a light emission enhancement by several orders of magnitude [22]. Thereby, two-photon transitions, as well as multipolar transitions (e.g., electric quadrupolar), can even outperform the electric dipole single-photon transition [22, 28, 29], making their exploitation accessible.

Despite the recent studies about TPSE near plasmonic nanostructures, they are hampered by a lack of efficient theoretical and numerical methods. For one-photon spontaneous emission (OPSE), it is known that the influence of the environment on the emission rate of a quantum emitter is identical to that on the power emitted by a classical point source [30], enabling the calculation of the Purcell effect by modeling classical sources in electromagnetic simulations. However, this link was not yet been established in the case of the two-photon Purcell effect, i.e., the influence of the environment on the TPSE rate. This link is not straightforward as in the case of OPSE, and it was first derived by Muniz et al. in 2019. In Ref. 31, he establishes the expression for it as a function of the one-photon Purcell factors, i.e., the ratio between the one-photon spontaneous emission rate of a quantum emitter within a photonic environment and in vacuum. However, the expression is not general as it is limited to symmetric situations and only considers the two-electric dipole transition. Hence, we develop an efficient and general framework which can be used for arbitrarily shaped nanostructures and for any emitter positions. Moreover, we include higher-order multipolar contributions to the TPSE, such as the contribution of the magnetic dipole and electric quadrupole, since multipolar interactions are also enhanced with plasmonic nanostructures [22].

## 1.2 Outline

In this thesis, we develop a general framework to compute the two-photon Purcell effect of a quantum emitter near arbitrarily shaped nanostructures via the classical computation of the one-photon Purcell factors. To do so, we take into account the interaction up to the electric quadrupolar order, as well as the interference effects between the multipolar pathways. Furthermore, we consider the simplest emitter, namely the hydrogen atom, and we study the two-photon transition between two spherically symmetric states. Then, we verify our numerical calculation of Purcell factors by reproducing results from the literature [26]. Afterwards, we study for the first time to our knowledge the interference between the multipolar pathways of the TPSE. Finally, we do a first step towards the design of innovative two-photon nanoantennas, where photons are emitted in different directions.

This thesis is structured into 6 chapters. Chapter 2 is devoted to the basic concepts, Chapters 3 and 4 to the development of the framework, Chapter 5 to the calculation of the emitter contribution, Chapter 6 to the computation of the environment contribution, and Chapter 7 to the application in specific plasmonic nanostructures. Each chapter is followed by a summary of the important information and equations.

Chapter 2 provides an overall understanding of the various key concepts of this thesis. We begin

by introducing the process of spontaneous emission and examine the different pathways by which a quantum emitter can decay. We include interferences when multiple decay pathways coexist, and discuss efficiency of the process when emission takes place within a photonic environment. Moreover, we address the electric dipole approximation, which is generally used to study light-matter interactions. It states that electric dipole (single-photon) transitions dominate the other transitions, such as multipolar and multiquanta transitions, called (electric-dipole) forbidden transitions. Then, we explain that in structures confining light at the nanoscale, such as plasmonic nanostructures, forbidden transitions become accessible due to the Purcell effect. Afterwards, we provide an overview of the historical background, applications, and recent research about the two-photon spontaneous emission (TPSE) process, the core subject of this thesis. Next, we introduce the Fermi's golden rule, which will be used to calculate spontaneous emission rates, and recall the selection rules for the hydrogen atom. We also introduce the Green's function that gives the power emitted by classical sources, and present the link between classical and quantum sources: the Purcell factors. Lastly, we provide a concise introduction to surface plasmons, as plasmonic nanostructures are considered in this thesis to enhance two-photon spontaneous emission rates.

Chapter 3 is devoted to the one-photon spontaneous emission (OPSE) process. Starting with Fermi's golden rule and with the Hamiltonian describing the emitter-field interaction up to the electric quadrupolar order. We derive the electric dipole (ED), magnetic dipole (MD) and electric quadrupole (EQ) contributions to the OPSE, as well as the interferences between these multipolar pathways. By doing so, we obtain equations that are valid regardless of the quantum emitter and of the photonic environment. Next, the special case where the emission takes place in vacuum is considered. We then make the link with the power emitted by classical point sources by writing the multipolar contributions to the OPSE using Green's function, highlighting that the Purcell effect can be computed by considering classical point sources in electromagnetic simulations. Afterwards, we introduce a modified version of the Voigt notation to simplify the equations relative to the EQ transition. Finally, the obtained expressions are decomposed into Purcell factors bases, which will be useful to establish the link between the two-photon Purcell effect and the one-photon Purcell factors.

We go one step further in Chapter 4 by considering the two-photon spontaneous emission process, the core subject of this thesis. Thereby, similar developments than for the OPSE are performed, but starting with the second-order Fermi's golden rule instead of the first-order one. We derive general expressions for the multipolar contributions to the TPSE rate, namely the two-electric dipole (2ED), two-magnetic dipole (2MD), the two-electric quadrupole (2EQ), and their interference. Next, the special case where the emission takes place in vacuum is considered. We then express the TPSE rates via the Green's function and use the modified Voigt notation. Lastly, we use the decomposition into Purcell factor bases of the OPSE rates to express the TPSE rates as a function of the Purcell factors of the two photons emitted during the process, enabling the classical computation of the two-photon Purcell effect. Furthermore, a comparison with the less general formula derived in Ref. 31 for the 2ED transition rate is made.

In the equations derived for the multipolar contributions to the TPSE rate, the emitter contribution (i.e., the second-order transition moments) is decoupled from the contribution of the environment (i.e., the Purcell factors). In Chapter 5, we calculate analytically the emitter contribution, for the transition considered throughout this thesis: a transition between two spherically symmetric

states ($s$ states) of a hydrogen atom. Firstly, we calculate the normalized second-order transition moments, which are sufficient to calculate the two-photon Purcell effect, i.e., the change of the TPSE rate due to the environment. Subsequently, we calculate the vacuum TPSE rates, which require the calculation of the norm of the transition moments, enabling the calculation of the absolute TPSE rates.

With the emitter contribution to the equations calculated, we explain the method used to calculate the Purcell factors in Chapter 6. For this purpose, we use the commercial software COMSOL Multiphysics® which is based on the finite element method, and a short introduction to this numerical method is provided. We also introduce the weak formulation of the master equation which is solved: the wave equation of the electric field. In addition, since only the electric and magnetic point dipoles are available in the software, we derive the weak formulation of the electric point quadrupole. Then, we describe the COMSOL models employed to compute the Purcell factors. Finally, we present the optical models of silver and graphene, the two metallic materials employed.

Chapter 7 is dedicated to the computation of TPSE spectra for transitions between $s$ states of a hydrogen atom close to different plasmonic nanostructures. Firstly, we validate our Purcell factors computation by comparison with results of Ref. [26], where they used an analytical calculation of the Purcell factors to calculate the 2ED transition rate for the emitter placed on the axis of symmetry of a silver nanodisk. In addition, we exploit the flexibility of our framework to study the case of an off-axis emitter, and we calculate the 2EQ transition rate. Secondly, we design a graphene nanotriangle close to which the 2EQ transition rate is of the same order of magnitude as the 2ED transition rate. We demonstrate a breakdown of the electric dipole approximation in the TPSE process, and we study the interference between these two multipolar emission channels. We find both destructive and constructive interferences, e.g., an increase of 67 % of the total transition rate. Thirdly, an important challenge for two-photon sources is the design of systems emitting the photons in separate directions at different frequencies. To address this issue, we design two nanoantenna systems based on silver nanorods, that operate via different mechanisms.

## 1.3 Publications and conferences

In this section, we list all the papers published or submitted during the PhD thesis. Furthermore, we list all the contributions to national and international conferences.

### 1.3.1 Publications

- **S. Smeets**, B. Maes, and G. Rosolen, General framework for two-photon spontaneous emission near plasmonic nanostructures, *Physical Review A* **107**, 063516 (2023).
- L. Rassinfosse, J. Müller, O. Deparis, **S. Smeets**, G. Rosolen, and S. Lucas, Convergence and accuracy of FDTD modelling for periodic plasmonic systems, *Opt. Continuum* **3**, 844-858 (2024).
- **S. Smeets**, B. Maes, and G. Rosolen, Interference between multipolar two-photon transitions in quantum emitters near plasmonic nanostructures, *Discover Nano* **19**, 155 (2024).
- **S. Smeets**, B. Maes, and G. Rosolen, Tailoring directivity of two-photon spontaneous emission using plasmonic nanoantennas, submitted in Optics Letters (2024).

### 1.3.2 Conferences

- **S. Smeets**, B. Maes, and G. Rosolen, Photonic modeling of high-order light-matter interactions (**Poster**), Paris-Saclay/Munich Summer School on Surface Plasmons, Paris-Saclay University, France, 12-16th July 2021.
- **S. Smeets**, B. Maes, and G. Rosolen, Photonic modeling of high-order light-matter interactions (**Poster**), Belgian Photonics Online Meetup, Online, Belgium, 23-24th September 2021.
- **S. Smeets**, B. Maes, and G. Rosolen, Photonic modeling of two-photon spontaneous emission processes beyond the electric dipole approximation (**Poster**), Belgian Physical Society Scientific Meeting, Tabloo Dessel, Belgium, 18th May 2022.
- **S. Smeets**, B. Maes, and G. Rosolen, Photonic modeling of two-photon spontaneous emission processes (**Poster**), Metamaterials, Siena, Italy, 12-15th September 2022.
- **S. Smeets**, B. Maes, and G. Rosolen, Photonic modeling of two-photon spontaneous emission processes (**Poster**), Belgian Photonics Online Meetup, Online and Brussels, Belgium, 29-30th September 2022.
- **S. Smeets**, B. Maes, and G. Rosolen, General framework for two-photon spontaneous emission near plasmonic nanostructures (**Poster**), Quantum Nanophotonics, Benasque, Spain, 13-17th March 2023.
- **S. Smeets**, B. Maes, and G. Rosolen, A general framework for two-photon spontaneous emission near plasmonic nanostructures (**Talk**), Belgian Physical Society Scientific Meeting, Namur, Belgium, 17th May 2023.
- **S. Smeets**, B. Maes, and G. Rosolen, Photonic modeling of two-photon Purcell effect near plasmonic nanostructures (**Paper in proceedings** and **Talk**), Metamaterials, Platanias, Greece, 11-14th September 2023.
- **S. Smeets**, B. Maes, and G. Rosolen, Tailoring two-photon spontaneous emission: framework and nanoantenna design for interference and directionality (**Talk**), European Optical Society Annual Meeting, Naples, Italy, 9-13th September 2024.

Chapter 2

# Spontaneous emission and Purcell effect

In this chapter, we start by introducing in Section 2.1 the spontaneous emission process and we examine the various pathways by which a quantum emitter can decay. We also explain how to enhance the slowest decay pathways via the Purcell effect, we describe the interferences when multiple decay pathways coexist, and we discuss about the efficiency of the spontaneous emission inside a photonic environment. Then, we present in Section 2.2 the historical background, the applications, as well as the recent studies about the two-photon spontaneous emission process, the core subject of this thesis. Next, in Section 2.3, we introduce the Fermi's golden rule used to calculate spontaneous emission rates and we discuss about the selection rules for the hydrogen atom. Subsequently, we take the time in Section 2.4 to present a textbook case to illustrate all the different types of transitions we have introduced. Afterwards, we calculate in Section 2.5 the power radiated by classical sources, and we introduce the Purcell factors that link them to transition rates of quantum emitters. Finally, in Section 2.6, we provide a concise introduction to surface plasmons, as plasmonic nanostructures are considered in this thesis to enhance two-photon spontaneous emission rates. This chapter ends with a summary of the important notions necessary for this thesis.

## 2.1 Introduction to the spontaneous emission process

Through interaction with the surrounding electromagnetic field, the electron of a quantum emitter (e.g., an atom, a molecule, a quantum dot) can transit from one state to another according to three different processes: absorption, stimulated emission, and spontaneous emission [2]. These are illustrated and explained in Figure 2.1. In this thesis, we are interested in the spontaneous emission (SE) process which is a fundamental quantum process in the field of light-matter interaction [32]. The term "spontaneous" refers to the fact that the emission seems to occur spontaneously without any interaction. Indeed, unlike the stimulated emission and absorption processes that only require the quantification of the emitter levels, SE cannot be understood without a quantum treatment of the electromagnetic field [33]. It is through the interaction between an emitter's excited state and the vacuum modes of the electromagnetic field that this process can take place. Thus, the SE can be understood as an emission stimulated by vacuum [32].

SE is responsible for most of the light we see all around us and many names are used to refer to it depending on the emitter's excitation mechanism [Fig. 2.2]. For example, SE is called bioluminescence if the emission results from biochemical reactions in a living organism, electroluminescence if light is emitted due to an electric current, or photoluminescence if the emitter is excited by the absorption of radiation (if the radiation stops within nanoseconds after the shutdown of the exciting radiation, it is fluorescence, whereas if it stops after few microseconds to several hours, it is phos-

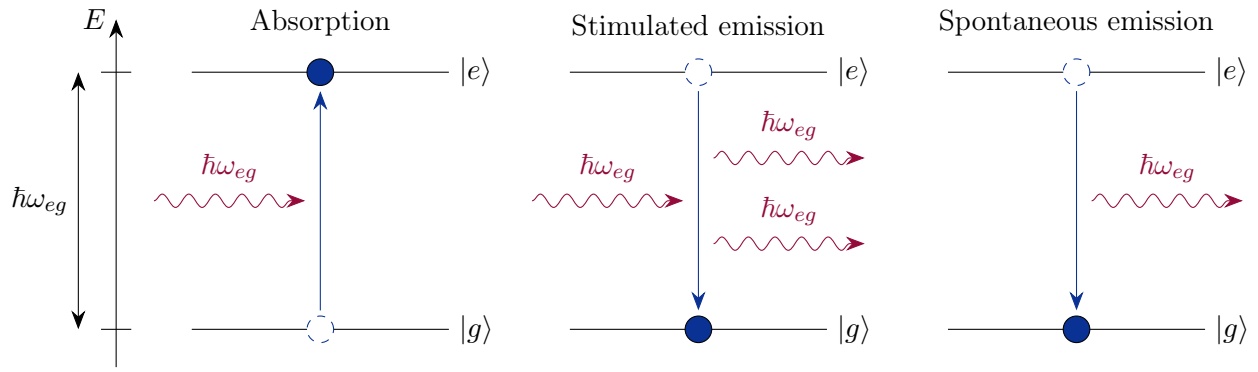


Figure 2.1: Energy representation of the absorption, stimulated emission and spontaneous emission processes [2]. In an absorption process, an incident photon is absorbed by an electron that transits towards a higher energy state $|e\rangle$. In a stimulated emission process, an incident photon causes the transition of an electron towards a lower energy state $|g\rangle$ by emitting a photon with characteristics similar to those of the incident photon, resulting in a coherent emission. In a spontaneous emission process, an electron decays spontaneously to a lower energy state by emitting a photon in a random direction. The energy of the photons involved in these processes is equal to the energy difference between the two emitter states: $\hbar\omega_{eg}$.

phorescence [34]). Furthermore, the photon initiating the stimulated emission in lasers comes from the SE and using a thermodynamical argument, one can show that the radiation from the sun is mainly due to the SE [32].

Historically, the theory of electromagnetism predicts that oscillating charges radiate, which was confirmed by Hertz's experiments in 1887 [32]. Then, Lorentz attributed the radiation by atoms to the oscillation of the atomic electrons, without understanding why atoms emit only at certain frequencies. This was understood in 1913 thanks to Bohr's theory of the hydrogen atom [32]. In 1916, Einstein introduced coefficients, later named Einstein coefficients, to describe spontaneous emission, stimulated emission and absorption processes using thermodynamical arguments [32]. The first person to derive the expression of the SE rate from first principles was Dirac in 1926 in his quantum theory of radiation [40], later named quantum electrodynamics. In the 1940s, Purcell discovered that the environment of a quantum emitter affects its SE rates [25, 30]. Concretely, the Purcell effect results from a modification of the photon local density of states at the emitter position. This discovery leads, with the Jaynes-Cummings model developed in 1963 to describe the interaction between a two-level system and the quantified vacuum mode of the electromagnetic field inside a cavity [41], to the cavity quantum electrodynamics theory [30]. Thereby, SE rates can be enhanced, reduced, or even suppressed, via the boundary conditions imposed on the electromagnetic field of the surrounding vacuum [42].

In addition to being responsible for most of the light we perceive every day, SE is responsible for the fingerprint of atoms and molecules, which is their emission spectrum [43]. Usually, because the size of a quantum emitter is typically three orders of magnitude smaller than the wavelength of the light it emits, it is sufficient to study the interaction between a quantum emitter and the surrounding electromagnetic field under the electric dipole approximation [30, 44, 45]. In the latter approach, the emitter "feels" a uniform electric field, thus neglecting the spatial variations of the field over it and consequently neglecting higher-order multipolar interactions that depend on the derivatives of the electric field (this will be explained mathematically in Section 3.2 when the Hamiltonian describing

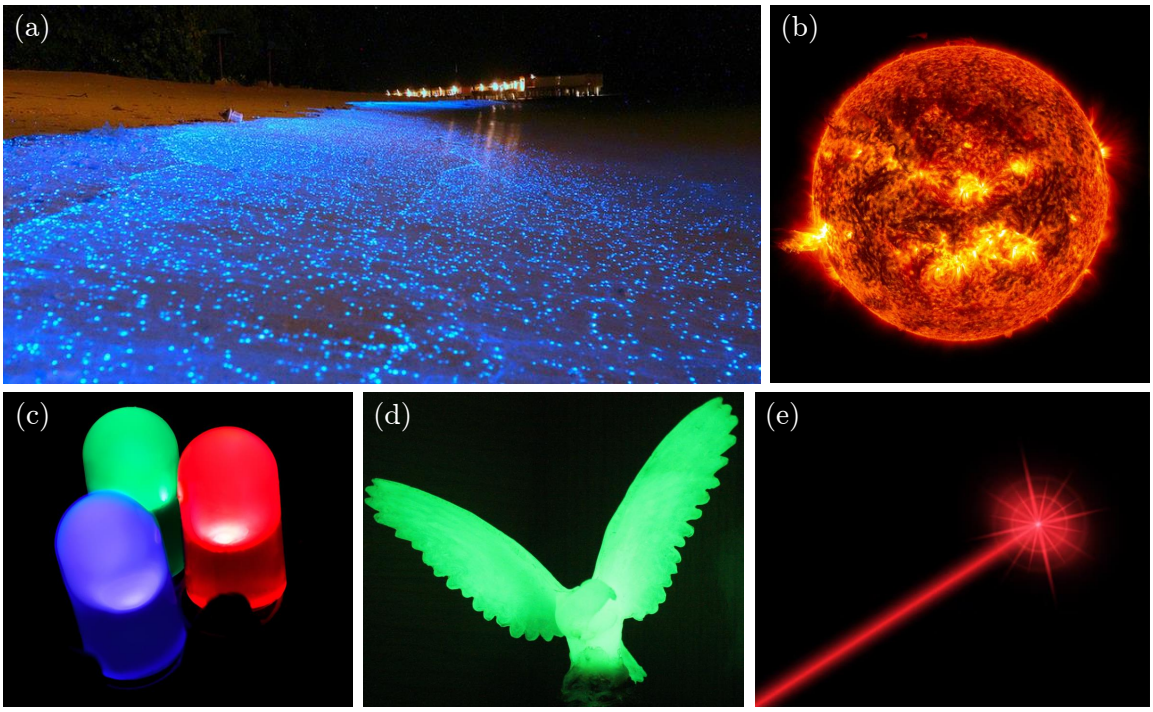


Figure 2.2: Illustration of different types of spontaneous emission (SE). (a) Bioluminescence from phytoplanktons [35]. (b) Solar radiation is mainly due to SE [36]. (c) Electroluminescence from light-emitting diodes [37]. (d) Phosphorescence [38]. (e) Laser emission starts with SE [39].

the interaction between the emitter and the field is introduced) [45, 46]. Therefore, the emitter is assumed to be a point and electric dipole transitions dominate, unless prohibited by selection rules between the considered initial and final states of the emitter. The selection rules for the hydrogen atom are addressed in Section 2.3. In atoms, electric dipole transitions are characterized by a variation of one unit in the azimuthal quantum number of the electron performing the transition and by the emission of a single quantum [45, 47].

Thereby, most of the decay pathways of an emitter have a low or a zero probability to occur, making much of the emission spectrum invisible and inaccessible [22]. These pathways are called (electric dipole) forbidden transitions, with the nuance that zero probability transitions, i.e., transitions that are not allowed by the emitter's selection rules [47], are called strictly forbidden transitions [22]. The forbidden transitions are classified into three distinct categories: multipolar, spin-flip, and multiquanta emission processes [22]. Firstly, in atoms, multipolar transitions are characterized by a change in the electron's azimuthal quantum number of more than one unit. Typically, if the change in azimuthal quantum number increases by one, the transition rate decreases by 4 to 6 orders of magnitude [22]. This is the result of the large difference between the wavelength of the emitted light ($\approx$ 100 to 1000 nm) and the orbital size involved in the transition ($\approx$ 0.1 to 1 nm). Secondly, multiquanta transitions are higher-order processes characterized by the emission of more than one photon. In addition to the mismatch between the emitter's size and the light that is emitted, these processes involve the fine-structure constant $\alpha \approx 1/137$ to the power of the order of the transition (e.g., squared for the emission of two quanta), thus explaining their slowness in comparison with first-order (single-photon) transitions [48]. For example, the two-photon spontaneous emission (second-order process) is 8 to 10 orders of magnitude slower than the competing spontaneous emission of a single photon [22, 48]. Thirdly, during spin-flip transitions, light is emitted when the spin

of an electron flips. An historical example is the 21-centimeter line of hydrogen that has several cosmological applications [49].

Despite the difficulty of accessing these forbidden transitions, they can lead to a wide variety of applications [22]. For example, it enables the conception of spectroscopy platforms to access a larger part of the electronic energy levels of atoms and molecules, the development of entangled two-photon sources based on the two-photon spontaneous emission as well as the design of broadband absorbers and light sources. However, it is possible to design systems in which the spatial extent of the emitter is no longer negligible compared to the wavelength of the light it emits. Thus, the point dipole approximation is no longer valid, opening access to otherwise forbidden transitions. This can happen with emitters having a large spatial extent, such as quantum dots or organic molecules [50–53], and in systems confining light [28], such as photonic crystals [18, 54], plasmonic nanocavities [22, 28, 29, 50, 55–62], nanomagnonic cavities[1] [63, 64], and phonon polaritonic nanocavities [48, 65]. Therefore, in systems that confine light at the nanoscale, the forbidden transitions can be enhanced and even outperform the electric dipole single-photon transition [22, 28]. For example, the electric quadrupole transition rate can become locally 100 times larger than the dipolar one for a hydrogen-like emitter near graphene nanoislands [29]. In addition, the two-quanta emission can be two orders of magnitude greater than the emission of a single quantum with phonon polaritons (quasiparticles arising from the coupling between the light and the vibrations in a crystal) in boron nitride or silicon carbide [48]. In this thesis, we focus on plasmonic nanocavities where the wavelength of the light can be squeezed by two orders of magnitude in the form of localized surface plasmons [22] (quasiparticles arising from the coupling between the light and the oscillations of electrons in a sub-wavelength conductive nanostructure [66]). An introduction to surface plasmons is given later in this chapter, in Section 2.6.

When several decay pathways coexist between two given states of an emitter, the overall transition rate is the sum of the individual rates. However, if in a system (atom plus environment) several decay channels are dominant, it is necessary to take into account the interference effects between them, potentially resulting in an increase or a decrease in the overall transition rate [2]. Note that in vacuum, multipolar transitions cannot interfere with each other because each multipolar emitter generates its unique field distribution that remains decoupled from other multipolar sources at the same location [2]. Inside a photonic environment, the multipolar field distributions are modified and interference between multipolar emission channels can occur [2].

Between two states of an atom, the selection rules [45, 47] tell us that there is only one possible decay channel for the emission of a single photon (e.g., electric dipole, magnetic dipole, electric quadrupole, etc.), and therefore no interference. However, in the case of molecules and asymmetric quantum dots, multiple multipolar single-photon emission channels can occur simultaneously, and therefore can interfere. For example, interference effects were studied between the one-photon magnetic dipole and electric quadrupole transitions in molecules [62] and between one-photon electric dipole, magnetic dipole and electric quadrupole transitions in quantum dots [51]. In the two-photon spontaneous emission (TPSE) process, the second-order transition is mediated by virtual intermediate states, allowing multiple multipolar emission channels to exist simultaneously [5] and to interfere, but these interferences have never been studied to our knowledge. However, interferences between a cascade of two single-photon (first-order) transitions and two-photon (second-order) transitions

[1] A magnon is the quasiparticle associated to an elementary excitation of a spin wave in a crystal lattice [63, 64].

have been studied [8].

In vacuum, SE processes result in the emission of photons in random directions. However, inside a photonic environment, an excited emitter can decay either radiatively in the case of photon emission in the far-field or non-radiatively in the case of energy dissipation in the environment in the form of, for example, phonons or plasmons [30]. Thus, one defines the quantum efficiency of a system as the ratio between the radiative and the total (radiative plus non-radiative) transition rates: $\eta := \Gamma_{\mathrm{rad}}/\Gamma_{\mathrm{tot}}$ [30, 67]. In addition to the design of nanoantennas with high quantum efficiency and high Purcell factor (i.e., a high enhancement of SE rates) [67, 68], their overall efficiency can be further improved by enhancing their directivity, thus increasing the proportion of photons that are emitted in a desired direction, e.g., to couple to a waveguide [69]. For example, Yagi-Uda [70, 71], bull's eye [72, 73], and hybrid metal-dielectric nanostructures [68, 74] can typically improve the directivity by a factor of 2 to more than two orders of magnitude compared with the directivity of a dipolar source in vacuum [Fig. 2.3]. Note that hybrid metal-dielectric nanostructures combine the advantages of both structures: a large Purcell factor due to the high confinement of the electromagnetic energy in the surroundings of the metal as well as a high scattering directivity with low losses in the dielectric part [68, 74].

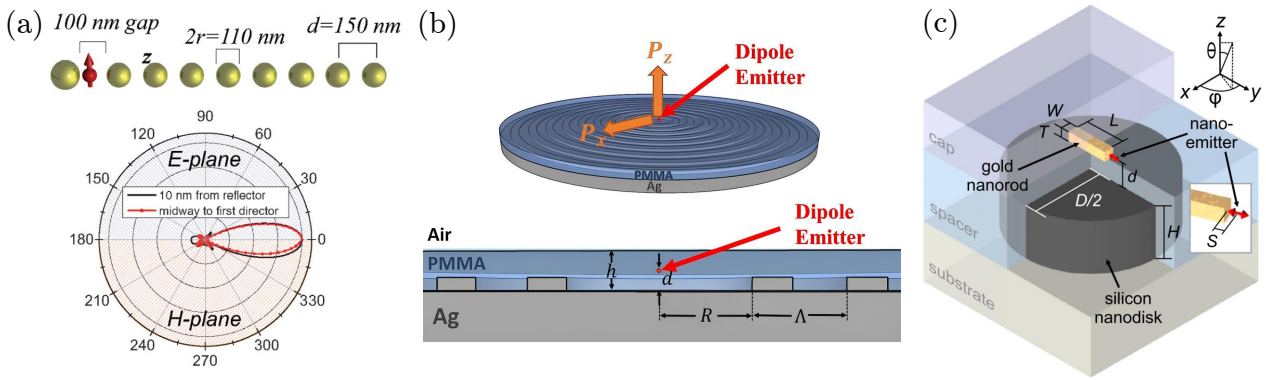


Figure 2.3: Schematic representations of nanoantenna examples for tailoring directivity. The figures are taken from the articles cited. (a) Yagi-Uda inspired nanoantenna consisting of one oriented emitter (red arrow), one reflector silver nanosphere at its left, and an array of director silver nanospheres at its right [71]. The emission pattern shows directional emission in the direction of the director nanospheres. (b) Bull's eye silver nanoantenna consisting of a dipole emitter placed at the central area surrounded by concentric rings [72]. (c) Hybrid metal-dielectric nanoantenna [74]. The emission from a dipole emitter (red arrow) is enhanced by a gold nanorod and redirected by a silicon nanodisk in the $y$ direction.

## 2.2 Two-photon spontaneous emission: state of the art

In this thesis, we study the two-photon spontaneous emission (TPSE) process. Historically, this second-order process in perturbation theory was predicted by Göppert-Mayer in 1931 [1] and is responsible for the mean lifetime of the 2s state of hydrogen [3]. It is at the origin of the continuous spectrum coming from planetary nebulae [Fig. 2.4] where about one third of electron captures by hydrogen atoms leads to the 2s state and so to the TPSE [4]. Also, the $2s \to 1s$ transition in hydrogen has a significant role in the control of the dynamics of cosmological hydrogen recombination [6–8]. Therefore, its consideration improves the accuracy in the determination of the cosmological

parameter measurements from the cosmic microwave background [75]. The first estimate of this two-electric dipole transition rate was made by Breit and Teller in 1940 [3], and one decade later, Spitzer and Greenstein realized a refinement and found a value of 8.23 $s^{-1}$ [4]. It was not until 1975 that the first experimental measurement of a two-photon emission rate, in hydrogen, was carried out [9]. In 1981, Goldman and Drake realized the first calculations that include multipolar contributions to the TPSE process [5]. For the hydrogen atom, they found that the two-magnetic dipole and the two-electric quadrupole transition rates are, respectively, 12 and 13 orders of magnitude smaller than the two-electric dipole one. Recently, the TPSE has been investigated in systems other than hydrogen, such as in atoms [10, 76], Rydberg atoms [11], molecules [12], quantum dots [17–19], semiconductors [13–16], epsilon-near-zero-materials [77], plasmonic nanostructures [21, 26, 27], and cosmic strings [78].

Figure 2.4: Hubble image of the Ring Nebula (Messier 57) [79].

Nowadays, the exploitation and the control of the TPSE process is of great interest as it promises several applications [20–23]. In addition to enabling the conception of broadband absorbers and light emitters since this is a continuous process [80], achieving high TPSE rates will enable the design of a new generation of entangled photon pair sources [13]. Indeed, efficient entangled photon sources are essential, especially in the telecommunication wavelengths, to test the foundations of quantum mechanics [81] and for many quantum applications [11, 13, 24, 82], including quantum computation, quantum teleportation, secured communications, etc. The most common approach to generating entangled photon pairs is the spontaneous parametric down conversion (SPDC) process in noncentrosymmetric crystals with second-order optical nonlinearity, in which pump photons are converted into photon pairs of lower energy [Fig. 2.5]. However, entangled photon sources based on the TPSE are promising alternatives [13]. Indeed, TPSE sources are theoretically expected to be 3 orders of magnitude more efficient than SPDC sources for equal pump levels [13] because it is a second-order process in the time-dependent perturbation theory, while SPDC is a third-order one [2, 83, 84]. In addition, TPSE should be more flexible for designing sources with given output wavelengths since there is no phase matching condition to satisfy[2] [11]. Furthermore, TPSE is promising for on-chip integrated two-photon sources where one proposes nanostructures coupled to waveguides [69], photonic crystals [85], or cavities [86].

In the 2000s, a high-intensity room-temperature TPSE source from semiconductor quantum wells in a photonic cavity has been proposed [13] and the first observations of TPSE from semiconduc-

[2]Due to the dispersion, only certain frequency triplets in the SPDC are allowed so that the laws of conservation of energy and momentum are respected.

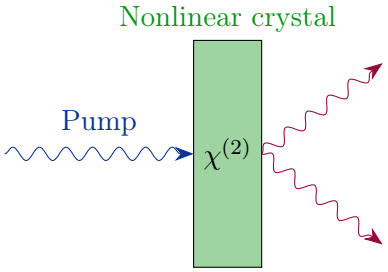


Figure 2.5: Schematic representation of the spontaneous parametric down-conversion (SPDC) process [24, 87]. In a nonlinear crystal characterized by a second-order susceptibility $\chi^{(2)}$, two photons are converted from a higher energy pump photon in accordance with the laws of conservation of energy and momentum.

tors have been reported [14]. In 2021, a source of heralded hyper-entangled (i.e., entanglement in various degrees of freedom verified through a measurement process) photons in the telecommunication wavelengths has been proposed, which uses TPSE in Rydberg atoms (atoms excited in a state characterized by a high principal quantum number, e.g., $n = 60$) placed inside a photonic cavity designed so that TPSE dominates [11]. Despite the interest in enhancing and controlling the TPSE process, its study near arbitrary photonic structures is hampered by a lack of efficient theoretical and numerical methods. In this direction, Muniz et al. derived a few years ago an expression for the TPSE transition rate of a quantum emitter as a function of the one-photon Purcell factors, with the restriction that structures are symmetric, that the emitter is at specific positions, and only for the two-electric dipole transition [31]. Therefore, there is a need for an efficient and general framework that considers higher-order multipolar interactions to study TPSE near arbitrary photonic structures. In this thesis, we develop this framework by taking into account the interaction up to the electric quadrupolar order, as well as the interference effects between the multipolar pathways.

## 2.3 Fermi's golden rule and selection rules

Now that SE processes have been introduced, let us see how to calculate the probability that a quantum system, defined here as the quantum emitter plus the electromagnetic field, transits form one state to another. For this purpose, consider the time-dependent Schrödinger equation that governs the time evolution of a quantum system [2, 88]:

$$i\hbar \frac{\partial \Psi(t)}{\partial t} = H(t)\,\Psi(t), \tag{2.1}$$

with $\hbar$ the reduced Planck's constant, $\Psi$ the wavefunction that contains all the information about the state of the system, and $H$ the Hamiltonian operator. However, solving this equation exactly is possible only for simple systems [2]. For more complex systems, the time-dependent perturbation theory gives good approximate solutions when the perturbation (interaction) is weak compared to the unperturbed system energy. This approximation method is particularly relevant for a quantum emitter interacting with the electromagnetic field surrounding it since, for example, the field acting on the electron in the ground state of the hydrogen atom is of the order of magnitude of $10^{11}$ V/m, which is much higher than the vacuum modes of the photonic environments usually studied and than the electromagnetic fields generally applied to an emitter [2].

In the time-dependent perturbation theory, the application of a perturbation to a two-level

quantum emitter (i.e., the interaction with the electromagnetic field), which is small compared to the emitter energy levels, causes the system to switch continuously from one state to another [2, 88]. Thus, the system's states after perturbation have not been altered, only the probability of being in one or the other. This perturbative approach leads to Fermi's golden rule that gives the probability per unit time that a system transits from an initial state $|i\rangle$ to a final state $|f\rangle$ due to a small interaction [88]:

$$\Gamma_{i\to f} = \frac{2\pi}{\hbar}|M_{fi}|^2\,\delta(E_f - E_i). \tag{2.2}$$

In SE processes, the initial state is characterized by the emitter in an excited state and by the field in the vacuum state, while in the final state, the emitter is in its ground state and the field is in a state containing one of several quanta. In this equation, $E_i$ and $E_f$ denote the energies of the initial and final states of the system (emitter plus field), respectively, while $\delta(E_f - E_i)$ is the Dirac delta distribution, which ensures the energy conservation during the transition. Moreover, $M_{fi}$ is the matrix element of the Hamiltonian $H_{\text{int}}$ describing the emitter-field interaction, which acts as a perturbation of the system. At the first order, it is given by [2, 88]:

$$M_{fi}^{(1)} = \langle f|\, H_{\text{int}}(t)\, |i\rangle\,, \tag{2.3}$$

whereas at the second order, it involves a summation over the intermediate states $|l\rangle$ of the system [2]:

$$M_{fi}^{(2)} = \sum_{|l\rangle} \frac{\langle f|\, H_{\text{int}}(t)\, |l\rangle\, \langle l|\, H_{\text{int}}\, |i\rangle}{E_i - E_l}, \tag{2.4}$$

where $M_{fi}^{(1)}$ and $M_{fi}^{(2)}$ describe one- and two-photon spontaneous emission processes, respectively. We will come back to this in the subsequent chapters when we address mathematically these processes.

Equation (2.2) can only be employed for transitions between discrete states of a system, so it is not complete for studying SE processes [2, 88]. Indeed, for a transition between two given states of a quantum emitter, there is a continuum of final states that is available for the emitted quanta, and it is therefore necessary to sum the transition rates relative to the transitions to each of these states [2, 88]. This is usually done by introducing the density of final states $\rho(E_f)$ that represents the number per unit of energy interval of available states at the energy $E_f$ [2, 88]. By adding an integration over $\rho(E_f)\,\mathrm{d}E_f$, which gives the number of final states within the energy interval $E_f$ and $E_f + \mathrm{d}E_f$, we find the most familiar form of Fermi's golden rule [2, 88, 89]:

$$\Gamma_{i\to f} = \frac{2\pi}{\hbar}|M_{fi}|^2\,\rho(E_i), \tag{2.5}$$

where $E_i = E_f$ by energy conservation. To study SE processes in the following chapters, we use the formulation of Fermi's golden rule expressed with the delta distribution [Eq. (2.2)], adding at the end of the developments a sum over all possible states for the emitted quanta.

### Selection rules

Having presented the method used to calculate SE rates, it is interesting to look at which transitions are allowed between two states of an emitter. These are given by the so-called selection rules and depend on the symmetry group to which the emitter belongs. In this thesis, we consider the simplest emitter, namely the hydrogen atom, which has spherical symmetry and the advantage of

being analytically calculable. Its wavefunction $\psi(\mathbf{r})$ can be written as a product between a radial function $R_{n,l}(r)$ and a spherical harmonic function $Y_l^m(\theta,\varphi)$ representing the angular part [45]:

$$\psi(\mathbf{r}) = R_{n,l}(r)\, Y_l^m(\theta,\varphi), \tag{2.6}$$

where $n$, $l$ and $m$ are, respectively, the principal, azimuthal and magnetic quantum numbers. The first one determines the energy level of the electron which is given by $-E_i/n^2$ with $n \in \mathbb{N}_0$ and $E_i = 13.6$ eV the ionization energy. The second one gives the shape of the orbital and can take $n-1$ values: $l = 0, 1, \ldots, n-1$. The last one sets the spatial orientation of the orbital and can take $2l+1$ values: $m = -l, -l+1, \ldots, l$. Hereafter, we use the spectroscopic notation to label the states. Thus, a state is written as $nl$ where $l = 0, 1, 2, 3$ is noted with the letters $s$, $p$, $d$, $f$, respectively.

To derive the selection rules for a given multipolar transition, it is sufficient to determine if the matrix element of the corresponding multipolar operator between the ground and the excited states of the emitter, noted respectively as $|g\rangle := |n_g, l_g, m_g\rangle$ and as $|e\rangle := |n_e, l_e, m_e\rangle$, is non-zero [47, 90]. For example, for electric dipole and quadrupole transitions, we determine for which conditions on the quantum numbers of the excited state $|e\rangle$ and of the ground state $|g\rangle$ the two following matrix elements are non-zero [47, 90]:

$$\langle g|\mathbf{d}|e\rangle = -e\,\langle n_g, l_g, m_g|\,\mathbf{r}\,|n_e, l_e, m_e\rangle\,, \tag{2.7a}$$

$$\langle g|\mathbf{Q}|e\rangle = -\frac{e}{2}\,\langle n_g, l_g, m_g|\,\mathbf{rr}\,|n_e, l_e, m_e\rangle\,, \tag{2.7b}$$

with $\mathbf{d}$, $\mathbf{Q}$, and $\mathbf{r}$ being the electric dipole, electric quadrupole, and position operators, respectively. By expressing the position vectors in terms of spherical harmonics, one finds the selection rules for electric dipole (ED) and electric quadrupole (EQ) transitions for the hydrogen atom [47, 90]:

$$\text{ED transition:} \quad \Delta n \neq 0, \quad \Delta l = \pm 1, \quad \Delta m = 0, \pm 1, \tag{2.8a}$$

$$\text{EQ transition:} \quad \Delta n \neq 0, \quad \Delta l = 0, \pm 2, \quad \Delta m = 0, \pm 1, \pm 2, \tag{2.8b}$$

where EQ transitions between two states characterized by $l = 0$ are forbidden. We will have the opportunity to calculate these matrix elements when we will calculate TPSE rates in Chapter 5.

## 2.4 Textbook case

In order to clarify the different types of transitions of the SE process that we have introduced and to further understand the characteristics of the two-photon spontaneous emission (TPSE) process, let us consider an isolated hydrogen atom with its electron being in an initial and excited state and let us examine the transitions that are allowed towards the ground state depending on the initial state. For this example, we consider only the electric dipole (ED) and the electric quadrupole (EQ) interactions, and we consider one and two-photon transitions. In the case of a two-photon transition, it follows from equations (2.8) that $\Delta l = 0, \pm 2$ for a two-electric dipole (2ED) transition, $\Delta l = 0, \pm 2, \pm 4$ for a two-electric quadrupole (2EQ) transition, and $\Delta l = \pm 1, \pm 3$ for the mixed transitions ED-EQ and EQ-ED.

First of all, one distinguishes two different processes among the two-photon transitions: the cascade of two independent single-photon transitions (i.e., two first-order transitions) and the quasi

simultaneous emission of two photons via the TPSE process (i.e., one second-order transition) [8]. The difference between these two decay mechanisms lies in the nature of the intermediate state that connects the initial state with the final state. In the cascade of two single-photon transitions, the intermediate state is a resonant state having an energy lower than the energy of the initial state and so both single-photon transitions have a pure Lorentzian shape. In the TPSE transition, the intermediate state has an energy equal or greater than the energy of the initial state. As a result, the law of conservation of energy is temporarily violated since the energy of the emitter increases while a photon is emitted. The intermediate states that mediate transitions without energy conservation are called virtual states [2, 42, 91] and their existence is limited in the time by the uncertainty principle. Indeed, they can exist only during a time shorter than the reduced Planck constant divided by the amount of energy violated: $t \leq \hbar/\Delta E$ [42]. Therefore, quasi simultaneously with the first transition towards the virtual intermediate state, the emitter decays to its ground state by emitting a second photon. Note that unlike first-order processes that connect two resonant states of the emitter, second-order processes connect non-resonant states. Therefore, the energy of a photon is not equal to the energy difference between two emitter states (e.g., between the intermediate and the ground states) since the conservation of energy is temporarily violated. Overall, the law of conservation of energy is respected: the energy of the two photons is equal to the energy difference between the excited and the ground state of the emitter, noted as $\hbar\omega_{eg}$. Thereby, this second-order transition can only be understood as a whole. Furthermore, since only the sum of the energies of the two photons is fixed, the frequency $\omega$ of one photon can take any value between 0 an $\omega_{eg}$ and the second photon will have the complementary frequency $\omega_{eg} - \omega$, leading to a broad continuous and symmetric spectrum with respect to $\omega_{eg}/2$ [92].

Let us start by considering the electron in the first excited level ($n = 2$) and let us examine the possible transitions towards the ground state, i.e., the $1s$ state ($n = 1$, $l = 0$). In the $n = 2$ shell, either the electron is in the $2s$ ($l = 0$) or in the $2p$ ($l = 1$) states, which have the same energy. In the first case, single-photon ED and EQ transitions are prohibited by the selection rules. Among two-photon transitions, the cascade of two single-photon transitions is also forbidden due to the absence of an intermediate resonant state between the excited and the ground states. Therefore, the only possibility for the emitter is to decay via a TPSE transition. Thereby, either the emitter performs a 2ED transition which is mediated by $p$ states or a 2EQ transition which is mediated by $d$ states. In the case where the electron is initially in the $2p$ state, the ED transition is now allowed, while the EQ transition and the cascade of two single-photon transitions are still forbidden. Among TPSE transitions, it is now the mixed transitions, mediated by $d$ states, that are permitted by selection rules.

Let us now consider an electron in the $n = 3$ shell, and more specifically in the $3d$ state ($l = 2$). In this case, the ED transition is forbidden towards the ground state while the EQ transition is allowed (red transition in Fig. 2.6). However, the electron can perform a first ED transition to the $2p$ state and then a second one to reach the ground state (green transitions in Fig. 2.6): it performs a cascade of two first-order ED transitions. In addition, the emitter can perform second-order transitions, where the 2ED transition is mediated by virtual states of type $p$ (blue transitions in Fig. 2.6) while the 2EQ transition is mediated by virtual states of type $d$ (not shown). Note that these transitions can interfere with each other [2, 8].

In order to get an idea of the order of magnitude of these transitions, the rates of some of them

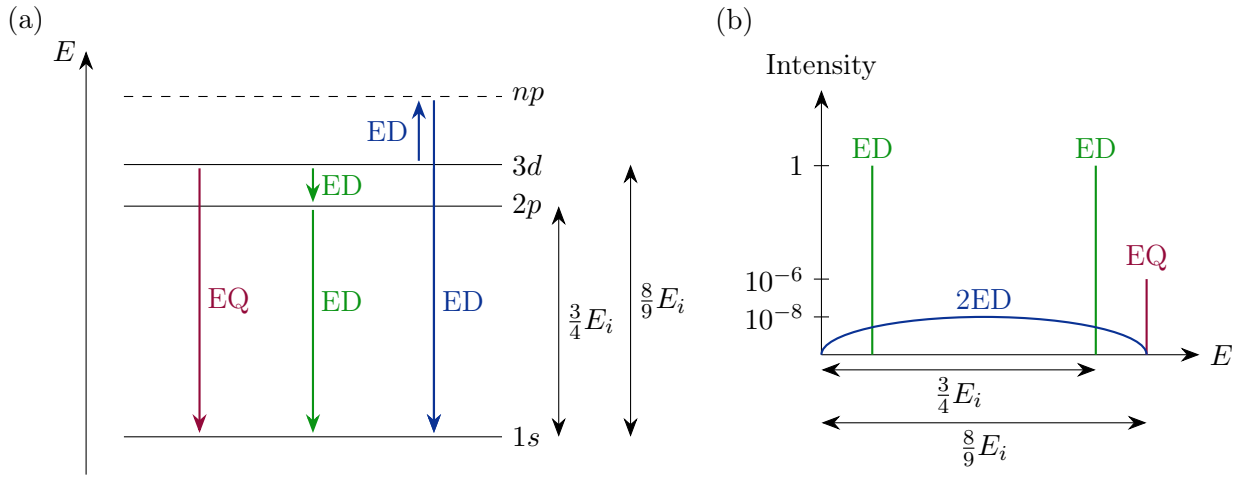


Figure 2.6: Energy representation and spectra of three possible transitions from the excited state $3d$ to the ground state $1s$. The EQ transition is drawn in red, the cascade of two ED transitions in green, and the 2ED TPSE transition in blue. The energy difference between two states is given by $\Delta E = E_i(\frac{1}{n_f^2} - \frac{1}{n_i^2})$ with $E_i$ the ionization energy of hydrogen and $n_i > n_f$. (a) In the energy representation, real states are sketched with solid lines while virtual states are drawn with dashed lines. As the law of conservation of energy is temporarily violated during the TPSE transition (blue), it is not possible to draw a picture that correctly represents both the energy of the intermediate state (which is greater than the energy of the excited state) and the energy of the two photons that are emitted (which their sum is equal to the energy difference between the excited and the ground state). Thus, for the TPSE transition, the photons do not have energies equal to the energy difference between the excited and the intermediate states, and between the intermediate and the ground states. (b) A log scale is used for the spectra intensity, which are given for comparison purposes only. Vertical lines represent resonant transitions of Lorentzian shape, while the blue spectrum represents the continuous and symmetric spectrum of the TPSE transition.

are given in Table 2.1 for the hydrogen atom in vacuum. Note that cascades of two first-order transitions have similar rates than single first-order transitions [8].

| 1-order transition | $\|e\rangle \to \|g\rangle$ | $\Gamma_0$ [$s^{-1}$] |
|---|---|---|
| ED | $2p \to 1s$ | $6.3 \times 10^8$ |
| EQ | $3d \to 1s$ | $5.9 \times 10^2$ |

| 2-order transition | $\|e\rangle \to \|g\rangle$ | $\Gamma_0$ [$s^{-1}$] |
|---|---|---|
| 2ED | $2s \to 1s$ | 8.2 |
| 2EQ | $2s \to 1s$ | $4.9 \times 10^{-12}$ |

Table 2.1: Examples of first-order and second-order vacuum transition rates for the hydrogen atom [5, 93].

## 2.5 From classical to quantum sources

Before dealing in the next chapters with quantum emitters, which can be seen as quantum sources since a decay rate multiplied by the energy of the emitted photon is equal to a power, let us take a mathematical look at the power emitted by classical sources. First, we introduce the dyadic Green's function that gives the fields produced by point sources. Then, we calculate the power emitted by an electric point dipole and quadrupole, and by the superposition of these two multipolar point sources. Finally, we present the Purcell factors that make the link between the spontaneous emission decay rate of a quantum system and the power emitted by classical point sources. It is this link that will

allow us in next chapters to calculate classically the impact of the environment on the spontaneous emission rate of quantum emitters. This section is mainly based on Chapters 2 and 8 of the book *Principles of Nano-Optics* [30].

### 2.5.1 The dyadic Green's function

Let us consider an infinite, linear, homogeneous, isotropic, and non-magnetic medium with a dielectric constant equal to 1 in which there is a source contained in a finite volume $V$. The source is described by a current density $\mathbf{j}$ and we assume a time harmonic dependency $e^{-i\omega t}$ for it and for the electromagnetic field, with $\omega$ the angular frequency. Starting from Maxwell's equations, one finds the wave equation for the electric field $\mathbf{E}(\mathbf{r})$ that describes its propagation in the presence of a source current density $\mathbf{j}(\mathbf{r})$ [30]:

$$\nabla\times\nabla\times\mathbf{E}(\mathbf{r}) - k^2\,\mathbf{E}(\mathbf{r}) = i\mu_0\,\omega\,\mathbf{j}(\mathbf{r}), \tag{2.9}$$

where $\nabla = (\frac{\partial}{\partial x}, \frac{\partial}{\partial y}, \frac{\partial}{\partial z})^T$ is a column vector with $T$ denoting the transpose, $k$ is the wavenumber, and $\mu_0$ represents the vacuum permeability. In addition to being a differential equation, it is inhomogeneous because of the right-hand side of the equation.

In this equation, $\left(\nabla\times\nabla\times - k^2\right)$ is a linear operator acting on the electric field $\mathbf{E}(\mathbf{r})$ representing the unknown response of the system due the source $\mathbf{j}(\mathbf{r})$. Generally, it is difficult to solve this equation. A mathematical trick is to consider the dyadic Green's function $\mathbf{G}(\omega;\mathbf{r},\mathbf{r}')$, a second-rank tensor, that obeys to the following equation[3] [30]:

$$\nabla\times\nabla\times\mathbf{G}(\omega;\mathbf{r},\mathbf{r}') - k^2\,\mathbf{G}(\omega;\mathbf{r},\mathbf{r}') = \mathbb{1}\,\delta(\mathbf{r}-\mathbf{r}'), \tag{2.10}$$

where $\mathbb{1}$ is the identity tensor and $\delta$ denotes the Dirac delta distribution, thus representing a point source at the position $\mathbf{r}'$. Thereby, the first, second, and third columns of the tensor $\mathbf{G}$ correspond to the field due to a point source in the $x$, $y$, and $z$ directions, respectively. Let us assume for the following that this equation is solved and therefore that the tensor $\mathbf{G}$ is known.

By multiplying the last equation by the source $\mathbf{j}(\mathbf{r}')$ and by integrating over the volume $V$ encompassing the source, one gets [30]:

$$\int_V \left(\nabla\times\nabla\times - k^2\right)\mathbf{G}(\omega;\mathbf{r},\mathbf{r}')\,\mathbf{j}(\mathbf{r}')\,\mathrm{d}V' = \int_V \mathbf{j}(\mathbf{r}')\,\delta(\mathbf{r}-\mathbf{r}')\,\mathrm{d}V' = \mathbf{j}(\mathbf{r}), \tag{2.11}$$

where the integral in the right-hand side has been calculated. Using the equation (2.9), we can replace $\mathbf{j}(\mathbf{r})$ in the right-hand side of the last equation. After a swap between the two equation sides, one finds [30]:

$$\left(\nabla\times\nabla\times - k^2\right)\mathbf{E}(\mathbf{r}) = i\mu_0\,\omega\int_V \left(\nabla\times\nabla\times - k^2\right)\mathbf{G}(\omega;\mathbf{r},\mathbf{r}')\,\mathbf{j}(\mathbf{r}')\,\mathrm{d}V'. \tag{2.12}$$

If the integrand has no singularities, the operator acting on $\mathbf{G}$ can be permuted with the integral and the equation reduces to [30]:

$$\mathbf{E}(\mathbf{r}) = i\mu_0\,\omega\int_V \mathbf{G}(\omega;\mathbf{r},\mathbf{r}')\,\mathbf{j}(\mathbf{r}')\,\mathrm{d}V'. \tag{2.13}$$

[3] Note that the Green's function is not only used in electromagnetism, it can be applied to solve the following general and inhomogeneous equation: $\mathcal{L}\,\mathbf{A}(\mathbf{r}) = \mathbf{B}(\mathbf{r})$, with $\mathcal{L}$ being a linear operator acting on an unknown vector field $\mathbf{A}$, which is the response due to a source vector field $\mathbf{B}$ [30].

Therefore, the unknown electric field $\mathbf{E}(\mathbf{r})$ produced by the source $\mathbf{j}(\mathbf{r}')$ can be calculated by integrating the product between the dyadic Green's function $\mathbf{G}(\omega; \mathbf{r}, \mathbf{r}')$, which represents the environment, and the source over the volume containing it [Fig. 2.7]. This is generally simpler to solve than the differential and inhomogeneous equation (2.9) when $\mathbf{G}(\omega; \mathbf{r}, \mathbf{r}')$ is known [30]. In addition, the Green's function depends only on the photonic environment, so once it is known, it is possible to obtain the electric field produced by any source.

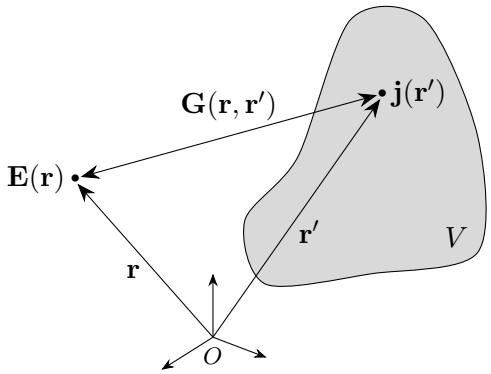


Figure 2.7: The dyadic Green's function $\mathbf{G}(\mathbf{r}, \mathbf{r}')$ represents the environment and gives the electric field at the position $\mathbf{r}$ due to a point source $\mathbf{j}$ at the position $\mathbf{r}'$ [30]. The electric field $\mathbf{E}(\mathbf{r})$ is obtained through the integration of the product between the tensor $\mathbf{G}(\mathbf{r}, \mathbf{r}')$ and the source $\mathbf{j}(\mathbf{r}')$ over the volume $V$ encompassing the source [Eq. (2.13)].

Now that the tensor $\mathbf{G}$ has been introduced, one can express the power emitted by a source as a function of it. The power emitted by the source is given by Poynting's theorem [30]:

$$W = -\frac{1}{2}\int_V \mathrm{Re}\left\{\mathbf{j}^*(\mathbf{r}) \cdot \mathbf{E}(\mathbf{r})\right\} \mathrm{d}V, \tag{2.14}$$

where Re denotes taking the real part. Using the equation (2.13), one gets

$$W = \frac{\mu_0\,\omega}{2}\int_V\int_V \mathrm{Im}\left\{\mathbf{j}^*(\mathbf{r}) \cdot \mathbf{G}(\omega; \mathbf{r}, \mathbf{r}') \cdot \mathbf{j}(\mathbf{r}')\right\} \mathrm{d}V'\,\mathrm{d}V, \tag{2.15}$$

where Im denotes taking the imaginary part and the obtained expression involves twice the source current density. In the next subsection, we calculate the power emitted by electric dipole and quadrupole point sources and we examine the case where these two sources are superposed, and therefore their interference. Note that these developments can also be made for the magnetic dipole, but the equations are similar to those relating to the electric dipole.

### 2.5.2 Point electric dipole and quadrupole

Let us consider an electric point dipole at the position $\mathbf{R}$ oscillating at the frequency $\omega$ with a time harmonic dependency, see sketch in Figure 2.8. Its current density is given by [30]:

$$\mathbf{j}_{\mathrm{ED}}(\mathbf{r}) = \frac{\mathrm{d}}{\mathrm{d}t}\mathbf{d}\,\delta(\mathbf{r} - \mathbf{R}) = -i\omega\,\mathbf{d}\,\delta(\mathbf{r} - \mathbf{R}), \tag{2.16}$$

with $\mathbf{d}$ being the electric dipole moment of the source:

$$\mathbf{d} = \int_V \rho(\mathbf{r})\,\mathbf{r}\,\mathrm{d}V, \tag{2.17}$$

with $\rho$ the volume charge density[4]. Using the expression of the current density in equation (2.13), we obtain the electric field produced by the electric point dipole [30]:

$$\mathbf{E}(\mathbf{r}) = \mu_0\,\omega^2\,\mathbf{G}(\omega;\mathbf{r},\mathbf{R})\,\mathbf{d}. \tag{2.18}$$

Thereby, each column of the Green's function gives the electric field at the position $\mathbf{r}$ produced by an electric point dipole at the position $\mathbf{R}$, oscillating at the frequency $\omega$, and whose axis is aligned with one of the coordinate axes [30].

Using equations (2.15) and (2.16), we obtain the power emitted by the electric point dipole inside an environment which is represented by the Green's function [30]:

$$W_{\mathrm{ED}} = \frac{\mu_0\,\omega^3}{2}\,\|\mathbf{d}\|^2\left\{\hat{\mathbf{d}}^*\cdot\operatorname{Im}\mathbf{G}(\omega;\mathbf{R},\mathbf{R})\cdot\hat{\mathbf{d}}\right\}, \tag{2.19}$$

where the caret denotes normalized vectors and where the imaginary part of the Green's function is evaluated at the source position $\mathbf{R}$. Note that $\operatorname{Im}\mathbf{G}(\omega;\mathbf{r},\mathbf{r}')$ is a symmetric tensor when $\mathbf{r}=\mathbf{r}'$ [30]. Using the free-space related expression of $\operatorname{Im}\mathbf{G}$, the emitted power in vacuum is given by [30, 94]:

$$W_{\mathrm{ED},0} = \frac{\mu_0\,\omega^4}{12\pi c}\,\|\mathbf{d}\|^2. \tag{2.20}$$

Thereby, the vacuum normalized power is given by

$$\frac{W_{\mathrm{ED}}}{W_{\mathrm{ED},0}} = \frac{6\pi c}{\omega}\left\{\hat{\mathbf{d}}^*\cdot\operatorname{Im}\mathbf{G}(\omega;\mathbf{R},\mathbf{R})\cdot\hat{\mathbf{d}}\right\}. \tag{2.21}$$

For an electric point quadrupole at the position $\mathbf{R}$, sketches in Figure 2.8, oscillating at the frequency $\omega$ with a time harmonic dependency, its current density is given by [2, 23]:

$$\mathbf{j}_{\mathrm{EQ}}(\mathbf{r}) = i\omega\,\mathbf{Q}\nabla\,\delta(\mathbf{r}-\mathbf{R}), \tag{2.22}$$

where $\nabla = (\frac{\partial}{\partial x},\frac{\partial}{\partial y},\frac{\partial}{\partial z})^T$ is a column vector with $T$ denoting the transpose and where the electric quadrupole moment is defined as[5]

$$\mathbf{Q} = \frac{1}{2}\int_V \rho(\mathbf{r})\left(\mathbf{rr}-\frac{r^2\mathbb{1}}{3}\right)\mathrm{d}V, \tag{2.23}$$

where $\mathbb{1}$ denotes the identity matrix and where the product $\mathbf{rr}$ is an outer product. Therefore, the power emitted by the point quadrupole is obtained by substituting $\mathbf{d}$ by $-\mathbf{Q}\nabla$ in equation (2.19):

$$W_{\mathrm{EQ}} = \frac{\mu_0\,\omega^3}{2}\,\|\mathbf{Q}\|^2\left\{\hat{\mathbf{Q}}^*\nabla\cdot\operatorname{Im}\mathbf{G}(\omega;\mathbf{r},\mathbf{r}')\cdot\hat{\mathbf{Q}}\nabla'\right\}_{\mathbf{r}=\mathbf{r}'=\mathbf{R}}, \tag{2.24}$$

where we defined the squared norm of a rank-$n$ tensor $\mathbf{U}$ with $n\geq 1$ as $\|\mathbf{U}\|^2 := \sum_{i_1,i_2,\ldots,i_n}|U_{i_1,i_2,\ldots,i_n}|^2$ and where $\nabla'$ means derivatives with respect to the coordinates $\mathbf{r}'$. Thereby, the power emitted by a quadrupole is related to the double derivatives of the imaginary part of the Green's function. Finally,

[4] Note that $\int_V \rho(\mathbf{r})\,\mathrm{d}V = 0$.

[5] The quadrupole moment is sometimes defined with a factor 3 instead of the factor 1/2. However, it is important to define the quadrupole moment as we did in order to have a correspondence with the electric quadrupole operator $\mathbf{Q} = -e\,\mathbf{rr}/2$ in quantum mechanics. In addition, $\mathbf{Q}$ can be taken traceless in source-free regions ($\int_V \rho(\mathbf{r})\,\mathrm{d}V = 0$) since $\nabla\cdot\mathbf{E} = 0$ [30, 46, 94, 95].

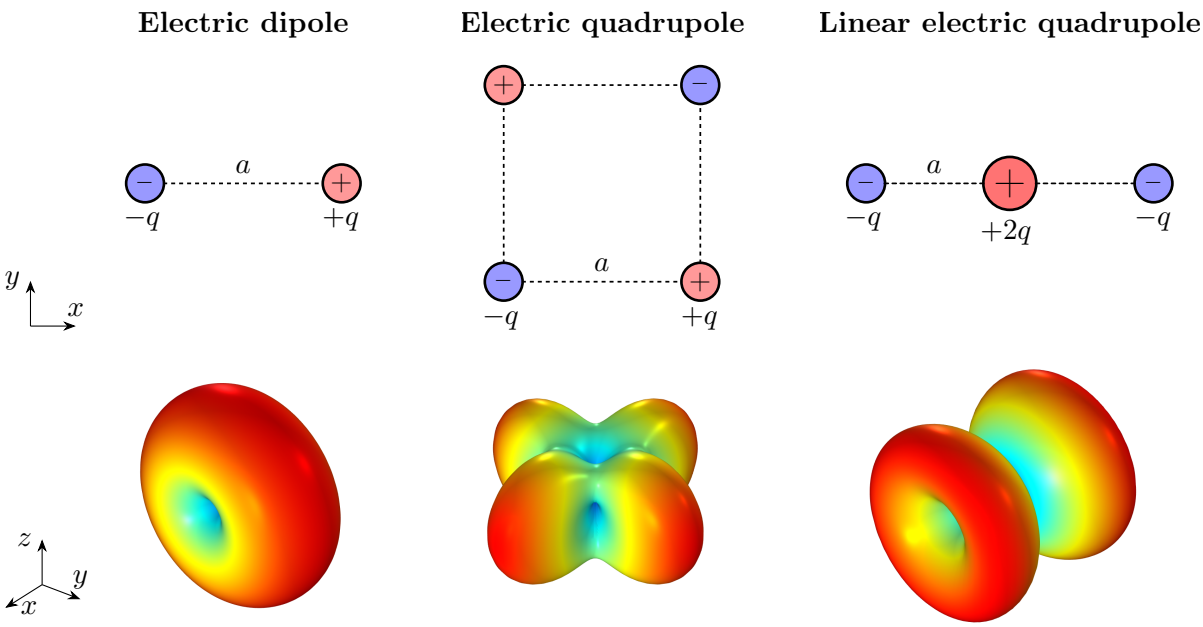


Figure 2.8: Representation of the charge distribution of an electric dipole, an electric quadrupole, and a linear electric quadrupole. They consist of, respectively, two charges $q$ of opposite sign, two positive and negative charges $q$ and $-q$ placed alternately on the corners of a square, and three charges $-q$, $2q$ and $-q$ aligned. The center of the three charge distributions is located by the vector $\mathbf{R}$. For the three systems, the total charge is zero (i.e., $\int_V \rho(\mathbf{r})\,\mathrm{d}V = 0$), and for the two electric quadrupoles, the dipole moment is zero. When the charges oscillate, there is a source current density leading to a radiation whose radiation pattern is sketched below each system. Radiation patterns have been obtained using the COMSOL Multiphysics® software. For point sources, the distance $a$ between charges tends towards zero by keeping their moments constant.

the power emitted in vacuum is expressed as follows [94]:

$$W_{\mathrm{EQ},0} = \frac{\mu_0\,\omega^6}{40\pi c^3}\,\|\mathbf{Q}\|^2\,, \tag{2.25}$$

and the vacuum normalized power is given by

$$\frac{W_{\mathrm{EQ}}}{W_{\mathrm{EQ},0}} = \frac{20\pi c^3}{\omega^3}\left\{\hat{\mathbf{Q}}^*\nabla\cdot\mathrm{Im}\,\mathbf{G}(\omega;\mathbf{r},\mathbf{r}')\cdot\hat{\mathbf{Q}}\nabla'\right\}_{\mathbf{r}=\mathbf{r}'=\mathbf{R}}. \tag{2.26}$$

It is important to note that when a source emits in an inhomogeneous environment (e.g., a quantum emitter in a cavity or near a plasmonic nanostructure), it is still possible to calculate the power it emits by integrating the Poynting vector on a surface $\delta V$ including the source [30]:

$$W = \int_{\delta V} \langle\mathbf{S}(\mathbf{r})\rangle\cdot\mathbf{n}\,\mathrm{d}S, \tag{2.27}$$

with $\mathbf{n}$ an unitary vector perpendicular to the surface and with $\langle\mathbf{S}(\mathbf{r})\rangle$ the time-averaged value of the Poynting vector that is given by

$$\langle\mathbf{S}(\mathbf{r})\rangle = \frac{1}{2}\,\mathrm{Re}\left\{\mathbf{E}\times\mathbf{H}^*\right\} \tag{2.28}$$

for fields with a time harmonic dependency. However, the electromagnetic field is the total field composed of the field produced by the source alone plus the scattered field from the environment [30].

As a result, the environment tailors the electric field at the emitter's position and with it the power emitted by the source: this is the Purcell effect. In the case of point sources, the equations (2.19) and (2.24) show that it is sufficient to know the electromagnetic field (or equivalently the Green's function) at the source position.

#### Superposition of multipolar sources

Let us now consider the superposition of two multipolar sources: an electric point dipole plus an electric point quadrupole at the same location. In this case, the source current density is given by

$$\mathbf{j}_{\mathrm{ED+EQ}}(\mathbf{r}) = -i\omega\,(\mathbf{d} - \mathbf{Q}\nabla)\,\delta(\mathbf{r} - \mathbf{R}), \tag{2.29}$$

which leads to the three following contributions to the emitted power [Eq. (2.15)]:

$$W_{\mathrm{ED+EQ}} = W_{\mathrm{ED}} + W_{\mathrm{EQ}} + W_{\mathrm{ED}\cap\mathrm{EQ}}. \tag{2.30}$$

In the last equation, we define $W_{\mathrm{ED}\cap\mathrm{EQ}}$ as the term describing the interference between the dipole and the quadrupole, which contains two equal cross terms[6] and which is expressed as follows:

$$W_{\mathrm{ED}\cap\mathrm{EQ}} = 2\,\frac{\mu_0\,\omega^3}{2}\,\|\mathbf{d}\|\,\|\mathbf{Q}\|\left\{\hat{\mathbf{d}}^*\cdot\mathrm{Im}\,\mathbf{G}(\omega;\mathbf{R},\mathbf{r}')\cdot\hat{\mathbf{Q}}\nabla'\right\}_{\mathbf{r}'=\mathbf{R}}. \tag{2.31}$$

Thereby, the interference term is related to the derivatives of the imaginary part of the Green's function. Note that there is no interference between multipolar sources in vacuum because each type of emitter generates its unique field distribution that remains decoupled from other multipolar sources at the same location [2]. We can nevertheless normalize it by the vacuum emitted power of the ED and EQ:

$$\frac{W_{\mathrm{ED}\cap\mathrm{EQ}}}{\sqrt{W_{\mathrm{ED},0}\,W_{\mathrm{EQ},0}}} = 2\,\frac{2\sqrt{30}\pi c^2}{\omega^2}\left\{\hat{\mathbf{d}}^*\cdot\mathrm{Im}\,\mathbf{G}(\omega;\mathbf{r},\mathbf{r}')\cdot\hat{\mathbf{Q}}\nabla'\right\}_{\mathbf{r}=\mathbf{r}'=\mathbf{R}}. \tag{2.32}$$

By looking at the equations of the power emitted by the multipolar sources [Eqs. (2.19), (2.24), and (2.31)], we notice that they involve twice the electric dipole moment $\mathbf{d}$ for the ED source, twice the electric quadrupole moment $\mathbf{Q}$ for the EQ source, and once the electric dipole and quadrupole moments for the term describing the interference between the dipolar and quadrupolar sources.

### 2.5.3 Link between classical and quantum sources: the Purcell factor

Since the work of Purcell in 1946 [25], we know that the spontaneous decay rate of a quantum emitter is not only an intrinsic property of the emitter but also depends on the photonic environment. Thereby, the environment can be designed to tailor the decay rate of an emitter, by increasing, decreasing or even suppressing it [30, 96–98]. Furthermore, the atom-field interaction domain is split into two distinct regimes: the strong and weak coupling regimes [30]. In the strong coupling regime, the interaction between the emitter and the field occurs faster than the emission of photons inside the cavity, whereas in the weak coupling regime, it is the opposite. As a result, one needs to use quantum electrodynamics theory to describe accurately the strong coupling regime. However, in the weak coupling regime, the classical theory gives the same modification of the spontaneous emission

[6] This can be proven using that the tensor $\mathrm{Im}\,\mathbf{G}(\omega;\mathbf{R},\mathbf{R})$ is symmetric [30].

rate as the quantum electrodynamics theory. Here, we develop the link between the modification of the power emitted by classical sources and the modification of transition rates when these systems are placed in a given environment.

We know that the transitions between the states of a non-extended quantum emitter are described by multipolar moments [47, 90] and can therefore be seen as quantum sources. However, for identical moments describing classical and quantum sources, the powers emitted by these two different systems are not equal [30]:

$$\Gamma\hbar\omega \neq W, \tag{2.33}$$

where $\Gamma$ denotes the transition rate of the quantum emitter, $\hbar\omega$ is the energy of the emitted photons, and $W$ represents the power emitted by the classical source. However, when these powers are vacuum normalized, there is an equality between the modification of these quantities [30]:

$$\frac{\Gamma}{\Gamma_0} = \frac{W}{W_0} := P, \tag{2.34}$$

where $P$ is defined as the Purcell factor. Thereby, the Purcell factor makes the link between transition rates of quantum emitters and powers emitted by classical sources. Therefore, this equation makes it possible to calculate the Purcell effect (i.e., the change in transition rates of a quantum emitter in a given environment) by calculating the power emitted by classical sources having the same multipolar moments that those describing the emitter transitions.

Furthermore, the equation (2.34) is valid regardless of the multipole moment describing the transition (electric dipole, magnetic dipole, electric quadrupole transition moments, etc.), but also when several multipole channels contribute simultaneously to the emitter's total transition rate. For example, in the case where the electric dipole (ED) and the electric quadrupole (EQ) emission channels contribute to the total decay rate, the equation (2.34) becomes

$$\frac{\Gamma_{\mathrm{ED+EQ}}}{\Gamma_{\mathrm{ED},0} + \Gamma_{\mathrm{EQ},0}} = \frac{W_{\mathrm{ED+EQ}}}{W_{\mathrm{ED},0} + W_{\mathrm{EQ},0}}, \tag{2.35}$$

where $\Gamma_{\mathrm{ED+EQ}}$ denotes the total transition rate of the emitter due to the ED and EQ decay channels and contains the interference between the two emission pathways. Note that, as with classical sources, there is no interference in vacuum between different multipolar sources because each type of emitter generates its unique field distribution that remains decoupled from other multipolar sources at the same location [2]. By developing the contributions to the total transition rate and to the total emitted power [Eq. (2.30)], we get

$$\frac{\Gamma_{\mathrm{ED}} + \Gamma_{\mathrm{EQ}} + \Gamma_{\mathrm{ED\cap EQ}}}{\Gamma_{\mathrm{ED},0} + \Gamma_{\mathrm{EQ},0}} = \frac{W_{\mathrm{ED}} + W_{\mathrm{EQ}} + W_{\mathrm{ED\cap EQ}}}{W_{\mathrm{ED},0} + W_{\mathrm{EQ},0}}, \tag{2.36}$$

where $\Gamma_{\mathrm{ED}}$, $\Gamma_{\mathrm{EQ}}$, and $\Gamma_{\mathrm{ED\cap EQ}}$ represent, respectively, the ED and EQ transition rates as well as the interference between these two emission channels.

The exposed link is valid for the one-photon spontaneous emission process only. For the two-photon spontaneous emission, a first step in establishing the link with the Purcell factors of single-photon emission has been made, with some restriction on the system and only for the two-electric dipole transition [31]. In this thesis, we establish in Chapter 4 the general link between the TPSE rates and the Purcell factors, up to the electric quadrupolar order.

## 2.6 Surface plasmons

Before concluding this chapter with a summary of the key concepts necessary for this thesis, let us take a closer look at localized surface plasmons, as plasmonic nanostructures will be used to enhance TPSE rates. Firstly, surface plasmons are quasiparticles associated to the collective and longitudinal oscillations of free electrons in a metal [66]. Unlike volume plasmons, these oscillations are confined at the interface between a dielectric and a metal. Secondly, surface plasmon polaritons (SPPs) are propagating electromagnetic waves at a metal/dielectric interface arising from the coupling of photons from an exciting light with surface plasmons. Thirdly, localized surface plasmons are resonances appearing in sub-wavelength conductive nanostructures, such as metal nanoparticles, conductive 2D nanostructures and graphene nanoislands, characterized by non-propagating excitations of the electron plasma coupled to the electromagnetic field [66]. They enable sub-wavelength confinement and a significant enhancement of the electromagnetic field, but metals exhibit considerable losses [66]. In this section based on the book *Plasmonics: fundamentals and applications* [66], we start by deriving and discussing the dispersion relation of SPPs, then address localized surface plasmons.

The properties of metals are equivalently described by permittivity $\varepsilon$ or conductivity $\sigma$, which are related by

$$\varepsilon(\omega) = 1 + \frac{i\sigma(\omega)}{\varepsilon_0 \omega}, \tag{2.37}$$

with $\varepsilon_0$ being the vacuum permittivity [66]. Furthermore, the permittivity of metals is often described by the Drude model, which considers the metal as a plasma, i.e., a gas of free electrons moving against an environment of fixed positive nuclei [66]. Under an external driving electric field with a time harmonic dependency $e^{-i\omega t}$, the permittivity is given by

$$\varepsilon(\omega) = 1 - \frac{\omega_p^2}{\omega^2 + i\gamma\omega}, \tag{2.38}$$

with $\omega_p$ the plasma frequency, which represents the resonance frequency of volume plasmons within the bulk of the metal [66]. The losses are caused by the collisions of the electrons with the positive ions, where $\gamma = \tau^{-1}$ denotes the collision frequency with $\tau$ the scattering lifetime of electrons. When $\omega < \omega_p$, the real part of the permittivity, noted as $\mathrm{Re}\,(\varepsilon)$, is negative and the material behaves as a metal (evanescent waves), while for $\omega > \omega_p$, it is positive and the material acts like a dielectric (propagating waves).

In order to understand the properties of SPPs, let us derive their dispersion relation for a propagation at a metal/dielectric interface [Fig. 2.9]. As surface plasmon waves are not possible for a transverse electric (TE) polarization of the light (characterized by the three components $H_x$, $E_y$, and $H_z$ of the electromagnetic field) due to the field boundary conditions at the interface[7], the solution is written for the component $H_y$, and the other components of the transverse magnetic (TM) polarization $E_x$ and $E_z$ can be retrieved using Maxwell's equations. Thereby, the solution is a wave propagating along the interface with the propagation constant $\beta$, and evanescent in the direction

[7] Physically, the longitudinal oscillation of electrons along the propagation axis $z$ requires an electric field in that direction, and thus a TM polarization [66].

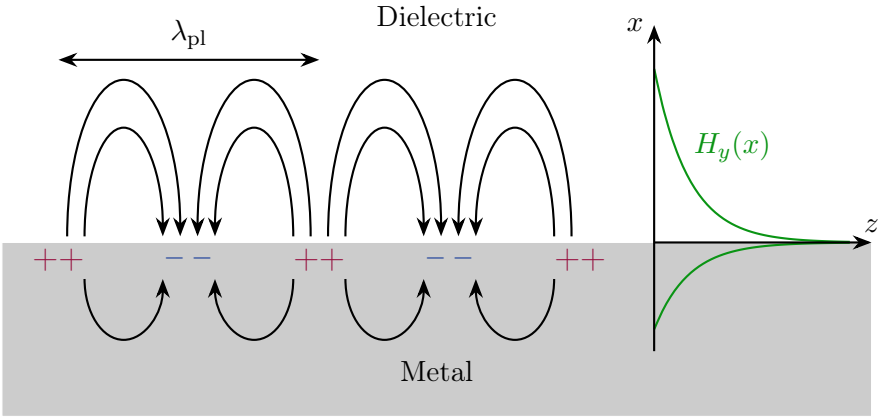


Figure 2.9: Schematic illustration of a surface plasmon wave propagating at the interface between a metal (bottom) and a dielectric (top). The metal is characterized by a complex permittivity $\varepsilon_m$ with a negative real part, while the dielectric is characterized by a real and positive permittivity $\varepsilon_d$. The field generated by the oscillation of the charge density decays exponentially in the two media, where the decrease is faster in the metal, confining the wave at the interface [66]. The surface plasmon wavelength $\lambda_{\text{pl}}$ can be two orders of magnitude smaller than the wavelength of the light in the dielectric [22].

perpendicular to the interface [66]:

$$\forall x > 0, \quad H_y(x,z) = A\, e^{i\beta z}\, e^{-\delta x}, \tag{2.39a}$$

$$\forall x < 0, \quad H_y(x,z) = A\, e^{i\beta z}\, e^{+\kappa x}, \tag{2.39b}$$

with $A$ a constant and

$$\delta = \sqrt{\beta^2 - \varepsilon_d k_0^2}, \tag{2.40a}$$

$$\kappa = \sqrt{\beta^2 - \varepsilon_m k_0^2}, \tag{2.40b}$$

where $k_0 := \omega/c$, with $c$ the speed of light. Note that $\delta$ and $\kappa$ are positive quantities in order to have exponential decay in the transverse direction and thus a confinement of the wave at the interface. In addition, the real part of the propagating constant is related to the effective wavelength of the surface plasmon wave which is given by $\lambda_{\text{pl}} = 2\pi/\text{Re}(\beta)$, while its imaginary part is linked to the decay of the plasmon wave during its propagation, and we define the propagation length as $L = 1/2\,\text{Im}(\beta)$ [66]. Using Maxwell's equations and continuity conditions for the tangential fields at the interface, one can show that

$$\frac{\delta}{\kappa} = -\frac{\varepsilon_d}{\varepsilon_m}, \tag{2.41}$$

which implies that $\varepsilon_d$ and $\text{Re}\,(\varepsilon_m)$ should have opposite sign in order to have $\delta$ and $\kappa$ positive [66]. Consequently, SPPs can only occur at the interface between a metal and a dielectric. Moreover, the decay is generally faster in the metal than in the dielectric since $|\text{Re}\,(\varepsilon_m)| > |\varepsilon_d|$ [66].

Using the equations (2.40) and (2.41), we get the dispersion relation of SPPs [66]:

$$\beta = k_0 \sqrt{\frac{\varepsilon_d \varepsilon_m}{\varepsilon_d + \varepsilon_m}}, \tag{2.42}$$

which is plotted in Figure 2.10 for a metal/air interface, where the metal is described by the Drude

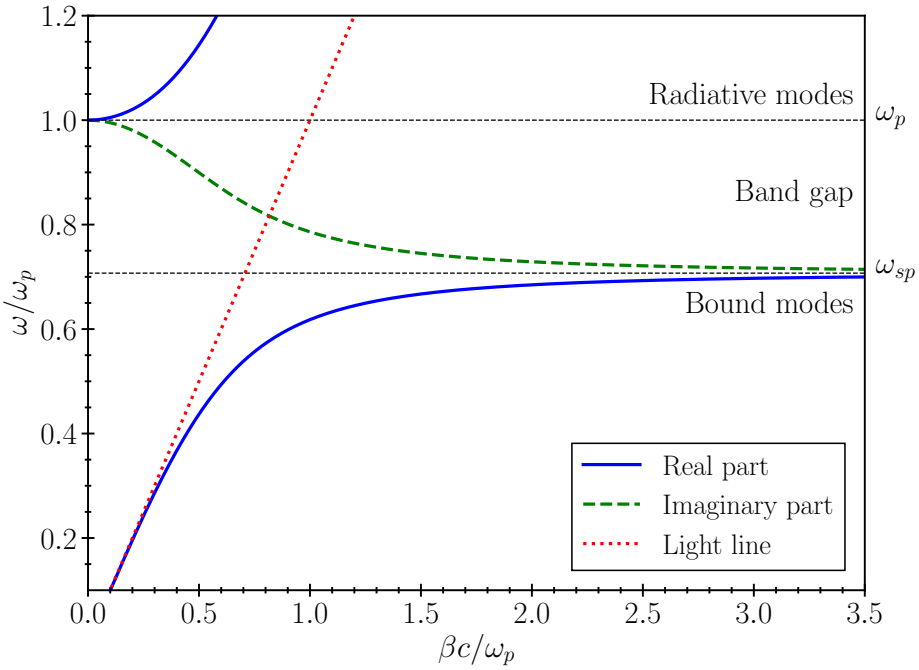


Figure 2.10: Plot of the dispersion relation of surface plasmons polaritons propagating at a metal/dielectric interface. The metal is described by the lossless Drude model (i.e., $\gamma = 0$ in Eq. (2.38)) and the dielectric is air ($\varepsilon_d = 1$). The real part of the propagation constant is plotted with a solid blue line, while its imaginary part is plotted with a dashed green line. The light line ($\omega = \beta c$) is also plotted, with a dotted red line. Three zones are distinguished, bound (confined) modes for $\omega < \omega_{sp}$, radiative modes for $\omega > \omega_p$, and a band gap between these two frequencies [66].

model without losses (i.e., $\gamma = 0$ in Eq. (2.38)). We distinguish three distinct parts in this dispersion relation. Firstly, due to their nature of confined modes that propagate at an interface (bound modes), SPPs correspond to the band of the dispersion curve at the right of the light line (below $\omega_{sp}$). Secondly, the band at the left of the light line (above $\omega_p$) corresponds to radiative modes that propagate in the metal since for $\omega > \omega_p$, the metal behaves like a dielectric ($\mathrm{Re}\,(\varepsilon_m) > 0$). Thirdly, there is a band gap between $\omega_{sp}$ and $\omega_p$ where $\beta$ is purely imaginary, prohibiting any propagation. Furthermore, when $\beta \to \infty$, the frequency tends asymptotically to the surface plasmon frequency[8]

$$\omega_{sp} = \frac{\omega_p}{\sqrt{1+\varepsilon_d}}, \tag{2.43}$$

and SPPs acquire an electrostatic character since the group velocity $\mathrm{d}\omega/\mathrm{d}\beta$ tends towards zero [66], and are therefore surface plasmons since they have lost their propagative character [66].

In the case of a "real" metal, losses exist ($\mathrm{Im}\,(\varepsilon_m) \neq 0$) and $\beta$ is a complex number, limiting the propagation of surface plasmon waves [66]. Moreover, $\mathrm{Re}\,(\beta)$ becomes non-zero between $\omega_{sp}$ and $\omega_p$, leading to quasibound modes (bound modes with high losses) instead of a band gap [Fig. 2.11]. As a result, the propagation constant reaches at $\omega = \omega_{sp}$ a limited value, imposing a lower limit on the effective wavelength: $\lambda_{\mathrm{pl}} = 2\pi/\mathrm{Re}(\beta_{\max})$ and thus on the confinement along $z$ (and also along $x$ given Eqs. (2.40)) [66]. Thereby, it is at this frequency that the confinement is highest (smallest $\lambda_{pl}$), but it is also at this frequency that losses are highest (smallest propagation length $L$). There is therefore a trade-off between confinement and losses [66].

[8] One can show that $\omega = \omega_{sp}$ when $\varepsilon_m(\omega) = -\varepsilon_d$ [66].

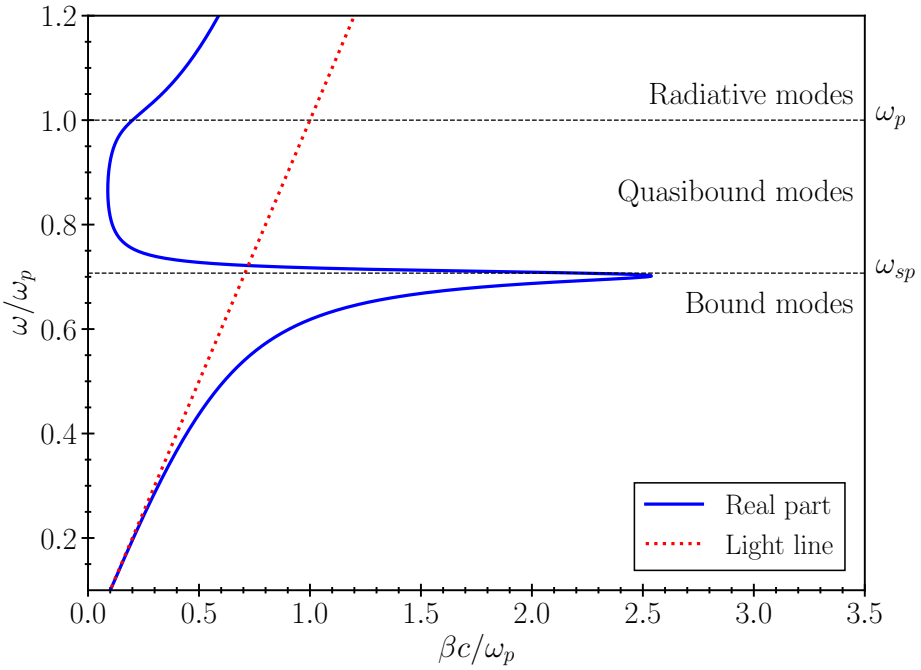


Figure 2.11: Plot of the dispersion relation of surface plasmons polaritons propagating at a metal/dielectric interface. The metal is described by the Drude model where we assumed that $\gamma/\omega_p = 7.5 \times 10^{-2}$, and the dielectric is air ($\varepsilon_d = 1$). The real part of the propagation constant is plotted with a solid blue line, and the light line ($\omega = \beta c$) is plotted with a dotted red line. Three zones are distinguished, bound (confined) modes for $\omega < \omega_{sp}$, radiative modes for $\omega > \omega_p$, and quasibound modes between these two frequencies [66].

So far we considered SPPs, which are surface plasmon waves propagating at an interface. On the other hand, localized surface plasmons are resonances appearing in sub-wavelength conductive nanostructures, which are characterized by non-propagating excitations of the electron plasma coupled to the electromagnetic field [66]. Indeed, an exciting light induces an oscillation of the electrons of a nanostructure, which is optimal at certain frequencies. Furthermore, these resonance frequencies depend on the size, shape, and material properties of the nanostructure, as well as the surrounding dielectric environment. Note that unlike SPPs that require phase-matching techniques to be excited by direct light illustration, such as prism and grating coupling, localized surface plasmons can be excited directly [66]. As with SPPs, it is possible to confine an electromagnetic wave by reducing its wavelength by two orders of magnitude compared with the wavelength of light in the dielectric medium [22]. We will see in Chapter 7 that these localized surface plasmon resonances correspond to modes characterized by a given profile of the surface charge density on the nanostructure.

## 2.7 Summary

Spontaneous emission (SE) is a fundamental process in the field of light-matter interaction in which an excited quantum emitter (e.g., an atom, a molecule, a quantum dot) decays spontaneously into its ground state by emitting one or several photons in random directions. This process is responsible for most of the light we see all around us and for the emission spectrum of atoms and molecules. It requires the quantification of the emitter and the electromagnetic field to be understood since it is through the interaction with the vacuum modes that this process can take place. Furthermore, when several decay pathways coexist between two states of an emitter, interference effects occur, po-

tentially leading to an increase or a decrease of the overall SE rate. Concretely, the time-dependent perturbation theory that leads to Fermi's golden rule [Eqs. (2.2)] is a good approximation to calculate SE rates because the interaction is weak relative to emitter energy levels. In addition, we presented the selection rules for the hydrogen atom relative to electric dipole and electric quadrupole transitions [Eqs. (2.8)].

The decay rate of a quantum emitter is not only an intrinsic property of the emitter, but also depends on its environment: this is the Purcell effect. Concretely, the environment modifies the boundary conditions applied to the vacuum field surrounding the emitter, thus modifying the photon local density of states. Moreover, an excited emitter can decay either radiatively in the case of photon emission in the far-field or non-radiatively in the case of energy dissipation in the environment in the form of, for example, phonons or plasmons. Thereby, the SE enhancement is performed through the design of a system (emitter plus environment) with a high SE rate, quantum efficiency (i.e., the proportion of radiative transitions), and directivity.

Usually, because the size of a quantum emitter is typically three orders of magnitude smaller than the wavelength of the emitted light, it is sufficient to study the influence of the environment on the emitter under the electric dipole approximation. In the latter approach, the spatial variations of the field over the emitter are neglected, thus ignoring higher-order multipolar interactions, and therefore only electric dipole transitions can occur. Nevertheless, when the electromagnetic field is confined at the nanometer scale, such as in plasmonic nanostructures that are considered in this thesis where the wavelength of the light can be squeezed by two orders of magnitude in the form of localized surface plasmons (coupling between the oscillations of electrons in a sub-wavelength conductive nanostructure and light), the electric dipole approximation is no longer valid, opening access to otherwise forbidden transitions (i.e., transitions that are slow with regard to the electric dipole single-photon transition). Thereby, higher-order transitions, such as multipolar and multiquanta transitions, can outperform the electric dipole single-photon transition.

In this thesis, we focus on the two-photon spontaneous emission (TPSE) which is a second-order process that involves the simultaneous emission of two photons from an emitter. This process is mediated by virtual non-resonant intermediate states that have very short lifetimes. It is characterized by a broad continuous and symmetric spectrum with respect to the half of the transition frequency. This process is promising for the design of a new generation of entangled photon pair sources, as a more efficient and flexible alternative to the conventional spontaneous parametric down conversion process, especially for on-chip integrated sources. Typically, the two-electric dipole (2ED) transition is 8 orders of magnitude slower than the electric dipole transition, while the two-magnetic dipole (2MD) and the two-electric quadrupole (2EQ) are 12 orders of magnitude slower than the 2ED transition. Despite the interest in controlling this process, its study is hampered by a lack of efficient theoretical and numerical methods: there is a need for an efficient and general framework that consider higher-order multipolar interactions to study TPSE near arbitrary photonic structures. In this thesis, we develop this framework by taking into account the interaction up to the electric quadrupolar order, as well as the interference effects between the multipolar pathways.

Concerning the mathematical developments, we derived expressions as a function of the dyadic Green's function, which gives the power emitted by point sources, for the modification of the power emitted by an electric dipole (ED) and an electric quadrupole (EQ) point sources due to the envi-

ronment, as well as for the term describing the interference between these two:

$$\frac{W_{\mathrm{ED}}}{W_{\mathrm{ED},0}} = \frac{6\pi c}{\omega}\left\{\hat{\mathbf{d}}^{*}\cdot \mathrm{Im}\,\mathbf{G}(\omega;\mathbf{R},\mathbf{R})\cdot\hat{\mathbf{d}}\right\}, \tag{2.44a}$$

$$\frac{W_{\mathrm{EQ}}}{W_{\mathrm{EQ},0}} = \frac{20\pi c^{3}}{\omega^{3}}\left\{\hat{\mathbf{Q}}^{*}\nabla\cdot \mathrm{Im}\,\mathbf{G}(\omega;\mathbf{r},\mathbf{r}')\cdot\hat{\mathbf{Q}}\nabla'\right\}_{\mathbf{r}=\mathbf{r}'=\mathbf{R}}, \tag{2.44b}$$

$$\frac{W_{\mathrm{ED}\cap\mathrm{EQ}}}{\sqrt{W_{\mathrm{ED},0}\,W_{\mathrm{EQ},0}}} = 2\,\frac{2\sqrt{30}\pi c^{2}}{\omega^{2}}\left\{\hat{\mathbf{d}}^{*}\cdot \mathrm{Im}\,\mathbf{G}(\omega;\mathbf{r},\mathbf{r}')\cdot\hat{\mathbf{Q}}\nabla'\right\}_{\mathbf{r}=\mathbf{r}'=\mathbf{R}}, \tag{2.44c}$$

where the caret denotes normalized tensors and where $W_{\mathrm{ED},0}$ and $W_{\mathrm{EQ},0}$ are the powers emitted in vacuum [Eqs. (2.20) and (2.25)]. All these equations involve the imaginary part of the Green's function evaluated the emitter's position, which is a symmetric tensor that gives the power emitted by point sources. For the EQ, the equation involves double derivatives of the imaginary part of the Green's function while the interference term involves single derivatives. Moreover, the Green's function is the result of the field produced by the source alone plus the field scattered by the environment, which explains how the power is modified by the environment of the emitter. Note that there is no interference between multipolar sources in vacuum. Furthermore, in an inhomogeneous environment, the power emitted by a source can be calculated by integrating the Poynting vector on a surface of a volume encompassing the source [Eq. (2.27)].

In the weak coupling regime, the Purcell factor makes the link between the modification of the one-photon decay rate of a quantum emitter, whose transitions are described by multipolar transitions moments, and the modification of the power emitted by classical multipolar point sources:

$$\frac{\Gamma}{\Gamma_{0}} = \frac{W}{W_{0}} := P. \tag{2.45}$$

This equation remains valid when several multipolar decay channels contribute simultaneously to the emitter's transition, including interference effects. Therefore, it is possible to classically calculate the change in transition rates of quantum systems by modeling multipolar point sources in electromagnetic simulations which have the same multipolar moments than those describing the emitter's transitions. In this thesis, we extend this link for the two-photon spontaneous emission.

Chapter 3

# One-photon spontaneous emission

In this chapter, we focus on the mathematical treatment of the one-photon spontaneous emission (OPSE) process. This will allow us to familiarize ourselves with the concepts before tackling the more complex process of two-photon spontaneous emission (TPSE). Furthermore, we should rather talk about the one-quantum spontaneous emission, since depending on the environment, quanta other than photons can be emitted, as for example plasmons or phonons [30]. This chapter is mainly based on Chapter 4 of the book *Molecular quantum electrodynamics: an introduction to radiation-molecule interactions* [2] in which they derive the electric dipole (ED), magnetic dipole (MD) and electric quadrupole (EQ) transition rates in vacuum, on Chapter 4 of the book *The quantum vacuum: an introduction to quantum electrodynamics* [42] where they derive the ED transition rate in an arbitrary environment, and on Chapter 8 of the book *Principles of Nano-Optics* [30] for the expression of the ED transition rate via the dyadic Green's function. Thereby, we present here a complete treatment of the OPSE process where the interaction Hamiltonian is taken up to the electric quadrupolar order. We do not make any assumptions about the quantum emitter and the environment and we include interference effects between the multipolar pathways, which are not presented in the books mentioned above, only briefly in Ref. [51]. At the end of this chapter, we introduce a notation to simplify the equations relative to the EQ transition and we decompose the multipolar contributions to the OPSE into Purcell factor bases, which will be used in the next chapter to express the two-photon spontaneous emission as a function of the one-photon Purcell factors.

First, we remind the Fermi's golden rule used to calculate transition rates of quantum systems and we present the multipolar expansion of the interaction Hamiltonian that describes the interaction between a quantum emitter and the electromagnetic field. Then, we derive the multipolar contributions to the OPSE, including interference effects, and we consider the case where the environment is vacuum. Next, the obtained expressions are expressed via the dyadic Green's function, vacuum normalized, and decomposed in Purcell factor bases. To do this, we introduce a modified version of Voigt notation to simplify the equations relative to the EQ transition. Finally, we close this chapter with a discussion about the derived equations and with a summary of them.

## 3.1 Fermi's golden rule

Let us consider a system composed of a two-level quantum emitter (e.g., an atom, a molecule, or a quantum dot) and its photonic environment. With a perturbative approach, the probability per unit time that a system carries out a first-order transition by emitting a quantum from an initial state $|i\rangle$ to a final state $|f\rangle$, upon an interaction between the emitter and the field described by the

Hamiltonian $H_{\text{int}}$, is given by Fermi's golden rule [Eqs. (2.2) and (2.3)]:

$$\Gamma_{i\to f} = \frac{2\pi}{\hbar}|M_{fi}|^2\,\delta(E_f - E_i), \tag{3.1}$$

with $M_{fi}$ the first-order matrix element of $H_{\text{int}}$, which acts as a small perturbation of the system:

$$M_{fi} = \langle f|\, H_{\text{int}}(t)\,|i\rangle\,, \tag{3.2}$$

where $\hbar$ is the reduced Planck constant and where $E_i$ and $E_f$ stand for the energy of the system in the initial and final state, respectively.

In this process, the initial state of the system is characterized by the emitter in an excited state $|e\rangle$ and the field in the vacuum state $|\text{vac}\rangle$, while in the final one the emitter is in a lower energy state $|g\rangle$ and the field is in a one-quantum state $|1_\alpha\rangle$ where $\alpha$ stands for the mode of the emitted quantum [2, 89]. Thus, they are respectively written as[1]

$$|i\rangle = |e;\text{vac}\rangle \tag{3.3a}$$

$$\text{and as } |f\rangle = |g;1_\alpha\rangle\,. \tag{3.3b}$$

Further on, the energy of the emitter in the state $|a\rangle$ will be denoted as $\varepsilon_a$ with $a = e, g$. In the subsequent developments, a sum over $\alpha$ will be added to consider all possible final states (modes) for the emitted quanta [Sec. 2.3]. This first-order transition is depicted in Figure 3.1.

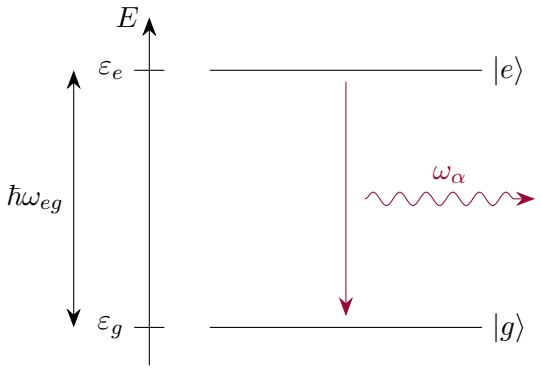


Figure 3.1: Energy representation of a first-order transition. The emitter carries-out a transition from its excited state $|e\rangle$ to its ground state $|g\rangle$ of lower energy by emitting a photon in the mode $\alpha$ of energy $\hbar\omega_\alpha$. The transition energy is given by $\hbar\omega_{eg} := \varepsilon_e - \varepsilon_g$. The conservation of energy implies that $\hbar\omega_\alpha = \hbar\omega_{eg}$.

## 3.2 Interaction Hamiltonian

As discussed in Chapter 2, when the spatial variation of the electric field at the emitter's position is not negligible, as this is the case in photonic structures where the field is highly confined such as in structures supporting localized surface plasmons, the standard electric dipole approximation is no longer appropriate [22, 29, 60–62]. Therefore, it is necessary to take into account higher order multipolar interactions. Thus, we study the interaction Hamiltonian $H_{\text{int}}$ of the system, which

[1] $|a;b\rangle$ is a shorthand notation used to represent the tensor product of the states $|a\rangle$ and $|b\rangle$.

describes the emitter-field interactions, up to the electric quadrupolar order[2] [30, 46]:

$$H_{\text{int}}(\mathbf{R},t) = \underbrace{-\mathbf{d}\cdot\mathbf{E}(\mathbf{R},t)}_{H_{\text{ED}}}\underbrace{-\mathbf{m}\cdot\mathbf{B}(\mathbf{R},t)}_{H_{\text{MD}}}\underbrace{-\mathbf{Q}:\nabla\mathbf{E}(\mathbf{R},t)}_{H_{\text{EQ}}}+\dots, \tag{3.4}$$

where the emitter's position $\mathbf{R}$ is taken at the center of its charge distribution and where the triple dots represent higher orders, which are not taken into account here. In this equation, $\nabla = (\frac{\partial}{\partial x}, \frac{\partial}{\partial y}, \frac{\partial}{\partial z})^T$ is a column vector with $T$ denoting the transpose, the dot product is the vector scalar product defined as $\mathbf{a}\cdot\mathbf{b} := \sum_i a_i b_i$, the components of the outer product $(\nabla\mathbf{E})_{ij}$ are $\nabla_i E_j$, whereas the double dot product is defined as $\mathbf{T}:\mathbf{U} := \sum_{i,j} T_{\dots ij} U_{ji\dots}$ with $\mathbf{T}$ and $\mathbf{U}$ two tensors of rank greater than or equal to two. Moreover, $\mathbf{d}$, $\mathbf{m}$, and $\mathbf{Q}$ are, respectively, the electric dipole (ED), the magnetic dipole (MD), and the electric quadrupole (EQ) moment operators[3] [30, 46, 90]:

$$\mathbf{d} := -e\,\mathbf{r}, \tag{3.5a}$$

$$\mathbf{m} := \frac{ie\hbar}{2m_e}\,\mathbf{r}\times\nabla, \tag{3.5b}$$

$$\mathbf{Q} := -\frac{e}{2}\left(\mathbf{rr} - \frac{1}{3}\mathbb{1}\,r^2\right), \tag{3.5c}$$

where the cross denotes the vector cross product, $r^2$ is the squared norm of the position operator $\mathbf{r}$, $e$ represents the elementary charge, $m_e$ denotes the electron mass, $\mathbb{1}$ is the identity operator and where $\mathbf{Q}$ can been taken traceless in source-free regions [46, 94, 95].

The electromagnetic field operators in the previous equation can be written as a function of the normal modes $\mathbf{A}_\alpha(\mathbf{r})$ of the vector potential [42, 99]:

$$\mathbf{E}(\mathbf{r},t) = i\sum_\alpha \sqrt{\frac{\hbar\omega_\alpha}{2\varepsilon_0}}\left\{a_\alpha(t)\,\mathbf{A}_\alpha(\mathbf{r}) - a_\alpha^\dagger(t)\,\mathbf{A}_\alpha^*(\mathbf{r})\right\}, \tag{3.6a}$$

$$\mathbf{B}(\mathbf{r},t) = \sum_\alpha \sqrt{\frac{\hbar}{2\varepsilon_0\omega_\alpha}}\left\{a_\alpha(t)\,\nabla\times\mathbf{A}_\alpha(\mathbf{r}) - a_\alpha^\dagger(t)\,\nabla\times\mathbf{A}_\alpha^*(\mathbf{r})\right\}. \tag{3.6b}$$

In these equations, $\varepsilon_0$ is the vacuum electric permittivity, whereas $a_\alpha(t) = a_\alpha\, e^{-i\omega_\alpha t}$ and $a_\alpha^\dagger(t) = a_\alpha^\dagger\, e^{i\omega_\alpha t}$ are the annihilation and creation operators of a photon in the mode $\alpha$ of energy $\hbar\omega_\alpha$. Thus, a photon is defined as an elementary excitation of a mode of the electromagnetic field [89, 99]. Given the previous equations, the electric dipole interaction is due to the field modes evaluated at the emitter's center of charge, whereas the magnetic dipolar and electric quadrupolar ones arise from the variation of the electric field. Therefore, in the electric dipole approximation that neglects the variation of the field over the emitter, the electric dipole interaction dominates, and the decays are dominated by electric dipole transitions [45, 46]. Note that the modes $\mathbf{A}_\alpha(\mathbf{r})$ are normalized and form a complete set of solutions of the Helmholtz equation, subject to the boundary conditions imposed by the photonic environment. These are also the conditions applied to the modes that lead to the Purcell effect [42].

In this single-photon process and upon this interaction considered up to the quadrupolar order,

[2] No notation is adopted to differentiate operators from other quantities. However, we will specify when a quantity is an operator.

[3] As already mentioned in Chapter 2 in Footnote 5, it is important to adopt the same definition for the classical EQ moment and for the corresponding operator to compare equivalent classical and quantum sources.

a photon can be emitted by three different multipolar emission pathways: ED, MD, and EQ, all contributing to the total rate. In addition, these multipolar channels can interfere with each other, potentially resulting in an increase or a decrease of the overall OPSE rate [2]. However, depending on the selection rules of the considered emitter, some emission channels can be forbidden. For example, only one multipolar transition can be allowed at a time between two states of the hydrogen atom [47], but several occur simultaneously in molecules and asymmetric quantum dots [51, 62]. Moreover, depending on the photonic environment, some multipolar transitions may be weaker than others, and therefore can be neglected. These multipolar contributions to the overall OPSE rate are derived in the following section.

## 3.3 Multipolar contributions

Now that Fermi's golden rule and the interaction Hamiltonian have been introduced, let us derive the different multipolar contributions to the OPSE rate. Given that the initial and the final energies[4] of the system are, respectively, $E_i = \varepsilon_e$ and $E_f = \varepsilon_g + \hbar\omega_\alpha$, the Dirac delta distribution in Fermi's golden rule [Eq. (3.1)] can be rewritten as

$$\delta(E_f - E_i) = \frac{1}{\hbar}\,\delta(\omega_{eg} - \omega_\alpha), \tag{3.7}$$

where we define $\hbar\omega_{ab} := \varepsilon_a - \varepsilon_b$ with $a, b = e, g$.

Now, let us calculate the matrix element $M_{fi}$ [Eq. (3.2)] with the interaction Hamiltonian given by the equation (3.4) and with the electromagnetic field operators given by the equations (3.6). As we are interested in emission processes, only the part of $\mathbf{E}$ and $\mathbf{B}$ involving creation operators, noted as $\mathbf{E}^{(-)}$ and $\mathbf{B}^{(-)}$, are kept in the calculation[5]:

$$\begin{aligned}
M_{fi} = \langle 1_\alpha|\,\langle g|\,H_{\text{int}}\,|e\rangle\,|\text{vac}\rangle &= \langle 1_\alpha|\,\langle g|\,-\mathbf{d}\cdot\mathbf{E}(\mathbf{R}) - \mathbf{m}\cdot\mathbf{B}(\mathbf{R}) - \mathbf{Q}:\nabla\mathbf{E}(\mathbf{R})\,|e\rangle\,|\text{vac}\rangle && \text{(3.8a)}\\
&= -\,\langle g|\,\mathbf{d}\,|e\rangle\,\cdot\,\langle 1_\alpha|\,\mathbf{E}^{(-)}(\mathbf{R})\,|\text{vac}\rangle\\
&\quad -\,\langle g|\,\mathbf{m}\,|e\rangle\,\cdot\,\langle 1_\alpha|\,\mathbf{B}^{(-)}(\mathbf{R})\,|\text{vac}\rangle\\
&\quad -\,\langle g|\,\mathbf{Q}\,|e\rangle\,:\nabla\,\langle 1_\alpha|\,\mathbf{E}^{(-)}(\mathbf{R})\,|\text{vac}\rangle && \text{(3.8b)}\\
&= -\mathbf{d}^{ge}\cdot\,\langle 1_\alpha|\,-\,i\sum_\beta\sqrt{\frac{\hbar\omega_\beta}{2\varepsilon_0}}a_\beta^\dagger\mathbf{A}_\beta^*(\mathbf{R})\,|\text{vac}\rangle\\
&\quad -\,\mathbf{m}^{ge}\cdot\,\langle 1_\alpha|\,-\sum_\beta\sqrt{\frac{\hbar}{2\varepsilon_0\omega_\beta}}a_\beta^\dagger\nabla\times\mathbf{A}_\beta^*(\mathbf{R})\,|\text{vac}\rangle\\
&\quad -\,\mathbf{Q}^{ge}:\langle 1_\alpha|\,-\,i\sum_\beta\sqrt{\frac{\hbar\omega_\beta}{2\varepsilon_0}}a_\beta^\dagger\nabla\mathbf{A}_\beta^*(\mathbf{R})\,|\text{vac}\rangle\,, && \text{(3.8c)}
\end{aligned}$$

where the multipolar operators only act on emitter states while the field operators solely act on field states. Within this equation, $\mathbf{d}^{ge} := \langle g|\mathbf{d}|e\rangle$, $\mathbf{m}^{ge} := \langle g|\mathbf{m}|e\rangle$, and $\mathbf{Q}^{ge} := \langle g|\mathbf{Q}|e\rangle$ stand, respectively, for the electric dipole, magnetic dipole and electric quadrupole transition moments (i.e., the first-order matrix elements of the operators $\mathbf{d}$, $\mathbf{m}$, and $\mathbf{Q}$) that describe the emitter's transition from

[4] The zero of energy is chosen to correspond to the energy of the electromagnetic field in vacuum.

[5] The time dependency in the annihilation and creation operators ($e^{-i\omega_\alpha t}$ and $e^{i\omega_\alpha t}$) is omitted since we take the modulus of $M_{fi}$.

the excited state $|e\rangle$ to the ground state $|g\rangle$. In the previous equation, only the terms involving the creation operator that creates a photon in the mode $\beta = \alpha$ leads to a non-zero term because the field states form an orthonormal basis[6]. Thus, we get the matrix element

$$M_{fi} = i\sqrt{\frac{\hbar\omega_\alpha}{2\varepsilon_0}}\left\{\mathbf{d}^{ge}\cdot\mathbf{A}^*_\alpha(\mathbf{R}) + \frac{1}{\omega_\alpha}\mathbf{m}^{ge}\cdot\nabla\times\mathbf{A}^*_\alpha(\mathbf{R}) + \mathbf{Q}^{ge}:\nabla\mathbf{A}^*_\alpha(\mathbf{R})\right\}\underbrace{\langle 1_\alpha|\, a^\dagger_\alpha\,|\mathrm{vac}\rangle}_{\langle 1_\alpha|1_\alpha\rangle=1}, \tag{3.9}$$

which is the result of three multipolar contributions:

$$M_{fi} = M^{\mathrm{ED}}_{fi} + M^{\mathrm{MD}}_{fi} + M^{\mathrm{EQ}}_{fi}, \tag{3.10}$$

which are respectively obtained when only the ED, MD or EQ interaction is taken into account in the interaction Hamiltonian [Eq. (3.4)].

Let us now take the complex conjugate[7] of $M_{fi}$:

$$M^*_{fi} = -i\sqrt{\frac{\hbar\omega_\alpha}{2\varepsilon_0}}\left\{\mathbf{d}^{eg}\cdot\mathbf{A}_\alpha(\mathbf{R}) + \frac{1}{\omega_\alpha}\mathbf{m}^{eg}\cdot\nabla\times\mathbf{A}_\alpha(\mathbf{R}) + \mathbf{Q}^{eg}:\nabla\mathbf{A}_\alpha(\mathbf{R})\right\}, \tag{3.11}$$

and then its square modulus:

$$|M_{fi}|^2 = \left|M^*_{fi}\right|^2 = \frac{\hbar\omega_\alpha}{2\varepsilon_0}\left|\mathbf{d}^{eg}\cdot\mathbf{A}_\alpha(\mathbf{R}) + \frac{1}{\omega_\alpha}\mathbf{m}^{eg}\cdot\nabla\times\mathbf{A}_\alpha(\mathbf{R}) + \mathbf{Q}^{eg}:\nabla\mathbf{A}_\alpha(\mathbf{R})\right|^2, \tag{3.12}$$

which can be injected, together with the equation (3.7), in Fermi's golden rule [Eq. (3.1)]:

$$\Gamma_{\mathrm{tot}}(\mathbf{R}) = \frac{\pi\omega_\alpha}{\varepsilon_0\hbar}\left|\mathbf{d}^{eg}\cdot\mathbf{A}_\alpha(\mathbf{R}) + \frac{1}{\omega_\alpha}\mathbf{m}^{eg}\cdot\nabla\times\mathbf{A}_\alpha(\mathbf{R}) + \mathbf{Q}^{eg}:\nabla\mathbf{A}_\alpha(\mathbf{R})\right|^2\delta(\omega_{eg}-\omega_\alpha). \tag{3.13}$$

As a final step, we take the summation over all the possible modes for the emitted quanta to get the total OPSE rate [Sec. 2.3]:

$$\Gamma_{\mathrm{tot}}(\mathbf{R}) = \frac{\pi}{\varepsilon_0\hbar}\sum_\alpha\omega_\alpha\left|\mathbf{d}^{eg}\cdot\mathbf{A}_\alpha(\mathbf{R}) + \frac{1}{\omega_\alpha}\mathbf{m}^{eg}\cdot\nabla\times\mathbf{A}_\alpha(\mathbf{R}) + \mathbf{Q}^{eg}:\nabla\mathbf{A}_\alpha(\mathbf{R})\right|^2\delta(\omega_{eg}-\omega_\alpha). \tag{3.14}$$

Since this expression has been obtained by considering simultaneously the three multipolar interactions in the Hamiltonian [Eq. (3.4)], it encompasses the ED, MD, and EQ contributions as well as the interference effects among them:

$$\Gamma_{\mathrm{tot}} = \Gamma_{\mathrm{ED}} + \Gamma_{\mathrm{MD}} + \Gamma_{\mathrm{EQ}} + \Gamma_{\mathrm{ED}\cap\mathrm{MD}} + \Gamma_{\mathrm{ED}\cap\mathrm{EQ}} + \Gamma_{\mathrm{MD}\cap\mathrm{ED}}. \tag{3.15}$$

In the last equation, $\Gamma_{\mathrm{ED}\cap\mathrm{MD}}$, $\Gamma_{\mathrm{ED}\cap\mathrm{EQ}}$, and $\Gamma_{\mathrm{MD},\cap\mathrm{ED}}$ are introduced as the terms representing the interferences between the multipolar transitions. Furthermore, the expression of the ED, MD and EQ transition rates are obtained by considering the multipolar contributions separately in the matrix

[6] An orthonormal basis satisfies $\langle 1_\alpha|1_\beta\rangle = \delta_{\alpha\beta}$.

[7] For an Hermitian operator: $\left(\mathbf{A}^{ab}\right)^* = (\langle a|\mathbf{A}|b\rangle)^* = \langle b|\mathbf{A}^\dagger|a\rangle = \langle b|\mathbf{A}|a\rangle = \mathbf{A}^{ba}$ where the dagger denotes the operation of taking the transpose and the complex conjugate.

element $M_{fi}$ [Eq. (3.10)]:

$$\Gamma_{\mathrm{ED}}(\mathbf{R}) = \frac{\pi}{\varepsilon_0 \hbar} \sum_{\alpha} \omega_\alpha \left| \mathbf{d}^{eg} \cdot \mathbf{A}_\alpha(\mathbf{R}) \right|^2 \delta(\omega_{eg} - \omega_\alpha), \tag{3.16a}$$

$$\Gamma_{\mathrm{MD}}(\mathbf{R}) = \frac{\pi}{\varepsilon_0 \hbar} \sum_{\alpha} \frac{1}{\omega_\alpha} \left| \mathbf{m}^{eg} \cdot \nabla \times \mathbf{A}_\alpha(\mathbf{R}) \right|^2 \delta(\omega_{eg} - \omega_\alpha), \tag{3.16b}$$

$$\Gamma_{\mathrm{EQ}}(\mathbf{R}) = \frac{\pi}{\varepsilon_0 \hbar} \sum_{\alpha} \omega_\alpha \left| \mathbf{Q}^{eg} : \nabla \mathbf{A}_\alpha(\mathbf{R}) \right|^2 \delta(\omega_{eg} - \omega_\alpha). \tag{3.16c}$$

Note that depending on the quantum emitter, the ED, MD, EQ transitions may not occur simultaneously between two given states.

By developing the square modulus in equation (3.14) of the total transition rate, we find the three multipolar transition rates given above as well as the three interference terms [51]:

$$\Gamma_{\mathrm{ED}\cap\mathrm{MD}}(\mathbf{R}) = 2\,\mathrm{Re}\left( \frac{\pi}{\varepsilon_0 \hbar} \sum_{\alpha} \left( \mathbf{d}^{eg} \cdot \mathbf{A}_\alpha(\mathbf{R}) \right) \left( \mathbf{m}^{eg} \cdot \nabla \times \mathbf{A}_\alpha(\mathbf{R}) \right)^* \delta(\omega_{eg} - \omega_\alpha) \right), \tag{3.17a}$$

$$\Gamma_{\mathrm{ED}\cap\mathrm{EQ}}(\mathbf{R}) = 2\,\mathrm{Re}\left( \frac{\pi}{\varepsilon_0 \hbar} \sum_{\alpha} \omega_\alpha \left( \mathbf{d}^{eg} \cdot \mathbf{A}_\alpha(\mathbf{R}) \right) \left( \mathbf{Q}^{eg} : \nabla \mathbf{A}_\alpha(\mathbf{R}) \right)^* \delta(\omega_{eg} - \omega_\alpha) \right), \tag{3.17b}$$

$$\Gamma_{\mathrm{MD}\cap\mathrm{EQ}}(\mathbf{R}) = 2\,\mathrm{Re}\left( \frac{\pi}{\varepsilon_0 \hbar} \sum_{\alpha} \left( \mathbf{m}^{eg} \cdot \nabla \times \mathbf{A}_\alpha(\mathbf{R}) \right) \left( \mathbf{Q}^{eg} : \nabla \mathbf{A}_\alpha(\mathbf{R}) \right)^* \delta(\omega_{eg} - \omega_\alpha) \right), \tag{3.17c}$$

where Re stands for the real part. Hereafter, we will omit the real part for clarity. Thereby, interference terms emerge from mixed products with one that is the complex conjugate of the other[8]. Note that these terms could have also been written by applying the complex conjugate to the other factor. Moreover, interference terms can be either positive or negative, potentially resulting in an increase or decrease of the total rate [Eq. (3.15)]. Afterwards, we focus on the interference between the ED and EQ channels, but similar developments can be performed for the terms $\Gamma_{\mathrm{ED}\cap\mathrm{MD}}$ and $\Gamma_{\mathrm{MD}\cap\mathrm{EQ}}$. Furthermore, all derived equations for the multipolar contributions to the OPSE rate, including the interference terms, are valid regardless of the emitter and its environment.

As a direct application, we derive in the next section the free-space transition rates, but we already know that the interference terms vanish. Indeed, there is no interference between different multipolar sources in vacuum because each type of emitter generates its unique field distribution that remains decoupled from other multipolar sources at the same location [2].

## 3.4 Vacuum transition rates

In vacuum, the field modes are plane waves defined by a wave vector $\mathbf{k}$ and a unitary polarization vector $\hat{\boldsymbol{\varepsilon}}_{\mathbf{k},s}$ where the parameter $s = 1, 2$ represents the two transverse polarizations [2, 42]. Consequently, the field modes in equations (3.16) become

$$\mathbf{A}_\alpha(\mathbf{r}) \longrightarrow \mathbf{A}_{\mathbf{k},s}(\mathbf{r}) = \frac{e^{i\mathbf{k}\cdot\mathbf{r}}}{\sqrt{V}} \hat{\boldsymbol{\varepsilon}}_{\mathbf{k},s}, \tag{3.18}$$

where $V$ stands for the arbitrary and finite box quantization volume in which the field is assumed to be confined. In addition, the angular frequency $\omega_\alpha$ becomes $\omega_k$ and the summation over the modes

[8] $\forall z \in \mathbb{C}, z + z^* = 2\,\mathrm{Re}(z)$.

$\alpha$ becomes $\sum_{s=1}^{2}\sum_{\mathbf{k}}$. By taking the limit to the continuum, the summation over the wave vectors $\mathbf{k}$ is replaced by an integral [2, 42]:

$$\sum_{s=1}^{2}\sum_{\mathbf{k}} \overset{V\to\infty}{\longrightarrow} \frac{V}{(2\pi)^3}\sum_{s=1}^{2}\int \mathrm{d}^3k = \frac{V}{(2\pi)^3}\sum_{s=1}^{2}\int k^2\,\mathrm{d}k\,\mathrm{d}\Omega_k = \frac{V}{(2\pi c)^3}\sum_{s=1}^{2}\int \omega_k^2\,\mathrm{d}\omega_k\,\mathrm{d}\Omega_k, \tag{3.19}$$

where we switched to spherical coordinates in the reciprocal space with $\mathrm{d}\Omega_k = \sin\theta_k\,\mathrm{d}\theta_k\,\mathrm{d}\phi_k$ the element of solid angle in the $\mathbf{k}$-space and where we used the free-space dispersion relation $\omega_k = c\,k$.

Let us now calculate the transition rates [Eqs. (3.16)] by carrying out the replacement given by the equation (3.19) as well as by calculating the following cross and outer products:

$$\nabla\times\mathbf{A}_{\mathbf{k},s}(\mathbf{r}) = i\mathbf{k}\times\frac{e^{i\mathbf{k}\cdot\mathbf{r}}}{\sqrt{V}}\hat{\boldsymbol{\varepsilon}}_{\mathbf{k},s} = i\frac{\omega_k}{c}\,\hat{\mathbf{k}}\times\frac{e^{i\mathbf{k}\cdot\mathbf{r}}}{\sqrt{V}}\hat{\boldsymbol{\varepsilon}}_{\mathbf{k},s}, \tag{3.20a}$$

$$\nabla\mathbf{A}_{\mathbf{k},s}(\mathbf{r}) = i\mathbf{k}\frac{e^{i\mathbf{k}\cdot\mathbf{r}}}{\sqrt{V}}\hat{\boldsymbol{\varepsilon}}_{\mathbf{k},s} = i\frac{\omega_k}{c}\,\hat{\mathbf{k}}\frac{e^{i\mathbf{k}\cdot\mathbf{r}}}{\sqrt{V}}\hat{\boldsymbol{\varepsilon}}_{\mathbf{k},s}, \tag{3.20b}$$

where the caret denotes normalized vectors. Thereby, the 2ED transition rate is given by

$$\Gamma_{\mathrm{ED},0}(\mathbf{R}) = \frac{\pi}{\varepsilon_0\hbar}\frac{V}{(2\pi c)^3}\sum_{s=1}^{2}\int \omega_k^3\left|\mathbf{d}^{eg}\cdot\frac{e^{i\mathbf{k}\cdot\mathbf{R}}}{\sqrt{V}}\hat{\boldsymbol{\varepsilon}}_{\mathbf{k},s}\right|^2\delta(\omega_{eg}-\omega_k)\,\mathrm{d}\omega_k\,\mathrm{d}\Omega_k \tag{3.21a}$$

$$\Leftrightarrow \Gamma_{\mathrm{ED},0} = \frac{1}{8\pi^2\varepsilon_0\hbar c^3}\int \omega_k^3\sum_{s=1}^{2}\left|\mathbf{d}^{eg}\cdot\hat{\boldsymbol{\varepsilon}}_{\mathbf{k},s}\right|^2\delta(\omega_{eg}-\omega_k)\,\mathrm{d}\omega_k\,\mathrm{d}\Omega_k, \tag{3.21b}$$

and the two others:

$$\Gamma_{\mathrm{MD},0} = \frac{1}{8\pi^2\varepsilon_0\hbar c^5}\int \omega_k^3\sum_{s=1}^{2}\left|\mathbf{m}^{eg}\cdot\hat{\mathbf{k}}\times\hat{\boldsymbol{\varepsilon}}_{\mathbf{k},s}\right|^2\delta(\omega_{eg}-\omega_k)\,\mathrm{d}\omega_k\,\mathrm{d}\Omega_k, \tag{3.22a}$$

$$\Gamma_{\mathrm{EQ},0} = \frac{1}{8\pi^2\varepsilon_0\hbar c^5}\int \omega_k^5\sum_{s=1}^{2}\left|\mathbf{Q}^{eg}:\hat{\mathbf{k}}\,\hat{\boldsymbol{\varepsilon}}_{\mathbf{k},s}\right|^2\delta(\omega_{eg}-\omega_k)\,\mathrm{d}\omega_k\,\mathrm{d}\Omega_k, \tag{3.22b}$$

where the transition rates are now independent of the emitter position $\mathbf{R}$ due to the homogeneity of space and where the subscript 0 reminds that the emission takes place in vacuum. As the vectors $\left\{\hat{\boldsymbol{\varepsilon}}_{\mathbf{k},1},\hat{\boldsymbol{\varepsilon}}_{\mathbf{k},2},\hat{\mathbf{k}}\right\}$ form an orthonormal basis, the cross product of two basis vectors is equal to the third one (or to the opposite vector). Consequently, the cross products $\hat{\mathbf{k}}\times\hat{\boldsymbol{\varepsilon}}_{\mathbf{k},1}$ and $\hat{\mathbf{k}}\times\hat{\boldsymbol{\varepsilon}}_{\mathbf{k},2}$ in equation (3.22a) can be replaced by $\hat{\boldsymbol{\varepsilon}}_{\mathbf{k},2}$ and $\hat{\boldsymbol{\varepsilon}}_{\mathbf{k},1}$, respectively[9]. Moreover, the integral over $\omega_k$ can already be calculated:

$$\Gamma_{\mathrm{ED},0} = \frac{\omega_{eg}^3}{8\pi^2\varepsilon_0\hbar c^3}\int_{4\pi}\sum_{s=1}^{2}\left|\mathbf{d}^{eg}\cdot\hat{\boldsymbol{\varepsilon}}_{\mathbf{k},s}\right|^2\mathrm{d}\Omega_k, \tag{3.23a}$$

$$\Gamma_{\mathrm{MD},0} = \frac{\omega_{eg}^3}{8\pi^2\varepsilon_0\hbar c^5}\int_{4\pi}\sum_{s=1}^{2}\left|\mathbf{m}^{eg}\cdot\hat{\boldsymbol{\varepsilon}}_{\mathbf{k},s}\right|^2\mathrm{d}\Omega_k, \tag{3.23b}$$

$$\Gamma_{\mathrm{EQ},0} = \frac{\omega_{eg}^5}{8\pi^2\varepsilon_0\hbar c^5}\int_{4\pi}\sum_{s=1}^{2}\left|\mathbf{Q}^{eg}:\hat{\mathbf{k}}\,\hat{\boldsymbol{\varepsilon}}_{\mathbf{k},s}\right|^2\mathrm{d}\Omega_k. \tag{3.23c}$$

[9]The sign is unimportant, since the change is made within a modulus.

Next, calculating the square modulus leads to

$$\Gamma_{\mathrm{ED},0} = \frac{\omega_{eg}^3}{8\pi^2\varepsilon_0\hbar c^3}\, d_i^{eg}\left(d_j^{eg}\right)^* \int_{4\pi}\sum_{s=1}^{2}\hat{\varepsilon}_{\mathbf{k},s,i}\,\hat{\varepsilon}^*_{\mathbf{k},s,j}\,\mathrm{d}\Omega_k, \tag{3.24a}$$

$$\Gamma_{\mathrm{MD},0} = \frac{\omega_{eg}^3}{8\pi^2\varepsilon_0\hbar c^5}\, m_i^{eg}\left(m_j^{eg}\right)^* \int_{4\pi}\sum_{s=1}^{2}\hat{\varepsilon}_{\mathbf{k},s,i}\,\hat{\varepsilon}^*_{\mathbf{k},s,j}\,\mathrm{d}\Omega_k, \tag{3.24b}$$

$$\Gamma_{\mathrm{EQ},0} = \frac{\omega_{eg}^5}{8\pi^2\varepsilon_0\hbar c^5}\, Q_{ij}^{eg}\left(Q_{ab}^{eg}\right)^* \int_{4\pi}\sum_{s=1}^{2}\hat{k}_j\,\hat{\varepsilon}_{\mathbf{k},s,i}\,\hat{k}_b\,\hat{\varepsilon}^*_{\mathbf{k},s,a}\,\mathrm{d}\Omega_k, \tag{3.24c}$$

where the Einstein summation convention is used and where $\hat{\varepsilon}_{\mathbf{k},s,i}$ and $\hat{\mathrm{k}}_i$ denote, respectively, the components in spherical coordinates of the unitary vectors $\hat{\boldsymbol{\varepsilon}}_{\mathbf{k},s}$ and of the normalized wave vector $\hat{\mathbf{k}}$ ($i = 1,2,3$). In addition, $\hat{\mathbf{k}}$ is a real vector since there are no losses in vacuum (in general, polarization vectors can be complex [94]).

In order to calculate the integrals over the solid angle, let us make use of the closure relation that satisfies the orthonormal basis $\left\{\hat{\boldsymbol{\varepsilon}}_{\mathbf{k},1}, \hat{\boldsymbol{\varepsilon}}_{\mathbf{k},2}, \hat{\mathbf{k}}\right\}$ [2]:

$$\sum_{s=1}^{2}\hat{\boldsymbol{\varepsilon}}_{\mathbf{k},s}\,\hat{\boldsymbol{\varepsilon}}^*_{\mathbf{k},s} + \hat{\mathbf{k}}\,\hat{\mathbf{k}} = \mathbb{1}_{3\times3}, \tag{3.25a}$$

$$\Leftrightarrow \sum_{s=1}^{2}\hat{\varepsilon}_{\mathbf{k},s,i}\,\hat{\varepsilon}^*_{\mathbf{k},s,j} = \delta_{ij} - \hat{\mathrm{k}}_i\,\hat{\mathrm{k}}_j, \tag{3.25b}$$

where $\mathbb{1}_{3\times3}$ is identity matrix in three dimensions. With the last equation, one can show that[10]

$$\int_{4\pi}\sum_{s=1}^{2}\hat{\varepsilon}_{\mathbf{k},s,i}\hat{\varepsilon}^*_{\mathbf{k},s,j}\,\mathrm{d}\Omega_k = \int_{4\pi}(\delta_{ij} - \hat{k}_i\hat{k}_j)\,\mathrm{d}\Omega_k = 4\pi\,\delta_{ij} - \frac{4\pi}{3}\delta_{ij} = \frac{8\pi}{3}\delta_{ij}, \tag{3.26}$$

and that

$$\int_{4\pi}\sum_{s=1}^{2}\hat{k}_j\,\hat{\varepsilon}_{\mathbf{k},s,i}\,\hat{k}_b\,\hat{\varepsilon}^*_{\mathbf{k},s,a}\,\mathrm{d}\Omega_k = \int_{4\pi}(\delta_{ia} - \hat{k}_i\hat{k}_a)\,\hat{k}_j\hat{k}_b\,\mathrm{d}\Omega_k \tag{3.27a}$$

$$= \delta_{ia}\int_{4\pi}\hat{k}_j\hat{k}_b\,\mathrm{d}\Omega_k - \int_{4\pi}\hat{k}_i\hat{k}_j\hat{k}_a\hat{k}_b\,\mathrm{d}\Omega_k \tag{3.27b}$$

$$= \frac{4\pi}{3}\delta_{ia}\delta_{jb} - \frac{4\pi}{15}\left(\delta_{ij}\delta_{ab} + \delta_{ia}\delta_{jb} + \delta_{ib}\delta ja\right). \tag{3.27c}$$

Multiplying the last result by the product $Q_{ij}^{eg}\left(Q_{ab}^{eg}\right)^*$ leads to

$$Q_{ij}^{eg}\left(Q_{ab}^{eg}\right)^* \int_{4\pi}\sum_{s=1}^{2}\hat{k}_j\,\hat{\varepsilon}_{\mathbf{k},s,i}\,\hat{k}_b\,\hat{\varepsilon}^*_{\mathbf{k},s,a}\,\mathrm{d}\Omega_k = \frac{4\pi}{5}\left\|\mathbf{Q}^{eg}\right\|^2, \tag{3.28}$$

where we define the squared norm of a rank-$n$ tensor $\mathbf{U}$ with $n \geq 1$ as $\|\mathbf{U}\|^2 := \sum_{i_1,i_2,\ldots,i_n}|U_{i_1,i_2,\ldots,i_n}|^2$.

Therefore, by using equations (3.26) and (3.28), the vacuum ED, MD and EQ transition rates

[10] The solid angle of the whole space is $4\pi$. Moreover, one can show that [94]: $\int_{4\pi}\hat{k}_i\hat{k}_j\,\mathrm{d}\Omega_k = \frac{4\pi}{3}\delta_{ij}$ and $\int_{4\pi}\hat{k}_i\hat{k}_j\hat{k}_a\hat{k}_b\,\mathrm{d}\Omega_k = \frac{4\pi}{15}\left(\delta_{ij}\delta_{ab} + \delta_{ia}\delta_{jb} + \delta_{ib}\delta ja\right)$ by using the expression of the vector $\hat{\mathbf{k}}$ in spherical coordinates: $\hat{\mathbf{k}} = \sin\theta\cos\varphi\,\mathbf{e}_x + \sin\theta\sin\varphi\,\mathbf{e}_y + \cos\theta\,\mathbf{e}_z$.

are expressed as follows [2]:

$$\Gamma_{\mathrm{ED},0} = \frac{\omega_{eg}^3}{3\pi\varepsilon_0\hbar c^3} \left\|\mathbf{d}^{eg}\right\|^2, \tag{3.29a}$$

$$\Gamma_{\mathrm{MD},0} = \frac{\omega_{eg}^3}{3\pi\varepsilon_0\hbar c^5} \left\|\mathbf{m}^{eg}\right\|^2, \tag{3.29b}$$

$$\Gamma_{\mathrm{EQ},0} = \frac{\omega_{eg}^5}{10\pi\varepsilon_0\hbar c^5} \left\|\mathbf{Q}^{eg}\right\|^2. \tag{3.29c}$$

As the spontaneous emission takes place in vacuum, the calculated rates are independent of the emitter position. Since there are no interferences in vacuum [2], the total OPSE rate is given by the three previous transition rates:

$$\Gamma_{\mathrm{tot},0} = \Gamma_{\mathrm{ED},0} + \Gamma_{\mathrm{MD},0} + \Gamma_{\mathrm{EQ},0}. \tag{3.30}$$

## 3.5 Expression via the Green's function

In Section 3.3, we derived the multipolar contributions to the OPSE as a function of the field modes [Eqs. (3.16) and (3.17)]. However, it is more convenient to express them via the dyadic Green's function and to normalize them with respect to vacuum. In this way, we obtain more elegant equations and we establish a direct link with the power emitted by classical point sources [Sec. 2.5]. The imaginary part of the Green's function admits a spectral representation that can be expanded in terms of the normal modes $\mathbf{A}_\alpha$ of the electromagnetic field [30]:

$$\operatorname{Im}\mathbf{G}(\omega;\mathbf{r},\mathbf{r}') = \frac{\pi c^2}{2\omega}\sum_\alpha \mathbf{A}_\alpha(\mathbf{r})\mathbf{A}_\alpha^*(\mathbf{r}')\,\delta(\omega-\omega_\alpha), \tag{3.31}$$

where $c$ denotes the speed of light in vacuum. Note that if $\mathbf{r} = \mathbf{r}'$, the imaginary part of the Green's function is symmetric [30].

### 3.5.1 Electric dipole transition

Let us start by introducing the imaginary part of the Green's function in equation (3.16a) of the ED transition rate [30]:

$$\Gamma_{\mathrm{ED}}(\mathbf{R}) = \frac{\pi}{\varepsilon_0\hbar}\sum_\alpha \omega_\alpha \left|\mathbf{d}^{eg}\cdot\mathbf{A}_\alpha(\mathbf{R})\right|^2 \delta(\omega_{eg}-\omega_\alpha) \tag{3.32a}$$

$$= \frac{\pi}{\varepsilon_0\hbar}\sum_\alpha \omega_\alpha\, \mathbf{d}^{eg}\cdot\mathbf{A}_\alpha(\mathbf{R})\left(\mathbf{d}^{eg}\cdot\mathbf{A}_\alpha(\mathbf{R})\right)^* \delta(\omega_{eg}-\omega_\alpha) \tag{3.32b}$$

$$= \frac{\pi}{\varepsilon_0\hbar}\sum_\alpha \omega_\alpha\, \mathbf{d}^{eg}\cdot\mathbf{A}_\alpha(\mathbf{R})\,\mathbf{A}_\alpha^*(\mathbf{R})\cdot\left(\mathbf{d}^{eg}\right)^* \delta(\omega_{eg}-\omega_\alpha) \tag{3.32c}$$

$$= \frac{\pi\,\omega_{eg}}{\varepsilon_0\hbar}\,\mathbf{d}^{eg}\cdot\left\{\sum_\alpha \mathbf{A}_\alpha(\mathbf{R})\,\mathbf{A}_\alpha^*(\mathbf{R})\,\delta(\omega_{eg}-\omega_\alpha)\right\}\cdot\left(\mathbf{d}^{eg}\right)^* \tag{3.32d}$$

$$= \frac{2\,\omega_{eg}^2}{\varepsilon_0\hbar c^2}\,\mathbf{d}^{eg}\cdot\operatorname{Im}\mathbf{G}(\omega_{eg};\mathbf{R},\mathbf{R})\cdot\left(\mathbf{d}^{eg}\right)^*. \tag{3.32e}$$

To go from one equation to the next, we developed the square modulus, we used that the scalar product is commutative, and we used that the delta function restricts all values of $\omega_\alpha$ to $\omega_{eg}$, which

can therefore be taken out of the sum over the modes to reveal the Green's function.

### 3.5.2 Magnetic dipole transition

Then, an equation similar to equation (3.32d) can be derived for the MD transition rate [Eq. (3.16b)]:

$$\Gamma_{\mathrm{MD}}(\mathbf{R}) = \frac{\pi}{\varepsilon_0 \hbar \omega_{eg}} \mathbf{m}^{eg} \cdot \left\{ \sum_{\alpha} \nabla \times \mathbf{A}_{\alpha}(\mathbf{R}) \, \nabla \times \mathbf{A}_{\alpha}^{*}(\mathbf{R}) \, \delta(\omega_{eg} - \omega_{\alpha}) \right\} \cdot (\mathbf{m}^{eg})^{*} \, . \tag{3.33}$$

In this equation, the cross product between vectors can be written using Levi-Civita symbols [100]: $\mathbf{A} \times \mathbf{B} = \varepsilon_{ijk} \, A_j B_k \, \hat{\mathbf{e}}_i$ where the Einstein summation convention is used and where the Levi-Civita symbol is defined as

$$\varepsilon_{ijk} := \begin{cases} +1 & \text{if } (i,j,k) = (1,2,3), (2,3,1), \text{ or } (3,1,2), \\ -1 & \text{if } (i,j,k) = (3,2,1), (1,3,2), \text{ or } (2,1,3), \\ \ \ 0 & \text{if } i = j, \text{ or } j = k, \text{ or } k = i. \end{cases} \tag{3.34}$$

Thereby, one obtains

$$\Gamma_{\mathrm{MD}}(\mathbf{R}) = \frac{\pi}{\varepsilon_0 \hbar \omega_{eg}} m_i^{eg} \left( m_j^{eg} \right)^{*} \left\{ \sum_{\alpha} \varepsilon_{ikl} \, \partial_k A_{\alpha,l}(\mathbf{R}) \, \varepsilon_{jmn} \, \partial_m A_{\alpha,n}^{*}(\mathbf{R}) \, \delta(\omega_{eg} - \omega_{\alpha}) \right\} . \tag{3.35}$$

To reveal the Green's function, the derivatives must be placed in front of the sum. To do so, we differentiate the spatial dependency of the normal modes and we take the limit $\mathbf{r}, \mathbf{r}' \to \mathbf{R}$ [23]:

$$\Gamma_{\mathrm{MD}}(\mathbf{R}) = \frac{\pi}{\varepsilon_0 \hbar \omega_{eg}} m_i^{eg} \left( m_j^{eg} \right)^{*} \left\{ \varepsilon_{ikl} \, \varepsilon_{jmn} \, \partial_k \partial'_m \sum_{\alpha} A_{\alpha,l}(\mathbf{r}) \, A_{\alpha,n}^{*}(\mathbf{r}') \, \delta(\omega_{eg} - \omega_{\alpha}) \right\}_{\mathbf{r}=\mathbf{r}'=\mathbf{R}} \tag{3.36a}$$

$$= \frac{2}{\varepsilon_0 \hbar c^2} m_i^{eg} \left( m_j^{eg} \right)^{*} \left\{ \varepsilon_{ikl} \, \varepsilon_{jmn} \, \partial_k \partial'_m \, \mathrm{Im} \, G_{ln}(\omega_{eg}; \mathbf{r}, \mathbf{r}') \right\}_{\mathbf{r}=\mathbf{r}'=\mathbf{R}} , \tag{3.36b}$$

where $\partial_k$ and $\partial_{m'}$ mean derivatives with respect to the coordinates $\mathbf{r}$ and $\mathbf{r}'$, respectively. By defining the Green's function of the magnetic dipole that gives the power emitted by a magnetic dipole point source [23]:

$$k^2 \, G_{ij}^{\mathrm{MD}}(\omega; \mathbf{R}, \mathbf{R}) := \left\{ \varepsilon_{ikl} \, \varepsilon_{jmn} \, \partial_k \partial'_m G_{ln}(\omega; \mathbf{r}, \mathbf{r}') \right\}_{\mathbf{r}=\mathbf{r}'=\mathbf{R}} , \tag{3.37}$$

the MD transition rate is expressed as follows [23]:

$$\Gamma_{\mathrm{MD}}(\mathbf{R}) = \frac{2 \, \omega_{eg}^2}{\varepsilon_0 \hbar c^4} m_i^{eg} \left( m_j^{eg} \right)^{*} \mathrm{Im} \, G_{ij}^{\mathrm{MD}}(\omega_{eg}; \mathbf{r}, \mathbf{r}') \tag{3.38a}$$

$$= \frac{2 \, \omega_{eg}^2}{\varepsilon_0 \hbar c^4} \mathbf{m}^{eg} \cdot \mathrm{Im} \, \mathbf{G}^{\mathrm{MD}}(\omega_{eg}; \mathbf{R}, \mathbf{R}) \cdot (\mathbf{m}^{eg})^{*} \, . \tag{3.38b}$$

Note that the derived equation is very similar to the one related to the ED transition [Eq. (3.32e)].

### 3.5.3 Electric quadrupole transition

Next, similar developments for the EQ transition rate [Eq. (3.16c)] lead to

$$\Gamma_{\mathrm{EQ}}(\mathbf{R}) = \frac{\pi\,\omega_{eg}}{\varepsilon_0\hbar}\,\mathbf{Q}^{eg} : \left\{\sum_\alpha \nabla\mathbf{A}_\alpha(\mathbf{R})\,\nabla\mathbf{A}_\alpha^*(\mathbf{R})\,\delta(\omega_{eg}-\omega_\alpha)\right\} : (\mathbf{Q}^{eg})^* \tag{3.39a}$$

$$= \frac{\pi\,\omega_{eg}}{\varepsilon_0\hbar}\,Q_{ij}^{eg}\left(Q_{kl}^{eg}\right)^*\left\{\sum_\alpha \partial_j A_{\alpha,i}(\mathbf{R})\,\partial_l A_{\alpha,k}^*(\mathbf{R})\,\delta(\omega_{eg}-\omega_\alpha)\right\} \tag{3.39b}$$

$$= \frac{\pi\,\omega_{eg}}{\varepsilon_0\hbar}\,Q_{ij}^{eg}\left(Q_{kl}^{eg}\right)^*\left\{\partial_j\partial_l'\sum_\alpha A_{\alpha,i}(\mathbf{r})\,A_{\alpha,k}^*(\mathbf{r}')\,\delta(\omega_{eg}-\omega_\alpha)\right\}_{\mathbf{r}=\mathbf{r}'=\mathbf{R}} \tag{3.39c}$$

$$= \frac{2\,\omega_{eg}^2}{\varepsilon_0\hbar c^2}\,Q_{ij}^{eg}\left(Q_{kl}^{eg}\right)^*\left\{\partial_j\partial_l'\,\mathrm{Im}\,G_{ik}(\omega_{eg};\mathbf{r},\mathbf{r}')\right\}_{\mathbf{r}=\mathbf{r}'=\mathbf{R}} \tag{3.39d}$$

$$= \frac{2\,\omega_{eg}^4}{\varepsilon_0\hbar c^4}\,\mathbf{Q}^{eg} : \mathrm{Im}\,\mathbf{G}^{\mathrm{EQ}}(\omega_{eg};\mathbf{R},\mathbf{R}) : (\mathbf{Q}^{eg})^*\,, \tag{3.39e}$$

where we used that the double dot product between two second-rank tensors is commutative and where we have defined the Green's function of the electric quadrupole as

$$k^2\,G_{jilk}^{\mathrm{EQ}}(\omega;\mathbf{R},\mathbf{R}) := \left\{\partial_j\partial_l'\,G_{ik}(\omega;\mathbf{r},\mathbf{r}')\right\}_{\mathbf{r}=\mathbf{r}'=\mathbf{R}}\,, \tag{3.40}$$

which is a fourth rank tensor. Furthermore, since the imaginary part of the defined tensor is real and by using equation (3.31), one can show that it satisfies the following property:

$$\forall i,j,k,l=1,2,3,\quad \mathrm{Im}\,G_{jilk}^{\mathrm{EQ}} = \mathrm{Im}\,G_{lkji}^{\mathrm{EQ}}. \tag{3.41}$$

### 3.5.4 Interference terms

Finally, for the interference term between the ED and EQ transitions [Eq. (3.17b)], we obtain

$$\Gamma_{\mathrm{ED}\cap\mathrm{EQ}}(\mathbf{R}) = 2\,\frac{\pi\,\omega_{eg}}{\varepsilon_0\hbar}\,\mathbf{d}^{eg}\cdot\left\{\sum_\alpha \mathbf{A}_\alpha(\mathbf{R})\,\nabla\mathbf{A}_\alpha^*(\mathbf{R})\,\delta(\omega_{eg}-\omega_\alpha)\right\} : (\mathbf{Q}^{eg})^* \tag{3.42a}$$

$$= 2\,\frac{\pi\,\omega_{eg}}{\varepsilon_0\hbar}\,d_i^{eg}\left(Q_{jk}^{eg}\right)^*\left\{\sum_\alpha A_{\alpha,i}(\mathbf{R})\,\partial_k A_{\alpha,j}^*(\mathbf{R})\,\delta(\omega_{eg}-\omega_\alpha)\right\} \tag{3.42b}$$

$$= 2\,\frac{\pi\,\omega_{eg}}{\varepsilon_0\hbar}\,d_i^{eg}\left(Q_{jk}^{eg}\right)^*\left\{\partial_k'\sum_\alpha A_{\alpha,i}(\mathbf{r})\,A_{\alpha,j}^*(\mathbf{r}')\,\delta(\omega_{eg}-\omega_\alpha)\right\}_{\mathbf{r}=\mathbf{r}'=\mathbf{R}} \tag{3.42c}$$

$$= 2\,\frac{2\,\omega_{eg}^2}{\varepsilon_0\hbar c^2}\,d_i^{eg}\left(Q_{jk}^{eg}\right)^*\left\{\partial_k'\,\mathrm{Im}\,G_{ij}(\omega_{eg};\mathbf{r},\mathbf{r}')\right\}_{\mathbf{r}=\mathbf{r}'=\mathbf{R}} \tag{3.42d}$$

$$= 2\,\frac{2\,\omega_{eg}^3}{\varepsilon_0\hbar c^3}\,\mathbf{d}^{eg}\cdot\mathrm{Im}\,\mathbf{G}^{\mathrm{ED}\cap\mathrm{EQ}} : (\mathbf{Q}^{eg})^*\,, \tag{3.42e}$$

where the real part is implied and where we have defined the third rank tensor $\mathbf{G}^{\mathrm{ED}\cap\mathrm{EQ}}$ as

$$k\,G_{ikj}^{\mathrm{ED}\cap\mathrm{EQ}}(\omega;\mathbf{R},\mathbf{R}) := \left\{\partial_k'\,G_{ij}(\omega;\mathbf{r},\mathbf{r}')\right\}_{\mathbf{r}=\mathbf{r}'=\mathbf{R}}\,. \tag{3.43}$$

Similar equations can be derived for the interference terms involving the MD channel, but will not be presented in this thesis.

### 3.5.5 Vacuum normalization and discussion

Now, let us normalize the derived equations by the free-space transition rates given by the equations (3.29) [23, 30, 51]:

$$\frac{\Gamma_{\mathrm{ED}}(\mathbf{R})}{\Gamma_{\mathrm{ED},0}} = \frac{6\pi c}{\omega_{eg}}\, \hat{\mathbf{d}}^{eg} \cdot \operatorname{Im} \mathbf{G}(\omega_{eg}; \mathbf{R}, \mathbf{R}) \cdot \left(\hat{\mathbf{d}}^{eg}\right)^{*}, \tag{3.44a}$$

$$\frac{\Gamma_{\mathrm{MD}}(\mathbf{R})}{\Gamma_{\mathrm{ED},0}} = \frac{6\pi c}{\omega_{eg}}\, \hat{\mathbf{m}}^{eg} \cdot \operatorname{Im} \mathbf{G}^{\mathrm{MD}}(\omega_{eg}; \mathbf{R}, \mathbf{R}) \cdot (\hat{\mathbf{m}}^{eg})^{*}, \tag{3.44b}$$

$$\frac{\Gamma_{\mathrm{EQ}}(\mathbf{R})}{\Gamma_{\mathrm{EQ},0}} = \frac{20\pi c}{\omega_{eg}}\, \hat{\mathbf{Q}}^{eg} : \operatorname{Im} \mathbf{G}^{\mathrm{EQ}}(\omega_{eg}; \mathbf{R}, \mathbf{R}) : \left(\hat{\mathbf{Q}}^{eg}\right)^{*}, \tag{3.44c}$$

$$\frac{\Gamma_{\mathrm{ED}\cap\mathrm{EQ}}(\mathbf{R})}{\sqrt{\Gamma_{\mathrm{ED},0}\,\Gamma_{\mathrm{EQ},0}}} = 2\,\frac{2\sqrt{30}\pi c}{\omega_{eg}}\, \hat{\mathbf{d}}^{eg} \cdot \operatorname{Im} \mathbf{G}^{\mathrm{ED}\cap\mathrm{EQ}}(\omega_{eg}; \mathbf{R}, \mathbf{R}) : \left(\hat{\mathbf{Q}}^{eg}\right)^{*}, \tag{3.44d}$$

where the caret denotes normalized tensors (i.e., for an $n^{\mathrm{th}}$ rank tensor $\mathbf{U}$ with $n \in \mathbb{N}_0$, $\hat{\mathbf{U}} := \mathbf{U}/\left\|\mathbf{U}\right\|$ with $\left\|\mathbf{U}\right\|^2 := \sum_{i_1,i_2,\ldots,i_n} |U_{i_1,i_2,\ldots,i_n}|^2$). Note that the derived equations are valid regardless of the emitter and its environment.

The first three equations represent the change of the multipolar transition rates due to the environment (i.e., the Purcell effect), and are therefore by definition the Purcell factors [Eq. (2.34)]. In addition, the obtained equations are identical with those obtained for the modification of the power emitted by classical multipolar point sources in Section 2.5.2 [Eqs. (2.44)]. Therefore, the comments made about the equations obtained for the classical sources apply here as well. In particular, the equations involve the imaginary part of the Green's function evaluated at the emitter's position, which is a symmetric tensor, with the nuance that MD and EQ transitions as well as interference terms involve derivatives of $\operatorname{Im} \mathbf{G}$.

To conclude this section, we proved the relation (2.34) which states that the modification due to the environment of the power emitted by classical sources is equal to the modification of transition rates of quantum emitters (in the weak coupling regime [30]). As a result, the Purcell effect [Eqs. (3.44)] can be computed by considering classical point sources in electromagnetic simulations, which have the same multipolar moment directions[11] as those describing the transitions of the quantum emitter [Subsec. 2.5.3]. Concerning the interference term [Eq. (3.44d)], it can be calculated by considering the superposition of dipolar and quadrupolar sources having the same multipolar moments as the emitter [Eq. (2.32)].

Despite that the obtained relations [Eqs. (3.44)] already enable the classical computation of the Purcell effect and of the interference effects, we decompose in Section 3.7 the equations into Purcell factor bases. This will allow us in the next chapter to express the Purcell effect for the two-photon spontaneous emission process as a function of the Purcell factors of the OPSE. In anticipation, we introduce in the following section a modified Voigt notation to simplify the equations relative to EQ transitions.

[11] The knowledge of the norm of the transition moments is not required to calculate the Purcell effect [Eqs. (2.44), (3.44)]. It is required only for the calculation of the vacuum rates [Eqs. (3.29)] and for the calculation of the interference term since the multipolar sources must be weighted according to the transition moments of the emitter [Eqs. (3.90) and (3.88)].

## 3.6 Simplification using a modified Voigt notation

The symmetry and traceless properties of electric quadrupole moments (i.e., $\forall i,j=1,2,3,\ Q_{ij}=Q_{ji}$ and $\sum_{i=1}^{3} Q_{ii}=0$) can be used to reduce the number of terms in the equations of the vacuum normalized rates of $\Gamma_{\mathrm{EQ}}$ and $\Gamma_{\mathrm{ED}\cap\mathrm{EQ}}$ [Eqs. (3.44c) and (3.44d)]. First of all, the first property is used to suppress the redundancy over the symmetric components of the tensor $\mathbf{Q}^{eg}$. This provides an expression involving $6^2$ terms instead of $9^2$ for the EQ transition rate [Eq. (3.44c)]:

$$\frac{\Gamma_{\mathrm{EQ}}(\mathbf{R})}{\Gamma_{\mathrm{EQ},0}}=\frac{20\pi c}{\omega_{eg}}\sum_{\mu,\nu=1}^{6}\hat{Q}_{\mu}^{eg}\left(\hat{Q}_{\nu}^{eg}\right)^{*}\mathrm{Im}\,U_{\mu\nu}^{\mathrm{EQ}}(\omega_{eg};\mathbf{R},\mathbf{R}), \tag{3.45}$$

with

$$U_{\mu\nu}^{\mathrm{EQ}}:=\begin{cases} G_{\mu\nu}^{\mathrm{EQ}} & \forall\mu,\nu=1,2,3 \\ G_{\mu\nu}^{\mathrm{EQ}}+G_{\mu\bar{\nu}}^{\mathrm{EQ}} & \forall\mu=1,2,3\ ;\ \nu=4,5,6 \\ G_{\mu\nu}^{\mathrm{EQ}}+G_{\bar{\mu}\nu}^{\mathrm{EQ}} & \forall\mu=4,5,6\ ;\ \nu=1,2,3 \\ G_{\mu\nu}^{\mathrm{EQ}}+G_{\mu\bar{\nu}}^{\mathrm{EQ}}+G_{\bar{\mu}\nu}^{\mathrm{EQ}}+G_{\bar{\mu}\bar{\nu}}^{\mathrm{EQ}} & \forall\mu,\nu=4,5,6. \end{cases} \tag{3.46}$$

To derive this equation, we used the Voigt notation. This mathematical convention exploits the symmetry property of a tensor, by removing its redundant components, to represent it by a lower rank tensor defined in a higher dimensional space. In this way the first-order electric quadrupole transition moment, which is a second rank tensor in three dimensions, is represented as a vector in six dimensions:

$$\left(Q_{ij}^{eg}\right)_{3\times3}\rightarrow\left(Q_{11}^{eg},Q_{22}^{eg},Q_{33}^{eg},Q_{23}^{eg},Q_{13}^{eg},Q_{12}^{eg}\right)^{T}\rightarrow\left(Q_{\mu}^{eg}\right)_{6}. \tag{3.47}$$

Table 3.1 establishes the correspondence between the new indices and the ones of the represented tensor. Furthermore, the bar over a pair of indices in equation (3.46) means taking the related symmetric one (e.g., $G_{2\bar{6}}^{\mathrm{EQ}}=G_{22\bar{1}\bar{2}}^{\mathrm{EQ}}=G_{2221}^{\mathrm{EQ}}$).

| $(i,j)$ | $(1,1)$ | $(2,2)$ | $(3,3)$ | $(2,3)$ | $(1,3)$ | $(1,2)$ |
|---|---|---|---|---|---|---|
| $\mu$ | 1 | 2 | 3 | 4 | 5 | 6 |

Table 3.1: Voigt notation: correspondence between the pair of indices $(i,j)$ of a symmetric tensor in three dimensions and the indices $\mu$ in six dimensions. The indices $\mu=1,2,3$ correspond to the diagonal components of a second rank tensor, while the indices $\mu=3,4,5$ correspond to its three independent off-diagonal components. By convention, the indices of this notation are denoted with Greek letters.

Similarly, using the symmetry property for the interference term $\Gamma_{\mathrm{ED}\cap\mathrm{EQ}}$ [Eq. (3.44d)] provides an expression involving $3\times6$ terms instead of $3\times9$:

$$\frac{\Gamma_{\mathrm{ED}\cap\mathrm{EQ}}(\mathbf{R})}{\sqrt{\Gamma_{\mathrm{ED},0}\,\Gamma_{\mathrm{EQ},0}}}=2\,\frac{2\sqrt{30}\pi c}{\omega_{eg}}\sum_{i=1}^{3}\sum_{\mu=1}^{6}\hat{d}_{i}^{eg}\left(\hat{Q}_{\mu}^{eg}\right)^{*}\mathrm{Im}\,U_{i\mu}^{\mathrm{ED}\cap\mathrm{EQ}}(\omega_{eg};\mathbf{R},\mathbf{R}), \tag{3.48}$$

with

$$U_{i\mu}^{\mathrm{ED}\cap\mathrm{EQ}}:=\begin{cases} G_{i\mu}^{\mathrm{ED}\cap\mathrm{EQ}} & \forall\mu=1,2,3 \\ G_{i\mu}^{\mathrm{ED}\cap\mathrm{EQ}}+G_{i\bar{\mu}}^{\mathrm{ED}\cap\mathrm{EQ}} & \forall\mu=4,5,6. \end{cases} \tag{3.49}$$

Then, by using the second property linked to the traceless property, we obtain a formula involving

$5^2$ terms for the EQ transition:

$$\frac{\Gamma_{\mathrm{EQ}}(\mathbf{R})}{\Gamma_{\mathrm{EQ},0}} = \frac{20\pi c}{\omega_{eg}} \sum_{\substack{\mu,\nu=1 \\ \mu\neq 3,\nu\neq 3}}^{6} \hat{Q}_{\mu}^{eg} \left(\hat{Q}_{\nu}^{eg}\right)^{*} \operatorname{Im} \widetilde{G}_{\mu\nu}^{\mathrm{EQ}}(\omega_{eg};\mathbf{R},\mathbf{R}), \tag{3.50}$$

with

$$\widetilde{G}_{\mu\nu}^{\mathrm{EQ}} := \begin{cases} U_{\mu\nu}^{\mathrm{EQ}} - U_{\mu 3}^{\mathrm{EQ}} - U_{3\nu}^{\mathrm{EQ}} + U_{33}^{\mathrm{EQ}} & \forall \mu,\nu = 1,2 \\ U_{\mu\nu}^{\mathrm{EQ}} - U_{3\nu}^{\mathrm{EQ}} & \forall \mu = 1,2 \quad ;\ \nu = 4,5,6 \\ U_{\mu\nu}^{\mathrm{EQ}} - U_{\mu 3}^{\mathrm{EQ}} & \forall \mu = 4,5,6\ ;\ \nu = 1,2 \\ U_{\mu\nu}^{\mathrm{EQ}} & \forall \mu,\nu = 4,5,6. \end{cases} \tag{3.51}$$

Note that the property of the tensor $\mathbf{G}^{\mathrm{EQ}}$ given by the equation (3.41) implies that the tensor $\widetilde{\mathbf{G}}^{\mathrm{EQ}}$ is symmetric. For the interference term, we obtain a formula involving $3 \times 5$ terms:

$$\frac{\Gamma_{\mathrm{ED}\cap\mathrm{EQ}}(\mathbf{R})}{\sqrt{\Gamma_{\mathrm{ED},0}\,\Gamma_{\mathrm{EQ},0}}} = 2\,\frac{2\sqrt{30}\pi c}{\omega_{eg}} \sum_{i=1}^{3} \sum_{\substack{\mu=1 \\ \mu\neq 3}}^{6} \hat{d}_{i}^{eg} \left(\hat{Q}_{\mu}^{eg}\right)^{*} \operatorname{Im} \widetilde{G}_{i\mu}^{\mathrm{ED}\cap\mathrm{EQ}}(\omega_{eg};\mathbf{R},\mathbf{R}), \tag{3.52}$$

with

$$\widetilde{G}_{i\mu}^{\mathrm{ED}\cap\mathrm{EQ}} := \begin{cases} U_{i\mu}^{\mathrm{ED}\cap\mathrm{EQ}} - U_{i3}^{\mathrm{ED}\cap\mathrm{EQ}} & \forall \mu = 1,2 \\ U_{i\mu}^{\mathrm{ED}\cap\mathrm{EQ}} & \forall \mu = 4,5,6. \end{cases} \tag{3.53}$$

Finally, we modify the Voigt notation to skip the last diagonal element of second-order tensors:

$$\left(Q_{ij}^{eg}\right)_{3\times 3} \to \left(Q_{11}^{eg}, Q_{22}^{eg}, Q_{23}^{eg}, Q_{13}^{eg}, Q_{12}^{eg}\right)^{T} \to \left(Q_{\mu}^{eg}\right)_{5}. \tag{3.54}$$

Table 3.2 establishes the correspondence between the indices in the modified Voigt notation and these of the represented tensors.

| $(i,j)$ | $(1,1)$ | $(2,2)$ | $(2,3)$ | $(1,3)$ | $(1,2)$ |
|---|---|---|---|---|---|
| $\mu$ | 1 | 2 | 3 | 4 | 5 |

Table 3.2: Modified Voigt notation: correspondence between the pair of indices $(i,j)$ of a symmetric and traceless tensor in three dimensions and the indices $\mu$ in five dimensions. The indices $\mu = 1,2$ correspond to the two independent diagonal components of a second rank tensor, while the indices $\mu = 3,4,5$ correspond to its three independent off-diagonal components. By convention, the indices of this notation are denoted with Greek letters.

With the modified Voigt notation, we obtain

$$\frac{\Gamma_{\mathrm{EQ}}(\mathbf{R})}{\Gamma_{\mathrm{EQ},0}} = \frac{20\pi c}{\omega_{eg}} \sum_{\mu,\nu=1}^{5} \hat{Q}_{\mu}^{eg} \left(\hat{Q}_{\nu}^{eg}\right)^{*} \operatorname{Im} \widetilde{G}_{\mu\nu}^{\mathrm{EQ}}(\omega_{eg};\mathbf{R},\mathbf{R}) \tag{3.55a}$$

$$= \frac{20\pi c}{\omega_{eg}}\, \hat{\mathbf{Q}}^{eg} \cdot \operatorname{Im} \widetilde{\mathbf{G}}^{\mathrm{EQ}}(\omega_{eg};\mathbf{R},\mathbf{R}) \cdot \left(\hat{\mathbf{Q}}^{eg}\right)^{*}, \tag{3.55b}$$

where the dot product denotes here the scalar product between vectors in five dimensions: $\mathbf{a}\cdot\mathbf{b} =$

$\sum_{\mu=1}^{5} a_\mu b_\mu$. For the interference term, we get

$$\frac{\Gamma_{\mathrm{ED}\cap\mathrm{EQ}}(\mathbf{R})}{\sqrt{\Gamma_{\mathrm{ED},0}\,\Gamma_{\mathrm{EQ},0}}} = 2\,\frac{2\sqrt{30}\pi c}{\omega_{eg}} \sum_{i=1}^{3}\sum_{\mu=1}^{5} \hat{d}_i^{eg} \left(\hat{Q}_\mu^{eg}\right)^* \mathrm{Im}\,\widetilde{G}_{i\mu}^{\mathrm{ED}\cap\mathrm{EQ}}(\omega_{eg};\mathbf{R},\mathbf{R}) \tag{3.56a}$$

$$= 2\,\frac{2\sqrt{30}\pi c}{\omega_{eg}}\, \hat{\mathbf{d}}^{eg} \cdot \mathrm{Im}\,\widetilde{\mathbf{G}}^{\mathrm{ED}\cap\mathrm{EQ}}(\omega_{eg};\mathbf{R},\mathbf{R}) \cdot \left(\hat{\mathbf{Q}}^{eg}\right)^*, \tag{3.56b}$$

where the first and second dot products are in three and five dimensions, respectively.

To summarize, using the modified Voigt notation that removes redundant components of the symmetric and traceless electric quadrupole transition moment $\mathbf{Q}^{eg}$ allows to reduce the number of terms in the equations. Thereby, we have rewritten the equations (3.39e) and (3.42e) that involves double dot products into equations that involve scalar products between lower rank tensors in five dimensions. Employing this notation results in all first-order transition moments being represented by first-rank tensors (the rank of the tensors is equal to the order of the transition), and all Green's functions also being of rank 2. In the next section, this convention will facilitate the decomposition of quadrupolar transitions into Purcell factor bases.

## 3.7 Decomposition in Purcell factor bases

In this section, we perform a decomposition of the multipolar contributions [Eqs. (3.44a), (3.44b), (3.55), and (3.56)] to the total OPSE rate in Purcell factor bases. These bases consist of Purcell factors related to multipolar transition moments aligned along basis vectors. This will allow us in the next chapter to express the two-photon Purcell effect as a function of the one-photon Purcell factors. To do this, the idea is to decompose the normalized first-order multipolar transition moments in bases and to assume them along the basis vectors to make the link with the diagonal components of the imaginary part of the Green's tensors, and along the vector formed by the sum of two basis vectors to make the link with the off-diagonal components. As a reminder, the tensors $\mathrm{Im}\,\mathbf{G}$, $\mathrm{Im}\,\mathbf{G}^{\mathrm{MD}}$, and $\mathrm{Im}\,\widetilde{\mathbf{G}}^{\mathrm{EQ}}$ are symmetric [Eqs. (3.31), (3.37), and (3.51)]. For the interference term, we superpose the basis vectors of the different multipolar transition moments.

### 3.7.1 Electric dipole transition

Since a general electric dipole moment involves up to three independent components, it can be expanded with an orthonormal basis of three vectors. Thus, let us take the electric dipole transition moment along one basis vector, i.e., $\hat{\mathbf{d}}^{eg} = \hat{\mathbf{e}}_i$ with $i = 1, 2, 3$. In this case, using the equation (3.44a) of the vacuum normalized ED transition rate, we define the three Purcell factors $P_i^{\mathrm{ED}}$ corresponding to the ratio between the ED transition rate of an emitter that has its electric dipole transition moment along the basis vector $\hat{\mathbf{e}}_i$ and the corresponding rate in free space as [30, 42]:

$$P_i^{\mathrm{ED}}(\omega;\mathbf{R}) := \frac{6\pi c}{\omega}\mathrm{Im}\,G_{ii}(\omega;\mathbf{R},\mathbf{R}). \tag{3.57}$$

The previous equation makes a link between the diagonal components of $\mathrm{Im}\,\mathbf{G}$ and the Purcell factors $P_i^{\mathrm{ED}}$. To establish a link with the off-diagonal components, let us take $\hat{\mathbf{d}}^{eg} = (\hat{\mathbf{e}}_i + \hat{\mathbf{e}}_j)/\sqrt{2}$ with $i, j = 1, 2, 3$ and $i < j$ in the equation (3.44a). In this case, we define the three Purcell factors $P_{ij}^{\mathrm{ED}}$ relative to an emitter that has its electric dipole transition moment aligned along the bisector

of the basis vectors $\hat{\mathbf{e}}_i$ and $\hat{\mathbf{e}}_j$ as

$$P_{ij}^{\mathrm{ED}}(\omega;\mathbf{R}) := \frac{6\pi c}{\omega}\frac{1}{2}\left[\mathrm{Im}\,G_{ii}(\omega;\mathbf{R},\mathbf{R}) + \mathrm{Im}\,G_{ij}(\omega;\mathbf{R},\mathbf{R}) + \mathrm{Im}\,G_{ji}(\omega;\mathbf{R},\mathbf{R}) + \mathrm{Im}\,G_{jj}(\omega;\mathbf{R},\mathbf{R})\right] \tag{3.58a}$$

$$:= \frac{1}{2}\left[P_i^{\mathrm{ED}}(\omega;\mathbf{R}) + P_j^{\mathrm{ED}}(\omega;\mathbf{R})\right] + \frac{6\pi c}{\omega}\mathrm{Im}\,G_{ij}(\omega;\mathbf{R},\mathbf{R}), \tag{3.58b}$$

where we used the definition of the Purcell factors $P_i^{\mathrm{ED}}$ [Eq. (3.57)] as well as the symmetry property of the tensor $\mathrm{Im}\,\mathbf{G}$ [30].

As all components of $\mathrm{Im}\,\mathbf{G}$ have been expressed as a function of Purcell factors, we can now rewrite the equation (3.44a) as

$$\frac{\Gamma_{\mathrm{ED}}(\mathbf{R})}{\Gamma_{\mathrm{ED},0}} = \hat{\mathbf{d}}^{eg}\cdot\mathbf{F}^{\mathrm{ED}}(\omega_{eg};\mathbf{R})\cdot\left(\hat{\mathbf{d}}^{eg}\right)^{*} = \sum_{i,j=1}^{3}\hat{d}_i^{eg}\left(\hat{d}_j^{eg}\right)^{*}F_{ij}^{\mathrm{ED}}(\omega_{eg};\mathbf{R}), \tag{3.59}$$

where the components of the tensor $\mathbf{F}^{\mathrm{ED}}$ are defined as

$$F_{ij}^{\mathrm{ED}}(\omega;\mathbf{R}) := \frac{6\pi c}{\omega}\,\mathrm{Im}\,G_{ij}(\omega;\mathbf{R},\mathbf{R}), \tag{3.60}$$

and linked to the Purcell factors by [Eqs. (3.57) and (3.58b)]:

$$F_{ij}^{\mathrm{ED}}(\omega;\mathbf{R}) = \begin{cases} P_i^{\mathrm{ED}}(\omega;\mathbf{R}) & \forall i = j \\ P_{ij}^{\mathrm{ED}}(\omega;\mathbf{R}) - \dfrac{1}{2}\left[P_i^{\mathrm{ED}}(\omega;\mathbf{R}) + P_j^{\mathrm{ED}}(\omega;\mathbf{R})\right] & \forall i \neq j. \end{cases} \tag{3.61}$$

Since the tensor $\mathbf{F}^{\mathrm{ED}}$ is also symmetric, we need to calculate in the most general case six Purcell factors to get the ED transition rate. For example, in a Cartesian basis we need to calculate these six components:

$$\left\{F_{xx}^{\mathrm{ED}},\, F_{yy}^{\mathrm{ED}},\, F_{zz}^{\mathrm{ED}},\, F_{yz}^{\mathrm{ED}},\, F_{xz}^{\mathrm{ED}},\, F_{xy}^{\mathrm{ED}}\right\}, \tag{3.62}$$

and thus these six Purcell factors:

$$\left\{P_x^{\mathrm{ED}},\, P_y^{\mathrm{ED}},\, P_z^{\mathrm{ED}},\, P_{yz}^{\mathrm{ED}},\, P_{xz}^{\mathrm{ED}},\, P_{xy}^{\mathrm{ED}}\right\}. \tag{3.63}$$

In the case where the system exhibits an azimuthal symmetry, there is an equivalence between the $X$ and $Y$ direction, As a result, some components are equal or zero:

$$\begin{cases} P_y^{\mathrm{ED}} = P_x^{\mathrm{ED}} \Rightarrow F_{yy}^{\mathrm{ED}} = F_{xx}^{\mathrm{ED}} & \text{(3.64a)} \\ P_{yz}^{\mathrm{ED}} = P_{xz}^{\mathrm{ED}} \Rightarrow F_{yz}^{\mathrm{ED}} := P_{yz}^{\mathrm{ED}} - \dfrac{1}{2}\left(P_y^{\mathrm{ED}} + P_z^{\mathrm{ED}}\right) = P_{xz}^{\mathrm{ED}} - \dfrac{1}{2}\left(P_x^{\mathrm{ED}} + P_z^{\mathrm{ED}}\right) = F_{xz}^{\mathrm{ED}} & \text{(3.64b)} \\ P_{xy}^{\mathrm{ED}} = P_x^{\mathrm{ED}} \Rightarrow F_{xy}^{\mathrm{ED}} := P_{xy}^{\mathrm{ED}} - \dfrac{1}{2}\left(P_x^{\mathrm{ED}} + P_y^{\mathrm{ED}}\right) = P_x^{\mathrm{ED}} - \dfrac{1}{2}\left(P_x^{\mathrm{ED}} + P_x^{\mathrm{ED}}\right) = 0. & \text{(3.64c)} \end{cases}$$

Consequently, the number of components of $\mathbf{F}^{\mathrm{ED}}$ and of Purcell factors to calculate is reduced to three:

$$\left\{F_{xx}^{\mathrm{ED}},\, F_{zz}^{\mathrm{ED}},\, F_{xz}^{\mathrm{ED}}\right\}, \tag{3.65a}$$

$$\left\{P_x^{\mathrm{ED}},\, P_z^{\mathrm{ED}},\, P_{xz}^{\mathrm{ED}}\right\}. \tag{3.65b}$$

Furthermore, by choosing a basis vector aligned with the electric dipole transition moment of the emitter, there is only one Purcell factor to calculate. In free space, all Purcell factors are equal to one and so the tensor $\mathbf{F}^{\mathrm{ED}}$ is equal to the identity matrix and thereby the equation (3.59) gives $\Gamma_{\mathrm{ED}} = \Gamma_{\mathrm{ED},0}$.

### 3.7.2 Magnetic dipole transition

Since the equations obtained for the ED and MD transition rates are similar [Eqs. (3.44a) and (3.44b)], the equations for the MD transition can be obtained from the equations of the ED transition by replacing the Green's function by the Green's function of the magnetic dipole and by replacing $\mathbf{d}^{eg}$ by $\mathbf{m}^{eg}$. Thereby, the MD transition rate is given by

$$\frac{\Gamma_{\mathrm{MD}}(\mathbf{R})}{\Gamma_{\mathrm{ED},0}} = \hat{\mathbf{m}}^{eg} \cdot \mathbf{F}^{\mathrm{MD}}(\omega_{eg};\mathbf{R}) \cdot (\hat{\mathbf{m}}^{eg})^* = \sum_{i,j=1}^{3} \hat{m}_i^{eg} \left(\hat{m}_j^{eg}\right)^* F_{ij}^{\mathrm{MD}}(\omega_{eg};\mathbf{R}), \tag{3.66a}$$

where the components of the symmetric tensor $\mathbf{F}^{\mathrm{MD}}$ are defined as

$$F_{ij}^{\mathrm{MD}}(\omega;\mathbf{R}) := \frac{6\pi c}{\omega} \mathrm{Im}\, G_{ij}^{\mathrm{MD}}(\omega;\mathbf{R},\mathbf{R}), \tag{3.67}$$

and linked to the Purcell factors by

$$F_{ij}^{\mathrm{MD}}(\omega;\mathbf{R}) = \begin{cases} P_i^{\mathrm{MD}}(\omega;\mathbf{R}) & \forall i = j \\ P_{ij}^{\mathrm{MD}}(\omega;\mathbf{R}) - \dfrac{1}{2}\left[P_i^{\mathrm{MD}}(\omega;\mathbf{R}) + P_j^{\mathrm{MD}}(\omega;\mathbf{R})\right] & \forall i \neq j, \end{cases} \tag{3.68}$$

where the Purcell factors are defined in the same way as for the ED transition, but with the magnetic dipole transition moment $\hat{\mathbf{m}}^{eg}$ instead.

### 3.7.3 Electric quadrupole transition

Let us now focus on the EQ transition. Since a general electric quadrupole moment involves up to five independent components, it can be expanded with an orthonormal basis of five quadrupoles. To construct this basis, we consider the two different types of quadrupoles sketched in Figure 3.2. In our modified Voigt notation [Tab. 3.2], these quadrupoles are represented by a vector in five dimensions where only the $\mu$-th component is non-zero and equal to $1/\sqrt{2}$ [12]. Note that we could have considered two linear quadrupoles [Fig. 2.8], defined by three diagonal components, instead of the two Type II quadrupoles to construct the basis.

Similarly to the developments made for the ED transition, let us first take the electric quadrupole transition moment along one basis vector, i.e., $\hat{\mathbf{Q}}^{eg} = \hat{\mathbf{e}}_\mu/\sqrt{2}$ with $\mu = 1,\ldots,5$ (i.e., the five quadrupoles illustrated in Fig. 3.2). In this case, using the equation (3.55) of the vacuum normalized EQ transition rate, we define the five Purcell factors $P_\mu^{\mathrm{ED}}$ corresponding to the ratio between the EQ transition rate of an emitter that has its electric quadrupole transition moment along the basis vector $\hat{\mathbf{e}}_\mu$ and the corresponding rate in free space as

$$P_\mu^{\mathrm{EQ}}(\omega;\mathbf{R}) := \frac{1}{2}\frac{20\pi c}{\omega} \mathrm{Im}\, \widetilde{G}_{\mu\mu}^{\mathrm{EQ}}(\omega;\mathbf{R},\mathbf{R}). \tag{3.69}$$

[12] The factor $1/\sqrt{2}$ for the quadrupoles is the normalization factor for quadrupoles that are described by two equal components in absolute value.

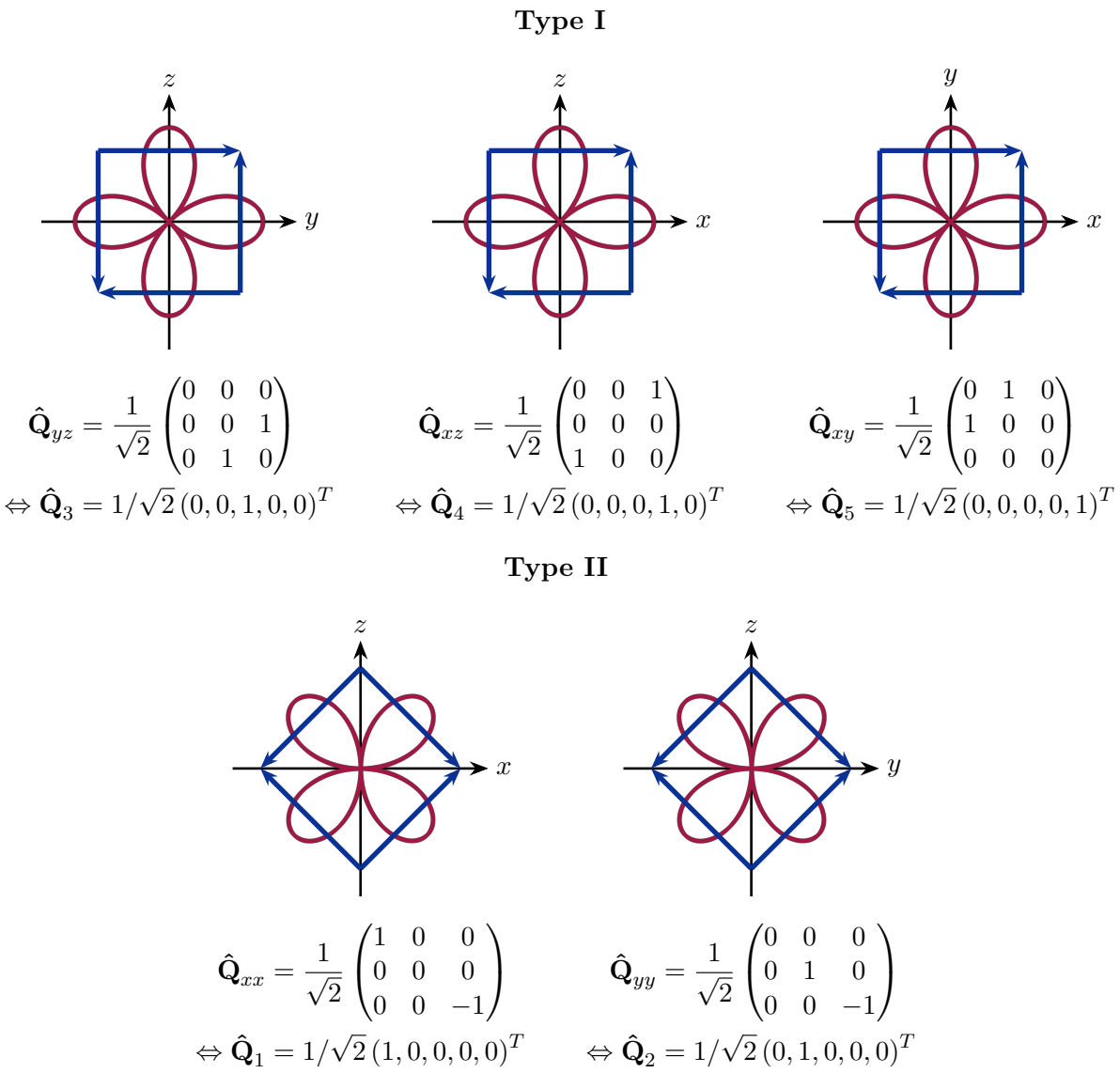


Figure 3.2: Representation of the two considered types of planar quadrupole configurations. Type II differs from type I by a rotation of 45° in the plane and involves only diagonal components, while type I involves solely off-diagonal components. They are represented by means of four dipoles of same norm (blue arrows) and the radiation patterns are sketched in dark red. The modified Voigt notation [Tab. 3.2] is used to represent their tensor by means of a five-dimensional vector.

The previous equation makes a link between the diagonal components of $\mathrm{Im}\,\widetilde{\mathbf{G}}^{\mathrm{EQ}}$ and the Purcell factors $P_\mu^{\mathrm{EQ}}$. To establish a link with the off-diagonal components, let us consider the combinations of the basis quadrupoles[13]:

$$\hat{\mathbf{Q}}^{eg} = \begin{cases} \dfrac{1}{\sqrt{6}}\,(\hat{\mathbf{e}}_\mu + \hat{\mathbf{e}}_\nu) & \text{if } (\mu,\nu) = (1,2) \\ \dfrac{1}{2}\,(\hat{\mathbf{e}}_\mu + \hat{\mathbf{e}}_\nu) & \forall \mu,\nu = 2,3,4,5\ ;\ \mu < \nu, \end{cases} \tag{3.70}$$

where the normalization constant is different according to the considered combination. By using the

[13]Note that all considered quadrupoles need to be normalized and that the quadrupole $\hat{\mathbf{Q}}_{xxyy} = (\hat{\mathbf{Q}}_{xx} + \hat{\mathbf{Q}}_{yy})/\sqrt{3}$ is the linear quadrupole represented by the diagonal matrix $1/\sqrt{6}\,\mathrm{diag}(1,1,-2)$.

normalized moment given above in the equation (3.55) of the EQ transition rate, we get

$$\frac{\Gamma_{\mathrm{EQ}}(\mathbf{R})}{\Gamma_{\mathrm{EQ},0}} = \frac{1}{N}\frac{20\pi c}{\omega_{eg}}\,\mathrm{Im}\left[\widetilde{G}^{\mathrm{EQ}}_{\mu\mu}(\omega_{eg};\mathbf{R},\mathbf{R}) + \widetilde{G}^{\mathrm{EQ}}_{\mu\nu}(\omega_{eg};\mathbf{R},\mathbf{R}) + \widetilde{G}^{\mathrm{EQ}}_{\nu\mu}(\omega_{eg};\mathbf{R},\mathbf{R}) + \widetilde{G}^{\mathrm{EQ}}_{\nu\nu}(\omega_{eg};\mathbf{R},\mathbf{R})\right] \tag{3.71a}$$

$$= \frac{2}{N}\left[P^{\mathrm{EQ}}_{\mu}(\omega_{eg};\mathbf{R}) + P^{\mathrm{EQ}}_{\nu}(\omega_{eg};\mathbf{R}) + \frac{20\pi c}{\omega_{eg}}\,\mathrm{Im}\,\widetilde{G}^{\mathrm{EQ}}_{\mu\nu}(\omega_{eg};\mathbf{R},\mathbf{R})\right], \tag{3.71b}$$

where $N = 6$ for $(\mu,\nu) = (1,2)$ and $N = 4$ otherwise. Moreover, we used the definition of the Purcell factors $P^{\mathrm{EQ}}_{\mu}$ [Eq. (3.69)] as well as the symmetry property of the tensor $\widetilde{\mathbf{G}}^{\mathrm{EQ}}$ [Eq. (3.51)]. Thereby, we have defined 10 Purcell factors $P^{\mathrm{EQ}}_{\mu\nu}$ relative to an emitter that has its electric quadrupole transition moment given by the equation (3.70) (i.e., an equal and linear combination of the basis quadrupoles) as

$$P^{\mathrm{EQ}}_{\mu\nu}(\omega;\mathbf{R}) := \begin{cases} \dfrac{1}{3}\left[P^{\mathrm{EQ}}_{\mu}(\omega;\mathbf{R}) + P^{\mathrm{EQ}}_{\nu}(\omega;\mathbf{R}) + \dfrac{20\pi c}{\omega}\,\mathrm{Im}\,\widetilde{G}^{\mathrm{EQ}}_{\mu\nu}(\omega;\mathbf{R},\mathbf{R})\right] & \text{if } (\mu,\nu) = (1,2) \\ \dfrac{1}{2}\left[P^{\mathrm{EQ}}_{\mu}(\omega;\mathbf{R}) + P^{\mathrm{EQ}}_{\nu}(\omega;\mathbf{R}) + \dfrac{20\pi c}{\omega}\,\mathrm{Im}\,\widetilde{G}^{\mathrm{EQ}}_{\mu\nu}(\omega;\mathbf{R},\mathbf{R})\right] & \forall \mu,\nu = 2,3,4,5\ ;\ \mu < \nu. \end{cases} \tag{3.72}$$

As all components of $\mathrm{Im}\,\widetilde{G}^{\mathrm{EQ}}$ have been expressed as a function of Purcell factors, we can now rewrite the equation (3.55) as

$$\frac{\Gamma_{\mathrm{EQ}}(\mathbf{R})}{\Gamma_{\mathrm{EQ},0}} = \hat{\mathbf{Q}}^{eg}\cdot\mathbf{F}^{\mathrm{EQ}}(\omega_{eg};\mathbf{R})\cdot\left(\hat{\mathbf{Q}}^{eg}\right)^{*} = \sum_{\mu,\nu=1}^{5}\hat{Q}^{eg}_{\mu}\left(\hat{Q}^{eg}_{\nu}\right)^{*}F^{\mathrm{EQ}}_{\mu\nu}(\omega_{eg};\mathbf{R}), \tag{3.73}$$

where the components of the tensor $\mathbf{F}^{\mathrm{EQ}}$ are defined

$$F^{\mathrm{EQ}}_{\mu\nu}(\omega;\mathbf{R}) := \frac{20\pi c}{\omega}\mathrm{Im}\,\widetilde{G}^{\mathrm{EQ}}_{\mu\nu}(\omega;\mathbf{R},\mathbf{R}), \tag{3.74}$$

and linked to the Purcell factors by [Eqs. (3.69) and (3.72)]:

$$F^{\mathrm{EQ}}_{\mu\nu}(\omega;\mathbf{R}) = \begin{cases} 2P^{\mathrm{EQ}}_{\mu}(\omega;\mathbf{R}) & \forall \mu = \nu \\ 3P^{\mathrm{EQ}}_{\mu\nu}(\omega;\mathbf{R}) - P^{\mathrm{EQ}}_{\mu}(\omega;\mathbf{R}) - P^{\mathrm{EQ}}_{\nu}(\omega;\mathbf{R}) & \text{if } (\mu,\nu) = (1,2) \\ 2P^{\mathrm{EQ}}_{\mu\nu}(\omega;\mathbf{R}) - P^{\mathrm{EQ}}_{\mu}(\omega;\mathbf{R}) - P^{\mathrm{EQ}}_{\nu}(\omega;\mathbf{R}) & \text{else.} \end{cases} \tag{3.75}$$

Since the tensor $\mathrm{Im}\,\widetilde{G}^{\mathrm{EQ}}$ is symmetric, the tensor $\mathbf{F}^{\mathrm{EQ}}$ is too. Thus, we need to calculate in the most general case these 15 Purcell factors to get the EQ transition rate. For example, in a Cartesian basis we need to calculate these 15 components:

$$\left\{F^{\mathrm{EQ}}_{\mu\nu}\right\}_{\mu\leq\nu}, \tag{3.76}$$

and thus these 15 Purcell factors:

$$\left\{P^{\mathrm{EQ}}_{\mu}\right\} \cup \left\{P^{\mathrm{EQ}}_{\mu\nu}\right\}, \tag{3.77}$$

where the indices $\mu,\nu = 1,\ldots,5$, with $\mu < \nu$, correspond to the indices $\{xx, yy, yz, xz, xy\}$ [Fig. 3.2]. In the case where the system exhibits an azimuthal symmetry, there is an equivalence between the

$X$ and $Y$ direction, As a result, some components are equal or zero:

$$\begin{cases} P_2^{\mathrm{EQ}} = P_1^{\mathrm{EQ}} \Rightarrow F_{22}^{\mathrm{EQ}} = F_{11}^{\mathrm{EQ}} & \text{(3.78a)} \\ P_3^{\mathrm{EQ}} = P_4^{\mathrm{EQ}} \Rightarrow F_{33}^{\mathrm{EQ}} = F_{44}^{\mathrm{EQ}} & \text{(3.78b)} \\ P_{12}^{\mathrm{EQ}} = P_1^{\mathrm{EQ}} \Rightarrow F_{12}^{\mathrm{EQ}} := 3P_{12}^{\mathrm{EQ}} - P_1^{\mathrm{EQ}} - P_2^{\mathrm{EQ}} = P_1^{\mathrm{EQ}} = \dfrac{F_{11}^{\mathrm{EQ}}}{2} & \text{(3.78c)} \\ P_{13}^{\mathrm{EQ}} = P_{14}^{\mathrm{EQ}} \Rightarrow F_{13}^{\mathrm{EQ}} := 2P_{13}^{\mathrm{EQ}} - P_1^{\mathrm{EQ}} - P_3^{\mathrm{EQ}} = F_{14}^{\mathrm{EQ}} & \text{(3.78d)} \\ P_{23}^{\mathrm{EQ}} = P_{14}^{\mathrm{EQ}} \Rightarrow F_{23}^{\mathrm{EQ}} = F_{14}^{\mathrm{EQ}} & \text{(3.78e)} \\ P_{24}^{\mathrm{EQ}} = P_{14}^{\mathrm{EQ}} \Rightarrow F_{24}^{\mathrm{EQ}} = F_{14}^{\mathrm{EQ}} & \text{(3.78f)} \\ P_{25}^{\mathrm{EQ}} = P_{15}^{\mathrm{EQ}} \Rightarrow F_{25}^{\mathrm{EQ}} = F_{15}^{\mathrm{EQ}} & \text{(3.78g)} \\ P_{34}^{\mathrm{EQ}} = P_4^{\mathrm{EQ}} \Rightarrow F_{34}^{\mathrm{EQ}} := 2P_{34}^{\mathrm{EQ}} - P_3^{\mathrm{EQ}} - P_4^{\mathrm{EQ}} = 0 & \text{(3.78h)} \\ P_{35}^{\mathrm{EQ}} = P_{45}^{\mathrm{EQ}} \Rightarrow F_{35}^{\mathrm{EQ}} = F_{45}^{\mathrm{EQ}}. & \text{(3.78i)} \end{cases}$$

As a result, the number of components of $\mathbf{F}^{\mathrm{EQ}}$ and of Purcell factors to calculate is reduced to six:

$$\left\{F_{11}^{\mathrm{EQ}}, F_{44}^{\mathrm{EQ}}, F_{55}^{\mathrm{EQ}}, F_{14}^{\mathrm{EQ}}, F_{15}^{\mathrm{EQ}}, F_{45}^{\mathrm{EQ}}\right\} = \left\{F_{xxxx}^{\mathrm{EQ}}, F_{xzxz}^{\mathrm{EQ}}, F_{xyxy}^{\mathrm{EQ}}, F_{xxxz}^{\mathrm{EQ}}, F_{xxxy}^{\mathrm{EQ}}, F_{xzxy}^{\mathrm{EQ}}\right\}, \tag{3.79a}$$

$$\left\{P_1^{\mathrm{EQ}}, P_4^{\mathrm{EQ}}, P_5^{\mathrm{EQ}}\, P_{14}^{\mathrm{EQ}}, P_{15}^{\mathrm{EQ}}, P_{45}^{\mathrm{EQ}}\right\} = \left\{P_{xx}^{\mathrm{EQ}}, P_{xz}^{\mathrm{EQ}}, P_{xy}^{\mathrm{EQ}}, P_{xxxz}^{\mathrm{EQ}}, P_{xxxy}^{\mathrm{EQ}}, P_{xzxy}^{\mathrm{EQ}}\right\}. \tag{3.79b}$$

Furthermore, by choosing a basis vector aligned with the electric quadrupole transition moment of the emitter, there is only one Purcell factor to calculate. In free space, all Purcell factors tend towards one and so $\mathbf{F}^{\mathrm{EQ}}$ is given by

$$F_{\mu\nu}^{\mathrm{EQ}} = \begin{cases} 2 & \forall \mu = \nu \\ 1 & \text{if } (\mu,\nu) = (1,2) \\ 0 & \text{else,} \end{cases} \tag{3.80}$$

and thereby equation (3.73) gives $\Gamma_{\mathrm{EQ}} = \Gamma_{\mathrm{EQ},0}$.

### 3.7.4 Interference term

To make the link between the term describing the interference between the ED and EQ transitions and the Purcell factors, let us consider a quantum emitter having simultaneously an ED transition and an EQ transition, described respectively by the transition moments $\mathbf{d}^{eg}$ and $\mathbf{Q}^{eg}$. In this case, its transition rate is given by the three following contributions [Eq. (3.15)]:

$$\Gamma_{\mathrm{ED+EQ}}(\mathbf{R}) = \Gamma_{\mathrm{ED}}(\mathbf{R}) + \Gamma_{\mathrm{EQ}}(\mathbf{R}) + \Gamma_{\mathrm{ED}\cap\mathrm{EQ}}(\mathbf{R}), \tag{3.81}$$

where the ED and EQ contributions have been written above as a function of the one-Purcell factors [Eqs. (3.59) and (3.73)]. In vacuum, there is no interference [2] and thus $\Gamma_{\mathrm{ED+EQ},0} = \Gamma_{\mathrm{ED},0} + \Gamma_{\mathrm{EQ},0}$.

Let us introduce the normalized vacuum transition rates to use the equations we have derived:

$$(\Gamma_{\mathrm{ED},0} + \Gamma_{\mathrm{EQ},0}) \frac{\Gamma_{\mathrm{ED+EQ}}(\mathbf{R})}{\Gamma_{\mathrm{ED},0} + \Gamma_{\mathrm{EQ},0}} = \Gamma_{\mathrm{ED},0} \frac{\Gamma_{\mathrm{ED}}(\mathbf{R})}{\Gamma_{\mathrm{ED},0}} + \Gamma_{\mathrm{EQ},0} \frac{\Gamma_{\mathrm{EQ}}(\mathbf{R})}{\Gamma_{\mathrm{EQ},0}} + \sqrt{\Gamma_{\mathrm{ED},0}\,\Gamma_{\mathrm{EQ},0}} \frac{\Gamma_{\mathrm{ED}\cap\mathrm{EQ}}(\mathbf{R})}{\sqrt{\Gamma_{\mathrm{ED},0}\,\Gamma_{\mathrm{EQ},0}}}. \tag{3.82}$$

As previously, let us take $\hat{\mathbf{d}}^{eg} = \hat{\mathbf{e}}_i$ and $\hat{\mathbf{Q}}^{eg} = \hat{\mathbf{e}}_\mu/\sqrt{2}$ (with $i = 1,2,3$ and $\mu = 1,\ldots,5$). In this case,

using the vacuum normalized equations (3.59), (3.73), and (3.56) for the ED, EQ, and interference contributions, the right-hand side of the equation (3.82) is rewritten as

$$(\Gamma_{\mathrm{ED},0}+\Gamma_{\mathrm{EQ},0})\,\frac{\Gamma_{\mathrm{ED+EQ}}(\mathbf{R})}{\Gamma_{\mathrm{ED},0}+\Gamma_{\mathrm{EQ},0}} = \Gamma_{\mathrm{ED},0}\,P_i^{\mathrm{ED}}(\omega_{eg};\mathbf{R}) + \Gamma_{\mathrm{EQ},0}\,P_\mu^{\mathrm{EQ}}(\omega_{eg};\mathbf{R}) + 2\,\sqrt{\Gamma_{\mathrm{ED},0}\,\Gamma_{\mathrm{EQ},0}}\,\frac{1}{\sqrt{2}}\,\frac{2\sqrt{30}\pi c}{\omega_{eg}}\,\mathrm{Im}\,\widetilde{G}_{i\mu}^{\mathrm{ED}\cap\mathrm{EQ}}(\omega_{eg};\mathbf{R},\mathbf{R}). \tag{3.83}$$

By definition, the fraction in the left-hand side is the Purcell factor $P_{i\mu}^{\mathrm{ED+EQ}}$ related to the superposition of an electric dipole aligned along $\hat{\mathbf{e}}_i$ and of an electric quadrupole aligned along $\hat{\mathbf{e}}_\mu$:

$$(\Gamma_{\mathrm{ED},0}+\Gamma_{\mathrm{EQ},0})\,P_{i\mu}^{\mathrm{ED+EQ}}(\omega_{eg};\mathbf{R}) = \Gamma_{\mathrm{ED},0}\,P_i^{\mathrm{ED}}(\omega_{eg};\mathbf{R}) + \Gamma_{\mathrm{EQ},0}\,P_\mu^{\mathrm{EQ}}(\omega_{eg};\mathbf{R}) + 2\,\sqrt{\Gamma_{\mathrm{ED},0}\,\Gamma_{\mathrm{EQ},0}}\,\frac{1}{\sqrt{2}}\,F_{i\mu}^{\mathrm{ED}\cap\mathrm{EQ}}(\omega_{eg};\mathbf{R}), \tag{3.84}$$

where we define the tensor $\mathbf{F}^{\mathrm{ED}\cap\mathrm{EQ}}$ as

$$\mathbf{F}^{\mathrm{ED}\cap\mathrm{EQ}}(\omega;\mathbf{R}) := \frac{2\sqrt{30}\pi c}{\omega}\,\mathrm{Im}\,\widetilde{\mathbf{G}}^{\mathrm{ED}\cap\mathrm{EQ}}(\omega;\mathbf{R},\mathbf{R}). \tag{3.85}$$

The equation (3.84) establishes the link between the Purcell factors and $\widetilde{\mathbf{G}}^{\mathrm{ED}\cap\mathrm{EQ}}$. These factors can be calculated via the power emitted by classical point sources [Eqs. (2.34), (2.35), and (2.36)]:

$$P_i^{\mathrm{ED}}(\omega;\mathbf{R}) = \frac{W_i^{\mathrm{ED}}(\omega;\mathbf{R})}{W_0^{\mathrm{ED}}(\omega)}, \tag{3.86a}$$

$$P_\mu^{\mathrm{EQ}}(\omega;\mathbf{R}) = \frac{W_\mu^{\mathrm{EQ}}(\omega;\mathbf{R})}{W_0^{\mathrm{EQ}}(\omega)}, \tag{3.86b}$$

$$P_{i\mu}^{\mathrm{ED+EQ}}(\omega;\mathbf{R}) = \frac{W_{i\mu}^{\mathrm{ED+EQ}}(\omega;\mathbf{R})}{W_0^{\mathrm{ED}}(\omega)+W_0^{\mathrm{EQ}}(\omega)} = \frac{W_i^{\mathrm{ED}}(\omega;\mathbf{R})+W_\mu^{\mathrm{EQ}}(\omega;\mathbf{R})+W_{i\mu}^{\mathrm{ED}\cap\mathrm{EQ}}(\omega;\mathbf{R})}{W_0^{\mathrm{ED}}(\omega)+W_0^{\mathrm{EQ}}(\omega)}. \tag{3.86c}$$

In these equations, the subscript 0 indicates quantities that refer to vacuum whereas $W_i^{\mathrm{ED}}$, $W_\mu^{\mathrm{EQ}}$, and $W_{i\mu}^{\mathrm{ED+EQ}}$ denote the power emitted by a classical dipole aligned along $\hat{\mathbf{e}}_i$, by a classical quadrupole aligned along $\hat{\mathbf{e}}_\mu$, and by the superposition of both sources, respectively. Furthermore, $W_{i\mu}^{\mathrm{ED+EQ}}$ is decomposed into three contributions where $W_{i\mu}^{\mathrm{ED}\cap\mathrm{EQ}}$ represents the interference term between the two classical sources. As a reminder, there is no interference in vacuum. Replacing the Purcell factor expressions into the equation (3.84) gives a system of three equations:

$$\begin{cases} (\Gamma_{\mathrm{ED},0}+\Gamma_{\mathrm{EQ},0})\,\dfrac{W_i^{\mathrm{ED}}}{W_0^{\mathrm{ED}}+W_0^{\mathrm{EQ}}} = \Gamma_{\mathrm{ED},0}\,\dfrac{W_i^{\mathrm{ED}}}{W_0^{\mathrm{ED}}} & \text{(3.87a)} \\ (\Gamma_{\mathrm{ED},0}+\Gamma_{\mathrm{EQ},0})\,\dfrac{W_\mu^{\mathrm{EQ}}}{W_0^{\mathrm{ED}}+W_0^{\mathrm{EQ}}} = \Gamma_{\mathrm{EQ},0}\,\dfrac{W_\mu^{\mathrm{EQ}}}{W_0^{\mathrm{EQ}}} & \text{(3.87b)} \\ (\Gamma_{\mathrm{ED},0}+\Gamma_{\mathrm{EQ},0})\,\dfrac{W_{i\mu}^{\mathrm{ED}\cap\mathrm{EQ}}}{W_0^{\mathrm{ED}}+W_0^{\mathrm{EQ}}} = \sqrt{2}\,\sqrt{\Gamma_{\mathrm{EQ},0}\,\Gamma_{\mathrm{EQ},0}}\,F_{i\mu}^{\mathrm{ED}\cap\mathrm{EQ}}, & \text{(3.87c)} \end{cases}$$

where the dependencies have been omitted. Solving the first or the second equation gives the relation:

$$\frac{W_0^{\mathrm{EQ}}(\omega_{eg})}{W_0^{\mathrm{ED}}(\omega_{eg})} = \frac{\Gamma_{\mathrm{EQ},0}}{\Gamma_{\mathrm{ED},0}}. \tag{3.88}$$

Indeed, the power emitted by the classical multipolar sources representing the multipolar transition moments of the emitter need to be set according to the multipolar transition rates in vacuum.

Now, by using equation (3.88) in the equation (3.87c), we obtain an expression for the components of the tensor $\mathbf{F}^{\mathrm{ED}\cap\mathrm{EQ}}$ (and so for the tensor $\widetilde{\mathbf{G}}^{\mathrm{ED}\cap\mathrm{EQ}}$ [Eq. (3.85)]):

$$F_{i\mu}^{\mathrm{ED}\cap\mathrm{EQ}}(\omega;\mathbf{R},\mathbf{R}) = \frac{W_{i\mu}^{\mathrm{ED}\cap\mathrm{EQ}}(\omega;\mathbf{R})}{\sqrt{2\,W_0^{\mathrm{ED}}(\omega)\,W_0^{\mathrm{EQ}}(\omega)}}, \tag{3.89}$$

which can be written using equations (3.86) as a function of the Purcell factors:

$$\sqrt{\Gamma_{\mathrm{ED},0}\,\Gamma_{\mathrm{EQ},0}}\,F_{i\mu}^{\mathrm{ED}\cap\mathrm{EQ}}(\omega;\mathbf{R}) = \frac{1}{\sqrt{2}}\left[(\Gamma_{\mathrm{ED},0}+\Gamma_{\mathrm{EQ},0})\,P_{i\mu}^{\mathrm{ED}+\mathrm{EQ}} - \Gamma_{\mathrm{ED},0}\,P_i^{\mathrm{ED}} - \Gamma_{\mathrm{EQ},0}\,P_\mu^{\mathrm{EQ}}\right], \tag{3.90}$$

where the dependencies have been omitted. Therefore, we have rewritten the interference term [Eq. (3.56)] as

$$\frac{\Gamma_{\mathrm{ED}\cap\mathrm{EQ}}(\mathbf{R})}{\sqrt{\Gamma_{\mathrm{ED},0}\,\Gamma_{\mathrm{EQ},0}}} = 2\,\hat{\mathbf{d}}^{eg}\cdot\mathbf{F}^{\mathrm{ED}\cap\mathrm{EQ}}(\omega_{eg};\mathbf{R})\cdot\left(\hat{\mathbf{Q}}^{eg}\right)^{*} = 2\sum_{i=1}^{3}\sum_{\mu=1}^{5}\hat{d}_i^{eg}\left(\hat{Q}_\mu^{eg}\right)^{*}F_{i\mu}^{\mathrm{ED}\cap\mathrm{EQ}}(\omega_{eg};\mathbf{R}), \tag{3.91}$$

where the real part is implied and where the tensor $\mathbf{F}^{\mathrm{ED}\cap\mathrm{EQ}}$ is expressed as a function of the Purcell factors [Eq. (3.90)], which can be calculated classically via the equations (3.86). Note that in vacuum, all Purcell factors tend towards one and the tensor $\mathbf{F}^{\mathrm{ED}\cap\mathrm{EQ}}$ tends towards 0, leading to an interference term equal to zero.

To calculate the 15 components $F_{i\mu}^{\mathrm{ED}\cap\mathrm{EQ}}$ [Eq. (3.90)], one needs to calculate an additional set of 15 Purcell factors: $\{P_{i\mu}^{\mathrm{ED}+\mathrm{EQ}}\}$ (the 3 factors $P_i^{\mathrm{ED}}$ and the 5 factors $P_\mu^{\mathrm{EQ}}$ are already calculated when calculating the ED and EQ transition rates [Eqs. (3.61), and (3.75)]). These factors must be calculated by respecting the equation (3.88), ensuring adequate weighting of multipolar sources. Consequently, vacuum rates are required to calculate interference effects.

In the case where the system exhibits an azimuthal symmetry, there is an equivalence between the $X$ and $Y$ direction. As a result, some components are equal ($i = 1, 2, 3$ corresponds to $x$, $y$ and $z$, while $\mu = 1, \ldots, 5$ corresponds to $xx$, $yy$, $yz$, $xz$, $xy$):

$$\begin{cases} \forall\mu = 1,\ldots,5 \quad F_{2\mu}^{\mathrm{ED}\cap\mathrm{EQ}} = F_{1\mu}^{\mathrm{ED}\cap\mathrm{EQ}} & \text{(3.92a)} \\ \forall i = 1,3, \quad F_{i2}^{\mathrm{ED}\cap\mathrm{EQ}} = F_{i1}^{\mathrm{ED}\cap\mathrm{EQ}} & \text{(3.92b)} \\ \forall i = 1,3, \quad F_{i3}^{\mathrm{ED}\cap\mathrm{EQ}} = F_{i4}^{\mathrm{ED}\cap\mathrm{EQ}}. & \text{(3.92c)} \end{cases}$$

Consequently, the number of components of $\mathbf{F}^{\mathrm{ED}\cap\mathrm{EQ}}$ and of Purcell factors to calculate is reduced to six:

$$\left\{F_{11}^{\mathrm{ED}}, F_{14}^{\mathrm{ED}}, F_{15}^{\mathrm{ED}}, F_{31}^{\mathrm{ED}}, F_{34}^{\mathrm{ED}}, F_{35}^{\mathrm{ED}}, \right\}, \tag{3.93a}$$

$$\left\{P_{11}^{\mathrm{ED}}, P_{14}^{\mathrm{ED}}, P_{15}^{\mathrm{ED}}, P_{31}^{\mathrm{ED}}, P_{34}^{\mathrm{ED}}, P_{35}^{\mathrm{ED}}, \right\}. \tag{3.93b}$$

Again, by considering bases where one basis vector is aligned with the multipolar moments of the emitter, there is only one additional Purcell factors to calculate the interference term $\Gamma_{\mathrm{ED}\cap\mathrm{EQ}}$.

## 3.8 Discussion

Throughout this chapter, we derived equations that are expressed via the dyadic Green's function [Eqs. (3.32e), (3.38b), and (3.55)] for the calculation of the Purcell effect of an arbitrary quantum emitter in an arbitrary photonic environment, by taking into account the interaction up the electric quadrupolar order. Going beyond the electric dipole approximation is relevant for large emitters [50–53] and in structures confining light at the nanoscale [28], such as plasmonic nanostructures [22, 28, 29, 50, 55–62]. We have also included the calculation of the interference between the ED and EQ emission channels of the OPSE [Eq. (3.56)], and similar equations can be derived for the other interference terms including the MD transition.

In the derived equations [Eqs. (3.32e), (3.38b), (3.55), and (3.56)], the contribution of the electronic structure of the emitter and of the photonic environment are decoupled, allowing their separate calculation. Indeed, each equation involves two different tensors. On the one hand, there is the normalized multipolar transition moment that depends only on the electronic structure of the emitter [2]. On the other hand, there is the dyadic Green's function that depends only on the photonic environment [30].

Moreover, the modification of the multipolar transition rates and the interference effects can be calculated classically by considering classical multipolar point sources in electromagnetic simulations [Sec. 2.5.2], thus allowing to consider arbitrarily shaped nanostructures. In addition, the Purcell factors can be decomposed into a radiative (emission of photons in the far-field) and a non-radiative part (absorption by the environment), allowing the separate calculation of these two channels, and so of the quantum efficiency [30]. We have also decomposed the Green's function into Purcell bases [Eqs. (3.59), (3.66), (3.73), and (3.91)], which will be useful in the chapter dedicated to the two-photon spontaneous emission process.

Since the derived equations in this chapter are based on Fermi's golden rule, they are limited to the weak coupling regime. Indeed, the perturbation theory is expected to fail when the ratio between the transition rate $\Gamma$ and the transition angular frequency $\omega_{eg}$ approaches 1 [22, 89]. Also, for the extreme cases of large emitters placed very close to a nanostructure ($\approx 1$ nm distance), their reduction to a point may require even higher orders than the quadrupolar order [53].

## 3.9 Summary

In this chapter, we presented a complete treatment of the OPSE process where the interaction Hamiltonian is taken up to the electric quadrupolar order by making no assumptions about the quantum emitter and the environment, including interference effects between the multipolar pathways. Concretely, the derivation as a function of the field modes and via the Green's function for the MD and EQ transitions as well as for the interference terms are in part personal developments, but some of these equations can be found in the literature [23, 51]. Furthermore, the introduction of a modified Voigt notation to simplify the equations relative to the EQ transition and the decomposition of the multipolar contributions to the OPSE into Purcell factor bases are personal developments.

Adopting a perturbative approach with Fermi's golden rule [Eq. (3.1)], and by considering the electric dipole (ED), magnetic dipole (MD) and electric quadrupole (EQ) interactions in the multipolar expansion of the interaction Hamiltonian [Eq. (3.4)], we found that the overall one-photon

spontaneous emission rate (OPSE) is given by six multipolar contributions [Eq. (3.15)]:

$$\Gamma_{\text{tot}} = \Gamma_{\text{ED}} + \Gamma_{\text{MD}} + \Gamma_{\text{EQ}} + \Gamma_{\text{ED}\cap\text{MD}} + \Gamma_{\text{ED}\cap\text{EQ}} + \Gamma_{\text{MD}\cap\text{EQ}}. \tag{3.94}$$

These contributions are the ED, MD, EQ transition rates and the interferences with each other, respectively. The interference terms can be either positive or negative, potentially leading to an increase or a decrease of the overall transitions rate. Note that depending on the quantum emitter, the ED, MD, EQ transitions may not occur simultaneously between two given states. In the case where the magnetic interaction is discarded, the overall OPSE is given by the three following multipolar contributions [Eq. (3.81)]:

$$\Gamma_{\text{ED+EQ}} = \Gamma_{\text{ED}} + \Gamma_{\text{EQ}} + \Gamma_{\text{ED}\cap\text{EQ}}. \tag{3.95}$$

Next, by considering plane waves for the field modes, we derived the vacuum OPSE rates [Eqs. (3.29)]:

$$\Gamma_{\text{ED},0} = \frac{\omega_{eg}^3}{3\pi\varepsilon_0\hbar c^3} \left\|\mathbf{d}^{eg}\right\|^2, \tag{3.96a}$$

$$\Gamma_{\text{MD},0} = \frac{\omega_{eg}^3}{3\pi\varepsilon_0\hbar c^5} \left\|\mathbf{m}^{eg}\right\|^2, \tag{3.96b}$$

$$\Gamma_{\text{EQ},0} = \frac{\omega_{eg}^5}{10\pi\varepsilon_0\hbar c^5} \left\|\mathbf{Q}^{eg}\right\|^2. \tag{3.96c}$$

As the spontaneous emission takes place in vacuum, there are no interferences between multipolar transitions. Afterwards, we introduced a modified Voigt notation [Eq. (3.54) and Tab. 3.2] to simplify equations involving the transition moment $\mathbf{Q}^{eg}$ by keeping only its 5 independent elements ($\mathbf{Q}^{eg}$ is traceless and symmetric) as a vector in five dimensions:

$$\left(Q_{ij}^{\text{eg}}\right)_{3\times3} \to \left(Q_{11}^{\text{eg}}, Q_{22}^{\text{eg}}, Q_{23}^{\text{eg}}, Q_{13}^{\text{eg}}, Q_{12}^{\text{eg}}\right)^T \to \left(Q_{\mu}^{\text{eg}}\right)_5. \tag{3.97}$$

Using this notation, all first-order transition moments are represented by tensors of rank equal to the order of the transition.

Then, we expressed the multipolar contributions via the dyadic Green's function, and then normalized them with respect to vacuum [Eqs. (3.44), (3.55), and (3.56)]:

$$\frac{\Gamma_{\text{ED}}(\mathbf{R})}{\Gamma_{\text{ED},0}} = \frac{6\pi c}{\omega_{eg}} \hat{\mathbf{d}}^{eg} \cdot \operatorname{Im}\mathbf{G}(\omega_{eg};\mathbf{R},\mathbf{R}) \cdot \left(\hat{\mathbf{d}}^{eg}\right)^*, \tag{3.98a}$$

$$\frac{\Gamma_{\text{MD}}(\mathbf{R})}{\Gamma_{\text{ED},0}} = \frac{6\pi c}{\omega_{eg}} \hat{\mathbf{m}}^{eg} \cdot \operatorname{Im}\mathbf{G}^{\text{MD}}(\omega_{eg};\mathbf{R},\mathbf{R}) \cdot (\hat{\mathbf{m}}^{eg})^*, \tag{3.98b}$$

$$\frac{\Gamma_{\text{EQ}}(\mathbf{R})}{\Gamma_{\text{EQ},0}} = \frac{20\pi c}{\omega_{eg}} \hat{\mathbf{Q}}^{eg} \cdot \operatorname{Im}\widetilde{\mathbf{G}}^{\text{EQ}}(\omega_{eg};\mathbf{R},\mathbf{R}) \cdot \left(\hat{\mathbf{Q}}^{eg}\right)^*, \tag{3.98c}$$

$$\frac{\Gamma_{\text{ED}\cap\text{EQ}}(\mathbf{R})}{\sqrt{\Gamma_{\text{ED},0}\,\Gamma_{\text{EQ},0}}} = 2\,\frac{2\sqrt{30}\pi c}{\omega_{eg}} \hat{\mathbf{d}}^{eg} \cdot \operatorname{Im}\widetilde{\mathbf{G}}^{\text{ED}\cap\text{EQ}}(\omega_{eg};\mathbf{R},\mathbf{R}) \cdot \left(\hat{\mathbf{Q}}^{eg}\right)^*, \tag{3.98d}$$

where the real part is implied for the last equation, where the caret denotes normalized tensors and where the dot product involving $\mathbf{Q}^{eg}$ denotes the scalar product between tensors in five dimensions [Eqs. (3.55) and (3.56)]. In these equations, the contribution of the environment and of the emitter are decoupled, allowing their separate calculation. The tensors $\mathbf{G}^{\text{MD}}$, $\widetilde{\mathbf{G}}^{\text{EQ}}$, and $\widetilde{\mathbf{G}}^{\text{ED}\cap\text{EQ}}$ are ex-

pressed as a function of the derivatives of the Green's function $\mathbf{G}$ [Eqs. (3.37), (3.40), (3.43), (3.51), and (3.53)]. By definition, the three first equations represent the Purcell factors of each multipolar transition. Moreover, these equations are identical with those obtained for the modification of the power emitter by classical point sources in Section 2.5.2, highlighting that the Purcell effect (i.e., the modification of transition rates due to the environment) can be computed classically via electromagnetic simulations with multipolar point sources whose their moments have the same orientation as those describing the multipolar transitions moments of the quantum emitter [Eq. (2.34)]. In addition, the interference effects between multipolar pathways can be computed via interference between classical sources [Eq. (2.36)], but their calculation requires the knowledge of vacuum rates to weight accordingly the power emitted by the classical sources [Eq. (3.88)].

Finally, we performed a decomposition in Purcell factor bases [Eqs. (3.59), (3.66), (3.73), and (3.91)]:

$$\frac{\Gamma_{\mathrm{ED}}(\mathbf{R})}{\Gamma_{\mathrm{ED},0}} = \hat{\mathbf{d}}^{eg} \cdot \mathbf{F}^{\mathrm{ED}}(\omega_{eg};\mathbf{R}) \cdot \left(\hat{\mathbf{d}}^{eg}\right)^{*} = \sum_{i,j=1}^{3} \hat{d}_i^{eg} \left(\hat{d}_j^{eg}\right)^{*} F_{ij}^{\mathrm{ED}}(\omega_{eg};\mathbf{R}), \tag{3.99a}$$

$$\frac{\Gamma_{\mathrm{MD}}(\mathbf{R})}{\Gamma_{\mathrm{ED},0}} = \hat{\mathbf{m}}^{eg} \cdot \mathbf{F}^{\mathrm{MD}}(\omega_{eg};\mathbf{R}) \cdot (\hat{\mathbf{m}}^{eg})^{*} = \sum_{i,j=1}^{3} \hat{m}_i^{eg} \left(\hat{m}_j^{eg}\right)^{*} F_{ij}^{\mathrm{MD}}(\omega_{eg};\mathbf{R}), \tag{3.99b}$$

$$\frac{\Gamma_{\mathrm{EQ}}(\mathbf{R})}{\Gamma_{\mathrm{EQ},0}} = \hat{\mathbf{Q}}^{eg} \cdot \mathbf{F}^{\mathrm{EQ}}(\omega_{eg};\mathbf{R}) \cdot \left(\hat{\mathbf{Q}}^{eg}\right)^{*} = \sum_{\mu,\nu=1}^{5} \hat{Q}_{\mu}^{eg} \left(\hat{Q}_{\nu}^{eg}\right)^{*} F_{\mu\nu}^{\mathrm{EQ}}(\omega_{eg};\mathbf{R}), \tag{3.99c}$$

$$\frac{\Gamma_{\mathrm{ED}\cap\mathrm{EQ}}(\mathbf{R})}{\sqrt{\Gamma_{\mathrm{ED},0}\,\Gamma_{\mathrm{EQ},0}}} = 2\,\hat{\mathbf{d}}^{eg} \cdot \mathbf{F}^{\mathrm{ED}\cap\mathrm{EQ}}(\omega_{eg};\mathbf{R}) \cdot \left(\hat{\mathbf{Q}}^{eg}\right)^{*} = 2\sum_{i=1}^{3}\sum_{\mu=1}^{5} \hat{d}_i^{eg} \left(\hat{Q}_{\mu}^{eg}\right)^{*} F_{i\mu}^{\mathrm{ED}\cap\mathrm{EQ}}(\omega_{eg};\mathbf{R}), \tag{3.99d}$$

where the real part is implied for the last equation. The tensors $\mathbf{F}^{\mathrm{ED}}$, $\mathbf{F}^{\mathrm{MD}}$, $\mathbf{F}^{\mathrm{EQ}}$, and $\mathbf{F}^{\mathrm{ED}\cap\mathrm{EQ}}$ are defined from the Green's functions [Eqs. (3.60), (3.67), (3.74), and (3.85)] and are expressed as a function of the Purcell factors. For MO $\in$ {ED, MD} [Eqs. (3.61) and (3.68)]:

$$F_{ij}^{\mathrm{MO}}(\omega;\mathbf{R}) = \begin{cases} P_i^{\mathrm{MO}}(\omega;\mathbf{R}) & \forall i = j \\ P_{ij}^{\mathrm{MO}}(\omega;\mathbf{R}) - \dfrac{1}{2}\left[P_i^{\mathrm{MO}}(\omega;\mathbf{R}) + P_j^{\mathrm{MO}}(\omega;\mathbf{R})\right] & \forall i \neq j, \end{cases} \tag{3.100}$$

where $P_i^{\mathrm{MO}}$ and $P_{ij}^{\mathrm{MO}}$ denote Purcell factors relative to a dipole (electric or magnetic) along $\hat{\mathbf{e}}_i$ and $\hat{\mathbf{e}}_i + \hat{\mathbf{e}}_j$, respectively. For the EQ transition [Eq. (3.75)]:

$$F_{\mu\nu}^{\mathrm{EQ}}(\omega;\mathbf{R}) = \begin{cases} 2P_{\mu}^{\mathrm{EQ}}(\omega;\mathbf{R}) & \forall \mu = \nu \\ 3P_{\mu\nu}^{\mathrm{EQ}}(\omega;\mathbf{R}) - P_{\mu}^{\mathrm{EQ}}(\omega;\mathbf{R}) - P_{\nu}^{\mathrm{EQ}}(\omega;\mathbf{R}) & \text{if } (\mu,\nu) = (1,2) \\ 2P_{\mu\nu}^{\mathrm{EQ}}(\omega;\mathbf{R}) - P_{\mu}^{\mathrm{EQ}}(\omega;\mathbf{R}) - P_{\nu}^{\mathrm{EQ}}(\omega;\mathbf{R}) & \text{else,} \end{cases} \tag{3.101}$$

where $P_{\mu}^{\mathrm{EQ}}$ and $P_{\mu\nu}^{\mathrm{EQ}}$ denote Purcell factors relative to an electric quadrupole described by one of the five basis quadrupole [Fig. 3.2] and relative to the combination of two basis quadrupoles [Eq. (3.70)], respectively. For the interference term [Eq. (3.90)]:

$$\sqrt{\Gamma_{\mathrm{ED},0}\,\Gamma_{\mathrm{EQ},0}}\,F_{i\mu}^{\mathrm{ED}\cap\mathrm{EQ}}(\omega;\mathbf{R}) = \frac{1}{\sqrt{2}}\left[(\Gamma_{\mathrm{ED},0} + \Gamma_{\mathrm{EQ},0})\,P_{i\mu}^{\mathrm{ED+EQ}} - \Gamma_{\mathrm{ED},0}\,P_i^{\mathrm{ED}} - \Gamma_{\mathrm{EQ},0}\,P_{\mu}^{\mathrm{EQ}}\right], \tag{3.102}$$

with $P_{i\mu}^{\mathrm{ED+EQ}}$ being the Purcell factor related to the superposition of an electric dipole along $\hat{\mathbf{e}}_i$

and of an electric quadrupole along $\hat{\mathbf{e}}_\mu$. Although this decomposition into Purcell factor bases is not useful for the OPSE (since only one Purcell factor needs to be calculated per multipolar contribution [Subsec. 3.5.5]), it will be useful for the expression of the two-photon spontaneous emission rates as a function of the one-photon Purcell factors.

The developments presented in this chapter have two limitations: they are limited to the weak coupling regime and the consideration of the interaction up to the electric quadrupolar order may be not sufficient for the extreme cases of large emitters placed very close to a nanostructure.

Chapter 4

# Two-photon spontaneous emission

In this chapter, we go one step further than in the previous chapter by considering a second-order process in the perturbation theory, namely the two-photon spontaneous emission (TPSE). The main difference with the one-photon spontaneous emission (OPSE) process studied in Chapter 3 is that the TPSE is mediated by virtual intermediates states, leading to two quasi simultaneous transitions, each emitting a quantum [2, 42, 91]. As a result, the TPSE is characterized by a continuous and symmetric spectrum whereas OPSE spectra are discrete [Sec. 2.4]. Furthermore, we should rather talk about the two-quanta spontaneous emission, since depending on the environment, quanta other than photons can be emitted, as for example plasmons or phonons [30]. In practice, the mathematical developments are very similar to those made for the OPSE, except that we start with the second-order Fermi's golden rule instead of the first-order one.

This chapter is mainly based on Chapter 5 of the book *Molecular quantum electrodynamics: an introduction to radiation-molecule interactions* [2] in which they derive the two-electric dipole (2ED) transition rate in vacuum and on the paper *Quantum two-photon emission in a photonic cavity* [31] where the 2ED transition rate is expressed via the Green's function and as a function of the one-photon Purcell factors, but only for a restricted set of systems. We present here a complete treatment of the TPSE process where the interaction Hamiltonian is taken up to the electric quadrupolar order. We do not make any assumptions about the quantum emitter and the environment and we include interference effects between the multipolar pathways, which have never been studied to our knowledge. Thus, we derive expressions for the two-electric dipole (2ED), two-magnetic dipole (2MD), and two-electric quadrupole (2EQ) transition rates and for the interferences between them as a function of the one-photon Purcell factors, which can be used for arbitrarily shaped nanostructures and for emitter at any position. These equations enable the classical evaluation of the impact of the environment on the TPSE (i.e., the two-photon Purcell effect), as this is the case for the OPSE.

First, we remind the second-order Fermi's golden rule used to calculate TPSE transition rates of quantum systems as well as the interaction Hamiltonian that describes the interaction between a quantum emitter and the electromagnetic field. Then, we derive the multipolar contributions to the TPSE, including interference effects, and we consider the case where the environment is vacuum. Next, the obtained expressions are expressed via the dyadic Green's function, vacuum normalized, and expressed as a function of the Purcell factors of the OPSE. To do this, we use the modified Voigt notation introduced in the previous chapter to simplify the equations relative to the 2EQ transition. Finally, we close this chapter with a discussion about the derived equations and with a summary of them.

## 4.1 Fermi's golden rule

Let us consider a system composed of a two-level quantum emitter (e.g., an atom, a molecule, or a quantum dot) and its photonic environment. With a perturbative approach, the probability per unit time that a system carries out a second-order transition from an initial state $|i\rangle$ to a final state $|f\rangle$, upon an interaction between the emitter and the field described by the Hamiltonian $H_{\text{int}}$, is given by Fermi's golden rule [Eqs. (2.2) and (2.4)]:

$$\Gamma^{(2)}_{i\to f} = \frac{2\pi}{\hbar}|M^{(2)}_{fi}|^2\,\delta(E_f - E_i), \tag{4.1}$$

with $M^{(2)}_{fi}$ the second-order matrix element of $H_{\text{int}}$, which acts as a small perturbation of the system:

$$M^{(2)}_{fi} = \sum_{|l\rangle} \frac{\langle f|\, H_{\text{int}}(t)\,|l\rangle\,\langle l|\, H_{\text{int}}(t)\,|i\rangle}{E_i - E_l}, \tag{4.2}$$

where the summation runs over all virtual intermediate states $|l\rangle$ of the system that are allowed by selection rules. In these equations, $\hbar$ is the reduced Planck constant, $E_a$ stands for the energy of the system in the state $|a\rangle$ with $a = i, l, f$, and the superscript (2) indicates that this is a second-order transition, in contrast with the first-order transitions studied in Chapter 3. In comparison with the first-order matrix element [Eq. (3.2)], $M^{(2)}_{fi}$ contains two matrix elements of the interaction Hamiltonian that describe the two successive transitions mediated by a virtual intermediate state [Fig. 4.1]. Thereby during this process, there are two interactions between the emitter and the field leading to the emission of two quanta.

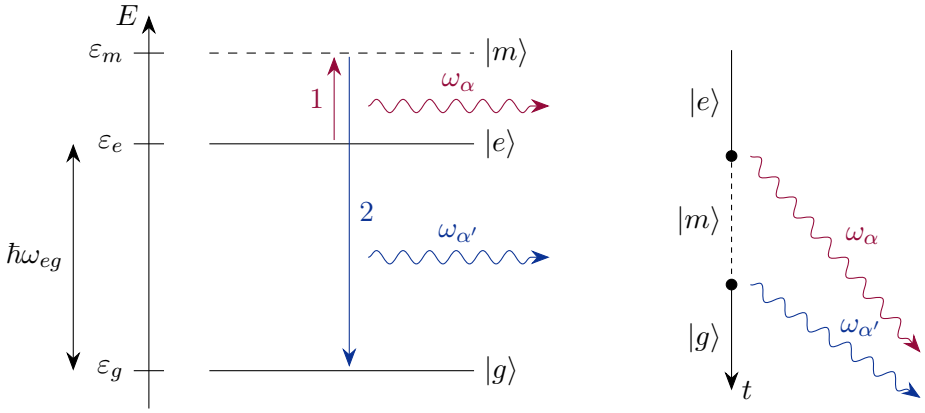


Figure 4.1: Energy and time representations of a second-order transition. The emitter carries-out a first transition from its excited state $|e\rangle$ to a virtual intermediate state $|m\rangle$ by emitting a photon in the mode $\alpha$. Then, a second transition is carried out to the ground state $|g\rangle$ of lower energy by emitting a photon in the mode $\alpha'$. The transition energy is given by $\hbar\omega_{eg} := \varepsilon_e - \varepsilon_g$. Even if the law of conservation of energy is temporarily violated after the emission of the first photon (since the energy of the emitter increases while emitting the first photon), overall this law is respected and the sum of the two photons' energies is equal to the transition energy: $\hbar\omega_\alpha + \hbar\omega_{\alpha'} = \hbar\omega_{eg}$ [Sec. 2.4]. This second-order process can therefore only be understood as a whole. Note that due to this violation, it is not possible to draw a picture that correctly represents both the energy of the intermediate state and the energy of the emitted photons, which are not equal to the energy difference between the emitter states. These representations only consider the intermediate state of the system $|l\rangle = |m; 1_\alpha\rangle$ where the first photon is emitted in the mode $\alpha$, but similar representations can be sketched by inverting the role of the two emitted quanta.

Regarding the states involved in this second-order process [2], the initial one is characterized by the emitter in an excited state $|e\rangle$ and the field in the vacuum state $|\text{vac}\rangle$, while in the final one the emitter is in a lower energy state $|g\rangle$ and the field is in a two-quanta state $|1_\alpha, 1_{\alpha'}\rangle$ where $\alpha$ and $\alpha'$ stand for the modes of the two emitted quanta. Thus, they are respectively written as[1]

$$|i\rangle = |e; \text{vac}\rangle \tag{4.3a}$$

$$\text{and as } |f\rangle = |g; 1_\alpha, 1_{\alpha'}\rangle\,. \tag{4.3b}$$

In the virtual intermediate states that connect these two states, the emitter is in the state $|m\rangle$ and the field is in a one-quantum state. Depending on in which mode is the emitted quantum, the intermediate states are written as

$$|l\rangle = |m; 1_\alpha\rangle \tag{4.4a}$$

$$\text{or as } |l\rangle = |m; 1_{\alpha'}\rangle\,. \tag{4.4b}$$

Further on, the energy of the emitter in the state $|a\rangle$ will be denoted as $\varepsilon_a$ with $a = e, m, g$. In the subsequent developments, a sum over $\alpha$ and $\alpha'$ will be added to consider all possible final states (modes) for the emitted quanta [Sec. 2.3].

## 4.2 Interaction Hamiltonian

As in Section 3.2 of the chapter dedicated to the OPSE, the multipolar expansion of the interaction Hamiltonian is considered up to the electric quadrupolar order [Eq. (3.4)]:

$$H_{\text{int}}(\mathbf{R}, t) = \underbrace{-\mathbf{d}\cdot\mathbf{E}(\mathbf{R}, t)}_{H_{\text{ED}}} \underbrace{-\mathbf{m}\cdot\mathbf{B}(\mathbf{R}, t)}_{H_{\text{MD}}} \underbrace{-\mathbf{Q}:\nabla\mathbf{E}(\mathbf{R}, t)}_{H_{\text{EQ}}} + \ldots \tag{4.5}$$

and therefore encompasses the interactions of the electric dipole (ED), magnetic dipole (MD) and electric quadrupole (EQ). Moreover, the multipolar moment operators are given by the equations (3.5) and the electromagnetic field operators are written as a function of the normal modes $\mathbf{A}_\alpha(\mathbf{r})$ of the vector potential [Eqs. (3.6)].

Upon this interaction, the quantum emitter can perform various two-photon transitions, each contributing to the overall TPSE rate [5]. As a quantum can be emitted by three distinct multipolar emission pathways (ED, MD, and EQ), there are nine multipolar contributions to this second-order process, three of which are illustrated in Figure 4.2. On the one hand, there are the two-electric dipole (2ED), the two-magnetic dipole (2MD) and the two-electric quadrupole (2EQ) transitions, under which both photons are emitted via the same multipolar first-order transition. On the other hand, there are the six mixed transitions ED–MD, ED–EQ, MD–ED, MD–EQ, EQ–ED, and EQ–MD in which the photons originate from different multipolar first-order transitions. In addition, these multipolar channels can interfere with each other, potentially resulting in an increase or a decrease of the overall TPSE rate [2]. However, depending on the selection rules of the considered emitter, some emission channels can be forbidden. For example, the mixed transitions ED–EQ and EQ–ED are not allowed between two states of a hydrogen atom that have the same azimuthal quantum

[1] $|a, b\rangle$ (or $|a; b\rangle$) is a shorthand notation used to represent the tensor product of the states $|a\rangle$ and $|b\rangle$.

number [Sec. 2.1]. Moreover, depending on the photonic environment, some multipolar transitions may be weaker than others, and therefore can be neglected. These multipolar contributions to the overall TPSE rate are derived in the following section.

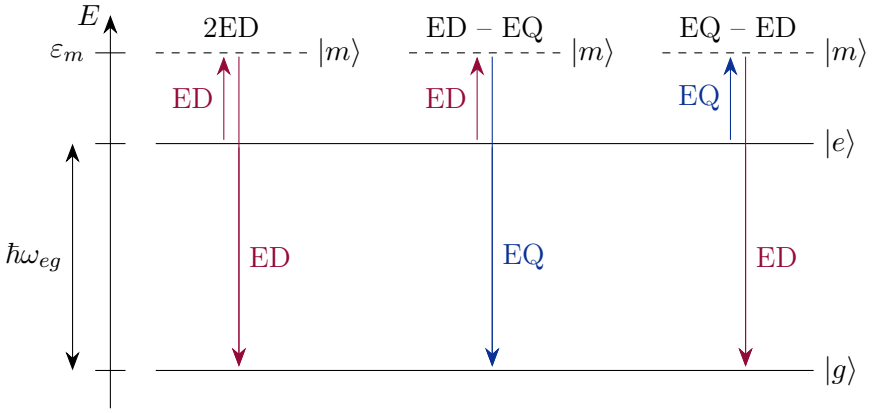


Figure 4.2: Representation of three of the nine multipolar contributions to the TPSE process. The 2ED transition is made up of two successive ED transitions, while the other two consist of one ED and one EQ transitions. These second-order transitions are mediated by different virtual intermediate states due to the selection rules [Eqs. (2.8) and Sec. 2.4] and can interfere.

## 4.3 Multipolar contributions

Now that the second-order Fermi's golden rule and all the states involved in the second-order transition have been introduced, let us derive the different multipolar contributions to the TPSE rate. Given that the initial and the final energies[2] of the system are, respectively, $E_i = \varepsilon_e$ and $E_f = \varepsilon_g + \hbar\omega_\alpha + \hbar\omega_{\alpha'}$, the Dirac delta distribution in Fermi's golden rule in equation (4.1) can be rewritten as

$$\delta(E_f - E_i) = \frac{1}{\hbar}\delta(\omega_{eg} - \omega_\alpha - \omega_{\alpha'}), \tag{4.6}$$

where we define $\hbar\omega_{ab} := \varepsilon_a - \varepsilon_b$ with $a, b = e, m, g$.

Then, given that there are two kinds of intermediate states [Eqs. (4.4)], the summation over them in the expression of the second-order matrix element $M_{fi}^{(2)}$ is split in two:

$$\begin{aligned} M_{fi}^{(2)} = &\sum_{|m\rangle} \frac{\langle 1_\alpha, 1_{\alpha'}| \langle g| H_{\text{int}} |m\rangle |1_\alpha\rangle \langle 1_\alpha| \langle m| H_{\text{int}} |e\rangle |\text{vac}\rangle}{\hbar(\omega_{em} - \omega_\alpha)} \\ &+ \sum_{|m\rangle} \frac{\langle 1_\alpha, 1_{\alpha'}| \langle g| H_{\text{int}} |m\rangle |1_{\alpha'}\rangle \langle 1_{\alpha'}| \langle m| H_{\text{int}} |e\rangle |\text{vac}\rangle}{\hbar(\omega_{em} - \omega_{\alpha'})}, \end{aligned} \tag{4.7}$$

where the first summation corresponds to the representations sketched in Figure 4.1. Note that the time dependency of $H_{\text{int}}$ (the time dependencies $e^{-i\omega t}$ and $e^{i\omega t}$ are in the annihilation and creation operators involved in the electromagnetic field operators [Eqs. (3.6)]) is omitted since we take the modulus of $M_{fi}$.

Let us first calculate the factor $\langle 1_\alpha, 1_{\alpha'}| \langle g| H_{\text{int}} |m\rangle |1_\alpha\rangle$ in $M_{fi}^{(2)}$ with the interaction Hamiltonian given by the equation (4.5) and with the electromagnetic field operators given by the equations (3.6).

[2]The zero of energy is chosen to correspond to the energy of the electromagnetic field in vacuum.

As we are interested in emission processes, only the part of $\mathbf{E}$ and $\mathbf{B}$ involving creation operators, noted as $\mathbf{E}^{(-)}$ and $\mathbf{B}^{(-)}$, are kept in the calculation:

$$\begin{aligned}
\langle 1_\alpha, 1_{\alpha'}| \langle g| H_{\text{int}} |m\rangle |1_\alpha\rangle &= \langle 1_\alpha, 1_{\alpha'}| \langle g| - \mathbf{d}\cdot\mathbf{E}(\mathbf{R}) - \mathbf{m}\cdot\mathbf{B}(\mathbf{R}) - \mathbf{Q}:\nabla\mathbf{E}(\mathbf{R}) |m\rangle |1_\alpha\rangle && \text{(4.8a)}\\
&= -\langle g|\,\mathbf{d}\,|m\rangle \cdot \langle 1_\alpha, 1_{\alpha'}|\,\mathbf{E}^{(-)}(\mathbf{R})\,|1_\alpha\rangle \\
&\quad -\langle g|\,\mathbf{m}\,|m\rangle \cdot \langle 1_\alpha, 1_{\alpha'}|\,\mathbf{B}^{(-)}(\mathbf{R})\,|1_\alpha\rangle \\
&\quad -\langle g|\,\mathbf{Q}\,|m\rangle : \nabla\langle 1_\alpha, 1_{\alpha'}|\,\mathbf{E}^{(-)}(\mathbf{R})\,|1_\alpha\rangle && \text{(4.8b)}\\
&= -\mathbf{d}^{gm}\cdot\langle 1_\alpha, 1_{\alpha'}| - i\sum_\beta \sqrt{\frac{\hbar\omega_\beta}{2\varepsilon_0}} a_\beta^\dagger \mathbf{A}_\beta^*(\mathbf{R})\,|1_\alpha\rangle \\
&\quad -\mathbf{m}^{gm}\cdot\langle 1_\alpha, 1_{\alpha'}| - i\sum_\beta \sqrt{\frac{\hbar}{2\varepsilon_0\omega_\beta}} a_\beta^\dagger \nabla\times\mathbf{A}_\beta^*(\mathbf{R})\,|1_\alpha\rangle \\
&\quad -\mathbf{Q}^{gm}:\langle 1_\alpha, 1_{\alpha'}| - i\sum_\beta \sqrt{\frac{\hbar\omega_\beta}{2\varepsilon_0}} a_\beta^\dagger \nabla\mathbf{A}_\beta^*(\mathbf{R})\,|1_\alpha\rangle\,, && \text{(4.8c)}
\end{aligned}$$

where the multipolar operators only act on emitter states while the field operators solely act on field states. Within this equation, $\mathbf{d}^{ba} := \langle b|\mathbf{d}|a\rangle$, $\mathbf{m}^{ba} := \langle b|\mathbf{m}|a\rangle$, and $\mathbf{Q}^{ba} := \langle b|\mathbf{Q}|a\rangle$ stand, respectively, for the electric dipole, magnetic dipole and electric quadrupole transition moments (i.e., the first-order matrix elements of the operators $\mathbf{d}$, $\mathbf{m}$, and $\mathbf{Q}$) that describe the emitter's transition from the state $|a\rangle$ to the state $|b\rangle$ ($a$, $b = e$, $m$, $g$). In the previous equation, only the term involving the creation operator $a_\beta^\dagger$ that creates a photon in the mode $\beta = \alpha'$ leads to a non-zero term because the field states form an orthonormal basis[3]. Thus, we get

$$\langle 1_\alpha, 1_{\alpha'}| \langle g| H_{\text{int}} |m\rangle |1_\alpha\rangle = i\sqrt{\frac{\hbar\omega_{\alpha'}}{2\varepsilon_0}} \left\{ \mathbf{d}^{gm}\cdot\mathbf{A}_{\alpha'}^*(\mathbf{R}) + \frac{1}{\omega_{\alpha'}}\mathbf{m}^{gm}\cdot\nabla\times\mathbf{A}_{\alpha'}^*(\mathbf{R}) + \mathbf{Q}^{gm}:\nabla\mathbf{A}_{\alpha'}^*(\mathbf{R}) \right\}. \tag{4.9}$$

Similar developments for the second factor in the first summation of the equation (4.7) lead to

$$\langle 1_\alpha| \langle m| H_{\text{int}} |e\rangle |\text{vac}\rangle = i\sqrt{\frac{\hbar\omega_\alpha}{2\varepsilon_0}} \left\{ \mathbf{d}^{me}\cdot\mathbf{A}_\alpha^*(\mathbf{R}) + \frac{1}{\omega_\alpha}\mathbf{m}^{me}\cdot\nabla\times\mathbf{A}_\alpha^*(\mathbf{R}) + \mathbf{Q}^{me}:\nabla\mathbf{A}_\alpha^*(\mathbf{R}) \right\}, \tag{4.10}$$

and therefore the first summation in equation (4.7) is given by

$$-\frac{\sqrt{\omega_\alpha\omega_{\alpha'}}}{2\varepsilon_0}\sum_{|m\rangle} \left\{ \frac{\left(\mathbf{d}^{gm}\cdot\mathbf{A}_{\alpha'}^* + \frac{1}{\omega_{\alpha'}}\mathbf{m}^{gm}\cdot\nabla\times\mathbf{A}_{\alpha'}^* + \mathbf{Q}^{gm}:\nabla\mathbf{A}_{\alpha'}^*\right)\left(\mathbf{d}^{me}\cdot\mathbf{A}_\alpha^* + \frac{1}{\omega_\alpha}\mathbf{m}^{me}\cdot\nabla\times\mathbf{A}_\alpha^* + \mathbf{Q}^{me}:\nabla\mathbf{A}_\alpha^*\right)}{\omega_{em} - \omega_\alpha} \right\}, \tag{4.11}$$

where the spatial dependency has been omitted.

Concerning the second summation present in equation (4.7), the result can be obtained by inverting the role of $\alpha$ and $\alpha'$ in the last obtained equation. Thus, the second-order matrix element

[3] An orthonormal basis satisfies $\langle 1_\alpha|1_\beta\rangle = \delta_{\alpha\beta}$ and $\langle 1_\alpha, 1_{\alpha'}|1_\beta, 1_{\beta'}\rangle = \langle 1_\alpha|1_\beta\rangle\langle 1_{\alpha'}|1_{\beta'}\rangle = \delta_{\alpha\beta}\,\delta_{\alpha'\beta'}$.

$M_{fi}^{(2)}$ is rewritten as

$$
\begin{aligned}
M_{fi}^{(2)} = -\frac{\sqrt{\omega_\alpha \omega_{\alpha'}}}{2\varepsilon_0} \sum_{|m\rangle} \Bigg\{ & \frac{\mathbf{d}^{gm}\cdot\mathbf{A}^*_{\alpha'}\,\mathbf{d}^{me}\cdot\mathbf{A}^*_{\alpha}}{\omega_{em}-\omega_\alpha} + \frac{\mathbf{d}^{gm}\cdot\mathbf{A}^*_{\alpha}\,\mathbf{d}^{me}\cdot\mathbf{A}^*_{\alpha'}}{\omega_{em}-\omega_{\alpha'}} \\
& + \frac{1}{\omega_\alpha\omega_{\alpha'}} \frac{\mathbf{m}^{gm}\cdot\nabla\times\mathbf{A}^*_{\alpha'}\,\mathbf{m}^{me}\cdot\nabla\times\mathbf{A}^*_{\alpha}}{\omega_{em}-\omega_\alpha} + \alpha \leftrightarrow \alpha' \\
& + \frac{\mathbf{Q}^{gm}:\nabla\mathbf{A}^*_{\alpha'}\,\mathbf{Q}^{me}:\nabla\mathbf{A}^*_{\alpha}}{\omega_{em}-\omega_\alpha} + \alpha \leftrightarrow \alpha' \\
& + \frac{1}{\omega_{\alpha'}} \frac{\mathbf{m}^{gm}\cdot\nabla\times\mathbf{A}^*_{\alpha'}\,\mathbf{d}^{me}\cdot\mathbf{A}^*_{\alpha}}{\omega_{em}-\omega_\alpha} + \alpha \leftrightarrow \alpha' \\
& + \frac{\mathbf{Q}^{gm}:\nabla\mathbf{A}^*_{\alpha'}\,\mathbf{d}^{me}\cdot\mathbf{A}^*_{\alpha}}{\omega_{em}-\omega_\alpha} + \alpha \leftrightarrow \alpha' \\
& + \frac{1}{\omega_{\alpha}} \frac{\mathbf{d}^{gm}\cdot\mathbf{A}^*_{\alpha'}\,\mathbf{m}^{me}\cdot\nabla\times\mathbf{A}^*_{\alpha}}{\omega_{em}-\omega_\alpha} + \alpha \leftrightarrow \alpha' \\
& + \frac{1}{\omega_{\alpha}} \frac{\mathbf{Q}^{gm}:\nabla\mathbf{A}^*_{\alpha'}\,\mathbf{m}^{me}\cdot\nabla\times\mathbf{A}^*_{\alpha}}{\omega_{em}-\omega_\alpha} + \alpha \leftrightarrow \alpha' \\
& + \frac{\mathbf{d}^{gm}\cdot\mathbf{A}^*_{\alpha'}\,\mathbf{Q}^{me}:\nabla\mathbf{A}^*_{\alpha}}{\omega_{em}-\omega_\alpha} + \alpha \leftrightarrow \alpha' \\
& + \frac{1}{\omega_{\alpha'}} \frac{\mathbf{m}^{gm}\cdot\nabla\times\mathbf{A}^*_{\alpha'}\,\mathbf{Q}^{me}:\nabla\mathbf{A}^*_{\alpha}}{\omega_{em}-\omega_\alpha} + \alpha \leftrightarrow \alpha' \Bigg\},
\end{aligned}
\tag{4.12}
$$

where the terms $\alpha \leftrightarrow \alpha'$ denote terms obtained by inverting the role of $\alpha$ and $\alpha'$ in the preceding terms, where the first one at the first line has been given for the example. The calculated matrix element is the result of nine multipolar contributions:

$$
\begin{aligned}
M_{fi}^{(2)} = {} & M_{fi}^{\mathrm{2ED}} + M_{fi}^{\mathrm{2MD}} + M_{fi}^{\mathrm{2EQ}} \\
& + M_{fi}^{\mathrm{ED-MD}} + M_{fi}^{\mathrm{ED-EQ}} + M_{fi}^{\mathrm{MD-ED}} + M_{fi}^{\mathrm{MD-EQ}} + M_{fi}^{\mathrm{EQ-ED}} + M_{fi}^{\mathrm{EQ-MD}},
\end{aligned}
\tag{4.13}
$$

where the first one corresponds to the first two terms in the summation over $|m\rangle$ in equation (4.12), the second to the next two, and so on. The contributions $M_{fi}^{\mathrm{2ED}}$, $M_{fi}^{\mathrm{2MD}}$, and $M_{fi}^{\mathrm{2EQ}}$ are, respectively, obtained when only the ED, MD, or EQ interaction is taken into account in the interaction Hamiltonian [Eq. (4.5)]. Thus, by considering these interactions separately, we will derive the transition rates relative to the 2ED, 2MD, and 2EQ transitions. When multiple interactions are present simultaneously in the interaction Hamiltonian, contributions appear from mixed transitions (second line in Eq. (4.13)).

Now and for the rest of this thesis, we put aside the contribution of mixed transitions to the second-order matrix element, but similar equations can be derived for them. Indeed, they are not involved in the transition studied in this thesis: namely the transition $s \to s$ of the hydrogen atom [Sec. 2.4]. Thus, we keep the three following multipolar contributions to $M_{fi}^{(2)}$:

$$
M_{fi}^{(2)} = M_{fi}^{\mathrm{2ED}} + M_{fi}^{\mathrm{2MD}} + M_{fi}^{\mathrm{2EQ}},
\tag{4.14}
$$

which correspond to the first three lines in equation (4.12). Using the commutation property of the

scalar and double dot products, one obtains the following equation

$$M_{fi}^{(2)} = -\frac{\sqrt{\omega_\alpha \omega_{\alpha'}}}{2\varepsilon_0} \sum_{|m\rangle} \left\{ \frac{\mathbf{A}_\alpha^* \cdot \mathbf{d}^{me}\, \mathbf{d}^{gm} \cdot \mathbf{A}_{\alpha'}^*}{\omega_{em} - \omega_\alpha} + \frac{\mathbf{A}_\alpha^* \cdot \mathbf{d}^{gm}\, \mathbf{d}^{me} \cdot \mathbf{A}_{\alpha'}^*}{\omega_{em} - \omega_{\alpha'}} \right.$$
$$+ \frac{1}{\omega_\alpha \omega_{\alpha'}} \left( \frac{\nabla \times \mathbf{A}_\alpha^* \cdot \mathbf{m}^{me}\, \mathbf{m}^{gm} \cdot \nabla \times \mathbf{A}_{\alpha'}^*}{\omega_{em} - \omega_\alpha} + \frac{\nabla \times \mathbf{A}_\alpha^* : \mathbf{m}^{gm}\, \mathbf{m}^{me} \cdot \nabla \times \mathbf{A}_{\alpha'}^*}{\omega_{em} - \omega_{\alpha'}} \right)$$
$$\left. + \frac{\nabla \mathbf{A}_\alpha^* : \mathbf{Q}^{me}\, \mathbf{Q}^{gm} : \nabla \mathbf{A}_{\alpha'}^*}{\omega_{em} - \omega_\alpha} + \frac{\nabla \mathbf{A}_\alpha^* : \mathbf{Q}^{gm}\, \mathbf{Q}^{me} : \nabla \mathbf{A}_{\alpha'}^*}{\omega_{em} - \omega_{\alpha'}} \right\}, \tag{4.15}$$

which can be reorganized as follows

$$M_{fi}^{(2)} = -\frac{\sqrt{\omega_\alpha \omega_{\alpha'}}}{2\varepsilon_0} \left( \mathbf{A}_\alpha^* \cdot \sum_{|m\rangle} \left\{ \frac{\mathbf{d}^{me}\mathbf{d}^{gm}}{\omega_{em} - \omega_\alpha} + \frac{\mathbf{d}^{gm}\mathbf{d}^{me}}{\omega_{em} - \omega_{\alpha'}} \right\} \cdot \mathbf{A}_{\alpha'}^* \right.$$
$$+ \frac{1}{\omega_\alpha \omega_{\alpha'}} \nabla \times \mathbf{A}_\alpha^* \cdot \sum_{|m\rangle} \left\{ \frac{\mathbf{m}^{me}\mathbf{m}^{gm}}{\omega_{em} - \omega_\alpha} + \frac{\mathbf{m}^{gm}\mathbf{m}^{me}}{\omega_{em} - \omega_{\alpha'}} \right\} \cdot \nabla \times \mathbf{A}_{\alpha'}^*$$
$$\left. + \nabla \mathbf{A}_\alpha^* : \sum_{|m\rangle} \left\{ \frac{\mathbf{Q}^{me}\mathbf{Q}^{gm}}{\omega_{em} - \omega_\alpha} + \frac{\mathbf{Q}^{gm}\mathbf{Q}^{me}}{\omega_{em} - \omega_{\alpha'}} \right\} : \nabla \mathbf{A}_{\alpha'}^* \right). \tag{4.16}$$

Let us now take the complex conjugate[4,5] of $M_{fi}^{(2)}$:

$$\left(M_{fi}^{(2)}\right)^* = -\frac{\sqrt{\omega_\alpha \omega_{\alpha'}}}{2\varepsilon_0} \left( \mathbf{A}_\alpha \cdot \sum_{|m\rangle} \left\{ \frac{\mathbf{d}^{em}\mathbf{d}^{mg}}{\omega_{em} - \omega_\alpha} + \frac{\mathbf{d}^{mg}\mathbf{d}^{em}}{\omega_{em} - \omega_{\alpha'}} \right\} \cdot \mathbf{A}_{\alpha'} \right.$$
$$+ \frac{1}{\omega_\alpha \omega_{\alpha'}} \nabla \times \mathbf{A}_\alpha \cdot \sum_{|m\rangle} \left\{ \frac{\mathbf{m}^{em}\mathbf{m}^{mg}}{\omega_{em} - \omega_\alpha} + \frac{\mathbf{m}^{mg}\mathbf{m}^{em}}{\omega_{em} - \omega_{\alpha'}} \right\} \cdot \nabla \times \mathbf{A}_{\alpha'}$$
$$\left. + \nabla \mathbf{A}_\alpha : \sum_{|m\rangle} \left\{ \frac{\mathbf{Q}^{em}\mathbf{Q}^{mg}}{\omega_{em} - \omega_\alpha} + \frac{\mathbf{Q}^{mg}\mathbf{Q}^{em}}{\omega_{em} - \omega_{\alpha'}} \right\} : \nabla \mathbf{A}_{\alpha'} \right) \tag{4.17a}$$
$$= -\frac{\sqrt{\omega_\alpha \omega_{\alpha'}}}{2\varepsilon_0} \left( \mathbf{A}_\alpha \cdot \boldsymbol{\mathcal{D}}^{eg} \cdot \mathbf{A}_{\alpha'} + \frac{1}{\omega_\alpha \omega_{\alpha'}} \nabla \times \mathbf{A}_\alpha \cdot \boldsymbol{\mathcal{M}}^{eg} \cdot \nabla \times \mathbf{A}_{\alpha'} + \nabla \mathbf{A}_\alpha : \boldsymbol{\mathcal{Q}}^{eg} : \nabla \mathbf{A}_{\alpha'} \right), \tag{4.17b}$$

where we define three tensors, the first two of rank two [Eqs. (4.18a) and (4.18b)] and the third one of rank four [Eq. (4.18c)], as

$$\boldsymbol{\mathcal{D}}^{eg}(\omega_\alpha, \omega_{\alpha'}) := \sum_{|m\rangle} \left( \frac{\mathbf{d}^{em}\, \mathbf{d}^{mg}}{\omega_{em} - \omega_\alpha} + \frac{\mathbf{d}^{mg}\, \mathbf{d}^{em}}{\omega_{em} - \omega_{\alpha'}} \right), \tag{4.18a}$$

$$\boldsymbol{\mathcal{M}}^{eg}(\omega_\alpha, \omega_{\alpha'}) := \sum_{|m\rangle} \left( \frac{\mathbf{m}^{em}\, \mathbf{m}^{mg}}{\omega_{em} - \omega_\alpha} + \frac{\mathbf{m}^{mg}\, \mathbf{m}^{em}}{\omega_{em} - \omega_{\alpha'}} \right), \tag{4.18b}$$

$$\boldsymbol{\mathcal{Q}}^{eg}(\omega_\alpha, \omega_{\alpha'}) := \sum_{|m\rangle} \left( \frac{\mathbf{Q}^{em}\, \mathbf{Q}^{mg}}{\omega_{em} - \omega_\alpha} + \frac{\mathbf{Q}^{mg}\, \mathbf{Q}^{em}}{\omega_{em} - \omega_{\alpha'}} \right), \tag{4.18c}$$

[4]For an Hermitian operator: $\left(\mathbf{A}^{ab}\right)^* = (\langle a|\mathbf{A}|b\rangle)^* = \langle b|\mathbf{A}^\dagger|a\rangle = \langle b|\mathbf{A}|a\rangle = \mathbf{A}^{ba}$ where the dagger denotes the operation of taking the transpose and the complex conjugate.

[5]It is more convenient to work with $\left(M_{fi}^{(2)}\right)^*$ to avoid the complex conjugate operation on the normal modes in order to derive equations similar than those of Refs. 2 and 31.

where the outer product is implied. The components of the tensor that come from the outer product of two tensors $\mathbf{U}$ and $\mathbf{V}$ are $(\mathbf{UV})_{i_1,i_2,\ldots,i_n,j_1,j_2,\ldots,j_n} := U_{i_1,i_2,\ldots,i_n} V_{j_1,j_2,\ldots,j_n}$. These tensors describe the two successive electric dipole, magnetic dipole, and electric quadrupole transitions of the emitter between the states $|e\rangle$ and $|g\rangle$ of the emitter. Consequently, they depend only on the electronic structure of the emitter. Subsequently, we will refer to them as the second-order multipolar transition moments. Since the operator $\mathbf{Q}$ is symmetric and can be taken traceless in source-free regions [Eq. (3.5c)], the fourth rank tensor $\boldsymbol{\mathcal{Q}}^{eg}$ is also symmetric:

$$\forall i,j,k,l = 1,2,3, \quad \mathcal{Q}^{eg}_{ijkl} = \mathcal{Q}^{eg}_{jikl} = \mathcal{Q}^{eg}_{ijlk} = \mathcal{Q}^{eg}_{jilk}, \tag{4.19}$$

and it satisfies the following property:

$$\forall i,j,k,l = 1,2,3, \quad \sum_i \mathcal{Q}^{eg}_{iikl} = \sum_k \mathcal{Q}^{eg}_{ijkk} = 0. \tag{4.20}$$

Let us now take the square modulus of $M^{(2)}_{fi}$:

$$\left|M^{(2)}_{fi}\right|^2 = \left|\left(M^{(2)}_{fi}\right)^*\right|^2 \tag{4.21a}$$

$$= \frac{\omega_\alpha \omega_{\alpha'}}{4\varepsilon_0^2} \left| \mathbf{A}_\alpha \cdot \boldsymbol{\mathcal{D}}^{eg} \cdot \mathbf{A}_{\alpha'} + \frac{1}{\omega_\alpha \omega_{\alpha'}} \nabla \times \mathbf{A}_\alpha \cdot \boldsymbol{\mathcal{M}}^{eg} \cdot \nabla \times \mathbf{A}_{\alpha'} + \nabla \mathbf{A}_\alpha : \boldsymbol{\mathcal{Q}}^{eg} : \nabla \mathbf{A}_{\alpha'} \right|^2, \tag{4.21b}$$

which can be injected, together with the equation (4.6), in Fermi's golden rule [Eq. (4.1)]:

$$\Gamma^{(2)}_{\text{tot}}(\mathbf{R}) = \frac{2\pi}{\hbar^2} \frac{\omega_\alpha \omega_{\alpha'}}{4\varepsilon_0^2} \left| \mathbf{A}_\alpha \cdot \boldsymbol{\mathcal{D}}^{eg} \cdot \mathbf{A}_{\alpha'} + \frac{1}{\omega_\alpha \omega_{\alpha'}} \nabla \times \mathbf{A}_\alpha \cdot \boldsymbol{\mathcal{M}}^{eg} \cdot \nabla \times \mathbf{A}_{\alpha'} + \nabla \mathbf{A}_\alpha : \boldsymbol{\mathcal{Q}}^{eg} : \nabla \mathbf{A}_{\alpha'} \right|^2 \times \delta(\omega_{eg} - \omega_\alpha - \omega_{\alpha'}). \tag{4.22}$$

As a final step, we take the summation over all the possible modes for the two emitted quanta to get the total TPSE rate [Sec. 2.3]. However, we must take into account a factor 1/2 to avoid double counting[6] [31]:

$$\Gamma^{(2)}_{\text{tot}}(\mathbf{R}) = \frac{\pi}{4\varepsilon_0^2 \hbar^2} \sum_{\alpha,\alpha'} \omega_\alpha \omega_{\alpha'} \left| \mathbf{A}_\alpha \cdot \boldsymbol{\mathcal{D}}^{eg} \cdot \mathbf{A}_{\alpha'} + \frac{1}{\omega_\alpha \omega_{\alpha'}} \nabla \times \mathbf{A}_\alpha \cdot \boldsymbol{\mathcal{M}}^{eg} \cdot \nabla \times \mathbf{A}_{\alpha'} + \nabla \mathbf{A}_\alpha : \boldsymbol{\mathcal{Q}}^{eg} : \nabla \mathbf{A}_{\alpha'} \right|^2 \times \delta(\omega_{eg} - \omega_\alpha - \omega_{\alpha'}), \tag{4.23}$$

where the spatial dependency of the field modes and the frequency dependency of the second-order multipolar transition moments have been omitted.

Since this expression has been obtained by putting aside the mixed transitions, the total TPSE rate encompasses the contributions of the 2ED, 2MD, and 2EQ emission channels as well as the interference effects among them:

$$\Gamma^{(2)}_{\text{tot}} = \Gamma^{(2)}_{\text{2ED}} + \Gamma^{(2)}_{\text{2MD}} + \Gamma^{(2)}_{\text{2EQ}} + \Gamma^{(2)}_{\text{2ED}\cap\text{2MD}} + \Gamma^{(2)}_{\text{2ED}\cap\text{2EQ}} + \Gamma^{(2)}_{\text{2MD}\cap\text{2EQ}}. \tag{4.24}$$

[6] The division by two is essential to take into account the indistinguishable nature of the photons being emitted. Indeed, the process of emitting a photon in the mode $\alpha$ and then a photon in the mode $\alpha'$ is indistinguishable from the process of emitting a photon in the mode $\alpha'$ and then a photon in the mode $\alpha$. Divide by a factor two ensures that each unique two-photon state is counted only once.

In the last equations, $\Gamma^{(2)}_{\mathrm{2ED}\cap\mathrm{2MD}}$, $\Gamma^{(2)}_{\mathrm{2ED}\cap\mathrm{2EQ}}$, $\Gamma^{(2)}_{\mathrm{2MD}\cap\mathrm{2EQ}}$ are introduced as the terms representing the interferences between the 2ED, 2MD, and 2EQ transitions. By developing the square modulus in equation (4.23), we find the three multipolar TPSE rates:

$$\Gamma^{(2)}_{\mathrm{2ED}}(\mathbf{R}) = \frac{\pi}{4\varepsilon_0^2\hbar^2}\sum_{\alpha,\alpha'}\omega_\alpha\omega_{\alpha'}\left|\mathbf{A}_\alpha(\mathbf{R})\cdot\boldsymbol{\mathcal{D}}^{eg}(\omega_\alpha,\omega_{\alpha'})\cdot\mathbf{A}_{\alpha'}(\mathbf{R})\right|^2\delta(\omega_{eg}-\omega_\alpha-\omega_{\alpha'}), \tag{4.25a}$$

$$\Gamma^{(2)}_{\mathrm{2MD}}(\mathbf{R}) = \frac{\pi}{4\varepsilon_0^2\hbar^2}\sum_{\alpha,\alpha'}\frac{1}{\omega_\alpha\omega_{\alpha'}}\left|\nabla\times\mathbf{A}_\alpha(\mathbf{R})\cdot\boldsymbol{\mathcal{M}}^{eg}(\omega_\alpha,\omega_{\alpha'})\cdot\nabla\times\mathbf{A}_{\alpha'}(\mathbf{R})\right|^2\delta(\omega_{eg}-\omega_\alpha-\omega_{\alpha'}), \tag{4.25b}$$

$$\Gamma^{(2)}_{\mathrm{2EQ}}(\mathbf{R}) = \frac{\pi}{4\varepsilon_0^2\hbar^2}\sum_{\alpha,\alpha'}\omega_\alpha\omega_{\alpha'}\left|\nabla\mathbf{A}_\alpha(\mathbf{R}):\boldsymbol{\mathcal{Q}}^{eg}(\omega_\alpha,\omega_{\alpha'}):\nabla\mathbf{A}_{\alpha'}(\mathbf{R})\right|^2\delta(\omega_{eg}-\omega_\alpha-\omega_{\alpha'}), \tag{4.25c}$$

and the three interference terms[7]:

$$\begin{aligned}\Gamma^{(2)}_{\mathrm{2ED}\cap\mathrm{2MD}}(\mathbf{R}) = 2\,\mathrm{Re}\Bigg(&\frac{\pi}{4\varepsilon_0^2\hbar^2}\sum_{\alpha,\alpha'}\left(\mathbf{A}_\alpha(\mathbf{R})\cdot\boldsymbol{\mathcal{D}}^{eg}(\omega_\alpha,\omega_{\alpha'})\cdot\mathbf{A}_{\alpha'}(\mathbf{R})\right)\\ &\times\left(\nabla\times\mathbf{A}_\alpha(\mathbf{R})\cdot\boldsymbol{\mathcal{M}}^{eg}(\omega_\alpha,\omega_{\alpha'})\cdot\nabla\times\mathbf{A}_{\alpha'}(\mathbf{R})\right)^*\delta(\omega_{eg}-\omega_\alpha-\omega_{\alpha'})\Bigg),\end{aligned} \tag{4.26a}$$

$$\begin{aligned}\Gamma^{(2)}_{\mathrm{2ED}\cap\mathrm{2EQ}}(\mathbf{R}) = 2\,\mathrm{Re}\Bigg(&\frac{\pi}{4\varepsilon_0^2\hbar^2}\sum_{\alpha,\alpha'}\omega_\alpha\omega_{\alpha'}\left(\mathbf{A}_\alpha(\mathbf{R})\cdot\boldsymbol{\mathcal{D}}^{eg}(\omega_\alpha,\omega_{\alpha'})\cdot\mathbf{A}_{\alpha'}(\mathbf{R})\right)\\ &\times\left(\nabla\mathbf{A}_\alpha(\mathbf{R}):\boldsymbol{\mathcal{Q}}^{eg}(\omega_\alpha,\omega_{\alpha'}):\nabla\mathbf{A}_{\alpha'}(\mathbf{R})\right)^*\delta(\omega_{eg}-\omega_\alpha-\omega_{\alpha'})\Bigg),\end{aligned} \tag{4.26b}$$

$$\begin{aligned}\Gamma^{(2)}_{\mathrm{2MD}\cap\mathrm{2EQ}}(\mathbf{R}) = 2\,\mathrm{Re}\Bigg(&\frac{\pi}{4\varepsilon_0^2\hbar^2}\sum_{\alpha,\alpha'}\left(\nabla\times\mathbf{A}_\alpha(\mathbf{R})\cdot\boldsymbol{\mathcal{M}}^{eg}(\omega_\alpha,\omega_{\alpha'})\cdot\nabla\times\mathbf{A}_{\alpha'}(\mathbf{R})\right)\\ &\times\left(\nabla\mathbf{A}_\alpha(\mathbf{R}):\boldsymbol{\mathcal{Q}}^{eg}(\omega_\alpha,\omega_{\alpha'}):\nabla\mathbf{A}_{\alpha'}(\mathbf{R})\right)^*\delta(\omega_{eg}-\omega_\alpha-\omega_{\alpha'})\Bigg),\end{aligned} \tag{4.26c}$$

where Re stands for the real part and the expression of the 2ED transition rate has been derived in Ref. 31. Hereafter, we will omit the real part for clarity. Thereby, interference terms emerge from mixed products with one that is the complex conjugate of the other[8]. Note that these terms could have also been written by applying the complex conjugate to the other factor. Moreover, interference terms can be either positive or negative, potentially resulting in an increase or decrease of the overall TPSE rate [Eq. (4.24)]. Afterwards, we focus on the interference between the 2ED and 2EQ channels, but similar developments can be performed for the other interference terms. Indeed, the plasmonic nanostructures studied in Chapter 7 do not contribute significantly to enhancing magnetic transitions [59], and thus the interferences with the 2MD transition are not calculated. Furthermore, all derived equations for the multipolar contributions to the TPSE rate are valid regardless of the emitter and its environment. As a direct application, we derive in the next section the free-space transition rates, without the interference terms as they vanish in vacuum [Sec. 3.3].

## 4.4 Vacuum transition rates

As mentioned in Section 3.4 of the previous chapter, in vacuum, the field modes are plane waves and the summation over the modes $\alpha$ is replaced by a summation over the two polarizations and an

[7] The cross product at the start of a new line in an equation indicates the product between scalars.
[8] $\forall z\in\mathbb{C}, z+z^* = 2\,\mathrm{Re}(z)$.

integral over the wave vectors that is expressed in spherical coordinates [Eqs. (3.18) and (3.19)]:

$$\mathbf{A}_\alpha(\mathbf{r}) \longrightarrow \mathbf{A}_{\mathbf{k},s}(\mathbf{r}) = \frac{e^{i\mathbf{k}\cdot\mathbf{r}}}{\sqrt{V}}\hat{\boldsymbol{\varepsilon}}_{\mathbf{k},s}, \tag{4.27a}$$

$$\sum_\alpha \to \frac{V}{(2\pi c)^3}\sum_{s=1}^{2}\int \omega_k^2\,\mathrm{d}\omega_k\,\mathrm{d}\Omega_k, \tag{4.27b}$$

with $\mathrm{d}\Omega_k = \sin\theta_k\,\mathrm{d}\theta_k\,\mathrm{d}\phi_k$ the element of solid angle in the $\mathbf{k}$-space and we used the free-space dispersion relation $\omega_k = c\,k$. Also, the gradient of the field modes is given by [Eq. (3.20b)]:

$$\nabla\mathbf{A}_{\mathbf{k},s}(\mathbf{r}) = i\frac{\omega_k}{c}\hat{\mathbf{k}}\frac{e^{i\mathbf{k}\cdot\mathbf{r}}}{\sqrt{V}}\hat{\boldsymbol{\varepsilon}}_{\mathbf{k},s}, \tag{4.28}$$

where the caret denotes normalized vectors.

Since we noted in Section 3.4 that the developments carried out for the MD transition are very similar to those carried out for the ED transition, only the developments for the 2ED and 2EQ transitions are presented. Let us now calculate the transition rates given by the equations (4.25) by carrying out the replacement given by the equations (4.27) and by using the gradient calculated in equation (4.28). Thereby, the 2ED transition rate is given by

$$\Gamma^{(2)}_{\mathrm{2ED},0}(\mathbf{R}) = \frac{\pi}{4\varepsilon_0^2\hbar^2}\frac{V^2}{(2\pi c)^6}\sum_{s,s'=1}^{2}\iint \omega_k^3\omega_{k'}^3\left|\frac{e^{i\mathbf{k}\cdot\mathbf{R}}}{\sqrt{V}}\hat{\boldsymbol{\varepsilon}}_{\mathbf{k},s}\cdot\boldsymbol{\mathcal{D}}^{eg}(\omega_k,\omega_{k'})\cdot\frac{e^{i\mathbf{k}\cdot\mathbf{R}}}{\sqrt{V}}\hat{\boldsymbol{\varepsilon}}_{\mathbf{k}',s'}\right|^2 \times \delta(\omega_{eg}-\omega_k-\omega_{k'})\,\mathrm{d}\omega_k\,\mathrm{d}\omega_{k'}\,\mathrm{d}\Omega_k\,\mathrm{d}\Omega_{k'} \tag{4.29a}$$

$$\Leftrightarrow \Gamma^{(2)}_{\mathrm{2ED},0} = \frac{1}{2^8\pi^5\varepsilon_0^2\hbar^2c^6}\iint \omega_k^3\omega_{k'}^3\sum_{s,s'=1}^{2}\left|\hat{\boldsymbol{\varepsilon}}_{\mathbf{k},s}\cdot\boldsymbol{\mathcal{D}}^{eg}(\omega_k,\omega_{k'})\cdot\hat{\boldsymbol{\varepsilon}}_{\mathbf{k}',s'}\right|^2\delta(\omega_{eg}-\omega_k-\omega_{k'}) \times\ \mathrm{d}\omega_k\,\mathrm{d}\omega_{k'}\,\mathrm{d}\Omega_k\,\mathrm{d}\Omega_{k'}, \tag{4.29b}$$

while the 2EQ transition rate is rewritten as

$$\Gamma^{(2)}_{\mathrm{2EQ},0}(\mathbf{R}) = \frac{\pi}{4\varepsilon_0^2\hbar^2}\frac{V^2}{(2\pi c)^6}\sum_{s,s'=1}^{2}\iint \omega_k^3\omega_{k'}^3\left|\left[i\frac{\omega_k}{c}\hat{\mathbf{k}}\frac{e^{i\mathbf{k}\cdot\mathbf{R}}}{\sqrt{V}}\hat{\boldsymbol{\varepsilon}}_{\mathbf{k},s}\right]:\boldsymbol{\mathcal{Q}}^{eg}(\omega_k,\omega_{k'}):\left[i\frac{\omega_{k'}}{c}\hat{\mathbf{k}}'\frac{e^{i\mathbf{k}'\cdot\mathbf{R}}}{\sqrt{V}}\hat{\boldsymbol{\varepsilon}}_{\mathbf{k}',s'}\right]\right|^2 \times \delta(\omega_{eg}-\omega_k-\omega_{k'})\,\mathrm{d}\omega_k\,\mathrm{d}\omega_{k'}\,\mathrm{d}\Omega_k\,\mathrm{d}\Omega_{k'} \tag{4.30a}$$

$$\Leftrightarrow \Gamma^{(2)}_{\mathrm{2EQ},0} = \frac{1}{2^8\pi^5\varepsilon_0^2\hbar^2c^{10}}\iint \omega_k^5\omega_{k'}^5\sum_{s,s'=1}^{2}\left|\hat{\mathbf{k}}\,\hat{\boldsymbol{\varepsilon}}_{\mathbf{k},s}:\boldsymbol{\mathcal{Q}}^{eg}(\omega_k,\omega_{k'}):\hat{\mathbf{k}}'\,\hat{\boldsymbol{\varepsilon}}_{\mathbf{k}',s'}\right|^2\delta(\omega_{eg}-\omega_k-\omega_{k'}) \times\ \mathrm{d}\omega_k\,\mathrm{d}\omega_k'\,\mathrm{d}\Omega_k\,\mathrm{d}\Omega_{k'}, \tag{4.30b}$$

where the transition rates are now independent of the emitter position $\mathbf{R}$ due to the homogeneity of space and where the subscript 0 reminds that the emission takes place in vacuum.

Next, calculating the dot and double dot products as well as the square modulus leads to

$$\Gamma^{(2)}_{\mathrm{2ED},0} = \frac{1}{2^8\pi^5\varepsilon_0^2\hbar^2c^6}\iint \omega_k^3\omega_{k'}^3\,\mathcal{D}^{eg}_{ij}(\omega_k,\omega_{k'})\left(\mathcal{D}^{eg}_{ab}(\omega_k,\omega_{k'})\right)^*\sum_{s=1}^{2}\hat{\varepsilon}_{\mathbf{k},s,i}\,\hat{\varepsilon}^*_{\mathbf{k},s,a}\sum_{s'=1}^{2}\hat{\varepsilon}_{\mathbf{k}',s',j}\,\hat{\varepsilon}^*_{\mathbf{k}',s',b} \times \delta(\omega_{eg}-\omega_k-\omega_{k'})\,\mathrm{d}\omega_k\,\mathrm{d}\omega_{k'}\,\mathrm{d}\Omega_k\,\mathrm{d}\Omega_{k'}, \tag{4.31}$$

and

$$\Gamma^{(2)}_{2\mathrm{EQ},0} = \frac{1}{2^8\pi^5\varepsilon_0^2\hbar^2c^{10}} \iint \omega_k^5\omega_{k'}^5\, \mathcal{Q}^{eg}_{ijhl}(\omega_k,\omega_{k'}) \left(\mathcal{Q}^{eg}_{abcd}(\omega_k,\omega_{k'})\right)^* \hat{\mathrm{k}}_j\,\hat{\mathrm{k}}_b\,\hat{\mathrm{k}}'_l\,\hat{\mathrm{k}}'_d \sum_{s=1}^{2} \hat{\varepsilon}_{\mathbf{k},s,i}\,\hat{\varepsilon}^*_{\mathbf{k},s,a} \times \sum_{s'=1}^{2} \hat{\varepsilon}_{\mathbf{k}',s',h}\,\hat{\varepsilon}^*_{\mathbf{k}',s',c}\,\delta(\omega_{eg}-\omega_k-\omega_{k'})\,\mathrm{d}\omega_k\,\mathrm{d}\omega_{k'}\,\mathrm{d}\Omega_k\,\mathrm{d}\Omega_{k'}, \tag{4.32}$$

where the Einstein summation convention is used and where $\hat{\varepsilon}_{\mathbf{k},s,i}$ and $\hat{\mathrm{k}}_i$ denote, respectively, the components in spherical coordinates of the unitary vectors $\hat{\boldsymbol{\varepsilon}}_{\mathbf{k},s}$ and of the normalized wave vector $\hat{\mathbf{k}}$ ($i = 1, 2, 3$). In addition, $\hat{\mathbf{k}}$ and $\hat{\mathbf{k}}'$ are real vectors since there are no losses in vacuum (in general, polarization vectors can be complex [94]).

Now, in order to calculate the integrals over the solid angles, we use the closure relation of the orthonormal basis $\left\{\hat{\boldsymbol{\varepsilon}}_{\mathbf{k},1}, \hat{\boldsymbol{\varepsilon}}_{\mathbf{k},2}, \hat{\mathbf{k}}\right\}$ [Eq. (3.25b)]:

$$\sum_{s=1}^{2} \hat{\varepsilon}_{\mathbf{k},s,i}\,\hat{\varepsilon}^*_{\mathbf{k},s,j} = \delta_{ij} - \hat{\mathrm{k}}_i\,\hat{\mathrm{k}}_j. \tag{4.33}$$

Thus, one can show that[9]:

$$\iint \sum_{s=1}^{2} \hat{\varepsilon}_{\mathbf{k},s,i}\,\hat{\varepsilon}^*_{\mathbf{k},s,a} \sum_{s'=1}^{2} \hat{\varepsilon}_{\mathbf{k}',s',j}\,\hat{\varepsilon}^*_{\mathbf{k}',s',b}\,d\Omega_k\,\mathrm{d}\Omega_{k'} = \iint (\delta_{ia}-\hat{\mathrm{k}}_i\hat{\mathrm{k}}_a)(\delta_{jb}-\hat{\mathrm{k}}'_j\hat{\mathrm{k}}'_b)\,d\Omega_k\,\mathrm{d}\Omega_{k'} \tag{4.34a}$$

$$= \left(\frac{8\pi}{3}\right)^2 \delta_{ia}\delta_{jb}, \tag{4.34b}$$

and that

$$\iint \hat{\mathrm{k}}_j\,\hat{\mathrm{k}}_b\,\hat{\mathrm{k}}'_l\,\hat{\mathrm{k}}'_d \sum_{s=1}^{2} \hat{\varepsilon}_{\mathbf{k},s,i}\,\hat{\varepsilon}^*_{\mathbf{k},s,a} \sum_{s'=1}^{2} \hat{\varepsilon}_{\mathbf{k}',s',h}\,\hat{\varepsilon}^*_{\mathbf{k}',s',c}\,d\Omega_k\,\mathrm{d}\Omega_{k'}$$

$$= \iint \hat{\mathrm{k}}_j\,\hat{\mathrm{k}}_b\,\hat{\mathrm{k}}'_l\,\hat{\mathrm{k}}'_d\,(\delta_{ia}-\hat{\mathrm{k}}_i\,\hat{\mathrm{k}}_a)\,(\delta_{hc}-\hat{\mathrm{k}}'_h\,\hat{\mathrm{k}}'_c)\,d\Omega_k\,\mathrm{d}\Omega_{k'} \tag{4.35a}$$

$$= \delta_{ia}\,\delta_{hc} \int \hat{\mathrm{k}}_j\hat{\mathrm{k}}_b\,\mathrm{d}\Omega_k \int \hat{\mathrm{k}}'_l\hat{\mathrm{k}}'_d\,\mathrm{d}\Omega_{k'} - \delta_{ia}\int \hat{\mathrm{k}}_j\hat{\mathrm{k}}_b\,\mathrm{d}\Omega_k \int \hat{\mathrm{k}}'_h\hat{\mathrm{k}}'_l\hat{\mathrm{k}}'_c\hat{\mathrm{k}}'_d\,\mathrm{d}\Omega_{k'}$$

$$- \delta_{hc}\int \hat{\mathrm{k}}_i\hat{\mathrm{k}}_j\hat{\mathrm{k}}_a\hat{\mathrm{k}}_b\,\mathrm{d}\Omega_k \int \hat{\mathrm{k}}'_l\hat{\mathrm{k}}'_d\,\mathrm{d}\Omega_{k'} + \int \hat{\mathrm{k}}_i\hat{\mathrm{k}}_j\hat{\mathrm{k}}_a\hat{\mathrm{k}}_b\,\mathrm{d}\Omega_k \int \hat{\mathrm{k}}'_h\hat{\mathrm{k}}'_l\hat{\mathrm{k}}'_c\hat{\mathrm{k}}'_d\,\mathrm{d}\Omega_{k'}. \tag{4.35b}$$

Multiplying the last result by the product $\mathcal{Q}^{eg}_{ijhl}\,(\mathcal{Q}^{eg}_{abcd})^*$, which depends only on the angular frequencies and not on the solid angles, leads to

$$\mathcal{Q}^{eg}_{ijhl}\,(\mathcal{Q}^{eg}_{abcd})^* \iint \hat{\mathrm{k}}_j\,\hat{\mathrm{k}}_b\,\hat{\mathrm{k}}'_l\,\hat{\mathrm{k}}'_d \sum_{s} \hat{\varepsilon}_{\mathbf{k},s,i}\,\hat{\varepsilon}^*_{\mathbf{k},s,a} \sum_{s'} \hat{\varepsilon}_{\mathbf{k}',s',h}\,\hat{\varepsilon}^*_{\mathbf{k}',s',c}\,d\Omega_k\,\mathrm{d}\Omega_{k'} = \left(\frac{4\pi}{5}\right)^2 \|\boldsymbol{\mathcal{Q}}^{eg}\|^2, \tag{4.36}$$

where we define the squared norm of a rank-$n$ tensor $\mathbf{U}$ with $n \geq 1$ as $\|\mathbf{U}\|^2 := \sum_{i_1,i_2,\ldots,i_n} |U_{i_1,i_2,\ldots,i_n}|^2$. To obtain the last result, the properties of the tensor $\boldsymbol{\mathcal{Q}}^{eg}$ given by the equations (4.19) and (4.20) have been used. Therefore, using equations (4.34b) and (4.36) in the equations (4.31) and (4.32),

[9] The solid angle of the whole space is $4\pi$. Moreover, one can show that [94]: $\int_{4\pi} \hat{k}_i\hat{k}_j\,\mathrm{d}\Omega_k = \frac{4\pi}{3}\delta_{ij}$ and $\int_{4\pi} \hat{k}_i\hat{k}_j\hat{k}_a\hat{k}_b\,\mathrm{d}\Omega_k = \frac{4\pi}{15}\,(\delta_{ij}\delta_{ab}+\delta_{ia}\delta_{jb}+\delta_{ib}\delta_{ja})$ by using the expression of the vector $\hat{\mathbf{k}}$ in spherical coordinates: $\hat{\mathbf{k}} = \sin\theta\cos\varphi\,\mathbf{e}_x + \sin\theta\sin\varphi\,\mathbf{e}_y + \cos\theta\,\mathbf{e}_z$.

we get

$$\Gamma^{(2)}_{\mathrm{2ED},0} = \frac{1}{36\pi^3\varepsilon_0^2\hbar^2c^6}\iint \omega_k^3\omega_{k'}^3 \left\|\boldsymbol{\mathcal{D}}^{eg}(\omega_k,\omega_{k'})\right\|^2 \delta(\omega_{eg}-\omega_k-\omega_{k'})\,\mathrm{d}\omega_k\,\mathrm{d}\omega_{k'}, \tag{4.37a}$$

$$\Gamma^{(2)}_{\mathrm{2EQ},0} = \frac{1}{400\pi^3\varepsilon_0^2\hbar^2c^{10}}\iint \omega_k^5\omega_{k'}^5 \left\|\boldsymbol{\mathcal{Q}}^{eg}(\omega_k,\omega_{k'})\right\|^2 \delta(\omega_{eg}-\omega_k-\omega_{k'})\,\mathrm{d}\omega_k\,\mathrm{d}\omega_{k'}. \tag{4.37b}$$

One of the two integrations in these equations can be solved with the following change of variables [2]:

$$\begin{cases} W = \omega_k + \omega_{k'} & \text{(4.38a)} \\ \omega = \omega_k & \text{(4.38b)} \\ \mathrm{d}\omega_k\,\mathrm{d}\omega_{k'} = \mathrm{d}W\,\mathrm{d}\omega. & \text{(4.38c)} \end{cases}$$

Thus, one obtains

$$\Gamma^{(2)}_{\mathrm{2ED},0} = \frac{1}{36\pi^3\varepsilon_0^2\hbar^2c^6}\iint \omega^3(W-\omega)^3 \left\|\boldsymbol{\mathcal{D}}^{eg}(\omega,W-\omega)\right\|^2 \delta(\omega_{eg}-W)\,\mathrm{d}\omega\,\mathrm{d}W \tag{4.39a}$$

$$= \frac{1}{36\pi^3\varepsilon_0^2\hbar^2c^6}\int \omega^3(\omega_{eg}-\omega)^3 \left\|\boldsymbol{\mathcal{D}}^{eg}(\omega,\omega_{eg}-\omega)\right\|^2 \mathrm{d}\omega, \tag{4.39b}$$

$$\Gamma^{(2)}_{\mathrm{2EQ},0} = \frac{1}{400\pi^3\varepsilon_0^2\hbar^2c^{10}}\int \omega^5(\omega_{eg}-\omega)^5 \left\|\boldsymbol{\mathcal{Q}}^{eg}(\omega,\omega_{eg}-\omega)\right\|^2 \mathrm{d}\omega. \tag{4.39c}$$

With similar developments to those carried out for calculating the MD transition rate [Sec. 3.4] and the 2ED transition rate in vacuum, one gets a similar equation for the 2MD transition rate in vacuum.

Finally, since the energy of an emitted quantum ranges from 0 to $\hbar\omega_{eg}$, we obtain for $\mathrm{2MO} \in \{\mathrm{2ED},\ \mathrm{2MD},\ \mathrm{2EQ}\}$ that the vacuum TPSE rate is given by

$$\Gamma^{(2)}_{\mathrm{2MO},0} = \int_0^{\omega_{eg}} \gamma^{(2)}_{\mathrm{2MO},0}(\omega)\,\mathrm{d}\omega, \tag{4.40}$$

where the multipolar contributions $\gamma^{(2)}_{\mathrm{2MO},0}(\omega)$ to the spectral distribution of the emitted quanta in vacuum are given by

$$\gamma^{(2)}_{\mathrm{2ED},0}(\omega) = \frac{1}{36\pi^3\varepsilon_0^2\hbar^2c^6}\,\omega^3(\omega_{eg}-\omega)^3 \left\|\boldsymbol{\mathcal{D}}^{eg}(\omega,\omega_{eg}-\omega)\right\|^2, \tag{4.41a}$$

$$\gamma^{(2)}_{\mathrm{2MD},0}(\omega) = \frac{1}{36\pi^3\varepsilon_0^2\hbar^2c^{10}}\,\omega^3(\omega_{eg}-\omega)^3 \left\|\boldsymbol{\mathcal{M}}^{eg}(\omega,\omega_{eg}-\omega)\right\|^2, \tag{4.41b}$$

$$\gamma^{(2)}_{\mathrm{2EQ},0}(\omega) = \frac{1}{400\pi^3\varepsilon_0^2\hbar^2c^{10}}\,\omega^5(\omega_{eg}-\omega)^5 \left\|\boldsymbol{\mathcal{Q}}^{eg}(\omega,\omega_{eg}-\omega)\right\|^2, \tag{4.41c}$$

where the expression of the 2ED transition rate in vacuum has been derived in Ref. 31. As the spontaneous emission takes place in vacuum, the calculated rates are independent of the emitter position. Since there are no interferences in vacuum [2], the total TPSE rate is given by the three previous transition rates:

$$\gamma^{(2)}_{\mathrm{tot},0}(\omega) = \gamma^{(2)}_{\mathrm{2ED},0}(\omega) + \gamma^{(2)}_{\mathrm{2MD},0}(\omega) + \gamma^{(2)}_{\mathrm{2EQ},0}(\omega). \tag{4.42}$$

## 4.5 Expression via the Green's function

In Section 4.3, we derived the multipolar contributions to the TPSE as a function of the field modes [Eqs. (4.25) and (4.26)]. However, it is more convenient to express them via the dyadic Green's function and to normalize them with respect to vacuum. In this way, we obtain more elegant equations, and we establish a direct link with the power emitted by classical point sources [Sec. 2.5]. Moreover, we will then be able to use the link between the Green's functions and the Purcell factors derived in Section 3.7 in order to express the TPSE rates as a function of Purcell factors. The imaginary part of the Green's function admits a spectral representation that can be expanded in terms of the normal modes $\mathbf{A}_\alpha$ of the electromagnetic field [30]:

$$\operatorname{Im}\mathbf{G}(\omega;\mathbf{r},\mathbf{r}') = \frac{\pi c^2}{2\omega}\sum_\alpha \mathbf{A}_\alpha(\mathbf{r})\mathbf{A}_\alpha^*(\mathbf{r}')\,\delta(\omega-\omega_\alpha), \tag{4.43}$$

where $c$ denotes the speed of light in vacuum. Note that if $\mathbf{r}=\mathbf{r}'$, the imaginary part of the Green's function is symmetric [30]. As a reminder, we have previously defined the Green's functions related to the MD, EQ, and to the interference between an ED and an EQ [Eqs. (3.37), (3.40) and (4.44c)]:

$$k^2\,G_{ij}^{\mathrm{MD}}(\omega;\mathbf{R},\mathbf{R}) := \left\{\varepsilon_{ikl}\,\varepsilon_{jmn}\,\partial_k\partial'_m G_{ln}(\omega;\mathbf{r},\mathbf{r}')\right\}_{\mathbf{r}=\mathbf{r}'=\mathbf{R}}, \tag{4.44a}$$

$$k^2\,G_{jilk}^{\mathrm{EQ}}(\omega;\mathbf{R},\mathbf{R}) := \left\{\partial_j\partial'_l\,G_{ik}(\omega;\mathbf{r},\mathbf{r}')\right\}_{\mathbf{r}=\mathbf{r}'=\mathbf{R}}, \tag{4.44b}$$

$$k\,G_{ikj}^{\mathrm{ED}\cap\mathrm{EQ}}(\omega;\mathbf{R},\mathbf{R}) := \left\{\partial'_k\,G_{ij}(\omega;\mathbf{r},\mathbf{r}')\right\}_{\mathbf{r}=\mathbf{r}'=\mathbf{R}}, \tag{4.44c}$$

where $\varepsilon_{ijk}$ denotes the Levi-Civita symbol [Eq. (3.34)] and where $\partial_i$ and $\partial_{i'}$ mean derivatives with respect to the coordinates $\mathbf{r}$ and $\mathbf{r}'$, respectively. First, we present the developments of Ref. 31 relative to the 2ED transition. Then, we perform similar developments for the 2MD and 2EQ transitions as well as for the interference term $\Gamma^{(2)}_{\mathrm{2ED}\cap\mathrm{2EQ}}$. Finally, we normalize the obtained equations with respect to vacuum and discuss them.

### 4.5.1 Two-electric dipole transition

Let us start by introducing the imaginary part of the Green's function [Eq. (4.43)] relative to the modes $\alpha'$ in equation (4.25a) of the 2ED transition rate [31]:

$$\Gamma^{(2)}_{\mathrm{2ED}}(\mathbf{R}) = \frac{\pi}{4\varepsilon_0^2\hbar^2}\sum_{\alpha,\alpha'}\omega_\alpha\omega_{\alpha'}\left|\mathbf{A}_\alpha(\mathbf{R})\cdot\boldsymbol{\mathcal{D}}^{eg}(\omega_\alpha,\omega_{\alpha'})\cdot\mathbf{A}_{\alpha'}(\mathbf{R})\right|^2\delta(\omega_{eg}-\omega_\alpha-\omega_{\alpha'}) \tag{4.45a}$$

$$= \frac{\pi}{4\varepsilon_0^2\hbar^2}\sum_{\alpha,\alpha'}\omega_\alpha\omega_{\alpha'}\left(A_{\alpha,i}(\mathbf{R})\,\mathcal{D}_{ia}(\omega_\alpha,\omega_{\alpha'})\,A_{\alpha',a}(\mathbf{R})\right)\left(A_{\alpha,j}(\mathbf{R})\,\mathcal{D}_{jb}(\omega_\alpha,\omega_{\alpha'})\,A_{\alpha',b}(\mathbf{R})\right)^*$$
$$\times\,\delta(\omega_{eg}-\omega_\alpha-\omega_{\alpha'}) \tag{4.45b}$$

$$= \frac{\pi}{4\varepsilon_0^2\hbar^2}\sum_{\alpha}\omega_\alpha(\omega_{eg}-\omega_\alpha)\,\mathcal{D}_{ia}(\omega_\alpha,\omega_{eg}-\omega_\alpha)\,\mathcal{D}^*_{jb}(\omega_\alpha,\omega_{eg}-\omega_\alpha)\,A_{\alpha,i}(\mathbf{R})A^*_{\alpha,j}(\mathbf{R})$$
$$\times\sum_{\alpha'}A_{\alpha',a}(\mathbf{R})A^*_{\alpha',b}(\mathbf{R})\,\delta(\omega_{eg}-\omega_\alpha-\omega_{\alpha'}) \tag{4.45c}$$

$$= \frac{1}{2\varepsilon_0^2\hbar^2c^2}\sum_{\alpha}\omega_\alpha(\omega_{eg}-\omega_\alpha)^2\,\mathcal{D}_{ia}(\omega_\alpha,\omega_{eg}-\omega_\alpha)\,\mathcal{D}^*_{jb}(\omega_\alpha,\omega_{eg}-\omega_\alpha)\,A_{\alpha,i}(\mathbf{R})A^*_{\alpha,j}(\mathbf{R})$$
$$\times\,\operatorname{Im}G_{ab}(\omega_{eg}-\omega_\alpha;\mathbf{R},\mathbf{R}). \tag{4.45d}$$

In equation (4.45b), we developed the square modulus and calculated the dot products using the Einstein summation convention. In equation (4.45c), we used that the delta function restricts all values of $\omega'_\alpha$ to $\omega_{eg}-\omega_\alpha$, which can therefore be taken out of the sum over the modes $\alpha'$ to introduce the Green's function at this frequency [Eq. (4.45d)]. In these developments, the $eg$ superscript has been omitted and $A_{\alpha,i}$ denotes the components of the vector $\mathbf{A}_\alpha$.

To introduce the Green's function relative to the modes $\alpha$, let us use the property $f(\omega_\alpha) = \int_{-\infty}^{\infty} f(\omega)\,\delta(\omega-\omega_\alpha)\,\mathrm{d}\omega$ in order to introduce a delta function [31]:

$$\Gamma^{(2)}_{\mathrm{2ED}}(\mathbf{R}) = \frac{1}{2\varepsilon_0^2\hbar^2c^2}\int_{-\infty}^{\infty}\omega(\omega_{eg}-\omega)^2\,\mathcal{D}_{ia}(\omega,\omega_{eg}-\omega)\,\mathcal{D}^*_{jb}(\omega,\omega_{eg}-\omega) \times\sum_\alpha A_{\alpha,i}(\mathbf{R})A^*_{\alpha,j}(\mathbf{R})\,\delta(\omega-\omega_\alpha)\,\mathrm{Im}\,G_{ab}(\omega_{eg}-\omega;\mathbf{R},\mathbf{R})\,\mathrm{d}\omega \tag{4.46a}$$

$$= \frac{1}{\pi\varepsilon_0^2\hbar^2c^4}\int_0^{\omega_{eg}}\omega^2(\omega_{eg}-\omega)^2\mathcal{D}_{ia}(\omega,\omega_{eg}-\omega)\,\mathcal{D}^*_{jb}(\omega,\omega_{eg}-\omega) \times\mathrm{Im}\,G_{ij}(\omega;\mathbf{R},\mathbf{R})\,\mathrm{Im}\,G_{ab}(\omega_{eg}-\omega;\mathbf{R},\mathbf{R})\,\mathrm{d}\omega, \tag{4.46b}$$

where the integration limits have been adapted since the photon frequency ranges from 0 to $\omega_{eg}$.

### 4.5.2 Two-magnetic dipole transition

Then, with similar developments to those carried out above for the 2ED transition and those realized in Subsection 3.5.2 for the MD transition, one finds

$$\Gamma^{(2)}_{\mathrm{2MD}}(\mathbf{R}) = \frac{1}{\pi\varepsilon_0^2\hbar^2c^8}\int_0^{\omega_{eg}}\omega^2(\omega_{eg}-\omega)^2\mathcal{M}_{ia}(\omega,\omega_{eg}-\omega)\,\mathcal{M}^*_{jb}(\omega,\omega_{eg}-\omega) \times\mathrm{Im}\,G^{\mathrm{MD}}_{ij}(\omega;\mathbf{R},\mathbf{R})\,\mathrm{Im}\,G^{\mathrm{MD}}_{ab}(\omega_{eg}-\omega;\mathbf{R},\mathbf{R})\,\mathrm{d}\omega, \tag{4.47}$$

where we have identified the Green's function of the MD [Eq. (4.44a)] for the photons emitted at the complementary frequencies $\omega$ and $\omega_{eg}-\omega$.

### 4.5.3 Two-electric quadrupole transition

Next, let us perform similar developments for the 2EQ transition rate [Eq. (4.25c)] in order to reveal the Green's function for the EQ [Eq. (4.44b)] relative to the modes $\alpha'$:

$$\Gamma^{(2)}_{\mathrm{2EQ}}(\mathbf{R}) = \frac{\pi}{4\varepsilon_0^2\hbar^2}\sum_{\alpha,\alpha'}\omega_\alpha\omega_{\alpha'}\left|\nabla\mathbf{A}_\alpha(\mathbf{R}):\boldsymbol{\mathcal{Q}}^{eg}(\omega_\alpha,\omega_{\alpha'}):\nabla\mathbf{A}_{\alpha'}(\mathbf{R})\right|^2\delta(\omega_{eg}-\omega_\alpha-\omega_{\alpha'}) \tag{4.48a}$$

$$= \frac{\pi}{4\varepsilon_0^2\hbar^2}\sum_{\alpha,\alpha'}\omega_\alpha\omega_{\alpha'}\left(\partial_jA_{\alpha,i}(\mathbf{R})\,\mathcal{Q}_{ijab}(\omega_\alpha,\omega_{\alpha'})\,\partial_bA_{\alpha',a}(\mathbf{R})\right) \times\left(\partial_lA_{\alpha,k}(\mathbf{R})\,\mathcal{Q}_{klcd}(\omega_\alpha,\omega_{\alpha'})\,\partial_dA_{\alpha',c}(\mathbf{R})\right)^*\delta(\omega_{eg}-\omega_\alpha-\omega_{\alpha'}) \tag{4.48b}$$

$$= \frac{\pi}{4\varepsilon_0^2\hbar^2}\sum_{\alpha}\omega_\alpha(\omega_{eg}-\omega_\alpha)\,\mathcal{Q}_{ijab}(\omega_\alpha,\omega_{eg}-\omega_\alpha)\,\mathcal{Q}^*_{klcd}(\omega_\alpha,\omega_{eg}-\omega_\alpha)\,\partial_jA_{\alpha,i}(\mathbf{R})\,\partial_lA^*_{\alpha,k}(\mathbf{R}) \times\sum_{\alpha'}\partial_bA_{\alpha',a}(\mathbf{R})\,\partial_dA^*_{\alpha',c}(\mathbf{R})\,\delta(\omega_{eg}-\omega_\alpha-\omega_{\alpha'}). \tag{4.48c}$$

To go from one equation to the next, we developed the square modulus, calculated the double dot products using the Einstein summation convention, and we used that the delta function restricts all

values of $\omega'_\alpha$ to $\omega_{eg}-\omega_\alpha$, which can therefore be taken out of the sum over the modes $\alpha'$. To reveal the Green's function at the frequency $\omega_{eg}-\omega_\alpha$, the derivatives must be placed in front of the sum over $\alpha'$. To do so, we differentiate the spatial dependency of the normal modes and we take the limit $\mathbf{r},\mathbf{r}'\to\mathbf{R}$ [23]:

$$\Gamma^{(2)}_{\mathrm{2EQ}}(\mathbf{R}) = \frac{\pi}{4\varepsilon_0^2\hbar^2}\sum_\alpha \omega_\alpha(\omega_{eg}-\omega_\alpha)\,\mathcal{Q}_{ijab}(\omega_\alpha,\omega_{eg}-\omega_\alpha)\,\mathcal{Q}^*_{klcd}(\omega_\alpha,\omega_{eg}-\omega_\alpha)\,\partial_j A_{\alpha,i}(\mathbf{R})\,\partial_l A^*_{\alpha,k}(\mathbf{R}) \times\left\{\partial_b\partial_{d'}\sum_{\alpha'} A_{\alpha',a}(\mathbf{r})A^*_{\alpha',c}(\mathbf{r}')\,\delta(\omega_{eg}-\omega_\alpha-\omega_{\alpha'})\right\}_{\mathbf{r}=\mathbf{r}'=\mathbf{R}} \tag{4.49a}$$

$$= \frac{1}{2\varepsilon_0^2\hbar^2c^2}\sum_\alpha \omega_\alpha(\omega_{eg}-\omega_\alpha)^2\,\mathcal{Q}_{ijab}(\omega_\alpha,\omega_{eg}-\omega_\alpha)\,\mathcal{Q}^*_{klcd}(\omega_\alpha,\omega_{eg}-\omega_\alpha)\,\partial_j A_{\alpha,i}(\mathbf{R})\,\partial_l A^*_{\alpha,k}(\mathbf{R}) \times\left\{\partial_b\partial_{d'}\mathrm{Im}G_{ac}(\omega_{eg}-\omega_\alpha;\mathbf{r},\mathbf{r}')\right\}_{\mathbf{r}=\mathbf{r}'=\mathbf{R}} \tag{4.49b}$$

$$= \frac{1}{2\varepsilon_0^2\hbar^2c^4}\sum_\alpha \omega_\alpha(\omega_{eg}-\omega_\alpha)^4\,\mathcal{Q}_{ijab}(\omega_\alpha,\omega_{eg}-\omega_\alpha)\,\mathcal{Q}^*_{klcd}(\omega_\alpha,\omega_{eg}-\omega_\alpha)\,\partial_j A_{\alpha,i}(\mathbf{R})\,\partial_l A^*_{\alpha,k}(\mathbf{R}) \times \mathrm{Im}\,G^{\mathrm{EQ}}_{badc}(\omega_{eg}-\omega_\alpha;\mathbf{R},\mathbf{R}). \tag{4.49c}$$

As before, to reveal the Green's function relative to the modes $\alpha$, let us use the property $f(\omega_\alpha)=\int_{-\infty}^{\infty} f(\omega)\,\delta(\omega-\omega_\alpha)\,\mathrm{d}\omega$ in order to introduce a delta function [31]:

$$\Gamma^{(2)}_{\mathrm{2EQ}}(\mathbf{R}) = \frac{1}{2\varepsilon_0^2\hbar^2c^4}\int_{-\infty}^{\infty}\omega(\omega_{eg}-\omega)^4\,\mathcal{Q}_{ijab}(\omega,\omega_{eg}-\omega)\,\mathcal{Q}^*_{klcd}(\omega,\omega_{eg}-\omega) \times\sum_\alpha \partial_j A_{\alpha,i}\,\partial_l A^*_{\alpha,k}\,\delta(\omega-\omega_\alpha)\,\mathrm{Im}\,G^{\mathrm{EQ}}_{badc}(\omega_{eg}-\omega;\mathbf{R},\mathbf{R})\,\mathrm{d}\omega \tag{4.50a}$$

$$= \frac{1}{\pi\varepsilon_0^2\hbar^2c^8}\int_0^{\omega_{eg}}\omega^4(\omega_{eg}-\omega)^4\mathcal{Q}_{ijab}(\omega,\omega_{eg}-\omega)\,\mathcal{Q}^*_{klcd}(\omega,\omega_{eg}-\omega) \times\mathrm{Im}\,G^{\mathrm{EQ}}_{jilk}(\omega;\mathbf{R},\mathbf{R})\,\mathrm{Im}\,G^{\mathrm{EQ}}_{badc}(\omega_{eg}-\omega;\mathbf{R},\mathbf{R})\,\mathrm{d}\omega, \tag{4.50b}$$

where the integration limits have been adapted since the photon frequency ranges from 0 to $\omega_{eg}$.

### 4.5.4 Interference term

Finally, similar developments can be made for the term describing the interference between the 2ED and 2EQ transitions [Eq. (4.26b)]:

$$\Gamma^{(2)}_{\mathrm{2ED\cap 2EQ}}(\mathbf{R}) = 2\,\frac{\pi}{4\varepsilon_0^2\hbar^2}\sum_{\alpha,\alpha'}\omega_\alpha\omega_{\alpha'}\,(\mathbf{A}_\alpha(\mathbf{R})\cdot\boldsymbol{\mathcal{D}}^{eg}(\omega_\alpha,\omega_{\alpha'})\cdot\mathbf{A}_{\alpha'}(\mathbf{R})) \times(\nabla\mathbf{A}_\alpha(\mathbf{R}):\boldsymbol{\mathcal{Q}}^{eg}(\omega_\alpha,\omega_{\alpha'}):\nabla\mathbf{A}_{\alpha'}(\mathbf{R}))^*\,\delta(\omega_{eg}-\omega_\alpha-\omega_{\alpha'}) \tag{4.51a}$$

$$= 2\,\frac{\pi}{4\varepsilon_0^2\hbar^2}\sum_{\alpha,\alpha'}\omega_\alpha\omega_{\alpha'}\left(A_{\alpha,i}\,\mathcal{D}_{ia}(\omega_\alpha,\omega_{\alpha'})\,A_{\alpha',a}\right) \times\left(\partial_k A_{\alpha,j}\,\mathcal{Q}_{jkbc}(\omega_\alpha,\omega_{\alpha'})\,\partial_c A_{\alpha',b}\right)^*\delta(\omega_{eg}-\omega_\alpha-\omega_{\alpha'}) \tag{4.51b}$$

$$= 2\,\frac{\pi}{4\varepsilon_0^2\hbar^2}\sum_{\alpha}\omega_\alpha(\omega_{eg}-\omega_\alpha)\,\mathcal{D}_{ia}(\omega_\alpha,\omega_{eg}-\omega_\alpha)\,\mathcal{Q}^*_{jkbc}(\omega_\alpha,\omega_{eg}-\omega_\alpha)\,A_{\alpha,i}\,\partial_k A^*_{\alpha,j} \times\sum_{\alpha'}A_{\alpha',a}\,\partial_c A^*_{\alpha',b}\,\delta(\omega_{eg}-\omega_\alpha-\omega_{\alpha'}) \tag{4.51c}$$

$$= 2\,\frac{\pi}{4\varepsilon_0^2\hbar^2}\sum_{\alpha}\omega_\alpha(\omega_{eg}-\omega_\alpha)\,\mathcal{D}_{ia}(\omega_\alpha,\omega_{eg}-\omega_\alpha)\,\mathcal{Q}^*_{jkbc}(\omega_\alpha,\omega_{eg}-\omega_\alpha)\,A_{\alpha,i}\,\partial_k A^*_{\alpha,j}$$
$$\times\left\{\partial_{c'}\sum_{\alpha'}A_{\alpha',a}(\mathbf{r})A^*_{\alpha',b}(\mathbf{r}')\,\delta(\omega_{eg}-\omega_\alpha-\omega_{\alpha'})\right\}_{\mathbf{r}=\mathbf{r}'=\mathbf{R}} \tag{4.51d}$$
$$= 2\,\frac{1}{2\varepsilon_0^2\hbar^2c^2}\sum_{\alpha}\omega_\alpha(\omega_{eg}-\omega_\alpha)^2\,\mathcal{D}_{ia}(\omega_\alpha,\omega_{eg}-\omega_\alpha)\,\mathcal{Q}^*_{jkbc}(\omega_\alpha,\omega_{eg}-\omega_\alpha)\,A_{\alpha,i}\,\partial_k A^*_{\alpha,j}$$
$$\times\left\{\partial_{c'}\mathrm{Im}G_{ab}(\omega_{eg}-\omega_\alpha;\mathbf{r},\mathbf{r}')\right\}_{\mathbf{r}=\mathbf{r}'=\mathbf{R}} \tag{4.51e}$$
$$= 2\,\frac{1}{2\varepsilon_0^2\hbar^2c^3}\sum_{\alpha}\omega_\alpha(\omega_{eg}-\omega_\alpha)^3\,\mathcal{D}_{ia}(\omega_\alpha,\omega_{eg}-\omega_\alpha)\,\mathcal{Q}^*_{jkbc}(\omega_\alpha,\omega_{eg}-\omega_\alpha)\,A_{\alpha,i}\,\partial_k A^*_{\alpha,j}$$
$$\times\,\mathrm{Im}\,G^{\mathrm{ED}\cap\mathrm{EQ}}_{acb}(\omega_{eg}-\omega_\alpha;\mathbf{R},\mathbf{R}), \tag{4.51f}$$

where we introduced $\mathbf{G}^{\mathrm{ED}\cap\mathrm{EQ}}$ [Eq. (4.44c)] for the photon emitted at the frequency $\omega_{eg}-\omega_\alpha$. By using the property $f(\omega_\alpha)=\int_{-\infty}^{\infty}f(\omega)\,\delta(\omega-\omega_\alpha)\,\mathrm{d}\omega$, one gets

$$\Gamma^{(2)}_{2\mathrm{ED}\cap2\mathrm{EQ}} = 2\,\frac{1}{2\varepsilon_0^2\hbar^2c^3}\int_{-\infty}^{\infty}\omega(\omega_{eg}-\omega)^3\,\mathcal{D}_{ia}(\omega,\omega_{eg}-\omega)\,\mathcal{Q}^*_{jkbc}(\omega,\omega_{eg}-\omega)$$
$$\times\sum_{\alpha}A_{\alpha,i}\,\partial_k A^*_{\alpha,j}\,\delta(\omega-\omega_\alpha)\,\mathrm{Im}\,G^{\mathrm{ED}\cap\mathrm{EQ}}_{acb}(\omega_{eg}-\omega;\mathbf{R},\mathbf{R})\,\mathrm{d}\omega \tag{4.52a}$$
$$= 2\,\frac{1}{\pi\varepsilon_0^2\hbar^2c^6}\int_0^{\omega_{eg}}\omega^3(\omega_{eg}-\omega)^3\,\mathcal{D}_{ia}(\omega,\omega_{eg}-\omega)\,\mathcal{Q}^*_{jkbc}(\omega,\omega_{eg}-\omega)$$
$$\times\,\mathrm{Im}\,G^{\mathrm{ED}\cap\mathrm{EQ}}_{ikj}(\omega;\mathbf{R},\mathbf{R})\,\mathrm{Im}\,G^{\mathrm{ED}\cap\mathrm{EQ}}_{acb}(\omega_{eg}-\omega;\mathbf{R},\mathbf{R})\,\mathrm{d}\omega, \tag{4.52b}$$

where the real part is implied and where we have identified the Green's function [Eq. (4.44c)] related to the photon emitted at the frequency $\omega$. Similar equations can be derived for the interference terms involving the 2MD decay channel, but will not be presented in this thesis.

### 4.5.5 Vacuum normalization and discussion

Now, let us normalize the integrand of the derived equations by the vacuum transition rates given by the equations (4.41). We obtain for $\mathrm{2MO}\in\{\mathrm{2ED},\ \mathrm{2MD},\ \mathrm{2EQ},\ \mathrm{2ED}\cap\mathrm{2EQ}\}$ that the TPSE rate is given by

$$\Gamma^{(2)}_{\mathrm{2MO}}(\mathbf{R}) = \int_0^{\omega_{eg}}\gamma^{(2)}_{\mathrm{2MO}}(\omega;\mathbf{R})\,\mathrm{d}\omega, \tag{4.53}$$

where the multipolar contributions $\gamma^{(2)}_{\mathrm{2MO}}(\omega;\mathbf{R})$ to the spectral distribution of the emitted quanta, normalized with respect to vacuum, are given by

$$\frac{\gamma^{(2)}_{\mathrm{2ED}}(\omega;\mathbf{R})}{\gamma^{(2)}_{\mathrm{2ED},0}(\omega)} = \frac{6\pi c}{\omega}\frac{6\pi c}{\omega_{eg}-\omega}\,\hat{\mathcal{D}}^{eg}_{ia}(\omega,\omega_{eg}-\omega)\left(\hat{\mathcal{D}}^{eg}_{jb}(\omega,\omega_{eg}-\omega)\right)^*$$
$$\times\,\mathrm{Im}\,G_{ij}(\omega;\mathbf{R},\mathbf{R})\,\mathrm{Im}\,G_{ab}(\omega_{eg}-\omega;\mathbf{R},\mathbf{R}), \tag{4.54a}$$
$$\frac{\gamma^{(2)}_{\mathrm{2MD}}(\omega;\mathbf{R})}{\gamma^{(2)}_{\mathrm{2MD},0}(\omega)} = \frac{6\pi c}{\omega}\frac{6\pi c}{\omega_{eg}-\omega}\,\hat{\mathcal{M}}^{eg}_{ia}(\omega,\omega_{eg}-\omega)\left(\hat{\mathcal{M}}^{eg}_{jb}(\omega,\omega_{eg}-\omega)\right)^*$$
$$\times\,\mathrm{Im}\,G^{\mathrm{MD}}_{ij}(\omega;\mathbf{R},\mathbf{R})\,\mathrm{Im}\,G^{\mathrm{MD}}_{ab}(\omega_{eg}-\omega;\mathbf{R},\mathbf{R}), \tag{4.54b}$$

$$\frac{\gamma^{(2)}_{\mathrm{2EQ}}(\omega;\mathbf{R})}{\gamma^{(2)}_{\mathrm{2EQ},0}(\omega)} = \frac{20\pi c}{\omega}\frac{20\pi c}{\omega_{eg}-\omega}\,\hat{\mathcal{Q}}^{eg}_{ijab}(\omega,\omega_{eg}-\omega)\left(\hat{\mathcal{Q}}^{eg}_{klcd}(\omega,\omega_{eg}-\omega)\right)^{*} \times \operatorname{Im} G^{\mathrm{EQ}}_{jilk}(\omega;\mathbf{R},\mathbf{R})\operatorname{Im} G^{\mathrm{EQ}}_{badc}(\omega_{eg}-\omega;\mathbf{R},\mathbf{R}), \tag{4.54c}$$

$$\frac{\gamma^{(2)}_{\mathrm{2ED}\cap\mathrm{2EQ}}(\omega;\mathbf{R})}{\sqrt{\gamma^{(2)}_{\mathrm{2ED},0}(\omega)\,\gamma^{(2)}_{\mathrm{2EQ},0}(\omega)}} = 2\,\frac{2\sqrt{30}\pi c}{\omega}\frac{2\sqrt{30}\pi c}{\omega_{eg}-\omega}\,\hat{\mathcal{D}}^{eg}_{ia}(\omega,\omega_{eg}-\omega)\left(\hat{\mathcal{Q}}^{eg}_{jkbc}(\omega,\omega_{eg}-\omega)\right)^{*} \times \operatorname{Im} G^{\mathrm{ED}\cap\mathrm{EQ}}_{ikj}(\omega;\mathbf{R},\mathbf{R})\operatorname{Im} G^{\mathrm{ED}\cap\mathrm{EQ}}_{acb}(\omega_{eg}-\omega;\mathbf{R},\mathbf{R}), \tag{4.54d}$$

where the caret indicates normalized tensors (i.e., for an $n^{\mathrm{th}}$ rank tensor $\mathbf{U}$ with $n \in \mathbb{N}_0$, $\hat{\mathbf{U}} := \mathbf{U}/\left\|\mathbf{U}\right\|$ with $\left\|\mathbf{U}\right\|^2 := \sum_{i_1,i_2,\ldots,i_n} |U_{i_1,i_2,\ldots,i_n}|^2$). Note that the derived equations are valid regardless of the emitter and its environment.

The derived equations are similar to those obtained for the OPSE (3.44) and their differences make sense, suggesting that the derived equations are correct. In particular, it is the second-order transition moments that are involved instead of the first-order ones and the Green's function (with the factor in front) intervenes twice, once for each photon that are emitted with the complementary frequencies $\omega$ and $\omega_{eg}-\omega$. Therefore, the impact of the environment on the two emitted photons is decoupled. Also, the first index of $\boldsymbol{\mathcal{D}}^{eg}$ and $\boldsymbol{\mathcal{M}}^{eg}$ and the first two indices of $\boldsymbol{\mathcal{Q}}^{eg}$ are related to the photon emitted at the frequency $\omega$ (first Green's function) while the others are related to the second photon emitted at the complementary frequency (second Green's function). Furthermore, the first three equations represent the change of the multipolar TPSE rates due to the environment, i.e., the two-photon Purcell effect.

## 4.6 Simplification using a modified Voigt notation

Before expressing the TPSE rates as a function of the one-photon Purcell factors, let us use the modified Voigt notation to simplify the equations relative to 2EQ transitions, in the same way that it has been used to simplify the equations relative to the ED transitions in Section 3.6. To do so, the following two properties of the second-order electric quadrupole transition moment $\boldsymbol{\mathcal{Q}}^{eg}$ are used [Eqs. (4.19) and (4.20)]:

$$\forall i,j,k,l=1,2,3, \quad \mathcal{Q}^{eg}_{ijkl} = \mathcal{Q}^{eg}_{jikl} = \mathcal{Q}^{eg}_{ijlk} = \mathcal{Q}^{eg}_{jilk}, \tag{4.55a}$$

$$\forall i,j,k,l=1,2,3, \quad \sum_i \mathcal{Q}^{eg}_{iikl} = \sum_k \mathcal{Q}^{eg}_{ijkk} = 0. \tag{4.55b}$$

As a reminder, the modified Voigt notation is a mathematical convention that exploits the symmetry and traceless properties of a tensor, by removing its redundant components, to represent it by a lower rank tensor defined in a higher dimensional space. Table 4.1 establishes the correspondence between the new indices and the ones of the represented tensor. In this way $\boldsymbol{\mathcal{Q}}^{eg}$, which is a fourth

rank tensor in three dimensions, is represented as a second rank tensor in five dimensions:

$$\left(\mathcal{Q}^{eg}_{ijab}\right)_{3\times3\times3\times3} \rightarrow \begin{pmatrix} \mathcal{Q}_{1111} & \mathcal{Q}_{1122} & \mathcal{Q}_{1123} & \mathcal{Q}_{1113} & \mathcal{Q}_{1112} \\ \mathcal{Q}_{2211} & \mathcal{Q}_{2222} & \mathcal{Q}_{2223} & \mathcal{Q}_{2213} & \mathcal{Q}_{2212} \\ \mathcal{Q}_{2311} & \mathcal{Q}_{2322} & \mathcal{Q}_{2323} & \mathcal{Q}_{2313} & \mathcal{Q}_{2312} \\ \mathcal{Q}_{1311} & \mathcal{Q}_{1322} & \mathcal{Q}_{1323} & \mathcal{Q}_{1313} & \mathcal{Q}_{1312} \\ \mathcal{Q}_{1211} & \mathcal{Q}_{1222} & \mathcal{Q}_{1223} & \mathcal{Q}_{1213} & \mathcal{Q}_{1212} \end{pmatrix} \rightarrow \left(\mathcal{Q}^{eg}_{\mu\alpha}\right)_{5\times5}. \tag{4.56}$$

| $(i,j)$ | $(1,1)$ | $(2,2)$ | $(2,3)$ | $(1,3)$ | $(1,2)$ |
|---|---|---|---|---|---|
| $\mu$ | 1 | 2 | 3 | 4 | 5 |

Table 4.1: Modified Voigt notation: correspondence between the pair of indices $(i,j)$ of a symmetric and traceless tensor in three dimensions and the indices $\mu$ in five dimensions. The indices $\mu = 1,2$ correspond to the two independent diagonal components of a second rank tensor, while the indices $\mu = 3,4,5$ correspond to its three independent off-diagonal components. By convention, the indices of this notation are denoted with Greek letters.

With identical developments as those presented in Section 3.6 for the OPSE, one finds an expression for the 2EQ transition involving $5^4$ terms instead of $9^4$ and an expression for the interference term involving $3^2 \times 5^2$ terms instead of $3^6$:

$$\begin{aligned} \frac{\gamma^{(2)}_{\mathrm{2EQ}}(\omega;\mathbf{R})}{\gamma^{(2)}_{\mathrm{2EQ},0}(\omega)} &= \frac{20\pi c}{\omega}\frac{20\pi c}{\omega_{eg}-\omega}\sum_{\mu,\nu,\alpha,\beta=1}^{5}\hat{\mathcal{Q}}^{eg}_{\mu\alpha}(\omega,\omega_{eg}-\omega)\left(\hat{\mathcal{Q}}^{eg}_{\nu\beta}(\omega,\omega_{eg}-\omega)\right)^{*} \\ &\quad\times \operatorname{Im}\widetilde{G}^{\mathrm{EQ}}_{\mu\nu}(\omega;\mathbf{R},\mathbf{R})\operatorname{Im}\widetilde{G}^{\mathrm{EQ}}_{\alpha\beta}(\omega_{eg}-\omega;\mathbf{R},\mathbf{R}), \end{aligned} \tag{4.57a}$$

$$\begin{aligned} \frac{\gamma^{(2)}_{\mathrm{2ED}\cap\mathrm{2EQ}}(\omega;\mathbf{R})}{\sqrt{\gamma^{(2)}_{\mathrm{2ED},0}(\omega)\gamma^{(2)}_{\mathrm{2EQ},0}(\omega)}} &= 2\,\frac{2\sqrt{30}\pi c}{\omega}\frac{2\sqrt{30}\pi c}{\omega_{eg}-\omega}\sum_{i,j=1}^{3}\sum_{\mu,\nu=1}^{5}\hat{\mathcal{D}}^{eg}_{ij}(\omega,\omega_{eg}-\omega)\left(\hat{\mathcal{Q}}^{eg}_{\mu\nu}(\omega,\omega_{eg}-\omega)\right)^{*} \\ &\quad\times \operatorname{Im}\widetilde{G}^{\mathrm{ED}\cap\mathrm{EQ}}_{i\mu}(\omega;\mathbf{R},\mathbf{R})\operatorname{Im}\widetilde{G}^{\mathrm{ED}\cap\mathrm{EQ}}_{j\nu}(\omega_{eg}-\omega;\mathbf{R},\mathbf{R}), \end{aligned} \tag{4.57b}$$

where the tensor $\widetilde{\mathbf{G}}^{\mathrm{EQ}}$ is a second-rank and symmetric tensor in five dimensions while the tensor $\widetilde{\mathbf{G}}^{\mathrm{EQ}}$ is represented with a $3\times5$ matrix. The links between the components of $\widetilde{\mathbf{G}}^{\mathrm{EQ}}$ and $\mathbf{G}^{\mathrm{EQ}}$ and between the components of $\widetilde{\mathbf{G}}^{\mathrm{ED}\cap\mathrm{EQ}}$ and $\mathbf{G}^{\mathrm{ED}\cap\mathrm{EQ}}$ are given in Section 3.6. Employing this notation results in all second-order transition moments being represented by second-rank tensors (the rank of the tensors is equal to the order of the transition), and all Green's functions also being of rank 2 (there is one Green's function for each emitter quanta). In the next section, we derive the connection between the vacuum normalized TPSE rates and the one-photon Purcell factors.

## 4.7 Expression as a function of the one-photon Purcell factors

In Section 3.7, we performed a decomposition of the OPSE rates in bases of Purcell factors, consisting of Purcell factors related to first-order multipolar transition moments aligned along basis vectors or a combination of them, allowing us to establish a link between the components of Green's functions and Purcell factors. Thereby, we use this link to write the TPSE rates as a function of them. However, since the expression derived for the interference between the ED and EQ emission channels depends on the vacuum OPSE rates [Eq. (3.89)], we need to perform new developments to derive an expression

for the interference between the 2ED and 2EQ channels that involves the vacuum TPSE rates.

### 4.7.1 Two-electric and two-magnetic dipole transitions

First, by using the definition of the tensors $\mathbf{F}^{\mathrm{ED}}$ and $\mathbf{F}^{\mathrm{MD}}$ [Eqs. (3.60) and (3.67)], the vacuum normalized 2ED and 2MD transition rates are rewritten as follows

$$\frac{\gamma^{(2)}_{\mathrm{2ED}}(\omega;\mathbf{R})}{\gamma^{(2)}_{\mathrm{2ED},0}(\omega)} = \sum_{i,j,a,b=1}^{3} \hat{\mathcal{D}}^{eg}_{ia}(\omega,\omega_{eg}-\omega)\left(\hat{\mathcal{D}}^{eg}_{jb}(\omega,\omega_{eg}-\omega)\right)^{*} F^{\mathrm{ED}}_{ij}(\omega;\mathbf{R})\, F^{\mathrm{ED}}_{ab}(\omega_{eg}-\omega;\mathbf{R}), \tag{4.58a}$$

$$\frac{\gamma^{(2)}_{\mathrm{2MD}}(\omega;\mathbf{R})}{\gamma^{(2)}_{\mathrm{2MD},0}(\omega)} = \sum_{i,j,a,b=1}^{3} \hat{\mathcal{M}}^{eg}_{ia}(\omega,\omega_{eg}-\omega)\left(\hat{\mathcal{M}}^{eg}_{jb}(\omega,\omega_{eg}-\omega)\right)^{*} F^{\mathrm{MD}}_{ij}(\omega;\mathbf{R})\, F^{\mathrm{MD}}_{ab}(\omega_{eg}-\omega;\mathbf{R}), \tag{4.58b}$$

where the components of the tensors $\mathbf{F}^{\mathrm{ED}}$ and $\mathbf{F}^{\mathrm{MD}}$ are defined as a function of the imaginary part of the Green's function of the ED and MD, respectively:

$$F^{\mathrm{ED}}_{ij}(\omega;\mathbf{R}) := \frac{6\pi c}{\omega}\,\mathrm{Im}\,G_{ij}(\omega;\mathbf{R},\mathbf{R}), \tag{4.59a}$$

$$F^{\mathrm{MD}}_{ij}(\omega;\mathbf{R}) := \frac{6\pi c}{\omega}\,\mathrm{Im}\,G^{\mathrm{MD}}_{ij}(\omega;\mathbf{R},\mathbf{R}). \tag{4.59b}$$

These tensors are expressed as a function of the one-photon Purcell factors [Eqs. (3.61) and (3.68)]:

$$F^{\mathrm{MO}}_{ij}(\omega;\mathbf{R}) = \begin{cases} P^{\mathrm{MO}}_{i}(\omega;\mathbf{R}) & \forall i = j \\ P^{\mathrm{MO}}_{ij}(\omega;\mathbf{R}) - \dfrac{1}{2}\left[P^{\mathrm{MO}}_{i}(\omega;\mathbf{R}) + P^{\mathrm{MO}}_{j}(\omega;\mathbf{R})\right] & \forall i \neq j, \end{cases} \tag{4.60}$$

where $\mathrm{MO} \in \{\mathrm{ED}, \mathrm{MD}\}$ and where $P^{\mathrm{MO}}_{i}$ and $P^{\mathrm{MO}}_{ij}$ denote Purcell factors relative to a dipole (electric or magnetic) along the basis vector $\hat{\mathbf{e}}_i$ and along the superposition of two basis vectors $\hat{\mathbf{e}}_i + \hat{\mathbf{e}}_j$, respectively.

Since the tensors $\mathbf{F}^{\mathrm{ED}}$ and $\mathbf{F}^{\mathrm{MD}}$ are symmetric, we need to calculate in the most general case six Purcell factors to get the 2ED or the 2MD transition rate. For example, in a Cartesian basis we need to calculate these six factors [Eq. (3.63)]:

$$\left\{P^{\mathrm{MO}}_{x},\, P^{\mathrm{MO}}_{y},\, P^{\mathrm{MO}}_{z},\, P^{\mathrm{MO}}_{yz},\, P^{\mathrm{MO}}_{xz},\, P^{\mathrm{MO}}_{xy}\right\}. \tag{4.61}$$

For a system with an azimuthal symmetry, the number of Purcell factors to calculate is reduced to three [Eq. (3.65)]. In free space, all Purcell factors are equal to one and so the tensors $\mathbf{F}^{\mathrm{ED}}$ and $\mathbf{F}^{\mathrm{MD}}$ are equal to the identity matrix and thereby the equations (4.58) gives $\gamma^{(2)}_{\mathrm{2ED}} = \gamma^{(2)}_{\mathrm{2ED},0}$ and $\gamma^{(2)}_{\mathrm{2MD}} = \gamma^{(2)}_{\mathrm{2MD},0}$.

As a consistency check, in the basis that diagonalizes the imaginary part of the Green's function[10] simultaneously at the frequencies of the two emitted quanta, we retrieve the formula derived in Ref. 31 for the 2ED transition that involves only the three Purcell factors $P^{\mathrm{ED}}_{i}$ linked to the diagonal components of the Green's function:

$$\frac{\gamma^{(2)}_{\mathrm{2ED}}(\omega;\mathbf{R})}{\gamma^{(2)}_{\mathrm{2ED},0}(\omega)} = \sum_{i,a=1}^{3} \left|\hat{\mathcal{D}}^{eg}_{ia}(\omega,\omega_{eg}-\omega)\right|^{2} P^{\mathrm{ED}}_{i}(\omega;\mathbf{R})\, P^{\mathrm{ED}}_{a}(\omega_{eg}-\omega;\mathbf{R}). \tag{4.62}$$

[10] Any real symmetric matrix is diagonalizable in an orthonormal basis.

However, finding a basis that diagonalizes Im $\mathbf{G}$ simultaneously at the complementary frequencies of the two emitted quanta for each frequency of a TPSE spectrum we want to calculate is restrictive. In addition, this basis might not exist depending on the photonic environment of the quantum emitter and, consequently, this equation is not general [31].

### 4.7.2 Two-electric quadrupole transition

Then, by using the definition of the tensors $\mathbf{F}^{\mathrm{EQ}}$ [Eq. (3.74)], the vacuum normalized 2EQ transition rate is rewritten as

$$\frac{\gamma^{(2)}_{\mathrm{2EQ}}(\omega;\mathbf{R})}{\gamma^{(2)}_{\mathrm{2EQ},0}(\omega)} = \sum_{\mu,\nu,\alpha,\beta=1}^{5} \hat{\mathcal{Q}}^{eg}_{\mu\alpha}(\omega,\omega_{eg}-\omega)\left(\hat{\mathcal{Q}}^{eg}_{\nu\beta}(\omega,\omega_{eg}-\omega)\right)^{*} F^{\mathrm{EQ}}_{\mu\nu}(\omega;\mathbf{R})\, F^{\mathrm{EQ}}_{\alpha\beta}(\omega_{eg}-\omega;\mathbf{R}), \tag{4.63}$$

where the components of the symmetric tensor $\mathbf{F}^{\mathrm{EQ}}$ are defined as a function of the imaginary part of the Green's function of the EQ:

$$F^{\mathrm{EQ}}_{\mu\nu}(\omega;\mathbf{R}) := \frac{20\pi c}{\omega}\mathrm{Im}\,\widetilde{G}^{\mathrm{EQ}}_{\mu\nu}(\omega;\mathbf{R},\mathbf{R}), \tag{4.64}$$

and are expressed as a function of the one-photon Purcell factors [Eq. (3.75)]:

$$F^{\mathrm{EQ}}_{\mu\nu}(\omega;\mathbf{R}) = \begin{cases} 2P^{\mathrm{EQ}}_{\mu}(\omega;\mathbf{R}) & \forall \mu=\nu \\ 3P^{\mathrm{EQ}}_{\mu\nu}(\omega;\mathbf{R}) - P^{\mathrm{EQ}}_{\mu}(\omega;\mathbf{R}) - P^{\mathrm{EQ}}_{\nu}(\omega;\mathbf{R}) & \text{if } (\mu,\nu)=(1,2) \\ 2P^{\mathrm{EQ}}_{\mu\nu}(\omega;\mathbf{R}) - P^{\mathrm{EQ}}_{\mu}(\omega;\mathbf{R}) - P^{\mathrm{EQ}}_{\nu}(\omega;\mathbf{R}) & \text{else.} \end{cases} \tag{4.65}$$

The Purcell factors $P^{\mathrm{EQ}}_{\mu}$ and $P^{\mathrm{EQ}}_{\mu\nu}$ denote Purcell factors relative to an electric quadrupole described by one of the five basis quadrupoles [Fig. 3.2] and two of the five basis quadrupoles [Eq. (3.70)], respectively.

Since the tensor $\mathbf{F}^{\mathrm{EQ}}$ is symmetric, we need to calculate in the most general case these 15 Purcell factors to get the EQ transition rate. For example, in a Cartesian basis we need to calculate these 15 factors [Eq. (3.77)]:

$$\left\{P^{\mathrm{EQ}}_{\mu}\right\} \cup \left\{P^{\mathrm{EQ}}_{\mu\nu}\right\}, \tag{4.66}$$

where the indices $\mu,\nu = 1,\ldots,5$, with $\mu<\nu$, correspond to the indices $\{xx, yy, yz, xz, xy\}$ [Fig. 3.2]. For a system with an azimuthal symmetry, the number of Purcell factors to calculate is reduced to six [Eq. (3.79)]. In free space, all Purcell factors tend towards one and so $\mathbf{F}^{\mathrm{EQ}}$ is given by

$$F^{\mathrm{EQ}}_{\mu\nu} = \begin{cases} 2 & \forall \mu=\nu \\ 1 & \text{if } (\mu,\nu)=(1,2) \\ 0 & \text{else,} \end{cases} \tag{4.67}$$

and thereby equation (4.63) gives $\gamma^{(2)}_{\mathrm{2EQ}} = \gamma^{(2)}_{\mathrm{2EQ},0}$.

### 4.7.3 Interference term

To make the link between the term describing the interference between the 2ED and 2EQ transitions and the Purcell factors, let us consider a quantum emitter having simultaneously a 2ED transition

and a 2EQ transition, described respectively by the transition moments $\boldsymbol{\mathcal{D}}^{eg}$ and $\boldsymbol{\mathcal{Q}}^{eg}$. In this case, its transition rate is given by the three following contributions [Eq. (4.24)]:

$$\gamma^{(2)}_{\mathrm{2ED+2EQ}}(\omega;\mathbf{R}) = \gamma^{(2)}_{\mathrm{2ED}}(\omega;\mathbf{R}) + \gamma^{(2)}_{\mathrm{2EQ}}(\omega;\mathbf{R}) + \gamma^{(2)}_{\mathrm{2ED\cap 2EQ}}(\omega;\mathbf{R}), \tag{4.68}$$

where $\gamma^{(2)}_{\mathrm{2ED+2EQ}}(\omega;\mathbf{R})$ is the spectral distribution of the emitted quanta of the total integrated TPSE rate, where the 2ED and 2EQ contributions have been written above as a function of the one-Purcell factors [Eqs. (4.58a) and (4.63)]. The interference term that we want to express as a function of the Purcell factors is given by the equation (4.57b). In vacuum, there is no interference [2] and the total rate is $\gamma^{(2)}_{\mathrm{2ED+2EQ},0} = \gamma^{(2)}_{\mathrm{2ED},0} + \gamma^{(2)}_{\mathrm{2EQ},0}$.

In Subsection 2.5.3, we saw that the Purcell factor is defined as the ratio between the one-photon transition rate of a quantum emitter in a given photonic environment and in vacuum: $P := \Gamma^{(1)}/\Gamma^{(1)}_0$. Moreover, they are calculated by considering classical radiating point sources [30]. In the case where multiple multipolar emission channels contribute to the transition rate, the classical source is described by the superposition of multipolar point sources, with multipolar moments identical to the multipolar transition moments of the emitter, allowing the calculation of interference effects between multipolar single-photon transitions [Subsec. 3.7.4]. In the TPSE process, we demonstrate above that the two-photon Purcell effect of multipolar transitions (e.g., 2ED and 2EQ transitions) can be written as a weighted summation of the product between the one-photon Purcell factors of the two emitted quanta [Eqs. (4.58a) and (4.63)]. The weighted summation runs over different source orientations and the weights correspond to the emitter contribution (the second-order multipolar transition moments).

As for the interference term [Eq. (4.57b)] there is also a decoupling with regard to the environment between the two emitted quanta through the product $\mathrm{Im}\,\widetilde{G}^{\mathrm{ED\cap EQ}}_{i\mu}(\omega)\,\mathrm{Im}\,\widetilde{G}^{\mathrm{ED\cap EQ}}_{j\nu}(\omega_{eg}-\omega)$, the link between the two-photon Purcell effect and the one-photon Purcell factors remains valid when several two-photon multipolar transitions contribute simultaneously to the TPSE process. Therefore, one can write

$$\frac{\gamma^{(2)}_{\mathrm{2ED+2EQ}}(\omega;\mathbf{R})}{x^2(\omega)} = \sum w\, P^{\mathrm{ED+EQ}}(\mathbf{R})\, P'^{\mathrm{ED+EQ}}(\mathbf{R}), \tag{4.69}$$

where $x^2(\omega)$ represents a function of the two-photon multipolar vacuum transition rates $\gamma^{(2)}_{\mathrm{2ED},0}$ and $\gamma^{(2)}_{\mathrm{2EQ},0}$[11]. Moreover, $P^{\mathrm{ED+EQ}}$ denotes the Purcell factor related to the superposition of an electric dipole and quadrupole and the summation runs over different source orientations with $w$ the weights. For clarity, we have adopted the following notation: when the prime symbol is not used, it denotes an evaluation at the frequency $\omega$, whereas when it is used, it denotes the evaluation at the complementary frequency $\omega_{eg}-\omega$.

To make the link between the Purcell factors $P^{\mathrm{ED+EQ}}$ and the tensor $\mathrm{Im}\,\widetilde{\mathbf{G}}^{\mathrm{ED\cap EQ}}$ involved in the interference term, the idea is to assume specific directions for the first-order multipolar transition moments involved in the definition of the second-order multipolar transitions moments [Eqs. (4.18)]. As a reminder, electric dipole and quadrupole moments are expanded with an orthonormal basis of 3 dipoles and 5 quadrupoles [Sec. 3.7]. For the dipolar moments, these are the three basis vectors, while for the quadrupolar ones, the basis is built from five different spatial configuration of plane quadrupoles [Fig.3.2]. In our modified Voigt notation, these quadrupoles are represented by a five

[11] The first intuition that $x^2$ is equal to the transition rate in vacuum $\gamma^{(2)}_{\mathrm{2ED+2EQ},0} = \gamma^{(2)}_{\mathrm{2ED},0} + \gamma^{(2)}_{\mathrm{2EQ},0}$ is wrong, as it leads to contradictory results. Therefore, we assume a function of these rates that we will find mathematically.

dimensional vector in which only the $\mu$-th component is non-zero and equal to $1/\sqrt{2}$ [12]. Thus, there are $3\times5$ combinations of the basis vectors of these two sources. As for the OPSE, let us take the two first-order electric dipole transition moments aligned along one basis vector, i.e., $\hat{\mathbf{d}}^{em} = \hat{\mathbf{d}}^{mg} = \hat{\mathbf{e}}_i$ with $i = 1, 2, 3$, and the two first-order electric quadrupole transition moments aligned along one basis vector, i.e., $\hat{\mathbf{Q}}^{em} = \hat{\mathbf{Q}}^{mg} = \hat{\mathbf{e}}_\mu/\sqrt{2}$ with $\mu = 1, \ldots, 5$. In this case, using equations (4.18), the normalized second-order multipolar transition moments are given by[13]

$$\hat{\boldsymbol{\mathcal{D}}}^{eg} = \hat{\mathbf{e}}_i\hat{\mathbf{e}}_i, \tag{4.70a}$$

$$\hat{\boldsymbol{\mathcal{Q}}}^{eg} = \frac{1}{2}\,\hat{\mathbf{e}}_\mu\hat{\mathbf{e}}_\mu. \tag{4.70b}$$

Therefore, using equations (4.58a) and (4.63) for the 2ED and 2EQ terms, equation (4.57b) for the interference term, and equations (4.70) for the multipolar moments, the total transition rate [Eq. (4.68)] is rewritten as

$$\gamma^{(2)}_{\mathrm{2ED+2EQ}} = \gamma^{(2)}_{\mathrm{2ED},0}\,P_i^{\mathrm{ED}}P_i'^{\mathrm{ED}} + \gamma^{(2)}_{\mathrm{2EQ},0}\,P_\mu^{\mathrm{EQ}}P_\mu'^{\mathrm{EQ}} + 2\sqrt{\gamma^{(2)}_{\mathrm{2ED},0}\,\gamma^{(2)}_{\mathrm{2EQ},0}}\,\frac{1}{2}\,F_{i\mu}^{\mathrm{ED}\cap\mathrm{EQ}}F_{i\mu}'^{\mathrm{ED}\cap\mathrm{EQ}}, \tag{4.71}$$

where the dependencies have been omitted. In this equation, $P_i^{\mathrm{ED}}$ and $P_\mu^{\mathrm{EQ}}$ correspond, respectively, to the Purcell factors related to an electric dipole aligned along $\hat{\mathbf{e}}_i$ and to an electric quadrupole aligned along $\hat{\mathbf{e}}_\mu$. Also, we introduced the tensor $\mathbf{F}^{\mathrm{ED}\cap\mathrm{EQ}}$ defined as [Eq. (3.85)]:

$$\mathbf{F}^{\mathrm{ED}\cap\mathrm{EQ}}(\omega;\mathbf{R}) := \frac{2\sqrt{30}\pi c}{\omega}\,\mathrm{Im}\,\widetilde{\mathbf{G}}^{\mathrm{ED}\cap\mathrm{EQ}}(\omega;\mathbf{R},\mathbf{R}). \tag{4.72}$$

As the second-order multipolar moments given by the equations (4.70) involve only one component, there is only one possible direction for the dipole ($\hat{\mathbf{e}}_i$) and for the quadrupole ($\hat{\mathbf{e}}_\mu$) and thereby the summation over the source orientations in equation (4.69) is reduced to a single term:

$$\gamma^{(2)}_{\mathrm{2ED+2EQ}} = x^2\,P_{i\mu}^{\mathrm{ED+EQ}}\,P_{i\mu}'^{\mathrm{ED+EQ}}, \tag{4.73}$$

where the dependencies have been omitted and where $P_{i\mu}^{\mathrm{ED+EQ}}$ is the Purcell factor related to a superposition of an electric dipole aligned along $\hat{\mathbf{e}}_i$ and of an electric quadrupole aligned along $\hat{\mathbf{e}}_\mu$. Combining the two last equations establishes a link between the Purcell factors and the tensors $\mathbf{F}^{\mathrm{ED}\cap\mathrm{EQ}}$:

$$x^2\,P_{i\mu}^{\mathrm{ED+EQ}}\,P_{i\mu}'^{\mathrm{ED+EQ}} = \gamma^{(2)}_{\mathrm{2ED},0}\,P_i^{\mathrm{ED}}\,P_i'^{\mathrm{ED}} + \gamma^{(2)}_{\mathrm{2EQ},0}\,P_\mu^{\mathrm{EQ}}\,P_\mu'^{\mathrm{EQ}} + \sqrt{\gamma^{(2)}_{\mathrm{2ED},0}\,\gamma^{(2)}_{\mathrm{2EQ},0}}\,F_{i\mu}^{\mathrm{ED}\cap\mathrm{EQ}}F_{i\mu}'^{\mathrm{ED}\cap\mathrm{EQ}}. \tag{4.74}$$

The Purcell factors in the previous equation can be calculated via the power emitted by classical point sources [Eqs. (3.86)]:

$$P_i^{\mathrm{ED}}(\omega;\mathbf{R}) = \frac{W_i^{\mathrm{ED}}(\omega;\mathbf{R})}{W_0^{\mathrm{ED}}(\omega)}, \tag{4.75a}$$

[12] The factor $1/\sqrt{2}$ for the quadrupoles is the normalization factor for quadrupoles that are described by two equal components in absolute value.

[13] Considering these transition moments is not a restrictive assumption. We could have considered moments containing more terms, but the number of terms in the developments will be greater and it will be more difficult to make the link between the Purcell factors $P^{\mathrm{ED+EQ}}$ and the tensor $\mathrm{Im}\,\widetilde{\mathbf{G}}^{\mathrm{ED}\cap\mathrm{EQ}}$.

$$P_{\mu}^{\mathrm{EQ}}(\omega;\mathbf{R}) = \frac{W_{\mu}^{\mathrm{EQ}}(\omega;\mathbf{R})}{W_{0}^{\mathrm{EQ}}(\omega)}, \tag{4.75b}$$

$$P_{i\mu}^{\mathrm{ED+EQ}}(\omega;\mathbf{R}) = \frac{W_{i\mu}^{\mathrm{ED+EQ}}(\omega;\mathbf{R})}{W_{0}^{\mathrm{ED}}(\omega)+W_{0}^{\mathrm{EQ}}(\omega)} = \frac{W_{i}^{\mathrm{ED}}(\omega;\mathbf{R})+W_{\mu}^{\mathrm{EQ}}(\omega;\mathbf{R})+W_{i\mu}^{\mathrm{ED}\cap\mathrm{EQ}}(\omega;\mathbf{R})}{W_{0}^{\mathrm{ED}}(\omega)+W_{0}^{\mathrm{EQ}}(\omega)}. \tag{4.75c}$$

In these equations, the subscript 0 indicates quantities that refer to vacuum whereas $W_{i}^{\mathrm{ED}}$, $W_{\mu}^{\mathrm{EQ}}$, and $W_{i\mu}^{\mathrm{ED+EQ}}$ denote the power emitted by a classical dipole aligned along $\hat{\mathbf{e}}_i$, by a classical quadrupole aligned along $\hat{\mathbf{e}}_\mu$, and by the superposition of both sources, respectively. Furthermore, $W_{i\mu}^{\mathrm{ED+EQ}}$ is decomposed into three contributions where $W_{i\mu}^{\mathrm{ED}\cap\mathrm{EQ}}$ represents the interference term between the two classical sources. As a reminder, there is no interference in vacuum.

Replacing the Purcell factor expressions into the equation (4.74) gives a left-hand side composed of nine terms, but a right-hand side consisting of only three terms. This is because in our developments based on Fermi's golden rule we discarded mixed transitions, which are consequently not included in the right-hand side. In the left-hand side, the terms involving the products $W_{i}^{\mathrm{ED}}\,W_{i}^{\prime\mathrm{ED}}$, $W_{\mu}^{\mathrm{EQ}}\,W_{\mu}^{\prime\mathrm{EQ}}$, and, $W_{i\mu}^{\mathrm{ED}\cap\mathrm{EQ}}\,W_{i\mu}^{\prime\mathrm{ED}\cap\mathrm{EQ}}$ correspond, respectively, to the 2ED, 2EQ, and interference contributions in the right-hand side. The 6 other terms in the left-hand side are related to mixed transitions, as for example the one that involves the product $W_{i}^{\mathrm{ED}}\,W_{\mu}^{\prime\mathrm{EQ}}$ describing an ED–EQ transition. Furthermore, the interference term in the left-hand side describes simultaneously the interference between the 2ED and 2EQ transitions and between the mixed transitions ED–EQ and EQ–ED. Indeed, as depicted in Figure 4.3, both situations are identical from an interference point of view since it is always a question of an interaction between an ED and EQ emission channel, leading to the same tensor $\mathbf{F}^{\mathrm{ED}\cap\mathrm{EQ}}$ and to the same interference term. It is therefore necessary to take only the half of the interference term in the left-hand side in order to equal it with the one on the right-hand side. Hence, by removing the terms related to mixed transitions in the left-hand side and by matching the remaining terms on either side of the equation, we obtain a system of three equations:

$$\begin{cases} x^2\dfrac{W_{i}^{\mathrm{ED}}}{W_{0}^{\mathrm{ED}}+W_{0}^{\mathrm{EQ}}}\dfrac{W_{i}^{\prime\mathrm{ED}}}{W_{0}^{\prime\mathrm{ED}}+W_{0}^{\prime\mathrm{EQ}}} = \gamma_{\mathrm{2ED},0}^{(2)}\dfrac{W_{i}^{\mathrm{ED}}}{W_{0}^{\mathrm{ED}}}\dfrac{W_{i}^{\prime\mathrm{ED}}}{W_{0}^{\prime\mathrm{ED}}} & \text{(4.76a)} \\ x^2\dfrac{W_{\mu}^{\mathrm{EQ}}}{W_{0}^{\mathrm{ED}}+W_{0}^{\mathrm{EQ}}}\dfrac{W_{\mu}^{\prime\mathrm{EQ}}}{W_{0}^{\prime\mathrm{ED}}+W_{0}^{\prime\mathrm{EQ}}} = \gamma_{\mathrm{2EQ},0}^{(2)}\dfrac{W_{\mu}^{\mathrm{EQ}}}{W_{0}^{\mathrm{EQ}}}\dfrac{W_{\mu}^{\prime\mathrm{EQ}}}{W_{0}^{\prime\mathrm{EQ}}} & \text{(4.76b)} \\ \dfrac{1}{2}x^2\dfrac{W_{i\mu}^{\mathrm{ED}\cap\mathrm{EQ}}}{W_{0}^{\mathrm{ED}}+W_{0}^{\mathrm{EQ}}}\dfrac{W_{i\mu}^{\prime\mathrm{ED}\cap\mathrm{EQ}}}{W_{0}^{\prime\mathrm{ED}}+W_{0}^{\prime\mathrm{EQ}}} = \sqrt{\gamma_{\mathrm{2EQ},0}^{(2)}\,\gamma_{\mathrm{2EQ},0}^{(2)}}\,F_{i\mu}^{\mathrm{ED}\cap\mathrm{EQ}}F_{i\mu}^{\prime\mathrm{ED}\cap\mathrm{EQ}}. & \text{(4.76c)} \end{cases}$$

The first two equations form a system of two equations with two unknowns: the ratio between the power emitted in vacuum by the classical ED and EQ sources and $x$ a function of the free-space TPSE rates. Indeed, the different classical multipolar sources need to be set to take into account the difference between the rates of the different multipolar decay pathways.

As a reminder, the vacuum TPSE rates are symmetric with respect to $\omega_{eg}/2$, and so the function $x$ is too. Thereby, we can write $x^2(\omega)$ and $\gamma_{\mathrm{2MO},0}^{(2)}(\omega)$ as the products $x(\omega)\,x(\omega_{eg}-\omega)$ and $\sqrt{\gamma_{\mathrm{2MO},0}^{(2)}(\omega)}\,\sqrt{\gamma_{\mathrm{2MO},0}^{(2)}(\omega_{eg}-\omega)}$, respectively. As a result, the three equations of the system can be

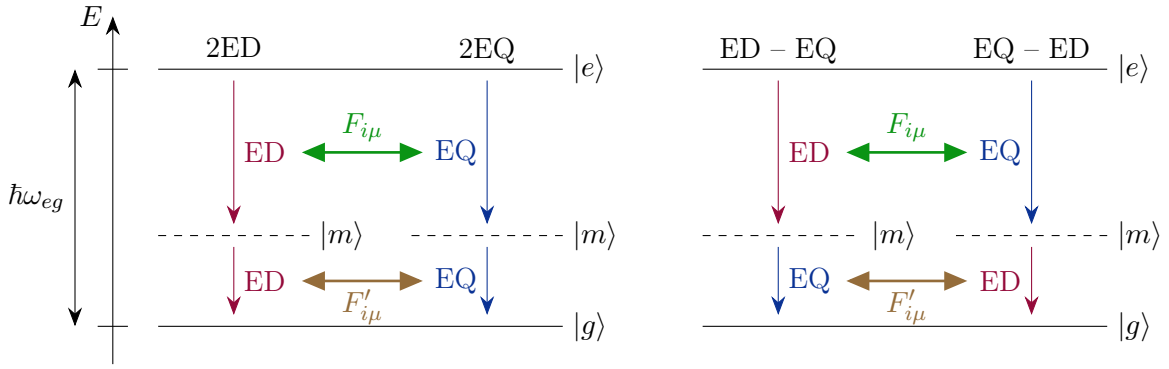


Figure 4.3: Illustration of the interference between the 2ED and 2EQ transitions (left) and between the mixed transitions ED–EQ and EQ–ED (right). Both situations are identical from an interference point of view since it is always a question of an interaction between an ED and EQ emission channels, leading to the same tensor $\mathbf{F}^{\mathrm{ED}\cap\mathrm{EQ}}$ and to the same interference term. Unlike other representations of two-photon transitions, we chose here to represent the intermediate states between the excited and ground states, even if their energy is greater than the energy of the excited state [Sec. 2.4]. Thus, the energy difference between two levels is equal to the energy of the emitted quanta, highlighting that the interference occurs between channels emitting photons of the same energy. Note that the 2ED and 2EQ transitions are mediated by different virtual intermediate states due to the selection rules [Eqs. (2.8) and Sec. 2.4].

written as $a\,a' = b\,b'$. Solving the first two equations gives:

$$x(\omega) = \sqrt{\gamma^{(2)}_{\mathrm{2ED},0}(\omega)} + \sqrt{\gamma^{(2)}_{\mathrm{2EQ},0}(\omega)}, \tag{4.77a}$$

$$\frac{W_0^{\mathrm{EQ}}(\omega)}{W_0^{\mathrm{ED}}(\omega)} = \sqrt{\frac{\gamma^{(2)}_{\mathrm{2EQ},0}(\omega)}{\gamma^{(2)}_{\mathrm{2ED},0}(\omega)}}. \tag{4.77b}$$

Thus, the function $x^2(\omega)$ in equation (4.69) establishing the general link between TPSE rates and one-photon Purcell factors is equal to $\left(\sqrt{\gamma^{(2)}_{\mathrm{2ED},0}(\omega)} + \sqrt{\gamma^{(2)}_{\mathrm{2EQ},0}(\omega)}\right)^2$, and not to $\gamma^{(2)}_{\mathrm{2ED},0}(\omega) + \gamma^{(2)}_{\mathrm{2EQ},0}(\omega)$. In addition, the power emitted by the classical sources is set as a function of the square root of the multipolar TPSE rates, whereas for the OPSE, it is as a function of the multipolar OPSE rates [Eq. (3.88)]. Now, by using the equation (4.76c) together with the last two, we obtain an expression for the components of the tensor $\mathbf{F}^{\mathrm{ED}\cap\mathrm{EQ}}$ (and so for the tensor $\widetilde{\mathbf{G}}^{\mathrm{ED}\cap\mathrm{EQ}}$ [Eq. (4.72)]):

$$F_{i\mu}^{\mathrm{ED}\cap\mathrm{EQ}}(\omega;\mathbf{R}) = \frac{W_{i\mu}^{\mathrm{ED}\cap\mathrm{EQ}}(\omega;\mathbf{R})}{\sqrt{2\,W_0^{\mathrm{ED}}(\omega)\,W_0^{\mathrm{EQ}}(\omega)}}, \tag{4.78}$$

which is identical to the expression derived for the interference between single-photon transitions [Eq. (3.89)]. Using equations (4.75) and (4.77b), the tensor can be written as a function of the Purcell factors:

$$\begin{aligned}&\left(\gamma^{(2)}_{\mathrm{2ED},0}(\omega)\,\gamma^{(2)}_{\mathrm{2EQ},0}(\omega)\right)^{1/4} F_{i\mu}^{\mathrm{ED}\cap\mathrm{EQ}}(\omega;\mathbf{R}) \\ &\qquad = \frac{1}{\sqrt{2}}\left[\left(\sqrt{\gamma^{(2)}_{\mathrm{2ED},0}} + \sqrt{\gamma^{(2)}_{\mathrm{2EQ},0}}\right) P_{i\mu}^{\mathrm{ED+EQ}} - \sqrt{\gamma^{(2)}_{\mathrm{2ED},0}}\,P_i^{\mathrm{ED}} - \sqrt{\gamma^{(2)}_{\mathrm{2EQ},0}}\,P_\mu^{\mathrm{EQ}}\right],\end{aligned} \tag{4.79}$$

where the dependencies have been omitted in the right-hand side. In comparison with the expression

obtained for the OPSE, this expression involves the square root of the TPSE rates, and not the OPSE rates [Eq. (3.90)]. Note that in vacuum, all Purcell factors tend towards one and the tensor $\mathbf{F}^{\mathrm{ED}\cap\mathrm{EQ}}$ tends towards 0, leading to an interference term equal to zero.

To conclude, we have rewritten the interference term [Eq. (4.57b)] as

$$\frac{\gamma^{(2)}_{2\mathrm{ED}\cap 2\mathrm{EQ}}(\omega;\mathbf{R})}{\sqrt{\gamma^{(2)}_{2\mathrm{ED},0}(\omega)\gamma^{(2)}_{2\mathrm{EQ},0}(\omega)}} = 2\sum_{i,j=1}^{3}\sum_{\mu,\nu=1}^{5}\hat{\mathcal{D}}^{eg}_{ij}(\omega,\omega_{eg}-\omega)\left(\hat{\mathcal{Q}}^{eg}_{\mu\nu}(\omega,\omega_{eg}-\omega)\right)^{*} \times F^{\mathrm{ED}\cap\mathrm{EQ}}_{i\mu}(\omega;\mathbf{R})\,F^{\mathrm{ED}\cap\mathrm{EQ}}_{j\nu}(\omega_{eg}-\omega;\mathbf{R}), \tag{4.80}$$

where the real part is implied and where the tensor $\mathbf{F}^{\mathrm{ED}\cap\mathrm{EQ}}$ is expressed as a function of the Purcell factors [Eq. (4.79)], which can be calculated classically via the equations (4.75). To calculate the 15 components $F^{\mathrm{ED}\cap\mathrm{EQ}}_{i\mu}$ [Eq. (4.79)], one needs to calculate an additional set of 15 Purcell factors: $\{P^{\mathrm{ED+EQ}}_{i\mu}\}$ (the 3 factors $P^{\mathrm{ED}}_{i}$ and the 5 factors $P^{\mathrm{EQ}}_{\mu}$ are already calculated when calculating the 2ED and 2EQ transition rates [Eqs. (4.60), and (4.65)]). For a system with an azimuthal symmetry, the number of Purcell factors to calculate is reduced to six [Eq. (3.93)]. These factors must be calculated by respecting the equation (4.77b), ensuring adequate weighting of multipolar sources. Consequently, vacuum rates are required to calculate interference effects.

## 4.8 Discussion

Throughout this chapter, we derived equations that are expressed as a function of the one-photon Purcell factors [Eqs. (4.58) and (4.63)] for the calculation of the two-photon Purcell effect of an arbitrary quantum emitter in an arbitrary photonic environment. To do so, the interaction has been taken up to the electric quadrupolar order, which is relevant for large emitters [50–53] and in structures confining light at the nanoscale [28], such as plasmonic nanostructures [22, 28, 29, 50, 55–62]. We have also included the calculation of the interference between the 2ED and 2EQ emission channels of the TPSE [Eq. (4.80)]. Similar equations can be derived for the interference terms including the 2MD transition as well as for the mixed transitions. The mixed transitions have not been developed in this thesis since they do not occur during the transition that will be studied afterwards [Sec. 2.4], namely the transition between two $s$ states of the hydrogen atom. Furthermore, the derived formulas do not impose any conditions on the basis of which Purcell factors are calculated, unlike the formula derived by Muniz [31] for calculating the 2ED transition rate.

In the derived equations [Eqs. (4.58), (4.63) and (4.80)], the contribution of the electronic structure of the emitter and of the photonic environment are decoupled, allowing their separate calculation. Indeed, each equation involves two different tensors. On the one hand, there is the normalized multipolar second-order transition moment that depends only on the electronic structure of the emitter [Eqs. (4.18)]. On the other hand, there are the $\mathbf{F}^{\mathrm{MO}}$ tensors, defined from Green's functions [Eqs. (4.59), (4.64), and (4.72)], present for the two emitted quanta of complementary energy. We express them as a function of the one-photon Purcell factors [Eqs. (4.60), (4.65), and (4.79)], and they depend only of the photonic environment. Thereby, the two-photon Purcell effect is proportional to the square of the Purcell factors, whereas the Purcell effect for the OPSE is proportional to the Purcell factors [Eqs. (3.99)]. For the interference term [Eq. (4.80)], the environment contribution involves one tensor $\mathbf{F}^{\mathrm{ED}\cap\mathrm{EQ}}$ for each emitted quantum, whose components can be either positive or

negative [Eq. (4.79)], leading to a positive or negative interference term. When two quanta (of same type) are emitted at the same frequency, the tensor $\mathbf{F}^{\mathrm{ED}\cap\mathrm{EQ}}$ appears squared and, consequently, the environment contribution is always positive. Therefore, in the case where the second-order transition moments $\boldsymbol{\mathcal{D}}^{eg}$ and $\boldsymbol{\mathcal{Q}}^{eg}$ involve mostly positive components, the system will always show a constructive interference.

By writing the multipolar contributions to the TPSE as a weighted summation of the product between the Purcell factors of the two emitted quanta, we demonstrated a general link between the TPSE and the one-photon Purcell factors. As a result, the modification due to the environment of the TPSE rates [Eqs. (4.58), (4.63) and (4.80)] can be computed by considering multiple orientations of classical point sources in electromagnetic simulations, where the different orientations are weighted according to the normalized multipolar second-order transition moments[14], thus allowing the consideration of arbitrarily shaped nanostructures. Moreover, this link remains valid when several two-photon multipolar transitions contribute simultaneously to the TPSE [Eq. (4.69)], allowing the calculation of the interference between the 2ED and 2EQ transitions via the computation of interferences between classical multipolar sources for the two emitted quanta [Eqs. (4.75) and (4.80)]. In the most general case, 6 Purcell factors are required to calculate the 2ED or 2MD transition rates [Eq. (4.61)], 15 for the 2EQ transition [Eq. (4.66)], and 15 additional for the interference between the 2ED and 2EQ transitions [Eq. (4.79)]. Furthermore, the Purcell factors can be decomposed into a radiative (emission of photons in the far-field) and a non-radiative part (absorption by the environment), allowing the separate calculation of these two channels, and so of the quantum efficiency [30].

The derived equations have the same limitations as those derived for the OPSE. Since the developments are based on Fermi's golden rule, they are limited to the weak coupling regime. Indeed, the perturbation theory is expected to fail when the ratio between the transition rate $\Gamma$ and the transition angular frequency $\omega_{eg}$ approaches 1 [22, 89]. Also, for the extreme cases of large emitters placed very close to a nanostructure ($\approx$ 1 nm distance), their reduction to a point may require even higher orders than the quadrupolar order [53].

Now that the theory has been developed, we consider in the next chapter the transition between two $s$ states of the hydrogen atom and we calculate the normalized second-order multipolar transition moments as well as the TPSE rates in vacuum. Afterwards, we address in Chapter 6 the method to calculate the Purcell factors by modeling classical multipolar point sources in electromagnetic simulations.

## 4.9 Summary

In this chapter, we presented a complete treatment of the two-photon spontaneous emission rate (TPSE) where the interaction Hamiltonian is taken up to the electric quadrupolar order by making no assumptions about the quantum emitter and the environment, including interference effects between the multipolar pathways, which have never been studied to our knowledge. We have set aside the mixed transitions (because they do not occur between two $s$ states of the hydrogen atom

[14]Note that the knowledge of the norm of the second-order transition moments is not required to calculate the two-photon Purcell effect [Eqs. (4.58), (4.63) and (4.80)]. It is required only for the calculation of the vacuum TPSE rates [Eqs. (4.41)] and for the calculation of the interference term since the multipolar sources must be weighted according to the vacuum TPSE rates of the emitter [Eqs. (4.79) and (4.77b)].

[Sec. 2.4]) and focused on the interference between the two-electric dipole (2ED) and the two-electric quadrupole (2EQ) transition, but similar developments can be performed for these contributions. Concretely, the derivation as a function of the field modes and via the Green's function for the 2MD and 2EQ transitions and for the interference term are personal developments, based on what has been done for the 2ED transition [31]. Furthermore, we introduced a modified Voigt notation to simplify the equations relative to the 2EQ transition. Finally, we have gone beyond the developments made by Muniz [31] for the 2ED transition since our equation [Eq. (4.58a)] is more general as it includes the off-diagonal components of the Green's function.

Adopting a perturbative approach with the second-order Fermi's golden rule [Eq. (4.1)], and by considering the electric dipole (ED), magnetic dipole (MD) and electric quadrupole (EQ) interactions in the multipolar expansion of the interaction Hamiltonian [Eq. (4.5)], we found that the overall TPSE is given by six multipolar contributions [Eq. (4.24)]:

$$\Gamma^{(2)}_{\text{tot}} = \Gamma^{(2)}_{\text{2ED}} + \Gamma^{(2)}_{\text{2MD}} + \Gamma^{(2)}_{\text{2EQ}} + \Gamma^{(2)}_{\text{2ED}\cap\text{2MD}} + \Gamma^{(2)}_{\text{2ED}\cap\text{2EQ}} + \Gamma^{(2)}_{\text{2MD}\cap\text{2EQ}}, \tag{4.81}$$

where the mixed transitions have been discarded. These contributions are the 2ED, 2MD, 2EQ transition rates and the interferences with each other, respectively. The interference terms can be either positive or negative, potentially leading to an increase or a decrease of the overall transition rate. In the case where the magnetic interaction is discarded, the overall TPSE is given by the three following multipolar contributions:

$$\Gamma^{(2)}_{\text{tot}} = \Gamma^{(2)}_{\text{2ED}} + \Gamma^{(2)}_{\text{2EQ}} + \Gamma^{(2)}_{\text{2ED}\cap\text{2EQ}}. \tag{4.82}$$

Next, by considering plane waves for the field modes, we derived the vacuum TPSE rates. For $\text{2MO} \in \{\text{2ED},\ \text{2MD},\ \text{2EQ}\}$ [Eq. (4.40)]:

$$\Gamma^{(2)}_{\text{2MO},0} = \int_0^{\omega_{eg}} \gamma^{(2)}_{\text{2MO},0}(\omega)\,\mathrm{d}\omega, \tag{4.83}$$

where the multipolar contributions $\gamma^{(2)}_{\text{2MO},0}(\omega)$ to the spectral distribution of the emitted quanta in vacuum are given by [Eqs. (4.41)]:

$$\gamma^{(2)}_{\text{2ED},0}(\omega) = \frac{1}{36\pi^3\varepsilon_0^2\hbar^2c^6}\,\omega^3(\omega_{eg}-\omega)^3\,\|\boldsymbol{\mathcal{D}}^{eg}(\omega,\omega_{eg}-\omega)\|^2\,, \tag{4.84a}$$

$$\gamma^{(2)}_{\text{2MD},0}(\omega) = \frac{1}{36\pi^3\varepsilon_0^2\hbar^2c^{10}}\,\omega^3(\omega_{eg}-\omega)^3\,\|\boldsymbol{\mathcal{M}}^{eg}(\omega,\omega_{eg}-\omega)\|^2\,, \tag{4.84b}$$

$$\gamma^{(2)}_{\text{2EQ},0}(\omega) = \frac{1}{400\pi^3\varepsilon_0^2\hbar^2c^{10}}\,\omega^5(\omega_{eg}-\omega)^5\,\|\boldsymbol{\mathcal{Q}}^{eg}(\omega,\omega_{eg}-\omega)\|^2\,. \tag{4.84c}$$

As the spontaneous emission takes place in vacuum, there are no interferences between multipolar transitions. These equations involve the second-order multipolar transition moments [Eqs. (4.18)]:

$$\boldsymbol{\mathcal{D}}^{eg}(\omega,\omega_{eg}-\omega) := \sum_{|m\rangle}\left(\frac{\mathbf{d}^{em}\,\mathbf{d}^{mg}}{\omega_{em}-\omega} + \frac{\mathbf{d}^{mg}\,\mathbf{d}^{em}}{\omega_{em}-(\omega_{eg}-\omega)}\right), \tag{4.85a}$$

$$\boldsymbol{\mathcal{M}}^{eg}(\omega,\omega_{eg}-\omega) := \sum_{|m\rangle}\left(\frac{\mathbf{m}^{em}\,\mathbf{m}^{mg}}{\omega_{em}-\omega} + \frac{\mathbf{m}^{mg}\,\mathbf{m}^{em}}{\omega_{em}-(\omega_{eg}-\omega)}\right), \tag{4.85b}$$

$$\boldsymbol{\mathcal{Q}}^{eg}(\omega,\omega_{eg}-\omega) := \sum_{|m\rangle}\left(\frac{\mathbf{Q}^{em}\,\mathbf{Q}^{mg}}{\omega_{em}-\omega}+\frac{\mathbf{Q}^{mg}\,\mathbf{Q}^{em}}{\omega_{em}-(\omega_{eg}-\omega)}\right), \tag{4.85c}$$

where the outer product is implied. These tensors that depend only on the electronic structure of the emitter, the first two of rank two and the third one of rank four, describe the two successive electric dipole, magnetic dipole, and electric quadrupole transitions of the emitter between the excited and ground states of the emitter. Since the operator $\mathbf{Q}$ is symmetric and can be taken traceless in source-free regions, $\boldsymbol{\mathcal{Q}}^{eg}$ is symmetric and satisfies the property given by the equation (4.20). Furthermore, we introduced a modified Voigt notation [Eq. (4.56) and Tab. 4.1] to simplify equations involving $\boldsymbol{\mathcal{Q}}^{eg}$ by keeping only its 25 independent components as a rank two tensor in five dimensions:

$$\left(\mathcal{Q}^{eg}_{ijab}\right)_{3\times3\times3\times3} \to \begin{pmatrix} \mathcal{Q}_{1111} & \mathcal{Q}_{1122} & \mathcal{Q}_{1123} & \mathcal{Q}_{1113} & \mathcal{Q}_{1112} \\ \mathcal{Q}_{2211} & \mathcal{Q}_{2222} & \mathcal{Q}_{2223} & \mathcal{Q}_{2213} & \mathcal{Q}_{2212} \\ \mathcal{Q}_{2311} & \mathcal{Q}_{2322} & \mathcal{Q}_{2323} & \mathcal{Q}_{2313} & \mathcal{Q}_{2312} \\ \mathcal{Q}_{1311} & \mathcal{Q}_{1322} & \mathcal{Q}_{1323} & \mathcal{Q}_{1313} & \mathcal{Q}_{1312} \\ \mathcal{Q}_{1211} & \mathcal{Q}_{1222} & \mathcal{Q}_{1223} & \mathcal{Q}_{1213} & \mathcal{Q}_{1212} \end{pmatrix} \to \left(\mathcal{Q}^{eg}_{\mu\alpha}\right)_{5\times5}. \tag{4.86}$$

Using this notation, all second-order transition moments are represented by tensors of rank equal to the order of the transition.

Then, we expressed the multipolar contributions via the dyadic Green's function, and then normalized them with respect to vacuum [Eqs. (4.54) and (4.57)]. In the obtained equations, the contribution of the environment and of the emitter are decoupled, allowing their separate calculation. Moreover, the Green's functions intervene twice, once for each emitted quantum, showing a decoupling with respect to the environment between the two emitted quanta.

Finally, we expressed the multipolar contributions to the TPSE as a function of the one-photon Purcell factors [Eqs. (4.58), (4.63), and (4.80)]:

$$\frac{\gamma^{(2)}_{\mathrm{2ED}}(\omega;\mathbf{R})}{\gamma^{(2)}_{\mathrm{2ED},0}(\omega)} = \sum_{i,j,a,b=1}^{3} \hat{\mathcal{D}}^{eg}_{ia}(\omega,\omega_{eg}-\omega)\left(\hat{\mathcal{D}}^{eg}_{jb}(\omega,\omega_{eg}-\omega)\right)^{*} F^{\mathrm{ED}}_{ij}(\omega;\mathbf{R})\,F^{\mathrm{ED}}_{ab}(\omega_{eg}-\omega;\mathbf{R}), \tag{4.87a}$$

$$\frac{\gamma^{(2)}_{\mathrm{2MD}}(\omega;\mathbf{R})}{\gamma^{(2)}_{\mathrm{2MD},0}(\omega)} = \sum_{i,j,a,b=1}^{3} \hat{\mathcal{M}}^{eg}_{ia}(\omega,\omega_{eg}-\omega)\left(\hat{\mathcal{M}}^{eg}_{jb}(\omega,\omega_{eg}-\omega)\right)^{*} F^{\mathrm{MD}}_{ij}(\omega;\mathbf{R})\,F^{\mathrm{MD}}_{ab}(\omega_{eg}-\omega;\mathbf{R}), \tag{4.87b}$$

$$\frac{\gamma^{(2)}_{\mathrm{2EQ}}(\omega;\mathbf{R})}{\gamma^{(2)}_{\mathrm{2EQ},0}(\omega)} = \sum_{\mu,\nu,\alpha,\beta=1}^{5} \hat{\mathcal{Q}}^{eg}_{\mu\alpha}(\omega,\omega_{eg}-\omega)\left(\hat{\mathcal{Q}}^{eg}_{\nu\beta}(\omega,\omega_{eg}-\omega)\right)^{*} F^{\mathrm{EQ}}_{\mu\nu}(\omega;\mathbf{R})\,F^{\mathrm{EQ}}_{\alpha\beta}(\omega_{eg}-\omega;\mathbf{R}), \tag{4.87c}$$

$$\begin{aligned}\frac{\gamma^{(2)}_{\mathrm{2ED}\cap\mathrm{2EQ}}(\omega;\mathbf{R})}{\sqrt{\gamma^{(2)}_{\mathrm{2ED},0}(\omega)\gamma^{(2)}_{\mathrm{2EQ},0}(\omega)}} = 2\sum_{i,j=1}^{3}\sum_{\mu,\nu=1}^{5} &\hat{\mathcal{D}}^{eg}_{ij}(\omega,\omega_{eg}-\omega)\left(\hat{\mathcal{Q}}^{eg}_{\mu\nu}(\omega,\omega_{eg}-\omega)\right)^{*} \\ &\times F^{\mathrm{ED}\cap\mathrm{EQ}}_{i\mu}(\omega;\mathbf{R})\,F^{\mathrm{ED}\cap\mathrm{EQ}}_{j\nu}(\omega_{eg}-\omega;\mathbf{R}),\end{aligned} \tag{4.87d}$$

where the real part is implied for the last equation. The tensors $\mathbf{F}^{\mathrm{ED}}$, $\mathbf{F}^{\mathrm{MD}}$, $\mathbf{F}^{\mathrm{EQ}}$, and $\mathbf{F}^{\mathrm{ED}\cap\mathrm{EQ}}$ are defined from the Green's functions [Eqs. (4.59), (4.64), and (4.72)] and are expressed as a function

of the Purcell factors. For MO $\in$ {ED, MD} [Eqs. (4.60)]:

$$F_{ij}^{\mathrm{MO}}(\omega;\mathbf{R}) = \begin{cases} P_i^{\mathrm{MO}}(\omega;\mathbf{R}) & \forall i = j \\ P_{ij}^{\mathrm{MO}}(\omega;\mathbf{R}) - \dfrac{1}{2}\left[P_i^{\mathrm{MO}}(\omega;\mathbf{R}) + P_j^{\mathrm{MO}}(\omega;\mathbf{R})\right] & \forall i \neq j, \end{cases} \tag{4.88}$$

where $P_i^{\mathrm{MO}}$ and $P_{ij}^{\mathrm{MO}}$ denote Purcell factors relative to a dipole (electric or magnetic) along $\hat{\mathbf{e}}_i$ and $\hat{\mathbf{e}}_i + \hat{\mathbf{e}}_j$, respectively. For the EQ transition [Eq. (4.65)]:

$$F_{\mu\nu}^{\mathrm{EQ}}(\omega;\mathbf{R}) = \begin{cases} 2P_{\mu}^{\mathrm{EQ}}(\omega;\mathbf{R}) & \forall \mu = \nu \\ 3P_{\mu\nu}^{\mathrm{EQ}}(\omega;\mathbf{R}) - P_{\mu}^{\mathrm{EQ}}(\omega;\mathbf{R}) - P_{\nu}^{\mathrm{EQ}}(\omega;\mathbf{R}) & \text{if } (\mu,\nu) = (1,2) \\ 2P_{\mu\nu}^{\mathrm{EQ}}(\omega;\mathbf{R}) - P_{\mu}^{\mathrm{EQ}}(\omega;\mathbf{R}) - P_{\nu}^{\mathrm{EQ}}(\omega;\mathbf{R}) & \text{else,} \end{cases} \tag{4.89}$$

where $P_{\mu}^{\mathrm{EQ}}$ and $P_{\mu\nu}^{\mathrm{EQ}}$ denote Purcell factors relative to an electric quadrupole described by one of the five basis quadrupoles [Fig. 3.2] and relative to the combination of two basis quadrupoles [Eq. (3.70)], respectively. For the interference term [Eq. (4.79)]:

$$\begin{aligned} &\left(\gamma_{\mathrm{2ED},0}^{(2)}(\omega)\,\gamma_{\mathrm{2EQ},0}^{(2)}(\omega)\right)^{1/4} F_{i\mu}^{\mathrm{ED}\cap\mathrm{EQ}}(\omega;\mathbf{R}) \\ &\qquad = \frac{1}{\sqrt{2}}\left[\left(\sqrt{\gamma_{\mathrm{2ED},0}^{(2)}} + \sqrt{\gamma_{\mathrm{2EQ},0}^{(2)}}\right) P_{i\mu}^{\mathrm{ED+EQ}} - \sqrt{\gamma_{\mathrm{2ED},0}^{(2)}}\, P_i^{\mathrm{ED}} - \sqrt{\gamma_{\mathrm{2EQ},0}^{(2)}}\, P_{\mu}^{\mathrm{EQ}}\right], \end{aligned} \tag{4.90}$$

with $P_{i\mu}^{\mathrm{ED+EQ}}$ being the Purcell factor related to the superposition of an electric dipole along $\hat{\mathbf{e}}_i$ and of an electric quadrupole along $\hat{\mathbf{e}}_\mu$. These Purcell factors are computable by modeling multiple orientations of classical multipolar point sources in electromagnetic simulations [Eqs. (4.75)]. In the equations, the different orientations are weighted according to the normalized second-order transition moments. For the calculation of the interference, the knowledge of the vacuum TPSE rates is required and the multipolar sources must be set according to the equation (4.77b) to take into account the difference between the rates in vacuum of the different multipolar decay pathways of the emitter.

The developments presented in this chapter have two limitations: they are limited to the weak coupling regime and the consideration of the interaction up to the electric quadrupolar order may not be sufficient for the extreme cases of large emitters placed very close to a nanostructure.

Chapter 5

# Second-order multipolar transition moments of the hydrogen atom

In the previous chapter, we investigated the multipolar contributions to the TPSE process. To evaluate the modification of the multipolar contributions to the total TPSE rate with respect to the vacuum [Eqs. (4.58), (4.63) and (4.80)], it is sufficient to calculate the normalized version of the second-order multipolar transition moments $\boldsymbol{\mathcal{D}}^{eg}$, $\boldsymbol{\mathcal{M}}^{eg}$, and $\boldsymbol{\mathcal{Q}}^{eg}$ [Eqs. (4.18)], which depend only on the electronic structure of the emitter. However, it is necessary to know the norm of these transition moments to get the vacuum transition rates [Eqs. (4.41)] and therefore to be able to calculate absolute TPSE rates, i.e., rates that are not vacuum normalized. Then, it will be possible to sum up all the contributions to retrieve the overall TPSE rate:

$$\gamma^{(2)}_{\mathrm{tot}}(\omega;\mathbf{R}) \approx \frac{\gamma^{(2)}_{\mathrm{2ED}}}{\gamma^{(2)}_{\mathrm{2ED},0}}\gamma^{(2)}_{\mathrm{2ED},0} + \frac{\gamma^{(2)}_{\mathrm{2EQ}}}{\gamma^{(2)}_{\mathrm{2EQ},0}}\gamma^{(2)}_{\mathrm{2EQ},0} + \frac{\gamma^{(2)}_{\mathrm{2ED}\cap\mathrm{2EQ}}}{\sqrt{\gamma^{(2)}_{\mathrm{2ED},0}\,\gamma^{(2)}_{\mathrm{2EQ},0}}}\sqrt{\gamma^{(2)}_{\mathrm{2ED},0}\,\gamma^{(2)}_{\mathrm{2EQ},0}}, \tag{5.1}$$

where for this example mixed and magnetic two-photon transitions have been discarded and where the dependencies have been omitted. In addition, for calculating the quantum interference between the 2ED and 2EQ multipolar two-photon transitions [Eqs. (4.80)], it is necessary to know the vacuum TPSE rates to weight accordingly the classical multipolar point sources [Eq. (3.88)] that are superposed when calculating the environmental contribution [Eq. (4.79)].

In this chapter, we calculate the second-order multipolar transition moments $\boldsymbol{\mathcal{D}}^{eg}$ and $\boldsymbol{\mathcal{Q}}^{eg}$ for a transition between two spherically symmetric states ($s$ states) of the hydrogen atom, the simplest quantum emitter, which allows analytical calculations. The presented developments can be adapted to study other transitions in hydrogen-like atoms and to calculate $\boldsymbol{\mathcal{M}}^{eg}$. Note that the mixed transitions are forbidden between these states [Sec. 2.4]. This chapter is organized as follows. First, we introduce the wavefunctions of the hydrogen atom. Then, we calculate the normalized tensors $\hat{\boldsymbol{\mathcal{D}}}^{eg}$ and $\hat{\boldsymbol{\mathcal{Q}}}^{eg}$ and, after, the vacuum TPSE rates. Finally, this chapter ends with a summary.

## 5.1 Hydrogen atom wavefunctions

The hydrogen wavefunctions $\psi(\mathbf{r})$ can be written as a product between a radial function $R_{N,L}(r)$ and a spherical harmonic function $Y_L^M(\theta,\varphi)$ representing the angular part [Eq. (2.6)]:

$$\psi(\mathbf{r}) = R_{N,L}(r)\,Y_L^M(\theta,\varphi), \tag{5.2}$$

where $N$, $L$ and $M$ are, respectively, the principal, azimuthal and magnetic quantum numbers. In this chapter, we use capital letters for quantum numbers to avoid confusion between the magnetic quantum number and the intermediate states $|m\rangle$. The Appendix A summarizes the properties of the spherical harmonics that will be used in this chapter, and gives some expressions of them. Since we consider an $s \to s$ transition, the excited and the ground states are characterized by the following quantum numbers [45]:

$$|e\rangle = |N_e; L_e = 0; M_e = 0\rangle \,, \tag{5.3a}$$

$$|g\rangle = |N_g; L_g = 0; M_g = 0\rangle \,, \tag{5.3b}$$

with $\{N_e, L_e, M_e\}$ and $\{N_g, L_g, M_g\}$ the quantum numbers characterizing, respectively, the excited and the ground states. Note that for consistency of notation, we retain the ground state label for the final state of the emitter, even though it is not necessarily the ground one. Using the selection rules for the different studied transitions [Eqs. (2.8)], it is possible to deduce the nature of the virtual intermediate states $|m\rangle$ involved in the two-photon transition. In general, they are written as

$$|m\rangle = |N_m; L_m; M_m\rangle \,, \tag{5.4}$$

with $\{N_m, L_m, M_m\}$ their quantum numbers. Therefore, given the equation (5.2), the wavefunctions of the three states involved in the second-order transition are written as follows:

$$\begin{cases} \psi_e(\mathbf{r}) = R_{N_e,0}(r)\, Y_0^0 & \text{(5.5a)} \\ \psi_g(\mathbf{r}) = R_{N_g,0}(r)\, Y_0^0 & \text{(5.5b)} \\ \psi_m(\mathbf{r}) = R_{N_m,L_m}(r)\, Y_{L_m}^{M_m}(\theta,\varphi), & \text{(5.5c)} \end{cases}$$

where $Y_0^0 = 1/\sqrt{4\pi}$ and where the excited and the ground states are independent of the angles.

## 5.2 Normalized second-order multipolar transition moments

In this section, we present the developments made in Ref. 31 for the calculation of the normalized tensor $\hat{\boldsymbol{\mathcal{D}}}^{eg}$ and, in the same way, we calculate the normalized tensor $\hat{\boldsymbol{\mathcal{Q}}}^{eg}$. As a reminder, the second-order electric dipole and quadrupole transition moments that describe the two-photon transition between the excited state $|e\rangle$ and the ground state $|g\rangle$ of the emitter are defined as [Eqs. (4.18)]:

$$\boldsymbol{\mathcal{D}}^{eg}(\omega_\alpha, \omega_{\alpha'}) := \sum_{|m\rangle} \left( \frac{\mathbf{d}^{em}\, \mathbf{d}^{mg}}{\omega_{em} - \omega_\alpha} + \frac{\mathbf{d}^{mg}\, \mathbf{d}^{em}}{\omega_{em} - \omega_{\alpha'}} \right) , \tag{5.6a}$$

$$\boldsymbol{\mathcal{Q}}^{eg}(\omega_\alpha, \omega_{\alpha'}) := \sum_{|m\rangle} \left( \frac{\mathbf{Q}^{em}\, \mathbf{Q}^{mg}}{\omega_{em} - \omega_\alpha} + \frac{\mathbf{Q}^{mg}\, \mathbf{Q}^{em}}{\omega_{em} - \omega_{\alpha'}} \right) , \tag{5.6b}$$

where the summation runs over all possible emitter's virtual intermediate states $|m\rangle$, where $\omega_\alpha$ and $\omega_{\alpha'}$ represent the frequencies of the two emitted quanta, and where $\hbar\omega_{em}$ is the transition energy between the excited state $|e\rangle$ and the virtual intermediate state $|m\rangle$. Moreover, $\mathbf{d}^{ab} := \langle a|\mathbf{d}|b\rangle$ and $\mathbf{Q}^{ab} := \langle a|\mathbf{Q}|b\rangle$, with $\mathbf{d}$ and $\mathbf{Q}$ the electric dipole and quadrupole operators [Eqs. (3.5)], stand for the first-order multipolar transition moments that describe the emitter's transition from the state $|b\rangle$ to the state $|a\rangle$ ($a$, $b = e$, $m$, $g$).

### 5.2.1 Normalized second-order electric dipole transition moment

For an electric dipole (ED) transition, the selection rules impose that $\Delta L = \pm 1$ and $\Delta M = 0, \pm 1$ [Eq. (2.8a)]. Thus, the intermediate states leading to non-zero electric dipole transition moments are $p$ states:

$$|m\rangle = |N_m; L_m = 1; M_m = 0, \pm 1\rangle\,, \tag{5.7a}$$

$$\psi_m(\mathbf{r}) = R_{N_m,1}(r)\, Y_1^{M_m}(\theta,\varphi), \quad \text{with } M_m = 0, \pm 1. \tag{5.7b}$$

As the type of all involved states in this second-order transition have been determined, we can now calculate the electric dipole transition moment corresponding, first, to the transition between the excited state $|e\rangle$ and an intermediate state $|m\rangle$:

$$\mathbf{d}^{em} = \langle e|\,\mathbf{d}\,|m\rangle \tag{5.8a}$$

$$= -e \int_{\mathbb{R}^3} R^*_{N_e,0}(r)\, \left(Y_0^0\right)^*\, \mathbf{r}\, R_{N_m,1}(r)\, Y_1^{M_m}(\theta,\varphi)\, \mathrm{d}^3 r \tag{5.8b}$$

$$= -\frac{e}{\sqrt{4\pi}} \int_0^\infty r^3 R^*_{N_e,0}(r) R_{N_m,1}(r)\, \mathrm{d}r \int_{4\pi} \hat{\mathbf{r}}\, Y_1^{M_m}(\theta,\varphi)\, \mathrm{d}\Omega, \tag{5.8c}$$

where we used the expression of the electric dipole moment operator[1] $\mathbf{d} = q\,\mathbf{r} = -e\,\mathbf{r}$ [Eq. (3.5a)] and that $Y_0^0 = 1/\sqrt{4\pi}$ [Tab. A.1]. Moreover, we switched to spherical coordinates with $\mathrm{d}\Omega = \sin\theta\,\mathrm{d}\theta\,\mathrm{d}\varphi$ the element of solid angle and with $\hat{\mathbf{r}} := \mathbf{r}/r$ an unitary vector. Notice that the radial integral depends only on the principal quantum numbers of the two states, while the angular integrals depend solely on the magnetic quantum number $M_m$ of the intermediate state $|m\rangle$ [31]. Similarly, the electric dipole transition moment corresponding to the transition between an intermediate state $|m\rangle$ and the ground state $|g\rangle$ is given by

$$\mathbf{d}^{mg} = \langle m|\,\mathbf{d}\,|g\rangle \tag{5.9a}$$

$$= -\frac{e}{\sqrt{4\pi}} \int_0^\infty r^3 R^*_{N_m,1}(r) R_{N_g,0}(r)\, \mathrm{d}r \int_{4\pi} \left(Y_1^{M_m}(\theta,\varphi)\right)^*\, \hat{\mathbf{r}}\, \mathrm{d}\Omega. \tag{5.9b}$$

To calculate the angular integrals, let us express the unitary vector $\hat{\mathbf{r}}$ as a function of the spherical harmonics [100]:

$$\hat{\mathbf{r}} = \sqrt{\frac{4\pi}{3}} \left[ \frac{Y_1^{-1} - Y_1^1}{\sqrt{2}}\, \hat{\mathbf{e}}_x + i\, \frac{Y_1^{-1} + Y_1^1}{\sqrt{2}}\, \hat{\mathbf{e}}_y + Y_1^0\, \hat{\mathbf{e}}_z \right]. \tag{5.10}$$

Indeed, by using the expressions of the spherical harmonics given in Table A.1, we find the expression of $\hat{\mathbf{r}}$ in spherical coordinates[2]. Now, let us use the complex conjugate and the orthonormality properties of these functions [100]:

$$\left(Y_L^M(\theta,\varphi)\right)^* = (-1)^M\, Y_L^{-M}(\theta,\varphi), \tag{5.11a}$$

$$\int_{4\pi} \left(Y_L^M(\theta,\varphi)\right)^*\, Y_{L'}^{M'}(\theta,\varphi)\, \mathrm{d}\Omega = \delta_{LL'}\, \delta_{MM'}. \tag{5.11b}$$

[1] The position operator $\mathbf{r}$ applied to a state $|\psi\rangle$ gives the position vector [45], but in our notations we do not distinguish operators with other quantities.

[2] In spherical coordinates: $\hat{\mathbf{r}} = \sin\theta\cos\varphi\,\hat{\mathbf{e}}_x + \sin\theta\sin\varphi\,\hat{\mathbf{e}}_y + \cos\theta\,\hat{\mathbf{e}}_z$.

Thus, one can calculate the two angular integrals present in equations (5.8c) and (5.9b) and find

$$\int_{4\pi} \hat{\mathbf{r}}\, Y_1^{M_m}(\theta,\varphi)\,\mathrm{d}\Omega = \sqrt{\frac{4\pi}{3}}\,\hat{\mathbf{e}}_{M_m}, \tag{5.12a}$$

$$\int_{4\pi} \left(Y_1^{M_m}(\theta,\varphi)\right)^* \hat{\mathbf{r}}\,\mathrm{d}\Omega = \sqrt{\frac{4\pi}{3}}\,\hat{\mathbf{e}}^*_{M_m}, \tag{5.12b}$$

where $\{\hat{\mathbf{e}}_{-1},\hat{\mathbf{e}}_0,\hat{\mathbf{e}}_1\}$ [100] forms an orthonormal basis and are given by

$$\begin{cases} \hat{\mathbf{e}}_{-1} := \dfrac{\hat{\mathbf{e}}_x - i\,\hat{\mathbf{e}}_y}{\sqrt{2}} & \text{(5.13a)} \\ \hat{\mathbf{e}}_0 := \hat{\mathbf{e}}_z & \text{(5.13b)} \\ \hat{\mathbf{e}}_1 := -\dfrac{\hat{\mathbf{e}}_x + i\,\mathbf{e_y}}{\sqrt{2}}, & \text{(5.13c)} \end{cases}$$

and satisfy the following relation:

$$\forall M_m = 0,\pm 1, \quad \hat{\mathbf{e}}^*_{M_m} = (-1)^{M_m}\,\hat{\mathbf{e}}_{-M_m}. \tag{5.14}$$

Injecting these results in equations (5.8c) and (5.38b), one gets:

$$\mathbf{d}^{em} = -\frac{e}{\sqrt{3}}\int_0^\infty r^3 R^*_{N_e,0}(r)R_{N_m,1}(r)\,\mathrm{d}r\,\hat{\mathbf{e}}_{M_m} = d^{em}\,\hat{\mathbf{e}}_{M_m}, \tag{5.15a}$$

$$\mathbf{d}^{mg} = -\frac{e}{\sqrt{3}}\int_0^\infty r^3 R^*_{N_m,1}(r)R_{N_g,0}(r)\,\mathrm{d}r\,\hat{\mathbf{e}}^*_{M_m} = d^{mg}\,\hat{\mathbf{e}}^*_{M_m}, \tag{5.15b}$$

where $d^{em}$ and $d^{mg}$ denote the norm of these vectors, which depend only on the principal quantum numbers of the involved states, while the magnetic quantum number $M_m$ of the intermediate state $|m\rangle$ fixes the orientation of the transition moments.

Since we have calculated the first-order transition moments $\mathbf{d}^{em}$ and $\mathbf{d}^{mg}$ in the last two equations, we can now calculate the second-rank tensor $\boldsymbol{\mathcal{D}}^{eg}$ given by the equation (5.6a), where the summation runs over all possible intermediate states. This summation is rewritten as a summation over the quantum numbers $N_m$ and $M_m$, the azimuthal quantum number $L_m$ being fixed to 1:

$$\boldsymbol{\mathcal{D}}^{eg}(\omega_\alpha,\omega_{\alpha'}) = \sum_{N_m}\sum_{M_m}\left(\frac{d^{em}\,\hat{\mathbf{e}}_{M_m}\,d^{mg}\,\hat{\mathbf{e}}^*_{M_m}}{\omega_{em}-\omega_\alpha} + \frac{d^{mg}\,\hat{\mathbf{e}}^*_{M_m}\,d^{em}\,\hat{\mathbf{e}}_{M_m}}{\omega_{em}-\omega_{\alpha'}}\right) \tag{5.16a}$$

$$= \sum_{N_m} d^{em}d^{mg}\left\{\frac{\sum_{M_m}\hat{\mathbf{e}}_{M_m}\hat{\mathbf{e}}^*_{M_m}}{\omega_{em}-\omega_\alpha} + \frac{\sum_{M_m}\hat{\mathbf{e}}^*_{M_m}\hat{\mathbf{e}}_{M_m}}{\omega_{em}-\omega_{\alpha'}}\right\}, \tag{5.16b}$$

where we remind that $d^{em}$, $d^{mg}$ and $\omega_{em}$ depend only on $N_m$[3] while $\hat{\mathbf{e}}_{M_m}$ depends only on $M_m$. Since the set of vectors $\{\hat{\mathbf{e}}_{-1},\hat{\mathbf{e}}_0,\hat{\mathbf{e}}_1\}$ forms an orthonormal basis, the closing relation is satisfied:

$$\sum_{M_m}\hat{\mathbf{e}}^*_{M_m}\hat{\mathbf{e}}_{M_m} = \sum_{M_m}\hat{\mathbf{e}}_{M_m}\hat{\mathbf{e}}^*_{M_m} = \mathbb{1}_{3\times 3}, \tag{5.17}$$

[3]The energy of the intermediate states, and therefore $\omega_{em}$, depends only on $N_m$ [Sec. 2.3].

where $\mathbb{1}_{3\times3}$ represents the identity matrix in three dimensions. Using the last property, one gets:

$$\boldsymbol{\mathcal{D}}^{eg}(\omega_\alpha,\omega_{\alpha'}) = \sum_{N_m} d^{em}d^{mg}\left(\frac{1}{\omega_{em}-\omega_\alpha}+\frac{1}{\omega_{em}-\omega_{\alpha'}}\right)\mathbb{1}_{3\times3}. \tag{5.18}$$

Therefore, the normalized tensor is given by [31]:

$$\hat{\boldsymbol{\mathcal{D}}}^{eg} = \frac{\boldsymbol{\mathcal{D}}^{eg}(\omega_\alpha,\omega_{\alpha'})}{\|\boldsymbol{\mathcal{D}}^{eg}(\omega_\alpha,\omega_{\alpha'})\|} = \frac{\mathbb{1}_{3\times3}}{\sqrt{3}}, \tag{5.19}$$

and is independent of the frequencies of the emitted quanta and where the norm of an $n^{\text{th}}$ rank tensor $\mathbf{U}$ with $n\in\mathbb{N}_0$ has been defined as $\|\mathbf{U}\|^2 := \sum_{i_1,i_2,\ldots,i_n}|U_{i_1,i_2,\ldots,i_n}|^2$. Note that this tensor implies that all components of the tensor $\mathbf{F}^{\text{ED}}$ must be calculated (some can be equal or zero due to the environment) in the calculation of the 2ED transition rate [Eq. (4.58a)], because the emitter is spherically symmetric.

### 5.2.2 Normalized second-order electric quadrupole transition moment

For an electric quadrupole (EQ) transition, the selection rules impose that $\Delta L = 0,\pm2$ and that $\Delta M = 0,\pm1,\pm2$, by noting that the transition between two $s$ states is forbidden [47]. Thus, the intermediate states leading to non-zero electric quadrupole transition moments are $d$ states:

$$|m\rangle = |N_m; L_m = 2; M_m = 0,\pm1,\pm2\rangle\,, \tag{5.20a}$$

$$\psi_m(\mathbf{r}) = R_{N_m,2}(r)\,Y_2^{M_m}(\theta,\varphi), \quad \text{with } M_m = 0,\pm1,\pm2. \tag{5.20b}$$

As the type of all involved states in this second-order transition have been determined, we can now calculate the electric quadrupole transition moment corresponding, first, to the transition between the excited state $|e\rangle$ and an intermediate state $|m\rangle$:

$$Q_{ij}^{em} = \langle e|\,Q_{ij}\,|m\rangle \tag{5.21a}$$

$$= -\frac{e}{2}\int_{\mathbb{R}^3} R^*_{N_e,0}(r)\left(Y_0^0\right)^*\left(x_ix_j - r^2\frac{\delta_{ij}}{3}\right)R_{N_m,2}(r)\,Y_2^{M_m}(\theta,\varphi)\,\mathrm{d}^3r \tag{5.21b}$$

$$= -\frac{e}{2}\int_0^\infty r^4 R^*_{N_e,0}(r)R_{N_m,2}(r)\,\mathrm{d}r\int_{4\pi}\left(Y_0^0\right)^*\left(\frac{x_ix_j}{r^2}-\frac{\delta_{ij}}{3}\right)Y_2^{M_m}(\theta,\varphi)\,\mathrm{d}\Omega, \tag{5.21c}$$

where we used the traceless form of the electric quadrupole moment operator $Q_{ij} = -\frac{e}{2}\left(x_ix_j - r^2\frac{\delta_{ij}}{3}\right)$ [Eq. (3.5c)] and we switched to spherical coordinates. Notice that the radial integral depends only on the principal quantum numbers of the two states, while the angular integrals depend solely on the magnetic quantum number $M_m$ of the intermediate state $|m\rangle$.

Let us now calculate the following angular integrals:

$$\int_{4\pi}\left(Y_0^0\right)^*\left(\frac{x_ix_j}{r^2}-\frac{\delta_{ij}}{3}\right)Y_2^{M_m}(\theta,\varphi)\,\mathrm{d}\Omega. \tag{5.22}$$

Using the orthonormality relation given by equation (5.11b), we notice directly that the term

$$\int_{4\pi}\left(Y_0^0\right)^*\frac{\delta_{ij}}{3}Y_2^{M_m}(\theta,\varphi)\,\mathrm{d}\Omega \tag{5.23}$$

in the last equation vanishes, showing that trace and traceless versions of electric quadrupole moments lead to the same results. Thus, we still have to calculate the following integral for the five possible values of $M_m$ $(0, \pm 1, \pm 2)$:

$$\int_{4\pi} \left(Y_0^0\right)^* \frac{x_i x_j}{r^2} Y_2^{M_m}(\theta,\varphi)\,\mathrm{d}\Omega = (-1)^{M_m} \frac{1}{\sqrt{4\pi}} \int_{4\pi} \frac{x_i x_j}{r^2} \left(Y_2^{-M_m}(\theta,\varphi)\right)^* \mathrm{d}\Omega, \tag{5.24}$$

where we used the complex conjugate property given by the equation (5.11a) and that $Y_0^0 = 1/\sqrt{4\pi}$ [Tab. A.1].

To simplify the calculations, the idea is to express the products $x_i x_j / r^2$ as a function of the spherical harmonics [100]:

$$\begin{cases} \dfrac{x^2}{r^2} = \dfrac{\sqrt{4\pi}}{3} Y_0^0 - \dfrac{1}{3}\sqrt{\dfrac{4\pi}{5}} Y_2^0 + \sqrt{\dfrac{2\pi}{15}} \left(Y_2^2 + Y_2^{-2}\right) & \text{(5.25a)} \\ \dfrac{y^2}{r^2} = \dfrac{\sqrt{4\pi}}{3} Y_0^0 - \dfrac{1}{3}\sqrt{\dfrac{4\pi}{5}} Y_2^0 - \sqrt{\dfrac{2\pi}{15}} \left(Y_2^2 + Y_2^{-2}\right) & \text{(5.25b)} \\ \dfrac{z^2}{r^2} = \dfrac{\sqrt{4\pi}}{3} Y_0^0 + \dfrac{2}{3}\sqrt{\dfrac{4\pi}{5}} Y_2^0 & \text{(5.25c)} \\ \dfrac{xy}{r^2} = i\sqrt{\dfrac{2\pi}{15}} \left(Y_2^{-2} - Y_2^2\right) & \text{(5.25d)} \\ \dfrac{yz}{r^2} = i\sqrt{\dfrac{2\pi}{15}} \left(Y_2^{-1} + Y_2^1\right) & \text{(5.25e)} \\ \dfrac{xz}{r^2} = \sqrt{\dfrac{2\pi}{15}} \left(Y_2^{-1} - Y_2^1\right). & \text{(5.25f)} \end{cases}$$

Thus, for each value of $M_m$ and by using the orthonormality property [Eq. (5.11b)], the non-zero integrals can be easily identified and calculated. By doing so, one gets

$$\mathbf{Q}^{em} = -\frac{e}{\sqrt{30}} \int_0^\infty r^4 R_{N_e,0}^*(r) R_{N_m,2}(r)\,\mathrm{d}r\, \mathbf{S}^{M_m} = q^{em}\, \mathbf{S}^{M_m}, \tag{5.26}$$

where $q^{em}$ denotes the norm of the tensor $\mathbf{Q}^{em}$, which depends only on the principal quantum numbers of the excited and intermediate states. Moreover, the tensor $\mathbf{S}^{M_m}$ is normalized, gives the orientation of the transition moment, and depends only on the quantum number $M_m$ of the intermediate state. Depending on the value of $M_m$, it is given by

$$\begin{gathered} \mathbf{S}^{-2} := \frac{1}{2}\begin{pmatrix} 1 & -i & 0 \\ -i & -1 & 0 \\ 0 & 0 & 0 \end{pmatrix}, \; \mathbf{S}^{-1} := \frac{1}{2}\begin{pmatrix} 0 & 0 & 1 \\ 0 & 0 & -i \\ 1 & -i & 0 \end{pmatrix}, \; \mathbf{S}^{0} := \frac{1}{\sqrt{6}}\begin{pmatrix} -1 & 0 & 0 \\ 0 & -1 & 0 \\ 0 & 0 & 2 \end{pmatrix}, \\ \mathbf{S}^{2} := \frac{1}{2}\begin{pmatrix} 1 & i & 0 \\ i & -1 & 0 \\ 0 & 0 & 0 \end{pmatrix}, \; \mathbf{S}^{1} := \frac{1}{2}\begin{pmatrix} 0 & 0 & -1 \\ 0 & 0 & -i \\ -1 & -i & 0 \end{pmatrix}. \end{gathered} \tag{5.27}$$

As electric quadrupole moments, these tensors are symmetric and traceless.

Concerning the moment $\mathbf{Q}^{mg}$ also involved in $\boldsymbol{\mathcal{Q}}^{eg}$ [Eq. (5.6b)], similar developments lead to

$$\mathbf{Q}^{mg} = -\frac{e}{\sqrt{30}} \int_0^\infty r^4 R_{N_m,2}^*(r) R_{N_g,0}(r)\,\mathrm{d}r \left(\mathbf{S}^{M_m}\right)^* = q^{mg} \left(\mathbf{S}^{M_m}\right)^*. \tag{5.28}$$

Since we have calculated the first-order transition moments $\mathbf{Q}^{em}$ and $\mathbf{Q}^{mg}$ [Eqs. (5.26) and (5.28)], we can now calculate the fourth-rank tensor $\boldsymbol{\mathcal{Q}}^{eg}$ given by the equation (5.6b), where the summation runs over all possible intermediate states. This summation is rewritten as a summation over the quantum numbers $N_m$ and $M_m$, the azimuthal quantum number $L_m$ being fixed to 2:

$$\boldsymbol{\mathcal{Q}}^{eg}(\omega_\alpha,\omega_{\alpha'}) = \sum_{N_m}\sum_{M_m}\left\{\frac{q^{em}\mathbf{S}^{M_m}q^{mg}\left(\mathbf{S}^{M_m}\right)^*}{\omega_{em}-\omega_\alpha}+\frac{q^{mg}\left(\mathbf{S}^{M_m}\right)^*q^{em}\mathbf{S}^{M_m}}{\omega_{em}-\omega_{\alpha'}}\right\} \tag{5.29a}$$

$$= \sum_{N_m} q^{em}q^{mg}\left\{\frac{\sum_{M_m}\mathbf{S}^{M_m}\left(\mathbf{S}^{M_m}\right)^*}{\omega_{em}-\omega_\alpha}+\frac{\sum_{M_m}\left(\mathbf{S}^{M_m}\right)^*\mathbf{S}^{M_m}}{\omega_{em}-\omega_{\alpha'}}\right\}, \tag{5.29b}$$

where we remind that $q^{em}$, $q^{mg}$ and $\omega_{em}$ depend only on $N_m$, while $\mathbf{S}^{M_m}$ depends only on $M_m$. Furthermore, one can show that

$$\forall i,j,k,l=1,2,3,\quad \sum_{M_m} S_{ij}^{M_m}\left(S_{kl}^{M_m}\right)^* = \sum_{M_m}\left(S_{ij}^{M_m}\right)^* S_{kl}^{M_m} = \frac{1}{2}\left(\delta_{ik}\delta_{jl}+\delta_{il}\delta_{jk}-\frac{2}{3}\delta_{ij}\delta_{kl}\right). \tag{5.30}$$

Thus, the components of the tensor $\boldsymbol{\mathcal{Q}}^{eg}$ are given by

$$\mathcal{Q}_{ijkl}^{eg}(\omega_\alpha,\omega_{\alpha'}) = \frac{1}{2}\sum_{N_m} q^{em}q^{mg}\left(\frac{1}{\omega_{em}-\omega_\alpha}+\frac{1}{\omega_{em}-\omega_{\alpha'}}\right)\left(\delta_{ik}\delta_{jl}+\delta_{il}\delta_{jk}-\frac{2}{3}\delta_{ij}\delta_{kl}\right), \tag{5.31}$$

whereas its normalized version is given by

$$\hat{\mathcal{Q}}_{ijkl}^{eg} := \frac{\mathcal{Q}_{ijkl}^{eg}(\omega_\alpha,\omega_{\alpha'})}{\|\boldsymbol{\mathcal{Q}}^{eg}(\omega_\alpha,\omega_{\alpha'})\|} = \frac{1}{\sqrt{20}}\left(\delta_{ik}\delta_{jl}+\delta_{il}\delta_{jk}-\frac{2}{3}\delta_{ij}\delta_{kl}\right), \tag{5.32}$$

which is independent of the frequencies of the emitted quanta. A representation of this tensor is sketched in Table 5.1. As a check, the calculated tensor satisfies the following properties [Eqs. (4.19) and (4.20)]:

$$\forall i,j,k,l=1,2,3,\quad \mathcal{Q}_{ijkl}^{eg}=\mathcal{Q}_{jikl}^{eg}=\mathcal{Q}_{ijlk}^{eg}=\mathcal{Q}_{jilk}^{eg}, \tag{5.33a}$$

$$\forall i,j,k,l=1,2,3,\quad \sum_i \mathcal{Q}_{iikl}^{eg}=\sum_k \mathcal{Q}_{ijkk}^{eg}=0, \tag{5.33b}$$

originating from the symmetric and the traceless properties of electric quadrupole moments.

Finally, using the modified Voigt notation introduced in Section 3.6 (see Table 3.2), the second-order electric quadrupole transition moment is rewritten as a second-rank tensor in five dimensions:

$$\hat{\boldsymbol{\mathcal{Q}}}^{eg} := \frac{\boldsymbol{\mathcal{Q}}^{eg}(\omega_\alpha,\omega_{\alpha'})}{\|\boldsymbol{\mathcal{Q}}^{eg}(\omega_\alpha,\omega_{\alpha'})\|} = \frac{1}{\sqrt{20}}\begin{pmatrix} 4/3 & -2/3 & 0 & 0 & 0\\ -2/3 & 4/3 & 0 & 0 & 0\\ 0 & 0 & 1 & 0 & 0\\ 0 & 0 & 0 & 1 & 0\\ 0 & 0 & 0 & 0 & 1\end{pmatrix}. \tag{5.34}$$

Note that this tensor implies that all components of the tensor $\mathbf{F}^{\mathrm{EQ}}$ must be calculated (some can be equal or zero due to the environment) in the calculation of the 2EQ transition rate [Eq. (4.63)], because the emitter is spherically symmetric.

| | | $j=1$ | | | $j=2$ | | | $j=3$ | | |
|---|---|---|---|---|---|---|---|---|---|---|
| | | $l=1$ | $l=2$ | $l=3$ | $l=1$ | $l=2$ | $l=3$ | $l=1$ | $l=2$ | $l=3$ |
| $i=1$ | $k=1$ | 4/3 | | | | 1 | | | | 1 |
| | $k=2$ | | -2/3 | | 1 | | | | | |
| | $k=3$ | | | -2/3 | | | | 1 | | |
| $i=2$ | $k=1$ | | 1 | | -2/3 | | | | | |
| | $k=2$ | 1 | | | | 4/3 | | | | 1 |
| | $k=3$ | | | | | | -2/3 | | 1 | |
| $i=3$ | $k=1$ | | | 1 | | | | -2/3 | | |
| | $k=2$ | | | | | | 1 | | -2/3 | |
| | $k=3$ | 1 | | | | 1 | | | | 4/3 |

Table 5.1: Representation of the fourth-rank tensor $\hat{\boldsymbol{\mathcal{Q}}}^{eg}$ (factor $1/\sqrt{20}$ in front) in the form of a $3 \times 3$ matrix, where each element is itself a $3 \times 3$ matrix.

## 5.3 Two-photon spontaneous emission transition rates in vacuum

Historically, the first estimate of a two-photon spontaneous emission rate was carried out in 1940 by Breit and Teller for the 2s state of hydrogen, for which this is the main process responsible for its mean lifetime [3]. One decade later, Spitzer and Greenstein realized a refinement and found a value of 8.23 $s^{-1}$ for the integrated two-electric dipole transition rate, i.e., the main multipolar contribution to this process [4]. In 1981, Goldman and Drake made the first calculations, relativistic, that include the first multipolar contributions to the TPSE process [5]. They found that the integrated 2ED and 2EQ transition rates are 8.229 $s^{-1}$ and $4.907 \times 10^{-12}$ $s^{-1}$, respectively. More recently in 2007, Chluba and Sunyaev studied the two-photon process for the $ns \to 1s$ and $nd \to 1s$ 2ED transitions in hydrogen and up to large $n$, where they provide analytical fittings of the spectra [8].

In conclusion, the only data available in the literature concerning 2ED and 2EQ transition rates in vacuum for hydrogen are, on the one hand, spectra involving the $1s$ state as the final state for the 2ED transition [8] and, on the other hand, the integrated rate between the $2s$ and $1s$ states for the 2EQ transition [5]. Nevertheless, Matsumoto derived in 1991 analytical expressions for the multipole matrix elements for the hydrogen atom [101]. Thus, we can use the method presented in Ref. 8 for their calculation of 2ED transition rates as well as the expressions of the multipole matrix elements in Ref. 101 to calculate the 2ED and 2EQ transition rates in vacuum between two $s$ states of the hydrogen atom.

The section starts with a reminder concerning the expressions of the 2ED and 2EQ transition rates in vacuum and about the multipolar second-order transition moments relative to a transition between two spherically symmetric states. Then, we derive in Subsection 5.3.2 the 2ED and 2EQ decay profiles and we discuss the two contributions to the summation over the virtual intermediate states. In Subsection 5.3.3, we give the expressions of the multipole matrix elements, which are radial integrals over the radial eigenfunctions of the hydrogen atom. Finally, our method and results are presented in Subsection 5.3.4.

### 5.3.1 Reminder

In Section 4.4, we showed that for each multipolar operator MO $\in$ {ED, EQ} the vacuum TPSE rate is given by

$$\Gamma^{(2)}_{\mathrm{2MO},0} = \int_0^{\omega_{eg}} \gamma^{(2)}_{\mathrm{2MO},0}(\omega)\,\mathrm{d}\omega, \tag{5.35}$$

where the multipolar contributions $\gamma^{(2)}_{\mathrm{2MO},0}(\omega)$ to the spectral distribution of the emitted quanta are given by

$$\gamma^{(2)}_{\mathrm{2ED},0}(\omega) = \frac{\omega^3(\omega_{eg}-\omega)^3}{36\pi^3\varepsilon_0^2\hbar^2c^6}\left\|\boldsymbol{\mathcal{D}}^{eg}(\omega,\omega_{eg}-\omega)\right\|^2, \tag{5.36a}$$

$$\gamma^{(2)}_{\mathrm{2EQ},0}(\omega) = \frac{\omega^5(\omega_{eg}-\omega)^5}{400\pi^3\varepsilon_0^2\hbar^2c^{10}}\left\|\boldsymbol{\mathcal{Q}}^{eg}(\omega,\omega_{eg}-\omega)\right\|^2, \tag{5.36b}$$

where $\omega$ and $\omega_{eg}-\omega$ are the frequencies of the two emitted quanta of complementary energy. In these equations, $\varepsilon_0$ is the vacuum electric permittivity, $\hbar\omega_{eg}$ represents the transition energy with $\hbar$ the reduced Planck constant, and $c$ denotes the speed of light in vacuum. These expressions involve the squared norm of $\boldsymbol{\mathcal{D}}^{eg}$ and $\boldsymbol{\mathcal{Q}}^{eg}$ reminded in equations (5.6). The squared norm of an $n^{\mathrm{th}}$ rank tensor $\mathbf{U}$ with $n \in \mathbb{N}_0$ is defined as $\|\mathbf{U}\|^2 := \sum_{i_1,i_2,\ldots,i_n} |U_{i_1,i_2,\ldots,i_n}|^2$.

In the case of a transition between two spherically symmetric states, we showed in the previous section that the second-order electric dipole transition moment is given by [Eq. (5.18)]:

$$\boldsymbol{\mathcal{D}}^{eg}(\omega,\omega_{eg}-\omega) = \sum_{N_m} d^{em}d^{mg}\left(\frac{1}{\omega_{em}-\omega}+\frac{1}{\omega_{em}-(\omega_{eg}-\omega)}\right)\mathbb{1}_{3\times3}, \tag{5.37}$$

where there is a summation over the principal quantum number $N_m$ of the intermediate states $|m\rangle$, where $\mathbb{1}_{3\times3}$ is the identity matrix in three dimensions, and where $d^{em}$ and $d^{mg}$ are the electric dipole radial matrix elements [Eqs. (5.15)]:

$$d^{em} := -\frac{e\,a_0}{\sqrt{3}}\,\langle R_{N_e,L_m-1}|r|R_{N_m,L_m}\rangle\,, \tag{5.38a}$$

$$d^{mg} := -\frac{e\,a_0}{\sqrt{3}}\,\langle R_{N_m,L_m}|r|R_{N_g,L_m-1}\rangle\,. \tag{5.38b}$$

In the previous equations, $e$ is the elementary charge, $a_0$ represents the Bohr radius, $r$ is the dimensionless position operator, and $R_{N,L}(r)$ denotes the radial component of the wavefunction of the hydrogen atom. Moreover, $L_m$ denotes the azimuthal quantum number of the intermediate state whereas $N_e$ and $N_g$ are the principal quantum numbers of the excited and ground states of the emitter, respectively. For consistency of notation, we retain the ground state label for the final state, even though it is not necessarily the ground state. Instead of working in the commonly used atomic

unit system, we have chosen to highlight the Bohr radius $a_0$ so that the radial integrals, discussed in Section 5.3.3, are dimensionless.

Concerning the 2EQ transition, for an $s \to s$ transition the second-order electric quadrupole transition moment is given by [Eq. (5.31)]:

$$\boldsymbol{\mathcal{Q}}^{eg}(\omega, \omega_{eg} - \omega) = \sqrt{5} \sum_{N_m} q^{em} q^{mg} \left( \frac{1}{\omega_{em} - \omega} + \frac{1}{\omega_{em} - (\omega_{eg} - \omega)} \right) \hat{\boldsymbol{\mathcal{Q}}}^{eg}, \tag{5.39}$$

where the elements of the normalized tensor are given by [Eq. (5.32)]:

$$\hat{\mathcal{Q}}^{eg}_{ijkl} := \frac{\mathcal{Q}^{eg}_{ijkl}(\omega, \omega_{eg} - \omega)}{\| \boldsymbol{\mathcal{Q}}^{eg}(\omega, \omega_{eg} - \omega) \|} = \frac{1}{\sqrt{20}} \left( \delta_{ik}\delta_{jl} + \delta_{il}\delta_{jk} - \frac{2}{3}\, \delta_{ij}\delta_{kl} \right), \tag{5.40}$$

and where $q^{em}$ and $q^{mg}$ are the electric quadrupole radial matrix elements [Eqs. (5.26) and (5.28)]:

$$q^{em} := -\frac{e\, a_0^2}{\sqrt{30}} \langle R_{N_e, L_m - 2} | r^2 | R_{N_m, L_m} \rangle \,, \tag{5.41a}$$

$$q^{mg} := -\frac{e\, a_0^2}{\sqrt{30}} \langle R_{N_m, L_m} | r^2 | R_{N_g, L_m - 2} \rangle \,. \tag{5.41b}$$

### 5.3.2 Vacuum decay profiles

To calculate TPSE rates in vacuum, let us rewrite the equations by introducing the dimensionless frequency $y := \omega/\omega_{eg}$ comprised between 0 and 1. By doing so, the equation (5.35) of the integrated transition rate is rewritten as follows [8]:

$$\Gamma^{(2)}_{\mathrm{2MO},0} = \int_0^{\omega_{eg}} \gamma^{(2)}_{\mathrm{2MO},0}(\omega)\, \mathrm{d}\omega = \frac{1}{2} \int_0^1 \phi^{(2)}_{\mathrm{2MO},0}(y)\, \mathrm{d}y = \int_0^{1/2} \phi^{(2)}_{\mathrm{2MO},0}(y)\, \mathrm{d}y, \tag{5.42}$$

with the decay profile

$$\phi^{(2)}_{\mathrm{2MO},0}(y) = 2\, \omega_{eg}\, \gamma^{(2)}_{\mathrm{2MO},0}(\omega), \tag{5.43}$$

where $\phi^{(2)}_{\mathrm{2MO},0}(y)\, \mathrm{d}y$ denotes the number of photons emitted per second in the frequency interval between $y$ and $y + \mathrm{d}y$. The latter spectrum encompasses the photons emitted simultaneously during this second-order process at complementary frequencies, thus necessitating integration over only half of the spectrum[4]. Note that the probability to emit a photon at the frequency $\omega$ is equal to the probability to emit a photon at the complementary energy $\omega_{eg} - \omega$, leading to symmetric profiles with respect to $\omega_{eg}/2$.

Now, let us derive the expression of the decay profiles for the 2ED and 2EQ transitions in vacuum. Then, we discuss the different contributions to the summation over the virtual intermediate states.

#### Two-electric dipole decay profile in vacuum

Let us start by rewriting the equations of the spectral transition rate and of the second-order transition moment [Eqs. (5.36a) and (5.37)] by introducing the dimensionless frequency $y := \omega/\omega_{eg}$

[4] The definition of $\gamma^{(2)}_{\mathrm{2MO},0}(\omega)$ doesn't count the quanta emitted simultaneously at complementary frequencies, which explains the factor 2 difference with the definition of $\phi^{(2)}_{\mathrm{2MO},0}(y)$.

and by using the new definition of the spectrum [Eq. (5.43)]:

$$\phi^{(2)}_{\mathrm{2ED},0}(y) = \frac{\omega_{eg}^7}{18\pi^3\varepsilon_0^2\hbar^2c^6}\, y^3(1-y)^3 \left\|\boldsymbol{\mathcal{D}}^{eg}(y,1-y)\right\|^2, \tag{5.44a}$$

$$\boldsymbol{\mathcal{D}}^{eg}(y,1-y) = \frac{1}{\omega_{eg}} \sum_{N_m} d^{em} d^{mg} f_{N_m}(y)\, \mathbb{1}_{3\times 3}, \tag{5.44b}$$

where the function $f_{N_m}(y)$ has been defined as

$$f_{N_m}(y) := \left(\frac{1}{y_{em}-y} + \frac{1}{y_{em}-(1-y)}\right), \tag{5.45}$$

with

$$y_{em} := \frac{\omega_{em}}{\omega_{eg}} := \frac{E_e - E_m}{E_e - E_g} = \frac{N_g^2(N_e^2-N_m^2)}{N_m^2(N_e^2-N_g^2)}. \tag{5.46}$$

Thus, the function $f_{N_m}(y)$ depends only on the frequency and on the principal quantum number $N_m$ of the intermediate state (these of the initial and final ones are fixed). In the last equation, we used the expression of the eigenvalues, i.e., $E_N = -E_i/N^2$ with $E_i \approx 13.6$ eV the ionization energy of the hydrogen atom[5] [Sec. 2.3].

Using the expressions of the electric dipole radial matrix elements [Eqs. (5.38)], the squared norm of the second-order transition moment is rewritten as

$$\left\|\boldsymbol{\mathcal{D}}^{eg}(y,1-y)\right\|^2 = \frac{e^4a_0^4}{3\,\omega_{eg}^2} \underbrace{\left|\sum_{N_m} \langle R_{N_e,L_m-1}|r|R_{N_m,L_m}\rangle \langle R_{N_m,L_m}|r|R_{N_g,L_m-1}\rangle\, f_{N_m}(y)\right|^2}_{\left|M^{eg}_{\mathrm{2ED}}(y)\right|^2}. \tag{5.47}$$

Finally, by injecting the last equation in the expression of the 2ED vacuum transition rate [Eq. (5.44a)], we get the expression obtained in Ref. 8 for the 2ED decay profile:

$$\boxed{\phi^{(2)}_{\mathrm{2ED},0}(y) = G^{eg}_{\mathrm{2ED}}\, y^3(1-y)^3 \left|M^{eg}_{\mathrm{2ED}}(y)\right|^2, \quad G^{eg}_{\mathrm{2ED}} := \left(\frac{2}{3}\right)^3 \frac{\omega_{eg}^5 a_0^4 \alpha^2}{\pi c^4},} \tag{5.48}$$

where $\alpha = e^2/4\pi\varepsilon_0\hbar c$ is the fine-structure constant. Note that this expression is only valid for an $s \to s$ transition. For a $2s \to 1s$ transition, $\omega_{eg} = 3E_i/4\hbar$ and $G^{2s\,1s}_{\mathrm{2ED}} \approx 4.37\ \mathrm{s}^{-1}$, while for a $5s \to 3s$ transition, $\omega_{eg} = (4/15)^2 E_i/\hbar$ and $G^{5s\,3s}_{\mathrm{2ED}} \approx 3.35 \times 10^{-5}\ \mathrm{s}^{-1}$.

### Two-electric quadrupole decay profile in vacuum

Now, let us do the same developments for the spectral transition rate and for the second-order transition moment of the 2EQ transition [Eqs. (5.36b) and (5.39)]:

$$\phi^{(2)}_{\mathrm{2EQ},0}(y) = \frac{\omega_{eg}^{11}}{200\pi^3\varepsilon_0^2\hbar^2c^{10}}\, y^5(1-y)^5 \left\|\boldsymbol{\mathcal{Q}}^{eg}(y,1-y)\right\|^2, \tag{5.49a}$$

$$\boldsymbol{\mathcal{Q}}^{eg}(y,1-y) = \frac{\sqrt{5}}{\omega_{eg}} \sum_{N_m} q^{em} q^{mg} f_{N_m}(y)\, \hat{\boldsymbol{\mathcal{Q}}}^{eg}. \tag{5.49b}$$

[5] In contrast to previous chapters, $E$ represents here the energy of a state of the atom, not of the system (atom + field).

Using the expressions of the electric quadrupole radial matrix elements [Eqs. (5.41)], the squared norm of the second-order transition moment is rewritten as

$$\|\boldsymbol{\mathcal{Q}}^{eg}(y,1-y)\|^2 = \frac{e^4 a_0^8}{180\,\omega_{eg}^2} \underbrace{\left| \sum_{N_m} \langle R_{N_e,L_m-2}|r^2|R_{N_m,L_m}\rangle \langle R_{N_m,L_m}|r^2|R_{N_g,L_m-2}\rangle\, f_{N_m}(y) \right|^2}_{\left|M_{2\mathrm{EQ}}^{eg}(y)\right|^2}. \tag{5.50}$$

Finally, by injecting the last equation in the expression of the 2EQ vacuum transition rate given by the equation (5.49a), we get the 2EQ decay profile:

$$\boxed{\phi_{2\mathrm{EQ},0}^{(2)}(y) = G_{2\mathrm{EQ}}^{eg}\, y^5(1-y)^5 \left|M_{2\mathrm{EQ}}^{eg}(y)\right|^2, \quad G_{2\mathrm{EQ}}^{eg} := \frac{\omega_{eg}^9 a_0^8 \alpha^2}{2250\pi c^8}.} \tag{5.51}$$

Note that this expression is only valid for an $s \to s$ transition. For a $2s \to 1s$ transition, $\omega_{eg} = 3E_i/4\hbar$ and $G_{2\mathrm{EQ}}^{2s\,1s} \approx 3.67 \times 10^{-13}$ s$^{-1}$, while for a $5s \to 3s$ transition, $\omega_{eg} = (4/15)^2 E_i/\hbar$ and $G_{2\mathrm{EQ}}^{5s\,3s} \approx 2.27 \times 10^{-22}$ s$^{-1}$.

#### Summation over intermediate states

To calculate the decay profiles $\phi_{2\mathrm{ED},0}^{(2)}(y)$ and $\phi_{2\mathrm{ED},0}^{(2)}(y)$, we need to calculate the quantities $M_{2\mathrm{ED}}^{eg}(y)$ and $M_{2\mathrm{EQ}}^{eg}(y)$ [Eqs. (5.47) and (5.50)] that involve a summation over the principal quantum number of the virtual intermediate states. This one starts from $N_m = N_e$ and extends to infinity. Indeed, the summation for $N_g < N_m < N_e$ denotes a summation over real states and thus describes a cascade of two single-photon emissions and not a TPSE process [8]. Furthermore, we see that the virtual states involved in this multi-step process mediate otherwise forbidden transitions (i.e., a transition towards a state with $N_m \geq N_e$). These virtual states violate the law of conservation of energy since the energy of the atom increases by emitting a photon, but only during a very short time [Sec. 2.4].

Furthermore, there are two contributions to the summation over $N_m \geq N_e$:

$$\sum_{N_m} = \sum_{N_m=N_e}^{\infty} + \int_0^{\infty} \mathrm{d}x. \tag{5.52}$$

The first one is a summation over the discrete set of bound states ($E_N = -E_i/N^2 < 0, N \in \mathbb{N}_0$) while the second one is an integral over the continuum of free states ($E_x = x^2 E_i \geq 0, x \in \mathbb{R}^+$) [8]. Now, all that remains is to calculate, in the next subsection, the multipole matrix elements involved in the calculation of $M_{2\mathrm{ED}}^{eg}(y)$ and $M_{2\mathrm{EQ}}^{eg}(y)$ [Eqs. (5.47) and (5.50)].

### 5.3.3 Calculation of multipole matrix elements

For the radial component of the hydrogen atom's wavefunction, the dimensionless eigenfunctions can be written, in atomic unit of length, as follows [101, 102]:

$$R_{N,L}(r) = K_{N,L}\, e^{-r/N}\, r^L\, {}_1F_1\left(-N_r; 2L+2; 2\frac{r}{N}\right), \tag{5.53}$$

where $N$, $L$, and $N_r := N - L - 1$ are respectively the principal, azimuthal, and radial quantum numbers. Moreover, $K_{N,L}$ is a normalization constant and ${}_1F_1(a;b;z)$ denotes the confluent

hypergeometric function defined as [100, 103]:

$$ {}_1F_1(a,b;z) := \sum_{i=0}^{\infty} \frac{(a)_i}{(b)_i}\frac{z^i}{i!} = \frac{\Gamma(b)}{\Gamma(a)\Gamma(b-a)} \int_0^1 e^{zt}\, t^{a-1}(1-t)^{b-a-1}\,\mathrm{d}t, \tag{5.54} $$

where $(\,\cdot\,)_j$ is the Pochhammer symbol defined as

$$ (x)_j := \frac{\Gamma(x+j)}{\Gamma(x)} = x(x+1)(x+2)\dots(x+j-1), \tag{5.55} $$

with $\Gamma(x)$ the gamma function.

For the discrete set of bound states ($E<0$), the eigenvalues $E_N$ and the normalization constant are given by

$$ E_N = -\frac{E_i}{N^2} \qquad \text{with } N \in \mathbb{N}_0, \tag{5.56a} $$

$$ K_{N,L} = \frac{2^{L+1}}{(2L+1)!}\sqrt{\frac{(N+L)!}{(N-L-1)!}}N^{-L-2}. \tag{5.56b} $$

For the continuum of unbound states ($E \geq 0$), the principal quantum number $N = -i/x$ is imaginary. In this case, the eigenvalues and the normalization constant, now denoted $C_{x,L}$, are given by[6]

$$ E_x = x^2 E_i = -\frac{E_i}{N^2} \qquad \text{with } x \in \mathbb{R}^+, \tag{5.57a} $$

$$ C_{x,L} = \frac{2^{L+1}}{(2L+1)!}\frac{x^{L+\frac{1}{2}}}{\sqrt{1-e^{-\frac{2\pi}{x}}}}\prod_{s=1}^{L}\left(s^2+x^{-2}\right). \tag{5.57b} $$

Note that even though $N$ may be complex, the radial eigenfunctions remain real.

The expressions obtained for the 2ED and 2EQ vacuum TPSE rates involve, in $M_{2ED}^{eg}$ and $M_{2EQ}^{eg}$ [Eqs. (5.47) and (5.50)], the multipole matrix elements of the radial eigenfunctions that describe the transition from the state characterized by the quantum numbers $(N,L)$ to the state characterized by the quantum numbers $(P,J)$. These are calculated through a radial integral [101, 102]:

$$ \langle R_{N,L}|r^a|R_{P,J}\rangle := \frac{1}{a_0}\int_0^\infty R_{N,L}(r)\, r^{a+2}\, R_{P,J}(r)\,\mathrm{d}r, \tag{5.58} $$

where $r$ is the position operator and where the integral is dimensionless due to the division by the atomic unit of length, i.e., the Bohr radius $a_0$. Moreover, $a$ is equal to 1 for an ED transition and to 2 for an EQ transition. In the previous equation, $(N,L)$ are the quantum numbers of an intermediate state ($N_m$ and $L_m$), which can be a bound or a free state, while $(P,J)$ are the ones of the initial or final states ($P = N_e, N_g$ and $J = L_e, L_g$), which are always bound states. We therefore refer to bound-bound and bound-free radial integrals. In addition, as the radial wavefunctions of the hydrogen atom are real and as the position operator $r$ is Hermitian, this relation is satisfied:

$$ \langle R_{N,L}|r^a|R_{P,J}\rangle = \langle R_{P,J}|r^a|R_{N,L}\rangle^* = \langle R_{P,J}|r^a|R_{N,L}\rangle\,. \tag{5.59} $$

[6] The normalization constant depends on the scale chosen to integrate over the continuum [102]. A normalization in the energy-scale leads to a normalization constant $C_{E,l} = C_{x,L}/\sqrt{x}$ with $C_{x,L}$ the normalization constant in the x-scale. As we wrote the integral over the continuum in equation (5.52) as a function of the variable $x$, we need to take the normalization constant $C_{x,L}$.

For an ED transition ($a = 1$ and $J = L - 1$), one can show that [101, 102]:

$$\forall N \neq P, \quad \langle R_{N,L}|r|R_{P,L-1}\rangle = K_{N,L}\, K_{P,L-1}\, (-1)^{P-L}\, \frac{(2L+1)!}{2}\, N(NP)^{2L+2}\, \frac{(N-P)^{N+P-2L-2}}{(N+P)^{N+P}} \times \left[F(-N_r, -P_r; c; z) - \left(\frac{N-P}{N+P}\right)^2 F(-N_r - 2, -P_r; c; z)\right], \tag{5.60a}$$

$$\langle R_{N,L}|r|R_{N,L-1}\rangle = \frac{3}{2} N \sqrt{N^2 - L^2}, \tag{5.60b}$$

where $c := 2L$, $z := -4NP/(N-P)^2$, $P_r := P - J - 1$ and where $F$ is the hypergeometric function ${}_2F_1(a, b; c; z)$ defined as [100, 103]:

$${}_2F_1(a, b; c; z) := \sum_{i=0}^{\infty} \frac{(a)_i (b)_i}{(c)_i} \frac{z^i}{i!} = \frac{\Gamma(c)}{\Gamma(b)\Gamma(c-b)} \int_0^1 \frac{t^{b-1}(1-t)^{c-b-1}}{(1-tz)^a}\, \mathrm{d}t. \tag{5.61}$$

For an EQ transition ($a = 2$ and $J = L, L - 2$), one can show that[7] [101]:

$$\forall N \neq P,\ \langle R_{N,L}|r^2|R_{P,L-2}\rangle = K_{N,L}\, K_{P,L-2}\, (-1)^{P-L+1}\, \frac{(2L+1)!}{4}\, N^3 (NP)^{2L}\, \frac{(N-P)^{N+P-2L-1}}{(N+P)^{N+P-1}} \times \left[F(-N_r, -P_r; c-2; z) - 2\left(\frac{N-P}{N+P}\right) F(-N_r - 1, -P_r; c-2; z) + 2\left(\frac{N-P}{N+P}\right)^3 F(-N_r - 3, -P_r; c-2; z) - \left(\frac{N-P}{N+P}\right)^4 F(-N_r - 4, -P_r; c-2; z)\right], \tag{5.62a}$$

$$\forall N \neq P,\ \langle R_{N,L}|r^2|R_{P,L}\rangle = 8\, K_{N,L}\, K_{P,L}\, (-1)^{P-L}\, (2L+1)!\, (NP)^{2L+6}\, \frac{(N-P)^{N+P-2L-4}}{(N+P)^{N+P+2}} \times F(-N_r, -P_r; c-2; z). \tag{5.62b}$$

Note that the EQ transition is forbidden between two $s$ states ($L = J = 0$) [47] and that the case where $N = P$ has not been derived for an EQ transition. Consequently, we use the definition of the radial eigenfunctions (5.53) and of the multipole radial matrix elements (5.58) to calculate this case. Also the equations (5.60) and (5.62) are valid for the bound-free radial integrals, by replacing $K_{N,L}$ by $C_{x,L}$ with $x = -i/N \in \mathbb{R}^+$.

### 5.3.4 Method and results

To calculate the 2ED and 2EQ vacuum decay profiles $\phi^{(2)}_{\mathrm{2ED},0}(y)$ and $\phi^{(2)}_{\mathrm{2EQ},0}(y)$ [Eqs. (5.48) and (5.51)], one needs to calculate the two contributions arising from the bound-bound and from the bound-free radial integrals to the summation over the virtual intermediate states [Eq. (5.52)] when calculating $M^{eg}_{\mathrm{2ED}}(y)$ and $M^{eg}_{\mathrm{2EQ}}(y)$ [Eqs. (5.47) and (5.50)]. Moreover, the calculation of $M^{eg}_{\mathrm{2ED}}(y)$ and $M^{eg}_{\mathrm{2EQ}}(y)$ involves the function $f_{N_m}(y)$ [Eqs. (5.45) and (5.46)] as well as the bound-bound and bound-free radial integrals given by the equations (5.60) for an ED transition and given by the equations (5.62) for an EQ transition. Then, the integrated rates can be calculated via the integration over half of the spectrum of the decay profiles [Eq. (5.42)].

To compute the profiles, we use the *mpmath* Python library [104] for the confluent hypergeometric function ${}_1F_1(a; b; z)$ and for the hypergeometric function ${}_2F_1(a, b; c; z)$, and we use the *integrate.quad*

[7] There are several typographical errors in the formula provided in the reference [101].

| Transition | $\Delta E$ [eV] | $\omega_{eg}$ [rad/s] | $\lambda_{eg}$ [μm] | Type | $\Gamma^{(2)}_{2\mathrm{MO},0}$ [$\mathrm{s}^{-1}$] | $\phi^{(2)}_{2\mathrm{MO},0}(0.5)$ [$\mathrm{s}^{-1}$] | $\phi^{(2),\mathrm{b\text{-}b}}_{2\mathrm{MO},0}(0.5)$ [$\mathrm{s}^{-1}$] |
|---|---|---|---|---|---|---|---|
| $2s \to 1s$ | 10.2 | $1.55 \times 10^{16}$ | 0.122 | 2ED | 8.23 | 21.3 | 27.5 |
| | | | | 2EQ | $4.91 \times 10^{-12}$ | $2.40 \times 10^{-11}$ | $3.19 \times 10^{-11}$ |
| $4s \to 2s$ | 2.55 | $3.87 \times 10^{15}$ | 0.486 | 2ED | $1.59 \times 10^{-1}$ | $4.21 \times 10^{-1}$ | $4.91 \times 10^{-1}$ |
| | | | | 2EQ | $4.81 \times 10^{-14}$ | $2.02 \times 10^{-13}$ | $2.03 \times 10^{-13}$ |
| $5s \to 3s$ | 0.968 | $1.47 \times 10^{15}$ | 1.28 | 2ED | $1.18 \times 10^{-2}$ | $3.24 \times 10^{-2}$ | $3.45 \times 10^{-2}$ |
| | | | | 2EQ | $1.43 \times 10^{-15}$ | $5.96 \times 10^{-15}$ | $5.98 \times 10^{-15}$ |

Table 5.2: Computed data for 2ED and 2EQ transitions between the states $2s \to 1s$, $4s \to 2s$, and $5s \to 3s$, with $\Delta E = \hbar\omega_{eg} = hc/\lambda_{eg}$.

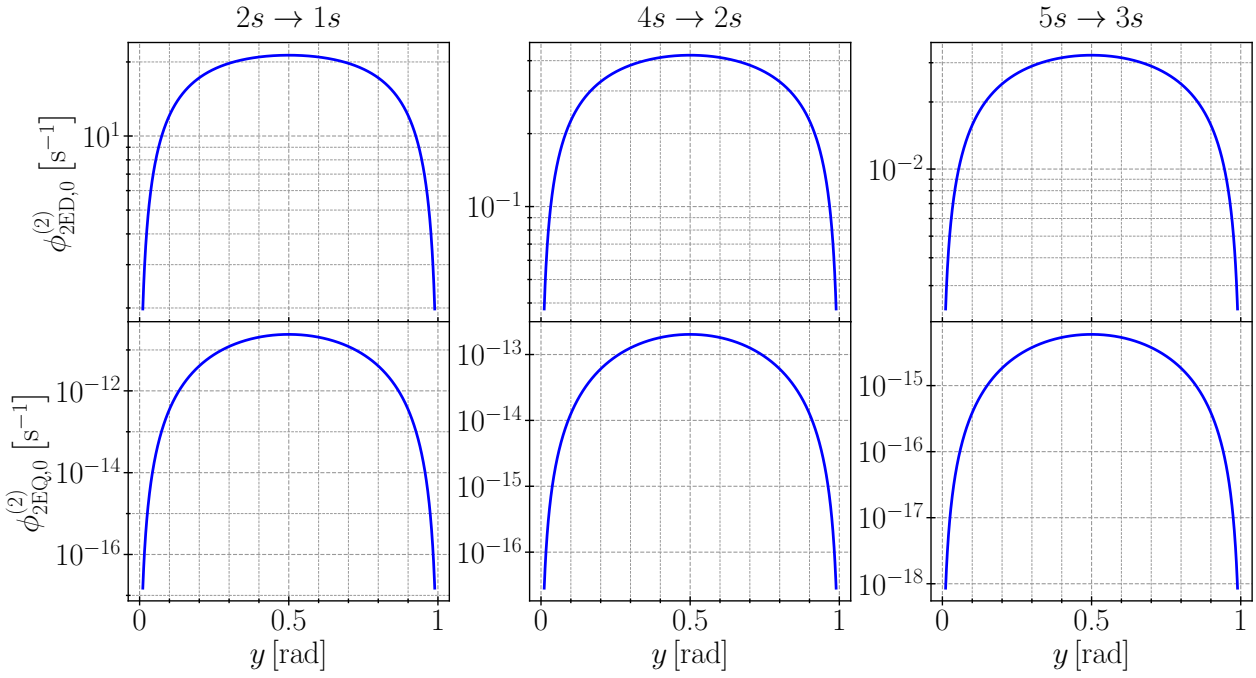


Figure 5.1: Profiles for 2ED (top) and 2EQ (bottom) transitions between the states $2s \to 1s$, $4s \to 2s$, and $5s \to 3s$.

function of the *SciPy* Python library [105] to integrate. In addition, the discrete summation over the principal quantum number of the virtual intermediate states [Eq. (5.52)] is truncated after the first 200 terms, as in Ref. 8. The computed data for the 2ED and 2EQ transitions between the states $2s \to 1s$, $4s \to 2s$, and $5s \to 3s$ are given in Table 5.2 and the corresponding profiles are sketched in Figure 5.1.

The relative difference between our computed values of $\phi^{(2)}_{2\mathrm{ED},0}(y = 0.5)$ for the transitions $N_e s \to 1s$ with $N_e$ ranging from 1 to 10 and those in Ref. [8] is less than 0.02 %. Also, the relative difference is less than 0.01 % between our computed values of $\Gamma^{(2)}_{2\mathrm{ED},0}$ and $\Gamma^{(2)}_{2\mathrm{EQ},0}$ for the $2s \to 1s$ transition and those in Ref. [5]. Furthermore, as there is only one 2EQ transition rate datum in vacuum, we checked that we can find the EQ transition rate value[8] for $N_e d \to N_g s$ single-photon transitions with a relative error less than 0.1 % [93].

[8]For an $N_e d \to N_g s$ transition, we can show that $\Gamma_{\mathrm{EQ},0} = \frac{\omega_{eg}^5 \alpha\, a_0}{75c^4} \langle R_{N_g,0}|r^2|R_{N_e,2}\rangle$.

The last column in Table 5.2, i.e., $\phi^{(2),\text{b-b}}_{\text{2MO},0}(0.5)$, corresponds to the rate calculated at $y = 0.5$ when only the bound states are taken into account in the summation over the intermediate states [Eq. (5.52)]. The values are greater than when the integral over the continuum of free states is also taken into account, because the summation over bound states in $M^{eg}_{\text{2ED}}(y)$ and $M^{eg}_{\text{2EQ}}(y)$ [Eqs. (5.47) and (5.50)] is negative while the integration of free states is positive. Furthermore, for the 2EQ $4s \to 2s$ and $5s \to 3s$ transitions, $\phi^{(2)}_{\text{2EQ},0}(0.5) \approx \phi^{(2),\text{b-b}}_{\text{2EQ},0}(0.5)$, and thus free states have a low impact on the calculated TPSE rate (at this frequency).

Finally, it is interesting to study the convergence with respect to the number of states considered in the summation over the bound intermediate states and with respect to the upper limit of the integral over the continuum of free intermediate states [Eq. (5.52)]. In this manner we have an idea of the number of bound states and of the range of free states to consider to calculate vacuum TPSE rates when using numerical methods to compute the bound-bound and bound-free radial integrals for more complex emitters. To do so we define an error score as follows:

$$\text{Error score}\,(\xi; y) := \frac{\phi^{(2),\text{b-b}}_{\text{2MO},0}(y;\xi) - \phi^{(2),\text{b-b}}_{\text{2MO},0}(y;\xi = 200)}{\phi^{(2),\text{b-b}}_{\text{2MO},0}(y;\xi = 200)} \tag{5.63}$$

for the convergence relative to bound states, with $\xi$ the number of bound intermediate states. For the convergence with respect to the upper limit of the integration over free states, noted $x_{\max}$, it is defined as

$$\text{Error score}\,(x_{\max}; y) := \frac{\phi^{(2),\text{b-f}}_{\text{2MO},0}(y;x_{\max}) - \phi^{(2),\text{b-f}}_{\text{2MO},0}(y;x_{\max} = \infty)}{\phi^{(2),\text{b-f}}_{\text{2MO},0}(y;x_{\max} = \infty)} \tag{5.64}$$

where $\phi^{(2),\text{b-f}}_{\text{2MO},0}$ denotes the rate calculated using only the integral over the free intermediate states. On the data plotted in Figs. 5.2 and 5.3, the error score is lower than 1 % starting from 20 bound states for the discrete summation, and starting from $x_{\max} = 1.5$ for the integration.

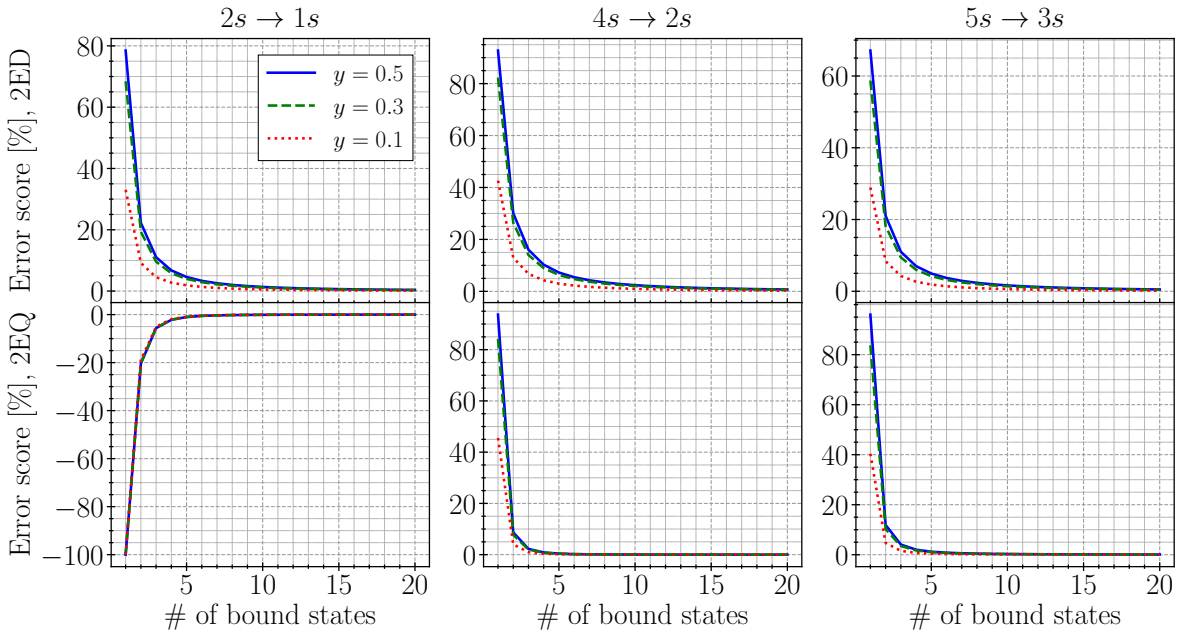


Figure 5.2: Plots of the error score [Eq. (5.63)] for the convergence with respect to the number of bound intermediate states. The graphs on top correspond to the 2ED transition while the graphs on bottom correspond to the 2EQ transition.

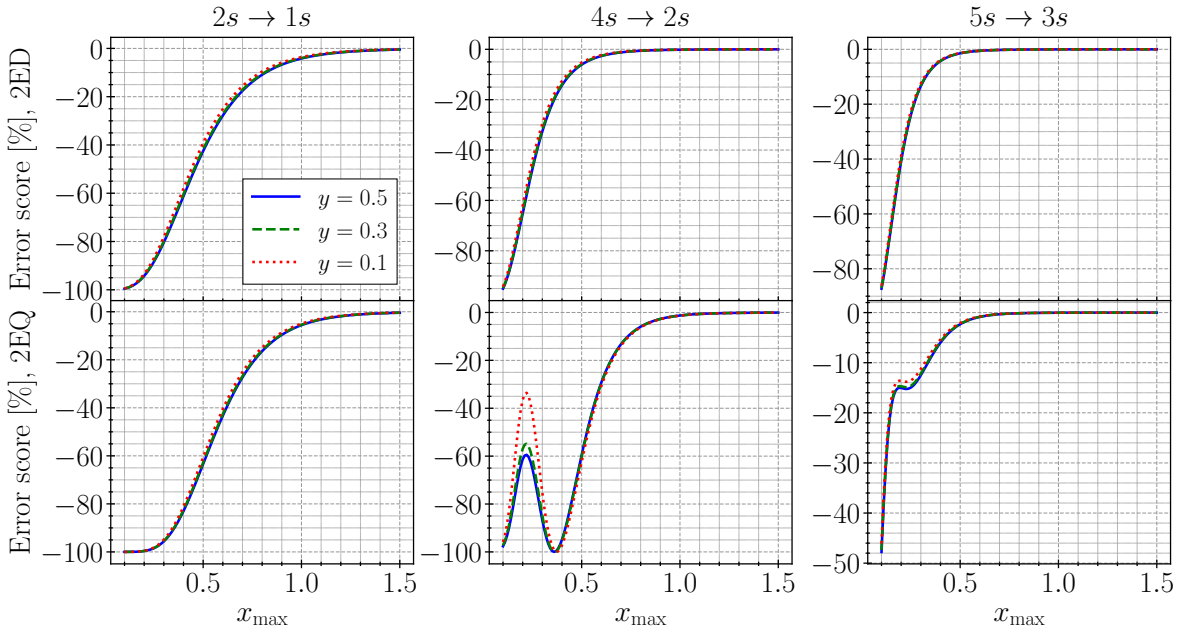


Figure 5.3: Plots of the error score [Eq. (5.64)] for the convergence with respect to the upper limit of the integration of the free intermediate states. The graphs on top correspond to the 2ED transition while the graphs on bottom correspond to the 2EQ transition.

## 5.4 Summary

In this chapter devoted to the calculation of the emitter contribution, we used the wavefunctions of the hydrogen atom to calculate analytically, the second-order electric dipole and quadrupole transition moments for $s \to s$ transitions. The 2ED transition is mediated by intermediate states which are $p$ states, while the 2EQ transition is mediated by $d$ states. The norm of $\boldsymbol{\mathcal{D}}^{eg}$ and $\boldsymbol{\mathcal{Q}}^{eg}$ (and thus the vacuum TPSE rates [Eqs. (4.41)]) depends only on the principal quantum numbers of the excited, ground, and intermediate states, whereas their orientation (i.e., the normalized tensors $\hat{\boldsymbol{\mathcal{D}}}^{eg}$ and $\hat{\boldsymbol{\mathcal{Q}}}^{eg}$) depends only on the azimuthal and on the magnetic quantum numbers of the intermediate states. First of all, we have calculated the normalized tensors $\hat{\boldsymbol{\mathcal{D}}}^{eg}$ [31] and $\hat{\boldsymbol{\mathcal{Q}}}^{eg}$ [Eq. (5.34)] that are given by

$$\hat{\boldsymbol{\mathcal{D}}}^{eg} = \frac{\mathbb{1}_{3\times 3}}{\sqrt{3}}, \tag{5.65a}$$

$$\hat{\boldsymbol{\mathcal{Q}}}^{eg} = \frac{1}{\sqrt{20}} \begin{pmatrix} 4/3 & -2/3 & 0 & 0 & 0 \\ -2/3 & 4/3 & 0 & 0 & 0 \\ 0 & 0 & 1 & 0 & 0 \\ 0 & 0 & 0 & 1 & 0 \\ 0 & 0 & 0 & 0 & 1 \end{pmatrix}, \tag{5.65b}$$

and which are sufficient to calculate the modification of TPSE rates with respect to vacuum [Eqs. (4.58), (4.63) and (4.80)]. These tensors implie that all components of the tensors $\mathbf{F}^{\mathrm{ED}}$, $\mathbf{F}^{\mathrm{EQ}}$, and $\mathbf{F}^{\mathrm{ED}\cap\mathrm{EQ}}$ must be calculated (some can be equal or zero due to the environment) in the calculation of the 2ED and 2EQ transition rates [Eqs. (4.58a) and (4.63)], and their interference [Eq. (4.80)], because the emitter is spherically symmetric.

Then, to calculate vacuum TPSE rates, which are required to calculate absolute rates and interferences, the two contributions arising from the bound-bound and from the bound-free multipole radial integrals to the summation over the virtual intermediate states [Eq. (5.52)] have been calculated numerically. The computed values, given in Table 5.2, are in agreement with those found in the literature, validating in passing the calculated tensor $\hat{\boldsymbol{\mathcal{Q}}}^{eg}$. We also discussed the convergence of the results as a function of the number of bound intermediate states in the summation and as a function of the upper limit of the integration over the free intermediate states.

Furthermore, similar analytical developments can be made for transitions between other states of the hydrogen atom, as well as for the second-order magnetic dipole transition moment $\hat{\boldsymbol{\mathcal{M}}}^{eg}$ and the 2MD vacuum transition rate. In the case of magnetic transitions, the spin of the electron performing the transition can change, and must therefore be taken into account [47, 90] in the calculation of the first-order transition moments involved in $\hat{\boldsymbol{\mathcal{M}}}^{eg}$ [Eq. (4.18b)]. To do so, the state space on which wave functions are defined is expanded to include the spin on which the spin angular momentum operator involved in the magnetic dipole moment operator acts [90].

Finally, in the case where it is not possible to calculate transition moments analytically (e.g., for molecules), one can use state-of-the-art quantum mechanical numerical methods [106] to compute the multipolar transition moments involved in the calculation of the second-order transition moments [Eqs. (4.18)], by considering a sufficient number of bound and free states in the summation over the intermediate states. Once the second-order transition moments are known, it is possible to calculate the vacuum TPSE rates [Eqs. (4.41)] and to use equations (4.87) to calculate the two-photon Purcell effect of the multipolar contribution to the TPSE.

Chapter 6

# Computation of Purcell factors

In the previous chapter, we calculated the emitter contribution to the TPSE rates for the hydrogen atom. All that remains is to calculate the contribution of the environment: the Purcell factors. To do this, we use the commercial software COMSOL Multiphysics® based on the finite element method, which is a method in numerical analysis used to solve partial differential equations that represent the dynamics of a physical system [107]. The advantages of this software are that it is easy to construct the geometry of the system under consideration thanks to its graphical user interface, it has efficient algorithms for meshing the geometry and solving Maxwell's equations, and it has various tools for post-processing the results.

First, we introduce the basic concepts of the finite element method (FEM), including the weak formulation of the master equation to solve in electrodynamics. Then, since the electric point quadrupole is not available in COMSOL, we derive its weak formulation to implement it in the software. Afterwards, we describe our COMSOL models used to compute the Purcell factors. Finally, we present the optical models of the materials that we will use to design plasmonic nanostructures.

## 6.1 Finite element method

The dynamics of a physical system are governed by partial differential equations (PDEs), which describe the spatial and time evolution of a physical quantity $\phi$. In general, a PDE can be written as

$$\mathcal{L}\,\phi = b, \tag{6.1}$$

with $\mathcal{L}$ being a differential operator acting on a unknown function $\phi$ and where $b$ is a source term [108]. In electrodynamics, the PDE is for example the wave equation for the electric field [Eq. (2.9)]. However, except for the simplest problems, it is not possible to solve these PDEs analytically, but one can use numerical approximation methods to search for approximate solutions [107, 108]. Among them, the finite element method (FEM) is widely used to solve boundary-value problems, i.e., PDEs with boundary conditions formulated at the frontier of the domain, such as in electromagnetics, mechanics, fluid dynamics, and heat transfer [108, 109]. The principle of the FEM is to replace an entire continuous domain by a finite number of subdomains, called elements, in which the unknown function is represented by simple interpolation functions with unknown coefficients [108, 109]. Thereby, the original boundary-value problem with an infinite number of degrees of freedom is converted into a problem with a finite number of degrees of freedom, i.e., the coefficients in each element [108]. Then, a system of algebraic equations is formed to calculate the coefficients, and finally solved [108, 109]. In the following subsection, we describe the four steps of the FEM, namely

domain discretization, selection of interpolation functions, formulation of the system of equations, and resolution of the latter [108, 109]. Then, in Subsection 6.1.2, the weak formulation of PDEs used in FEM is introduced and illustrated for the master equation to solve in electromagnetics.

### 6.1.1 Basic steps

First of all, the domain of interest $\Omega$ is discretized (meshed) into small elements, without any overlap or gaps between them [108, 109]. The elements must fit together smoothly to form a set of connected domains resembling the original structure [109]. To this end, different types of elements can be used [Fig. 6.1]. For a three-dimensional domain, tetrahedral elements are the most used, as they are the simplest and best suited to structures of arbitrary shape [108]. With these elements, surfaces are divided into triangular elements. However, depending on the structure to be meshed, other elements can be used such as hexahedral elements for structures having a rectangular geometry [Fig. 6.1], resulting in rectangular elements at the surfaces. Furthermore, the elements are represented with a set of nodes [107–109]. In linear elements, the nodes are the vertices of the polyhedron, while quadratic elements contain additional nodes, e.g., at the middle of the edges [Fig. 6.1]. Note that the manner in which this step is carried out affects the computing resources (time and memory) that will be used, as well as the accuracy of the approximate solution that will be obtained [107–109]. Indeed, smaller elements result in more accurate solutions, but increase the number of nodes, which requires more computing resources. The FEM has the advantage of being able to use adaptive meshing, i.e., to use smaller elements where the unknown function is expected to vary more strongly [107, 109].

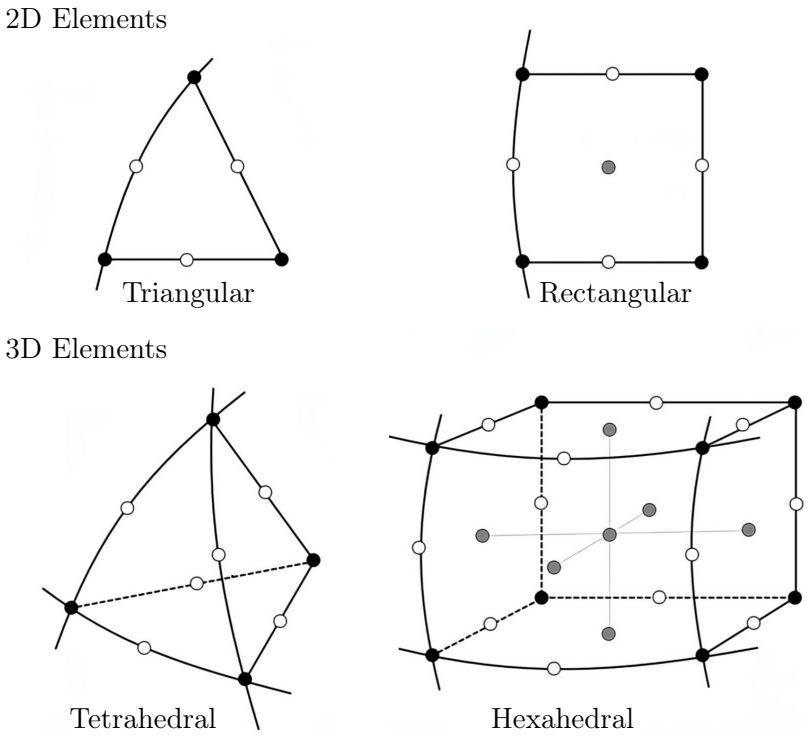


Figure 6.1: Illustrations of examples of elements used in FEM for two- and three-dimensional domains [107–109]. In linear elements, only the black nodes are used. In quadratic elements, the black and white nodes are used (serendipity elements), sometimes together with the grey ones (Lagrangian elements). Elements with curved edges and faces can be used to model more accurately curved structures. Figure adapted from Ref. 107.

Once the domain has been discretized, the next step is to choose an interpolation function to represent the unknown function $\phi$ (e.g., a component of the electric field) within each element with a set of coefficients [108, 109]. For example, $\phi$ can be written using a quadratic interpolation in each element $\Omega_i$ [108, 109]:

$$\forall \mathbf{r} \in \Omega_i, \quad \phi(\mathbf{r}) = a_i + b_i\, x + c_i\, y + d_i\, z + e_i\, xy + f_i\, xz + g_i\, yz + h_i\, x^2 + i_i\, y^2 + j_i\, z^2. \tag{6.2}$$

The ten coefficients $a_i, \ldots, j_i$ of the interpolation are obtained by imposing $\forall j = 1, \ldots, N_i,\ \phi(\mathbf{r}) = \phi(\mathbf{r}_{ij})$, with $N_i$ being the number of nodes within the $i$-th element and where $\mathbf{r}_{ij}$ denotes the position of the $j$-th node belonging to the $i$-th element. Consequently, to perform a quadratic interpolation, the elements must contain at least 10 nodes [108, 109]. As a result, an interpolation is used together with elements of the same order [109]. Furthermore, the higher the order, the greater the number of coefficients and nodes. Therefore, there are more degrees of freedom to solve, requiring more computing resources. In practice, a quadratic interpolation is suitable for the vast majority of problems to solve with the FEM, since it offers a good compromise between calculation time and solution accuracy, and is therefore used by default in COMSOL [107, 109]. By injecting the expression of these coefficients that are found by imposing $\phi(\mathbf{r}) = \phi(\mathbf{r}_{ij})$ at each node, the interpolation can be rewritten as

$$\forall \mathbf{r} \in \Omega_i, \quad \phi(\mathbf{r}) = \sum_{j=1}^{N_i} \psi_{i,j}(\mathbf{r})\, \phi(\mathbf{r}_{ij}), \tag{6.3}$$

where $\psi_{i,j}$ are called the basis (or shape) functions [108], which are quadratic since we assumed a quadratic interpolation and depend only on the mesh. A basis function $\psi_{i,j}$ is equal to 1 at the corresponding node, and decreases to reach 0 at the adjacent nodes [Fig. 6.2]. We can highlight here two advantages of the FEM [109]. Since an interpolation function exists in each element, the FEM produces a solution everywhere in the domain, not only at the nodes. In addition, the derivatives of the unknown function can be easily calculated using these interpolations.

In the third step, the original PDE [Eq. (6.1)] is turned in each element into an matrix equation by using the interpolation of the unknown function [Eq. (6.3)]. Then, the assembly of all elemental matrix equations results in a global matrix equation that represents the entire domain:

$$\mathbf{A}\, \boldsymbol{\phi} = \mathbf{b}, \tag{6.4}$$

with $\mathbf{A}$ being a matrix acting on an unknown vector $\boldsymbol{\phi}$ that contains the value of $\phi$ at each nodes of the domain, and where the vector $\mathbf{b}$ represents the source at each nodes [108, 109]. The matrix $\mathbf{A}$ is constructed according to the PDE, boundary conditions and shape functions. Thus, the obtained solution satisfies the requirements inside every element and is made continuous across elements [109, 110]. Note that a single global matrix element can be formed for several unknown functions, as for example the three components of the electric field [109].

Finally, the solution $\boldsymbol{\phi}$ is found by solving the system of linear equations [Eq. (6.4)]. In practice, solving this equation consists in inverting the matrix $A$ in order to isolate the vector of unknowns: $\boldsymbol{\phi} = \mathbf{A}^{-1}\mathbf{b}$ [111]. However, this matrix can quickly contain a very large number of elements, especially with three-dimensional domains [109]. Therefore, inverting this matrix can become very time-consuming and expensive [111]. Fortunately, efficient numerical methods exist that allow us to find $\boldsymbol{\phi}$ without the need of finding $\mathbf{A}^{-1}$ [111]. Among them, two different categories of algorithms

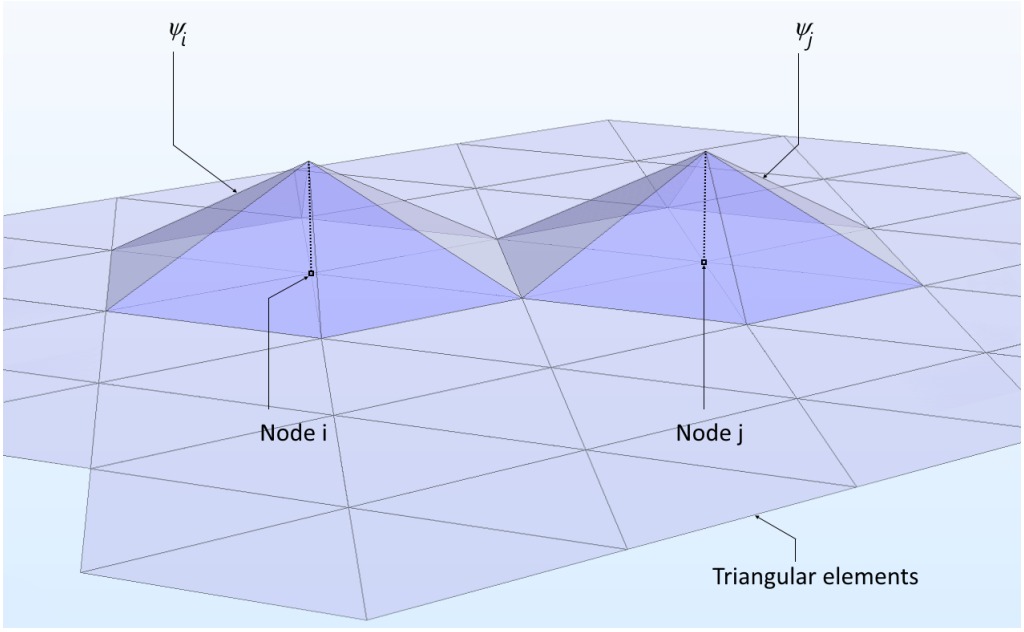


Figure 6.2: Illustration of two linear basis functions $\psi_i$ and $\psi_j$, related to the nodes $i$ and $j$ respectively, in a two-dimensional domain discretized with triangular elements (easier to represent than quadratic basis functions in 3D) [107]. Figure taken from Ref. 107.

can be employed [108, 111, 112]. On the one hand, direct methods theoretically yield to an exact solution and consist in a one large computational step [108, 112]. In COMSOL, they are based on the LU decomposition method[1] [112]. On the other hand, iterative methods start with an initial guess, then iterates to obtain an approximated solution [111, 112]. They require fewer computing resources, but depending on the system under consideration, the solver may not converge [112]. Note that as the solution obtained depends on the mesh used to discretize the domain, it is necessary to check that the solution has converged with the considered mesh fineness.

### 6.1.2 Weak formulation

In the FEM, PDEs and boundary conditions are not considered in their original formulation, but rather in their weak formulation [114]. Let us illustrate this by deriving the weak formulation of the master equation to solve in electromagnetics: the wave equation for the electric field. In a linear, macroscopic, and non-magnetic medium with a time harmonic dependency $e^{j\omega t}$ for the fields[2], the wave equation is given by [30, 115]:

$$\nabla\times\nabla\times\mathbf{E}(\mathbf{r}) - k_0^2\left(\varepsilon(\omega,\mathbf{r}) - \frac{j\sigma(\omega,\mathbf{r})}{\varepsilon_0\omega}\right)\mathbf{E}(\mathbf{r}) = -j\omega\mu_0\,\mathbf{j}_s(\mathbf{r}), \tag{6.5}$$

where $\varepsilon$ is the dielectric constant (a tensor in anisotropic media), where $k_0 := \omega/c$, and where the total current density $\mathbf{j}$ has been decomposed into a source current density $\mathbf{j}_s$ and an induced

[1] The LU decomposition method consist into the factorization of the matrix $\mathbf{A}$, if necessary after permutation of its rows and/or columns, as the product of a lower triangular matrix $\mathbf{L}$ and an upper triangular matrix $\mathbf{U}$ [113]. Thus, the system of equations is rewritten as $\mathbf{L}\mathbf{U}\,\boldsymbol{\phi} = \mathbf{b}$. Posing $\mathbf{U}\,\boldsymbol{\phi} := \mathbf{y}$, one gets $\mathbf{L}\,\mathbf{y} = \mathbf{b}$. Firstly, we find the components of $\mathbf{y}$ by elementary substitutions since $L_{11}y_1 = b_1$, $L_{21}y_1 + L_{22}y_2 = b_2$, and so on. Then, $\boldsymbol{\phi}$ is calculated in the same way with the equation $\mathbf{U}\,\boldsymbol{\phi} = \mathbf{y}$.

[2] For this chapter, we adopt the engineering convention used in COMSOL for time harmonic dependencies. To avoid any confusion, the letter $j$ is used for the imaginary unit (not to be confused with current density) when this convention is used.

conduction current $\mathbf{j}_c$ (given by Ohm's law $\mathbf{j}_c = \sigma\mathbf{E}$ with $\sigma$ the electrical conductivity [30]). This vectorial equation contains three scalar equations where the electric field $\mathbf{E}$ represents the unknown and where the right-hand side denotes the source term.

The basic idea of the weak formulation is the following: if $\mathbf{E}$ is a solution of the PDE, then it is also a solution of the following integral equations [107, 114, 116]:

$$\forall i = 1,2,3, \quad \int_\Omega \left[ \left(\nabla\times\nabla\times\mathbf{E}(\mathbf{r})\right)_i - k_0^2 \left(\varepsilon(\mathbf{r}) - \frac{j\sigma(\mathbf{r})}{\varepsilon_0\omega}\right) E_i(\mathbf{r}) \right] v_i \, \mathrm{d}r^3 = -j\omega\mu_0 \int_\Omega j_{s,i}(\mathbf{r})\, v_i \, \mathrm{d}r^3, \tag{6.6}$$

obtained by multiplying both sides of the three scalar equations by arbitrary functions $v_i$ and by integrating over the domain of interest $\Omega$. Inversely, if $\mathbf{E}$ is a solution of the previous integrals for a sufficiently large number of different functions $v_i$, then it is likely that it is also a solution of the original PDE [114, 116]. Concretely, the role of the functions $v_i$ is to limit the contribution of the integrand to a small portion of the domain, thus testing that the solution is good in the selected part of the domain [114]. For this reason, these functions are the basis functions defined previously and are called, in this context, test functions [107, 114]. Consequently, by taking different test functions, each selecting a different part of the domain, the solution obtained at the end is globally a good solution in each part of the domain [114]. Concretely, this formulation is used when the elemental matrix equations are formed [108, 109].

In other words, the weak formulation is obtained by requiring the last equation to hold for all test functions, instead of the PDE for all points in the domain $\Omega$ [107]. It is called "weak" because the PDE is solved globally via an integral over mesh elements, and therefore it does not need to be well-defined at every single point in the domain like the original PDE [107, 116]. In addition to finding a solution that verifies existence conditions that are easier to satisfy than those of the initial problem, another major advantage is that the order of derivatives is reduced by one-order as the weak formulation involves an integral [114].

In practice, the three scalar equations (6.6) is turned into a single one. Indeed, using a similar reasoning, if $\mathbf{E}$ is a solution of the previous integrals [Eq. (6.6)], then it is also a solution of the following integral equation:

$$\int_\Omega \left[ \nabla\times\nabla\times\mathbf{E}(\mathbf{r}) - k_0^2 \left(\varepsilon(\mathbf{r}) - \frac{j\sigma(\mathbf{r})}{\varepsilon_0\omega}\right) \mathbf{E}(\mathbf{r}) \right] \cdot \mathbf{v} \, \mathrm{d}r^3 = -j\omega\mu_0 \int_\Omega \mathbf{j}_s(\mathbf{r}) \cdot \mathbf{v} \, \mathrm{d}r^3, \tag{6.7}$$

where $\mathbf{v}$ denotes a vector of test functions. In COMSOL, $\mathbf{v}$ is implemented as test($\mathbf{E}$), highlighting the role of these test functions [116]. In conclusion, we have gone from solving a vectorial PDE to a single integral equation, where the solution verifies more relaxed existence conditions [107].

## 6.2 Weak formation of the electric point dipole and quadrupole

In COMSOL Multiphysics®, the only available point sources are the ED and MD. Consequently, we need to implement the weak formulation of the source term (right-hand side in the Eq. (6.7)) for the electric point quadrupole. Before that, let us derive it for the ED. As a reminder, the current density related to an electric point dipole at the position $\mathbf{R}$, oscillating at the frequency $\omega$ with a time harmonic dependency $e^{j\omega t}$, is given by [Eq. (2.16)]:

$$\mathbf{j}_{\mathrm{ED}}(\mathbf{r}) = \dot{\mathbf{d}}\, \delta(\mathbf{r} - \mathbf{R}), \tag{6.8}$$

with $\mathbf{d}$ being the electric dipole moment of the source [Eq. (2.17)] and where the point over $\mathbf{d}$ denotes the time derivative. By injecting the current density in the source term [Eq. (6.7)], we find the weak formulation for the electric point dipole which is implemented in COMSOL [115]:

$$-j\omega\mu_0\,\dot{\mathbf{d}}\cdot\int_\Omega \text{test}\left(\mathbf{E}(\mathbf{r})\right)\,\delta(\mathbf{r}-\mathbf{R})\,\mathrm{d}r^3 = -j\omega\mu_0\,\dot{\mathbf{d}}\cdot\text{test}(\mathbf{E}(\mathbf{R})), \tag{6.9}$$

where $\dot{\mathbf{d}} = j\omega\,\mathbf{d}$ denotes the electric current dipole moment.

Similarly, using the current density associated to an electric point quadrupole at the position $\mathbf{R}$ oscillating at the frequency $\omega$ with a time harmonic dependency $e^{j\omega t}$ [Eq. (2.22)]:

$$\mathbf{j}_{\text{EQ}}(\mathbf{r}) = -\dot{\mathbf{Q}}\nabla\,\delta(\mathbf{r}-\mathbf{R}), \tag{6.10}$$

with $\mathbf{Q}$ being the electric quadrupole moment of the source [Eq. (2.23)], one obtains

$$j\omega\mu_0\,\dot{\mathbf{Q}}\int_\Omega \nabla\,\delta(\mathbf{r}-\mathbf{R})\cdot\text{test}\left(\mathbf{E}(\mathbf{r})\right)\,\mathrm{d}r^3 \tag{6.11}$$

for the weak formulation of the source term for the EQ. To calculate this integral, let us make the use of the following property [117]:

$$\int \nabla\delta(\mathbf{r}-\mathbf{R})\cdot\mathbf{g}(\mathbf{r})\,\mathrm{d}r^3 = -\int \nabla\cdot\mathbf{g}(\mathbf{r})\,\delta(\mathbf{r}-\mathbf{R})\,\mathrm{d}r^3. \tag{6.12}$$

As a result, one gets

$$-j\omega\mu_0\,\dot{\mathbf{Q}}\int_\Omega \nabla\cdot\text{test}\left(\mathbf{E}(\mathbf{r})\right)\,\delta(\mathbf{r}-\mathbf{R})\,\mathrm{d}r^3 = -j\omega\mu_0\,\dot{\mathbf{Q}}\nabla\cdot\text{test}(\mathbf{E}(\mathbf{R})) \tag{6.13a}$$

$$= -j\omega\mu_0\,\dot{\mathbf{Q}} : \nabla\,\text{test}(\mathbf{E}(\mathbf{R})), \tag{6.13b}$$

where $\dot{\mathbf{Q}} = j\omega\,\mathbf{Q}$ denotes the electric current quadrupole moment.

As a validation step, we checked that the source implemented as a weak point contribution in our COMSOL models provides the radiation patterns characteristic of electric quadrupoles [Fig. 2.8], and that the power emitted in vacuum [Eq. (2.25)] is correct. Note that studies including point electric quadrupole source near a nanostructure converge with difficulty. Indeed, even with an increasingly fine mesh, the variation on the calculated values of 2EQ spectra is of the order of 5 to 10 %[3], whereas it is of the order of 1 % for 2ED spectra. This seems to be due to the fact that we simulate a structure at a distance from the source that is a fraction of the studied wavelength. Also the EQ, unlike the ED, involves derivatives of the electric field [Eqs. (6.13)], which is more sensitive to small variations.

## 6.3 Computation of Purcell factors using COMSOL Multiphysics

To calculate the multipolar contributions to the two-photon spontaneous emission (TPSE) spectrum and their interference, Purcell factors need to be calculated for different orientations of multipolar point sources and at different frequencies [Eqs. (4.81) and (4.87)]. As a reminder, the Purcell factors can be calculated by dividing the power emitted by a classical source in a photonic environment by

[3] These values have been calculated for an electric point quadrupole placed 10 nm under a silver nanodisk and 2 nm under a graphene nanotriangle [Chap. 7].

the power it emits in vacuum [Eq. (2.34)]:

$$P := \frac{W}{W_0}, \tag{6.14}$$

where the classical source is described by a multipolar point source, or by a superposition of different multipolar point sources [Eqs. (4.75)]. In total, there are 6 Purcell factors to calculate the 2ED or the 2MD transition rate by modeling electric or magnetic point dipoles [Eq. (4.61)], 15 to calculate the 2EQ transition rate by modeling electric point quadrupoles [Eq. (4.66)], and 15 to calculate the interference between the 2ED and 2EQ channels by modeling the superposition of electric point dipoles and quadrupoles [Eq. (4.79)]. These correspond to different source orientations and are computed over a range of frequencies to obtain spectra. Depending on the symmetry of the studied system, the number of Purcell factors to calculate can be reduced, as for example for systems having an azimuthal symmetry [Eqs. (3.65), (3.79), and (3.93)]. Furthermore, when simulating superposition of multipolar sources at the same position for the calculation of the interference, the power emitted by the classical sources is chosen in such a way that equation (4.77b) is satisfied, which allows to account for the branching fraction of the multipolar emission channels. In addition, due to the expression of the electric dipole and quadrupole moment operators [Eqs. (3.5)], the electric dipole moments are in phase with the electric quadrupole ones. In contrast, there is a $\pi/2$ phase shift between the electric and magnetic moments since the magnetic dipole moment operator contains a factor $i$ (or $-j$) [Eq. (3.5b)]. The expression of the power emitted in free space for the electric point sources are given by the equations (2.20) and (2.25), while for the MD it is given by [94]:

$$W_{\mathrm{MD},0} = \frac{\mu_0\,\omega^4}{12\pi c^3}\,\|\mathbf{m}\|^2\,, \tag{6.15}$$

with $\mathbf{m}$ being the magnetic dipole moment.

As already mentioned in Chapter 2, inside a photonic environment, a quantum emitter can decay either radiatively in the case of emission of photons (energy radiated in the far-field) or non-radiatively in the case of energy dissipation in the environment, for example in the form of plasmons or phonons [30]. Moreover, the separate calculation of the radiative and non-radiative channels is achieved through the decomposition of Purcell factors into a radiative part and a non-radiative part:

$$P = P_{\mathrm{r}} + P_{\mathrm{nr}}. \tag{6.16}$$

In the context of the emission of one quantum from an emitter close to a plasmonic nanostructure, the non-radiative channel is dominated by the excitation of plasmons[4]. As a result, the two-quanta spontaneous emission process is mainly given by three distinct emission pathways [Fig. 6.3]: the emission of a pair of photons (ph-ph), the emission of a photon and the excitation of one plasmon (ph-pl), and the excitation of two plasmons on the structure (pl-pl) [26]. This decomposition into three pathways is valid for the 2ED, 2MD, and 2EQ transitions. For example, these three channels

[4]Depending on the frequency, a material can behave like a metal when the real part of its permittivity is negative or like a dielectric when it is positive. For a dielectric, the excitation of plasmons is impossible [Sec. 2.6], and in this case the non-radiative channel is absorption within the material.

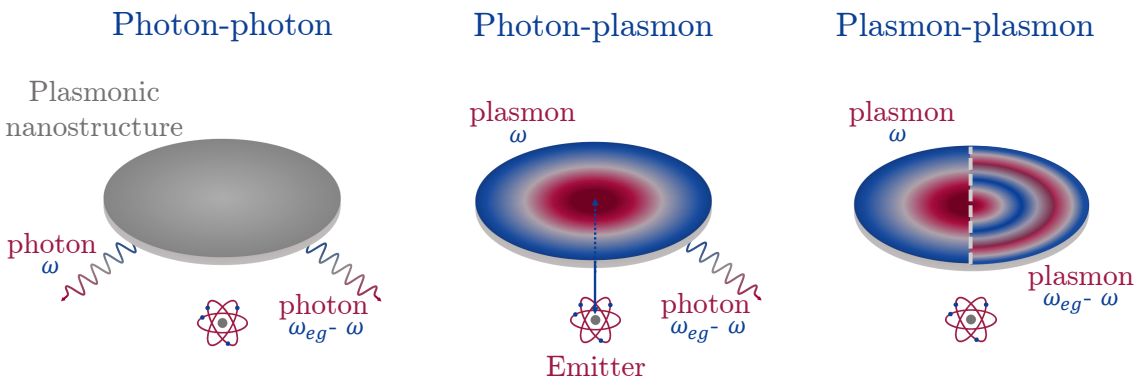


Figure 6.3: From left to right: photon-photon, photon-plasmon, and plasmon-plasmon emission channels of the TPSE of a quantum emitter placed near a plasmonic nanostructure (a nanodisk for the example). The first quantum is emitted at the frequency $\omega$ while the second one is emitted at the complementary frequency $\omega_{eg} - \omega$.

are calculated as follows for the 2ED transition:

$$\frac{\gamma^{(2)}_{\text{2ED,ph-ph}}(\omega;\mathbf{R})}{\gamma^{(2)}_{\text{2ED},0}(\omega)} = \sum_{i,j,a,b=1}^{3} \hat{\mathcal{D}}^{eg}_{ia}(\omega,\omega_{eg}-\omega)\left(\hat{\mathcal{D}}^{eg}_{jb}(\omega,\omega_{eg}-\omega)\right)^{*} F^{\text{ED}}_{ij,r}(\omega;\mathbf{R})\, F^{\text{ED}}_{ab,r}(\omega_{eg}-\omega;\mathbf{R}), \tag{6.17a}$$

$$\frac{\gamma^{(2)}_{\text{2ED,ph-pl}}(\omega;\mathbf{R})}{\gamma^{(2)}_{\text{2ED},0}(\omega)} = \sum_{i,j,a,b=1}^{3} \hat{\mathcal{D}}^{eg}_{ia}(\omega,\omega_{eg}-\omega)\left(\hat{\mathcal{D}}^{eg}_{jb}(\omega,\omega_{eg}-\omega)\right)^{*} \times \left[F^{\text{ED}}_{ij,r}(\omega;\mathbf{R})\, F^{\text{ED}}_{ab,nr}(\omega_{eg}-\omega;\mathbf{R}) + F^{\text{ED}}_{ij,nr}(\omega;\mathbf{R})\, F^{\text{ED}}_{ab,r}(\omega_{eg}-\omega;\mathbf{R})\right], \tag{6.17b}$$

$$\frac{\gamma^{(2)}_{\text{2ED,pl-pl}}(\omega;\mathbf{R})}{\gamma^{(2)}_{\text{2ED},0}(\omega)} = \sum_{i,j,a,b=1}^{3} \hat{\mathcal{D}}^{eg}_{ia}(\omega,\omega_{eg}-\omega)\left(\hat{\mathcal{D}}^{eg}_{jb}(\omega,\omega_{eg}-\omega)\right)^{*} F^{\text{ED}}_{ij,nr}(\omega;\mathbf{R})\, F^{\text{ED}}_{ab,nr}(\omega_{eg}-\omega;\mathbf{R}), \tag{6.17c}$$

where we can verify that the sum of these three channels yields to the total 2ED transition rate [Eq. (4.58a)]. In these equations, $\mathbf{F}^{\text{ED}}_{r}$ and $\mathbf{F}^{\text{ED}}_{nr}$ are calculated by using the radiative part and the non-radiative part of the Purcell factors, respectively [Eq. (4.60)]. Similar equations stand for the other multipolar contributions to the TPSE.

Concretely, we use the Wave Optics Module of COMSOL [115] in the frequency domain (i.e., assuming an harmonic dependency for the fields and sources) to build our models, of which a schematic illustration is given in Figure 6.4. As a first step, we define a spherical simulation domain on which perfectly matched layers (PMLs) are defined as an outer layer with a thickness equal to a quarter of the domain radius. Their role is to mimic an open infinite domain by absorbing all radiated waves and avoiding parasitic reflections towards the domain [109, 115]. Second, the classical emitter is positioned at the center of the domain and is modeled by a given orientation of a radiating electric point dipole, magnetic point dipole, electric point quadrupole, or the superposition of two of these. Third, the plasmonic nanostructure is placed close to the emitter, whose modeling is addressed in the next section. Fourth, Purcell factors are determined through the integration of the Poynting vector, which represents the energy flux density related to the propagation of an electromagnetic wave [Eqs. (2.27) and (2.28)]. For the radiative part, this integration is carried out on the inner surface of the PMLs, while for the total part (radiative plus non-radiative parts), it is performed

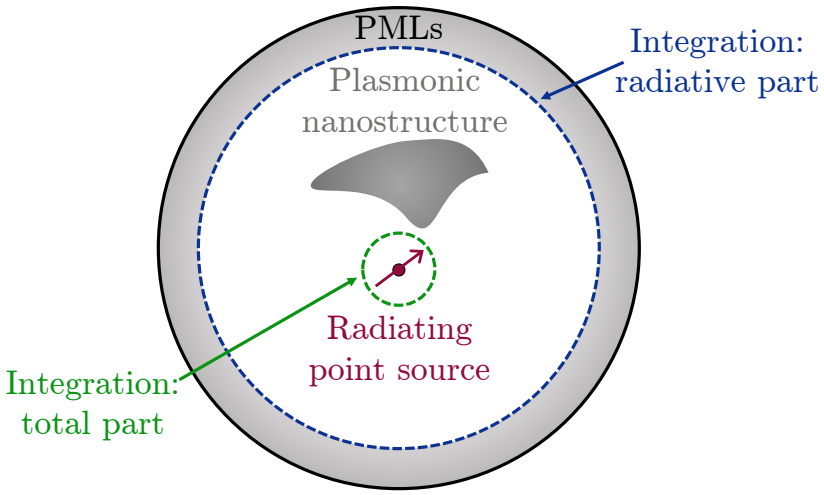


Figure 6.4: Schematic representation of the simulation domain. A point source is placed at the center of the simulation domain and near a plasmonic structure. The simulation domain is a sphere, where PMLs are defined as an outer layer. An integration on the inner surface of the PMLs is carried out to calculate the radiative part of the emitted power, while an integration on the surface of a fictional sphere centered on the emitter is performed to calculate the total emitted power (radiative plus non-radiative parts).

on the surface of a fictional sphere centered on the emitter. Fifth, the whole simulation domain is meshed, where the element sizes are chosen to have a convergence in the results. The mesh of one of our model is illustrated as an example in Figure 6.5. To do so, the PMLs are meshed in order to contain a fixed number of layers (typically between 6 and 12 [115]). For the rest (the domain inside the PMLs and the plasmonic structure if it is modeled with a 3D domain), a tetrahedral mesh is used. In the case where the structure is modeled by a surface, a triangular mesh is used. Sixth, a sweep over frequencies is implemented to calculate spectra. This sweep ranges from a minimal frequency $\omega_{\text{min}}$ to $\omega_{eg} - \omega_{\text{min}}$, with $\omega_{eg}$ the transition frequency, and must contains complementary frequencies to be able to mutliply a Purcell factor at a given frequency with a Purcell factor at the complementary frequency. In order to have the frequency $\omega_{eg}/2$ in our data, we work with an odd number of frequencies. Finally, we use the direct solver MUMPS, which is based on the LU decomposition method and takes the advantage of the multithreaded processors [112]. In all the tests we carried out during this thesis, it gives the most converged solutions, especially at low frequencies where other solvers fail. Iterative solvers, although faster and less RAM-intensive, do not always find a solution for the systems we are studying, and should therefore be avoided. The simulations are performed on a workstation using an AMD Ryzen Threadripper PRO 5995WX 64-core CPU and 512GB of RAM, thus enabling the computation of Purcell factors in parallel. Typically, calculating a Purcell factor on 99 frequencies takes between 20 minutes and 5 hours by using 1 to 8 cores, and uses between 10 and 35 GB of RAM for the systems studied in the next chapter.

In practice, for each studied structure, there is one model (simulation) per Purcell factor to calculate over a range of frequencies, which corresponds to a given emitter orientation. These models can be computed in parallel, according to the available computing resources. However, it is theoretically possible to reduce the number of simulations. Indeed, it is for example possible to calculate the three Purcell factors $P_{ij}^{\text{ED}}$ using the data obtained when calculating the three Purcell factors $P_i^{\text{ED}}$ by superposing the fields produced by a dipole along $\hat{\mathbf{e}}_i$ and $\hat{\mathbf{e}}_j$ in the calculation

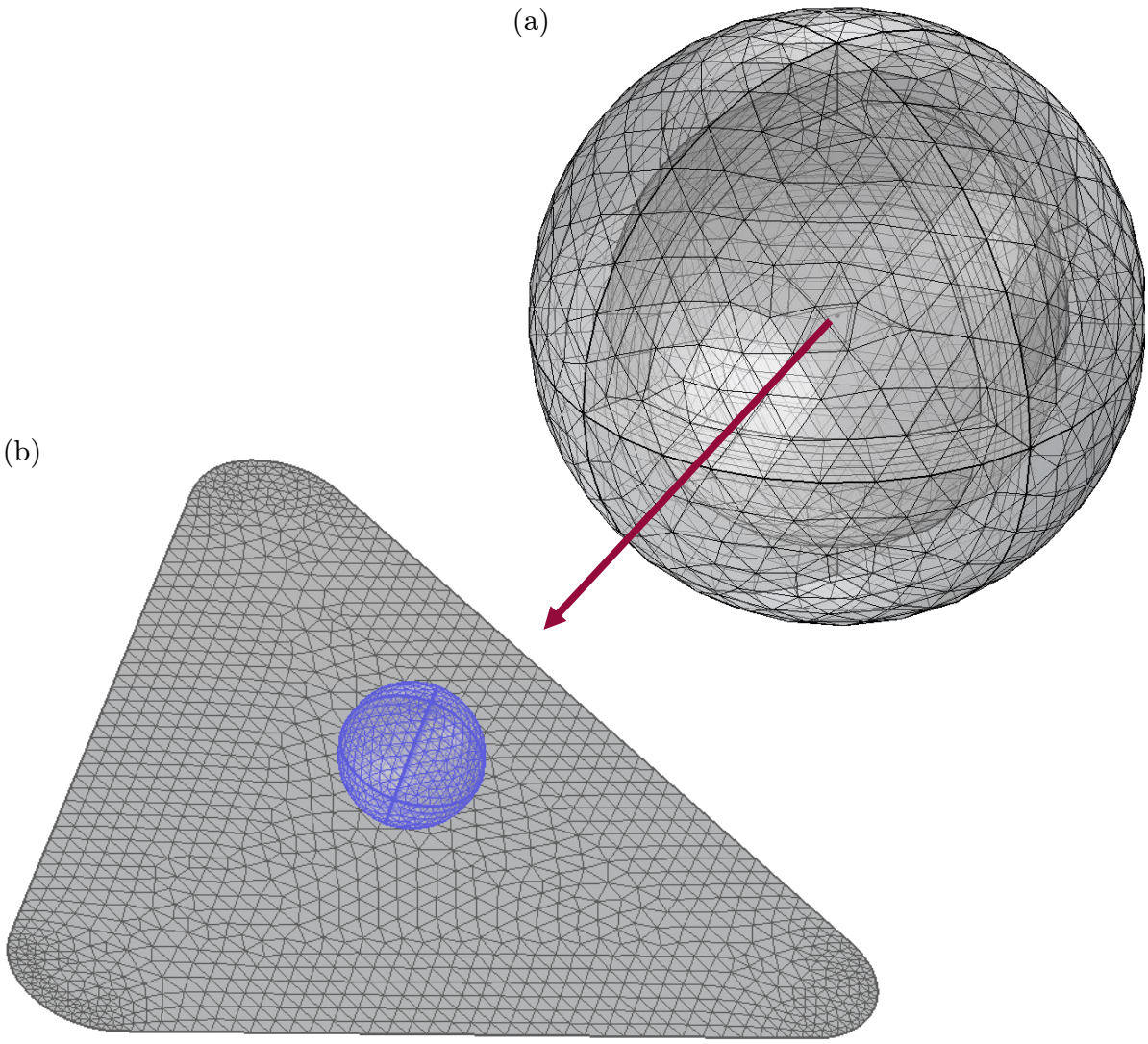


Figure 6.5: Screenshots from one of our COMSOL model to illustrate the mesh. (a) The domain is a sphere whose radius is, for this example, half the transition wavelength $\lambda_{eg} = 1.28$ µm. PMLs are made up of 6 layers and meshed using triangular prism elements, while tetrahedral elements are used for the rest. The structure and the emitter are placed on the center of the domain (small dot at the extremity of the red arrow). (b) The plasmonic structure, here a two-dimensional triangle with 23 nm sides and rounded edges, is meshed with triangular elements. The emitter is placed 2 nm above the structure and at the center of the fictional sphere (in blue) having a radius of 1.6 nm used to calculate the total emitted power.

of the Poynting vector [Eqs. (2.27) and (2.28)]. Thereby, the number of orientations to consider drops to 3 for the dipoles (dipoles along the three basis vectors) and 5 for the quadrupoles (the five quadrupoles depicted in Fig. 3.2). Moreover, there are no extra simulations to perform for calculating the interference because the Purcell factors $P_{i\mu}^{\mathrm{ED+EQ}}$ can be computed by superposing the field produced by a dipole along $\hat{\mathbf{e}}_i$ and by a quadrupole along $\hat{\mathbf{e}}_\mu$, provided that the moments of these sources have been properly calibrated according to the vacuum TPSE rates [Eq. (4.77b)]. Despite the drastic reduction in the number of simulations to be performed (e.g., from 36 to 8 for the calculation of the 2ED and 2EQ spectra as well as their interference), we did not take the time to implement this for the sake of simplicity in data processing and, above all, to devote more time to producing results.

## 6.4 Optical modeling of silver and graphene

In the next chapter, we will consider different plasmonic nanostructures (nanostructures supporting localized surface plasmon resonances). For this purpose, silver and graphene will be used as conductive materials.

On the one hand, silver is modeled with a three-dimensional domain and using the Drude model [Eq. (2.38)], with the plasma frequency $\hbar\omega_p = 9.1$ eV ($\omega_p = 1.38 \times 10^{16}$ rad/s) and the collision frequency $\hbar\gamma = 18$ meV ($\gamma = 2.73 \times 10^{13}$ Hz) [26]. As a reminder, the engineering convention is used in COMSOL for harmonic dependencies and so the factor $i$ in equation (2.38) must be replaced by $-j$. The permittivity of silver is plotted in Figure 6.6.

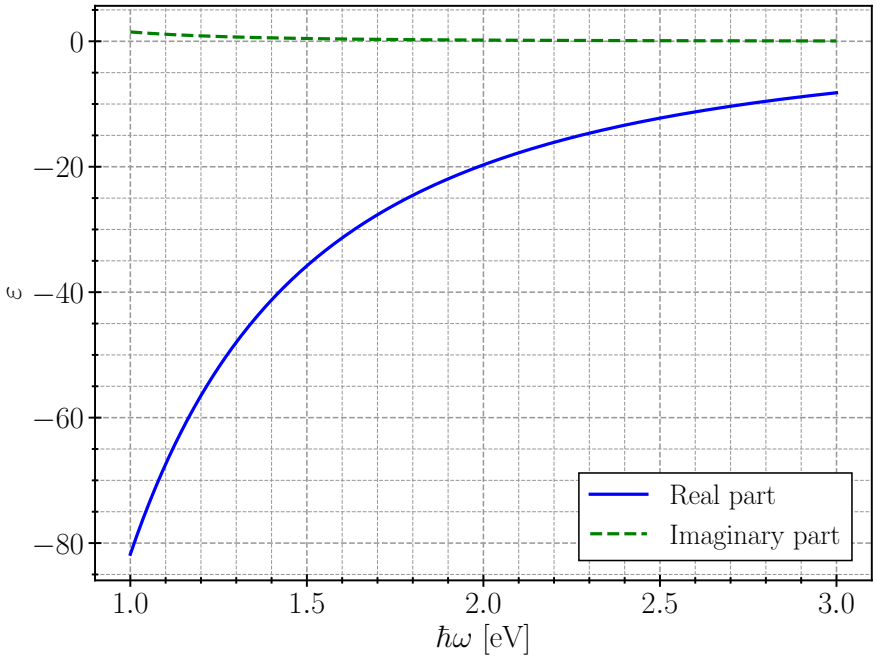


Figure 6.6: Plot of the Drude model [Eq. (2.38)] for silver characterized by $\omega_p = 9.1$ eV and $\hbar\gamma = 18$ meV. Note that in the engineering convention, the imaginary part is negative, but here it is represented by a positive number (i.e., not using this convention).

On the other hand, graphene is modeled in COMSOL using a transition boundary condition (TBC)[5], with an effective thickness $t = 0.335$ nm [119]. TBC is designed to model a geometrically thin structure, which physically represents a discontinuity in the tangential electric field due to the induced surface current density [118]. Unlike silver where only intraband transitions contribute to the optical response at the frequencies of interest (below 4 eV) [66], the optical response of graphene characterized by its two-dimensional surface conductivity [120, 121] results also of interband

[5]There are three ways of modeling a thin structure: with a surface current density boundary condition, a transition boundary condition, and a 3D domain. Using a boundary condition avoids the need to mesh a 3D domain with very thin elements, thus saving computing resources [118].

transitions [120, 121]:

$$\sigma_{2D} = \sigma_{\text{intra}} + \sigma_{\text{inter}}, \tag{6.18a}$$

$$\sigma_{\text{intra}} = -\frac{2je^2k_BT}{\pi\hbar^2(\omega - j\tau^{-1})}\ln\left[2\cosh\left(\frac{E_F}{2k_BT}\right)\right], \tag{6.18b}$$

$$\sigma_{\text{inter}} = \frac{e^2}{4\hbar}\left[\frac{1}{2} + \frac{1}{\pi}\arctan\left(\frac{\hbar\omega - 2E_F}{2k_BT}\right) + \frac{j}{2\pi}\ln\left(\frac{(\hbar\omega + 2E_F)^2}{(\hbar\omega - 2E_F)^2 + (2k_BT)^2}\right)\right], \tag{6.18c}$$

where the engineering convention is used. In these equations, $e$ represents the electron charge, $k_B$ is the Boltzmann constant, $T = 300$ K denotes the temperature, and $E_F$ stands for the Fermi energy, i.e., the doping level of graphene which can tune the graphene optical response. Moreover, the scattering lifetime of electrons in graphene is given by $\tau = \mu E_F/ev_F^2$, with $\mu \approx 10^4$ cm$^2$ V$^{-1}$s$^{-1}$ the impurity-limited DC conductivity and $v_F = 10^6$ m/s the graphene Fermi velocity [122, 123]. Figure 6.7 shows the graphene permittivity[6] as a function of its Fermi energy.

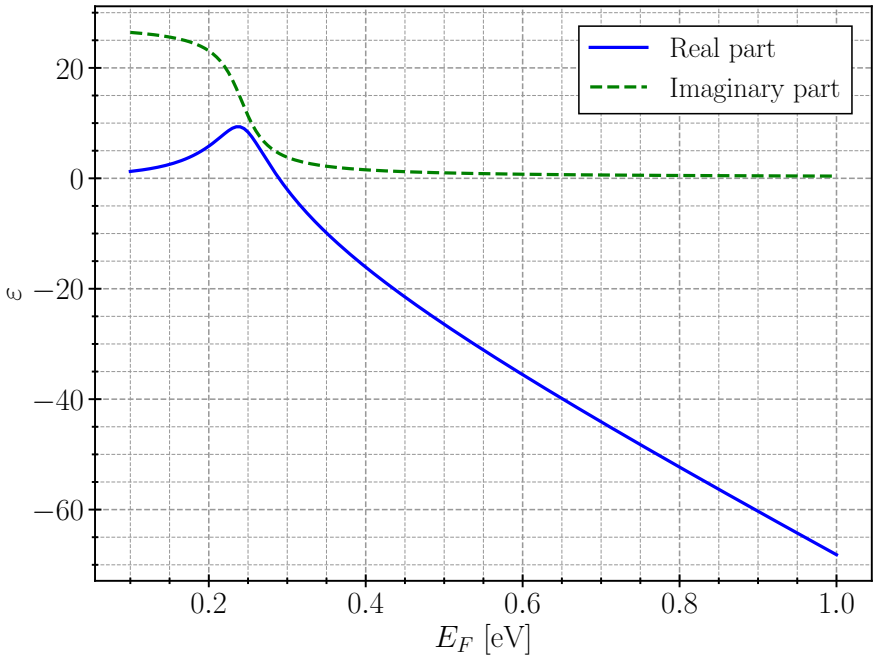


Figure 6.7: Plot of the real and imaginary parts of the graphene permittivity as a function of its Fermi energy for an effective thickness of 0.335 nm [119] and a frequency $\hbar\omega = 0.48$ eV ($\omega = 7.30 \times 10^{14}$ rad/s, $\lambda = 2.58$ µm). Below $E_F = 0.29$ eV, graphene assumes a dielectric behavior ($\text{Re}(\varepsilon) > 0$). The imaginary part of the permittivity increases when the Fermi energy decreases and approaches half of the photon energy ($E_F = \hbar\omega/2 = 0.24$ eV) due to interband transitions [124]. Note that in the engineering convention, the imaginary part is negative, but here it is represented by a positive number (i.e., not using this convention).

## 6.5 Summary

In this chapter, we introduced the finite element method (FEM) used in the commercial software COMSOL Multiphysics®. This numerical method seeks approximate solutions to partial differential equations (PDEs) by dividing the domain of interest into a finite number of elements, within which

[6] The graphene permittivity is calculated using its link with the (3D) conductivity [Eq. (2.37)], where $\sigma = \sigma_{2D}/t$.

the unknown function is represented by simple interpolation functions. A global matrix equation for the entire domain is then assembled and solved using either iterative or direct solvers. The FEM has the advantage of using adaptive meshing and producing solutions throughout the domain. Concretely, a weak formulation of the wave equation for the electric field (i.e., the master equation to solve [Eq. (6.5)]) is used. This formulation is obtained by multiplying the original PDE by a test function and integrating over the domain of interest [Eq. (6.6)]. It requires the integral equation to hold for all test functions rather than the PDE at each point in the domain. Thus, the PDE is solved globally, and the solution verifies existence conditions thay are easier to satisfy, and the order of derivatives is reduced by one.

Afterwards, we presented our COMSOL models used to compute Purcell factors (i.e., the environment contribution to TPSE rates). We implemented the weak formulation of the electric point quadrupole [Eqs. (6.13)], as it is not available in the software. In total, there are 6 Purcell factors to calculate the 2ED or the 2MD transition rate by modeling electric or magnetic point dipoles [Eq. (4.61)], 15 to calculate the 2EQ transition rate by modeling electric point quadrupoles [Eq. (4.66)], and 15 to calculate the interference between the 2ED and 2EQ channels by modeling the superposition of electric point dipoles and quadrupoles [Eq. (4.79)]. These correspond to different source orientations and are computed over a range of frequencies to obtain spectra. Furthermore, near a plasmonic nanostructure, the two-quanta spontaneous emission process is given by three emission pathways, which can be computed through the decomposition of Purcell factors into radiative and non-radiative parts: the emission of a pair of photons, the emission of a photon and the excitation of one plasmon, and the excitation of two plasmons on the structure. Finally, we provided the optical models of silver and graphene, the two materials that we will use in the next chapter to design plasmonic nanostructures. Silver is modeled using the Drude model, while the response of graphene is given by interband and intraband contributions, which can be tuned by its Fermi energy.

Chapter 7

# Two-photon spontaneous emission near plasmonic nanostructures

In this chapter, we use the framework we developed in the previous chapters to calculate two-photon spontaneous emission spectra of a quantum emitter placed near plasmonic nanostructures (i.e., nanostructures supporting localized surface plasmons resonances). To do so, we use the equations derived for the multipolar contributions to the TPSE rate [Eqs. (4.87)], which involve second-order multipolar transition moments (the emitter contribution) and Purcell factors for the two emitted quanta (the environment contribution). For all systems we study, we consider a hydrogen-like emitter, and more specifically transitions between two spherically symmetric states ($s$ states). The second-order multipolar transition moments and the vacuum TPSE rates were calculated analytically for these transitions in Section 5.2 [Eqs. (5.65)] and in Section 5.3, respectively. In addition, we use the software COMSOL Multiphysics® to compute the Purcell factors [Chap. 6]. Furthermore, as the plasmonic nanostructures considered in this chapter do not contribute significantly to enhancing magnetic transitions [59], we do not present the magnetic contribution to the TPSE rate. Moreover, one-photon and mixed two-photon transitions are not allowed between two $s$ states [Sec. 2.4]. As a result, it is sufficient in this chapter to calculate the two-electric dipole (2ED) and the two-electric quadrupole (2EQ) contributions, as well as their interference, to the TPSE spectra [Eq. (4.82)]:

$$\gamma^{(2)}_{\mathrm{tot}}(\omega;\mathbf{R}) = \gamma^{(2)}_{\mathrm{2ED}}(\omega;\mathbf{R}) + \gamma^{(2)}_{\mathrm{2EQ}}(\omega;\mathbf{R}) + \gamma^{(2)}_{\mathrm{2ED\cap 2EQ}}(\omega;\mathbf{R}). \tag{7.1}$$

First of all, we check in Section 7.1 that our numerical computation of Purcell factors allows to find the results of Muniz et al. [26]. In their study, they calculated the 2ED transition rate of a hydrogen-like emitter placed on the axis of symmetry of a silver nanodisk with an analytical calculation of Purcell factors. Here, we also calculate the 2EQ transition rate and we exploit the flexibility of our method to study the case of an off-axis emitter. The results presented in this first section, as well as the derivation made in Chapter 4 of the equations based on Purcell factors for the contribution of the 2ED, 2MD, and 2EQ to the TPSE rate [Eqs. (4.87a)-(4.87c)] and the analytical calculation of the second-order transition moments [Sec. 5.2], have been published in Physical Review A [125]. Then, we design in Section 7.2 a system in which the 2EQ transition rate is of the same order of magnitude as the 2ED transition rate, in order to study the interference between these two multipolar emission channels. This study, together with the derivation of the equation for calculating the interference between 2ED and 2EQ transition rates [Eq. (3.99d)] and with the analytical calculation of the vacuum TPSE rates [Sec. 5.3], has been published in Discover Nano [126]. Finally, we design in Section 7.3 two nanoantennas that emit the two photons from the TPSE in different directions, for which a paper is under submission.

## 7.1 Two-photon spontaneous emission near silver nanodisks

As a validation step of the developed framework, we study the two-photon Purcell effect for an $s \to s$ transition of a hydrogen atom placed 10 nm under a two-dimensional silver nanodisk [Fig. 7.1], with the same system's parameters as in Ref. 26. In their study, they used the equation (4.62) to calculate the 2ED contribution to the TPSE rate with an analytical calculation of Purcell factors [26]. As equation (4.62) can only be used in a basis that diagonalizes the Green's function simultaneously for all studied frequencies, their study is restricted to the specific case where the emitter is placed on the axis of symmetry of the disk. With our more general framework [Eqs. (4.87)], the Purcell factors are computed numerically, the 2EQ contribution is also determined, and we use the flexibility of our method to study the case of an off-axis emitter. In this case, the interference between the 2ED and 2EQ transitions has not been computed because the method had not yet been developed at the time of this study. However, the calculated non-normalized by vacuum 2EQ transition rate is much lower than the 2ED transition rate (difference of 6 orders of magnitude), leading to negligible interference in this system.

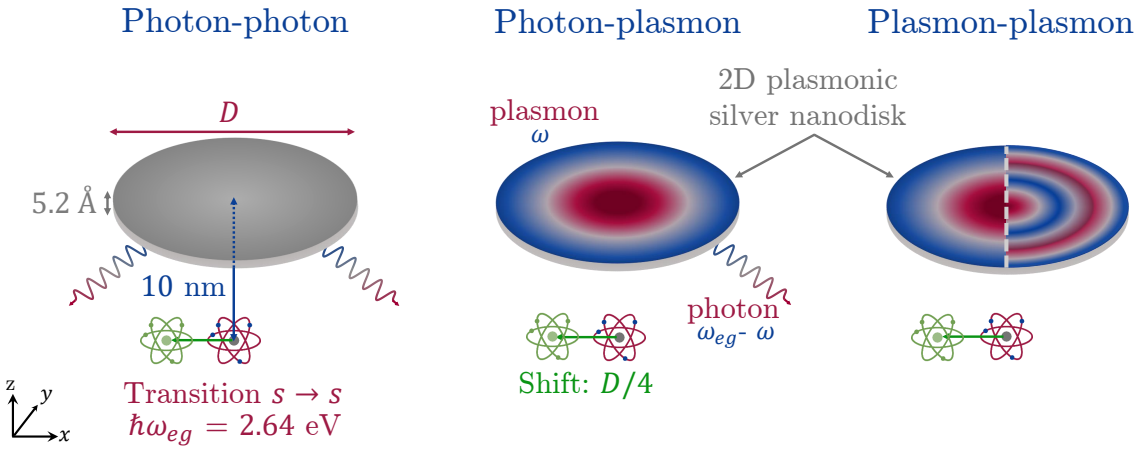


Figure 7.1: From left to right: photon-photon, photon-plasmon, and plasmon-plasmon emission channels of the TPSE. We study an $s \to s$ transition of a hydrogen-like emitter placed 10 nm below a 5.2 Å thick silver disk with a diameter $D$. The emitter is on-axis or shifted by a quantity $D/4$ in the $x$ direction. The transition frequency is $\hbar\omega_{eg} = 2.64$ eV, which corresponds to a wavelength of 470 nm. The first quantum is emitted at the frequency $\omega$ while the second one is emitted at the complementary frequency $\omega_{eg} - \omega$.

When the emitter is on-axis, the system has an azimuthal symmetry, reducing the number of Purcell factors to calculate due to the equivalence between the $X$ and $Y$ directions. Thereby, it is sufficient to calculate the three components $\left\{F^{\mathrm{ED}}_{xx}, F^{\mathrm{ED}}_{zz}, F^{\mathrm{ED}}_{xz}\right\}$ for the 2ED transition [Eq. (3.65)], and the six components $\left\{F^{\mathrm{EQ}}_{xxxx}, F^{\mathrm{EQ}}_{xzxz}, F^{\mathrm{EQ}}_{xyxy}, F^{\mathrm{EQ}}_{xxxz}, F^{\mathrm{EQ}}_{xxxy}, F^{\mathrm{EQ}}_{xzxy}\right\}$ for the 2EQ transition [Eq. (3.79)]. The calculation of these nine components requires the calculation of nine Purcell factors [Eqs. (3.65) and (3.79)]. When the emitter is shifted in the $x$ direction, the system has no longer an azimuthal symmetry and all components of the tensors $\mathbf{F}^{\mathrm{ED}}$ and $\mathbf{F}^{\mathrm{EQ}}$ (resp. 6 and 15) need to be computed [Eqs. (3.63) and (3.77)].

Concerning the COMSOL models [Sec. 6.3], first, the domain radius is equal to the studied wavelength $\lambda$ (i.e., $\lambda = 2\pi c/\omega$ with $\omega$ ranging from 0 to $\omega_{eg}$), and PMLs are made up of 10 layers. Second, the silver nanodisk is modeled with the Drude model [Sec. 6.4] and using a cylinder[1] with

[1] Given the thinness of the disk, we could have modeled it as a surface and applied a transition boundary condition

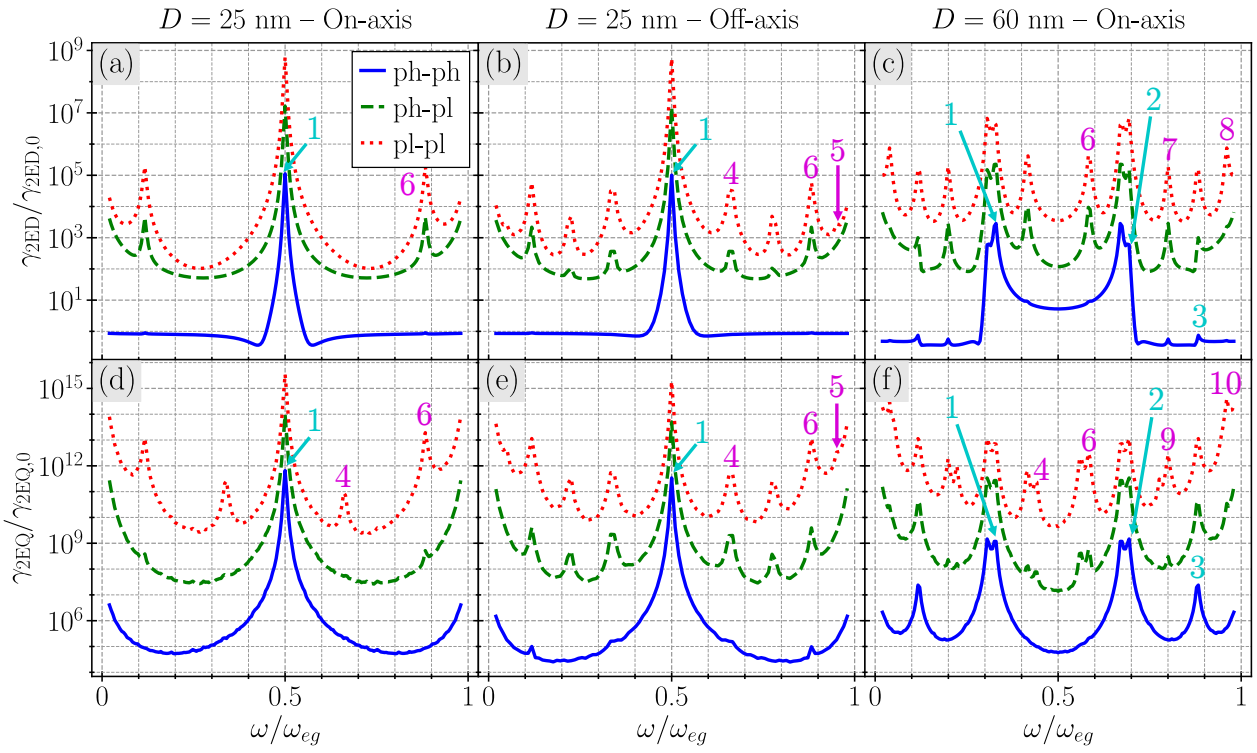


Figure 7.2: Photon-photon (ph-ph), photon-plasmon (ph-pl), and plasmon-plasmon (pl-pl) emission channels of the spectral TPSE rate for the 2ED (a - c) and 2EQ (d - f) contributions for the system sketched in Figure 7.1. The first two columns (a, b, d, e) correspond to a 25 nm diameter disk, while for the third one (c, f) the diameter is 60 nm. The emitter is placed on the axis of symmetry of the disk, except for the central column (b, e) where it is shifted in the $x$ direction parallel to the disk by $D/4$. The spectra were computed over 199 frequencies for the emitter on-axis and over 99 frequencies for the emitter off-axis. The first quantum is emitted at the frequency $\omega$ while the second one is emitted at the complementary frequency $\omega_{eg} - \omega$, leading to symmetric spectra. Some radiative and non-radiative peaks are identified by cyan and magenta numbers, respectively.

a height $t = 0.52$ nm and a diameter $D = 25$ or 60 nm. This height has been chosen in order to have a correspondence with the results of Y. Muniz et al. [26]. Third, the smallest element has a characteristic size of 0.25 nm on the disk and on the fictional sphere around the emitter used to calculate the emitted power, which have a radius of 5 nm. The computation on a single core of one Purcell factor over 199 frequencies has required 45 minutes and 13 GB of RAM for the 25 nm diameter disk, and 135 minutes and 30 GB of RAM for the 60 nm diameter one.

### Results and discussion

The photon-photon, photon-plasmon, and plasmon-plasmon relaxation channels of the spectral TPSE rate for the 2ED and 2EQ contributions are plotted in Figure 7.2. First of all, our results obtained for the 2ED transition where the emitter is placed on-axis [Figs. 7.2(a, c)] correspond to the results of Y. Muniz et al. [26] with their analytical calculation of Purcell factors, thus validating our numerical computation of Purcell factors. Furthermore, the 2ED and 2EQ transitions are strongly enhanced by the plasmonic disk. Indeed, with the 25 nm diameter disk [Figs. 7.2(a, d)] at $\omega = \omega_{eg}/2$, i.e., the frequency where both photons have the same energy, the 2ED and 2EQ

or a surface current density, instead as a 3D domain. We have chosen a 3D model in order to be able to study disks of greater thickness (results not shown), which is not possible with a 2D model.

transition rates are enhanced by, respectively, 8 and 15 orders of magnitude for the emission of two plasmons (dotted red line) and by, respectively, a factor $1.12 \times 10^5 (\pm 0.4\,\%)$ and $6.6 \times 10^{11} (\pm 5\,\%)$[2] for the emission of two photons (solid blue line). The percentage represents the standard deviation of the variation of the rate with finer meshes.

The TPSE spectra result from a summation over different components of the tensors $\mathbf{F}^{\mathrm{ED}}$ and $\mathbf{F}^{\mathrm{EQ}}$ [Eqs. (4.87)], i.e., a summation over different orientations of the multipolar point sources. In order to have a better understanding, the dominant components are plotted in Figure 7.3 for the 25 nm diameter disk, for an ED on-axis, an ED off-axis, and an EQ on-axis. Firstly, for the ED on the axis of symmetry of the disk [Figs. 7.3(a, d)], the component $F_{xz}^{\mathrm{ED}}$ is negligible and thus only the components $F_{xx}^{\mathrm{ED}}$ and $F_{zz}^{\mathrm{ED}}$ are required to calculate the 2ED transition rate. As a result, the equation used by Muniz [Eq. (4.62)] which does not involve the component $F_{xz}^{\mathrm{ED}}$ (linked to an off-diagonal component of the Green's function) is appropriate in the case of an on-axis emitter. In addition, there is one radiative peak at $\omega = \omega_{eg}/2$ (labeled 1) and one non-radiative peak (labeled 6). Therefore, the corresponding 2ED transition spectrum in Figure 7.2(a) have one radiative peak, and the non-radiative peak is doubled since TPSE spectra are symmetric with respect to $\omega_{eg}/2$. When the emitter is shifted in the plane parallel to the disk [Figs. 7.3(b, e)], there are now 4 of the 6 components of $\mathbf{F}^{\mathrm{ED}}$ that are non negligible. Among them, the component $F_{yy}^{\mathrm{ED}}$ is now different from $F_{xx}^{\mathrm{ED}}$ due to the breaking of azimuthal symmetry, while the component $F_{xz}^{\mathrm{ED}}$ is linked to an off-diagonal component of the Green's function. Therefore, our equation that involve the off-diagonal components of $\mathrm{Im}\,\mathbf{G}$ [Eq. (4.87a)] is required for an off-axis emitter. Moreover, three additional non-radiative peaks appear (two of which are labeled 4 and 5). For an EQ placed on the axis of symmetry [Figs. 7.3(c, f)], there is one radiative peak (labeled 1, the others peaks are too weak to be considered as radiative peaks) and two non-radiative peaks (labeled 4 and 6). In addition, the results are noisier than for ED, because the convergence for EQ is harder to achieve. The case of an EQ off-axis is not presented due to the important number of components to plot (9).

Concerning the comparison of the different spectra of Figure 7.2, the surface charge density of some modes excited on the disk is plotted in Figure 7.4. We first observe that the 2EQ spectrum relative to a 25 nm diameter disk [Fig. 7.2(d)] has an additional non-radiative peak compared to the 2ED one [Fig. 7.2(a)], which corresponds to the quadrupolar mode number 4 in Figure 7.4. Second, when the emitter is shifted [Figs. 7.2(b, e)], the breaking of the azimuthal symmetry leads to a greater wealth of excited modes (non-radiative modes number 4 and 5 in Fig. 7.4), but the central radiative peak is slightly reduced. Note that in the off-axis configuration, the 2ED spectra [Fig. 7.2(b)] exhibits a peak labeled 4 corresponding to a quadrupolar mode excited on the structure, which was not possible to excite in the more symmetric on-axis configuration [Fig. 7.2(a)]. Third, when the diameter of the disk increases [Figs. 7.2(c, f)], the frequency of the peaks changes and new radiative and non-radiative peaks appear, which correspond to higher order modes (modes number 2, 3, 7, 8, 9 and 10 in Fig. 7.4). Remark for example that the dipolar mode 1 appears multiple times, such as in Figure 7.2(a, c), but at different frequencies due to the different disk sizes.

[2] This value is slightly different from the value $7.5 \times 10^{11}$ given in our paper [125]. Indeed, there was a post-processing error in the calculation of 2EQ spectra, but this leads to an almost invisible change in the 2EQ spectra.

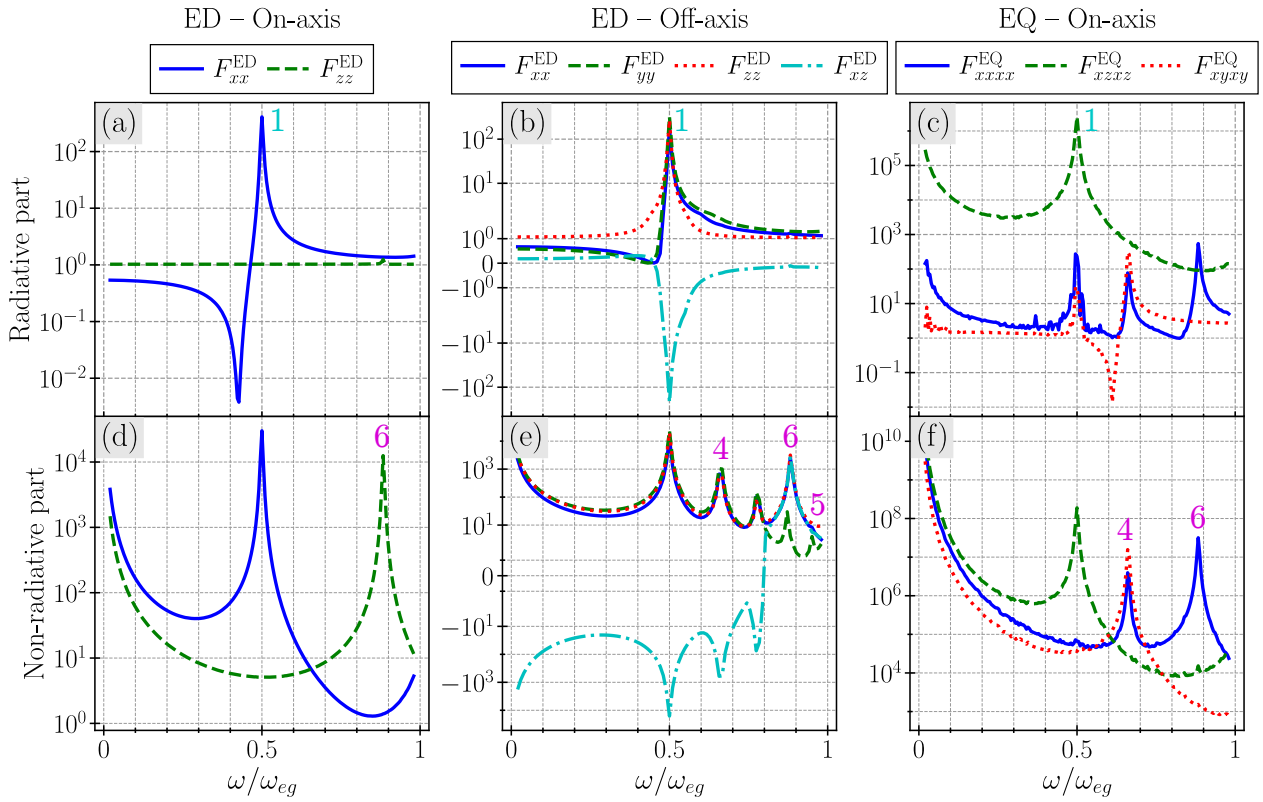


Figure 7.3: Plots of the radiative (a, b, c) and non-radiative parts (d, e, f) of the dominant components of the tensors $\mathbf{F}^{\mathrm{ED}}$ and $\mathbf{F}^{\mathrm{EQ}}$ for the 25 nm diameter disk. Subplots (a, d) correspond to an electric dipole on-axis, and are used to calculate the 2ED spectrum in Fig. 7.2(a). Subplots (b, e) correspond to an electric dipole off-axis, and are used to calculate the 2ED spectrum in Fig. 7.2(b). A symlog plot is used for these figures since the component $F_{xz}^{\mathrm{ED}}$ can be negative [Eq. (4.60)]. Subplots (c, f) correspond to an electric quadrupole on-axis, and are used to calculate the 2EQ spectrum in Fig. 7.2(d). Some radiative and non-radiative peaks are labeled, respectively with cyan and magenta numbers, and the corresponding modes on the disk are plotted in Figure 7.4.

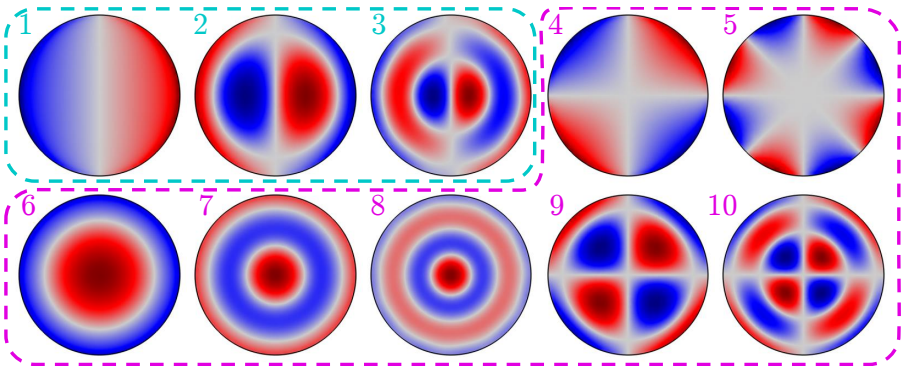


Figure 7.4: Surface charge density on the silver nanodisk relative to some radiative and non-radiative peaks, which are numbered in Figure 7.2 in cyan and magenta, respectively. These plots were obtained by the excitation of the modes on the structure with a specific orientation of the emitter, either a dipole or a quadrupole. For example, the mode 1 can be obtained with a dipole oriented along the $x$ axis but also with the quadrupole $\hat{\mathbf{Q}}_{xz}$, while the mode 10 can only be obtained with quadrupoles, with for example $\hat{\mathbf{Q}}_{xx}$ and $\hat{\mathbf{Q}}_{xy}$.

## 7.2 Interference between multipolar two-photon transitions near graphene nanotriangles

We study interference effects between the 2ED and 2EQ emission channels of the TPSE during a $5s \rightarrow 3s$ transition of a hydrogen atom placed 2 nm under a two-dimensional graphene nanotriangle. This structure is a good candidate to observe a 2EQ transition rate similar to the 2ED one [29], and thus highlight high interference effects. Indeed, it was shown in Ref. 29 for the one-photon spontaneous emission that the EQ transition rate can become locally 100 times larger than the dipolar one for a hydrogen-like emitter placed under the corners of a graphene nanotriangle (for specific dipole and quadrupole orientations). In addition, the $5s \rightarrow 3s$ transition has been chosen in order to match the half transition frequency ($\hbar\omega_{eg}/2 = 0.48$ eV, the frequency of the photons when they are emitted with the same energy) with the transition frequency used in Ref. 29 ($\hbar\omega_{eg} = 0.47$ eV).

For this system, all Purcell factors need to be calculated (6 for the 2ED transition, 15 for the 2EQ transition, and 15 for the interference [Sec. 4.7]). Concerning the COMSOL models [Sec. 6.3], first, the domain radius is equal to half the studied wavelength $\lambda$, and PMLs are made up of 12 layers. Second, the graphene nanotriangle is modeled using a transition boundary condition [Sec. 6.4] applied to a two-dimensional equilateral triangle with rounded corners of 2 nm, an effective thickness of $t = 0.335$ nm [119], and a side length $C$ ranging from 10 to 80 nm. Its optical response is described in Section 6.4 and can be tuned via its Fermi energy $E_F$, i.e., the doping level. Third, the smallest element has a characteristic size of 0.6 nm on the structure and 0.3 nm on the fictional sphere around the emitter used to calculate the emitted power, which have a radius of 1.5 nm. The computation on 4 cores of one Purcell factor over 145 frequencies has required 7.5 hours and 12 GB of RAM for a 23 nm side length triangle.

To underline the impact of interference effects on the overall TPSE rate, the following metric is used [62]:

$$R(\omega;\mathbf{R}) := \frac{\gamma^{(2)}_{\mathrm{2ED}\cap\mathrm{2EQ}}(\omega;\mathbf{R})}{\gamma^{(2)}_{\mathrm{2ED}}(\omega;\mathbf{R}) + \gamma^{(2)}_{\mathrm{2EQ}}(\omega;\mathbf{R})}, \tag{7.2}$$

which is comprised between $-1$ and 1. With this definition, the total TPSE rate [Eq. (7.1)] is rewritten as

$$\gamma^{(2)}_{\mathrm{2ED+2EQ}}(\omega;\mathbf{R}) = (1 + R(\omega;\mathbf{R}))\left(\gamma^{(2)}_{\mathrm{2ED}}(\omega;\mathbf{R}) + \gamma^{(2)}_{\mathrm{2EQ}}(\omega;\mathbf{R})\right). \tag{7.3}$$

Thus, a negative R value corresponds to a destructive interference while a positive one denotes a constructive interference. Moreover, values of -1 and 1 denote fully destructive and constructive effects, respectively, while a value of 0 indicates the absence of interference. By analogy with the interference between two waves[3], the maximum absolute value of $R$ is given by

$$R_{\max}(\omega;\mathbf{R}) = \frac{2\sqrt{\gamma^{(2)}_{\mathrm{2EQ}}/\gamma^{(2)}_{\mathrm{2ED}}}}{1 + \gamma^{(2)}_{\mathrm{2EQ}}/\gamma^{(2)}_{\mathrm{2ED}}}. \tag{7.4}$$

[3]The intensity of the wave resulting from the interference between two waves oscillating with time harmonic dependency of frequency $\omega$ is given by $I = I_1 + I_2 + 2\sqrt{I_1 I_2}\cos\Delta(\phi)$, with $I_1$ and $I_2$ the intensities of the two waves and $\Delta\phi$ the phase difference between them [94]. In this case, $R$ (the ratio between the interference and the intensities without interference) is $R = 2\sqrt{I_1 I_2}\cos\Delta(\phi)/(I_1 + I_2)$ and the maximum absolute value is $R_{\max} = 2\sqrt{I_1 I_2}/(I_1 + I_2)$.

Thus, the closer the ratio $\gamma^{(2)}_{\mathrm{2EQ}}/\gamma^{(2)}_{\mathrm{2ED}}$ is to 1, the greater the interference effects in the total TPSE rate can be, i.e., the larger the absolute values of $R$ can be. For example, ratios of $10^{-1}$, $10^{-2}$, and $10^{-3}$ give $R_{\max} = 57.5\,\%$, $19.8\,\%$, and $6.3\,\%$, respectively, while $R_{\max} = 10\,\%$ for a ratio equal to $2.5 \times 10^{-3}$. This shows that even if an emission channel is one, two or three orders of magnitude smaller than the other, interference effects must be taken into account. Furthermore, a ratio of $2.5 \times 10^{-3}$ between two multipolar channels indicates a possible threshold for the appearance of two-photon interference effects.

Note that in the case of 2D plasmonic infinite materials, the ratio can be written as a function of the confinement factor $\eta$: $\gamma^{(2)}_{\mathrm{2EQ}}/\gamma^{(2)}_{\mathrm{2ED}} = \eta^4\,\gamma^{(2)}_{\mathrm{2EQ,0}}/\gamma^{(2)}_{\mathrm{2ED,0}}$ [48], thus a threshold as a function of the confinement factor can be derived. For example, for the $2s \to 1s$ and $5s \to 3s$ transitions [Tab. 5.2], the confinement factor threshold (corresponding to $R_{\max} = 10\,\%$ and a ratio of $2.5\times10^{-3}$) is $\eta = 215$ and 340, which are achievable values with graphene nanostructures [48, 127].

### Results and discussion

The considered system [Fig. 7.5(a,b)] is defined by three parameters: the Fermi energy of graphene $E_F$, the triangle side length $C$, and the position of the emitter with respect to the structure. First, we show in Figure 7.5(c - h) the 2ED and 2EQ spectral transition rates at $\omega_{eg}/2$ as a function of $E_F$ and $C$ for an emitter placed under a corner of the triangle. Moreover, the surface charge density is plotted in Figure 7.6 for two set of parameters, showing two different responses of the structure. Then, these two rates and the metric $R$ are calculated in Figure 7.7 as a function of the emitter position for a specific value of the parameters $E_F$ and $C$, still at $\omega_{eg}/2$. Finally, spectra of the total TPSE rate and of $R$ are shown in Figure 7.8 and discussed for two sets of parameters, which are chosen to show constructive and destructive interferences.

Figure 7.5(c - h) shows the ph-ph and pl-pl emission pathways for the 2ED and 2EQ transition rates and their ratio as a function of the Fermi energy and of the structure size. For the photon-photon emission channel (first row), lines are present for the 2ED and 2EQ transitions [Figs. 7.5(c, d)] for Fermi energies roughly greater than 0.4 eV, which correspond to radiative modes excited on the structure (see Fig. 7.6(a)). For the plasmon-plasmon emission channel (second row), new lines appear corresponding to non-radiative modes. Note that in this case, both dipolar and quadrupolar excitations result in the excitation of the same modes [Figs. 7.5(f, g)], but the rate enhancement is higher for the 2EQ transition. Indeed, the maximum values for the ph-ph channel are: $\gamma^{(2)}_{\mathrm{2ED}}/\gamma^{(2)}_{\mathrm{2ED,0}} = 5.1\times10^{8}$, $\gamma^{(2)}_{\mathrm{2EQ}}/\gamma^{(2)}_{\mathrm{2EQ,0}} = 2.0\times10^{19}$, and $\gamma^{(2)}_{\mathrm{2EQ}}/\gamma^{(2)}_{\mathrm{2ED}} = 2.9\times10^{-2}$, while for the pl-pl channel they are: $\gamma^{(2)}_{\mathrm{2ED}}/\gamma^{(2)}_{\mathrm{2ED,0}} = 2.9 \times 10^{15}$, $\gamma^{(2)}_{\mathrm{2EQ}}/\gamma^{(2)}_{\mathrm{2EQ,0}} = 1.3 \times 10^{26}$, and $\gamma^{(2)}_{\mathrm{2EQ}}/\gamma^{(2)}_{\mathrm{2ED}} = 0.24$, showing a breakdown of the dipole approximation in the TPSE process since the 2EQ transition is not negligible. In contrast to the one-photon spontaneous emission process where the total EQ transition can be two orders of magnitude higher than the total ED transition for the plasmon channel for transition moments parallel to the triangle [29], the TPSE process implies a summation over all possible intermediate states and therefore a summation over the emitter's orientations, including these that are less favorable to exhibit a higher ratio between the 2ED and 2EQ channels.

Furthermore, the ratio $\gamma^{(2)}_{\mathrm{2EQ}}/\gamma^{(2)}_{\mathrm{2ED}}$ for the pl-pl channel [Fig. 7.5(h)] is the highest in a horizontal band roughly between $E_F = 0.29$ eV and 0.36 eV, which is independent of the structure size. Indeed when the Fermi energy decreases, graphene losses increase due to interband transitions [124, Fig. 6.7]. Thus, the plasmons excited on the structure are rapidly absorbed, leading to a localized response

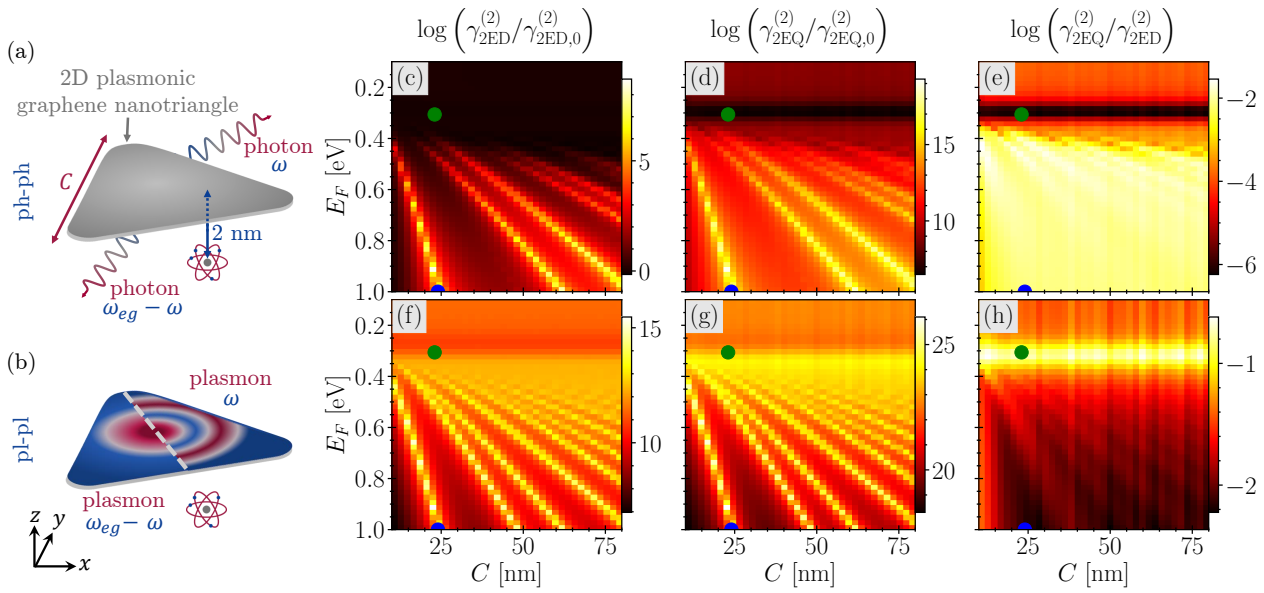


Figure 7.5: (a, b) Sketch of the ph-ph and pl-pl emission channels of the TPSE process for a $5s \to 3s$ transition of a hydrogen-like emitter. Its transition frequency is $\hbar\omega_{eg} = 0.967$ eV ($\lambda_{eg} = 1.28$ µm) and it is placed 2 nm below a 0.335 nm thickness graphene triangle of side length $C$. (c - h) Ph-ph (first row) and pl-pl (second row) emission channels of the spectral TPSE rate as a function of the graphene Fermi energy $E_F$ and of the triangle side length $C$ at $\omega = \omega_{eg}/2$, for an emitter placed below a corner of the triangle. The blue dots ($E_F = 1$ eV, $C = 23.9$ nm) and the green dots ($E_F = 0.31$ eV, $C = 23$ nm) correspond to a plasmonic mode and a localized response on the structure, respectively (see Fig. 7.6). (c, f) Logarithm of the vacuum normalized spectral TPSE rate for the 2ED transition. (d, g) Logarithm of the vacuum normalized spectral TPSE rate for the 2EQ transition. (e, h) Logarithm of the ratio between the 2EQ and 2ED transition rates.

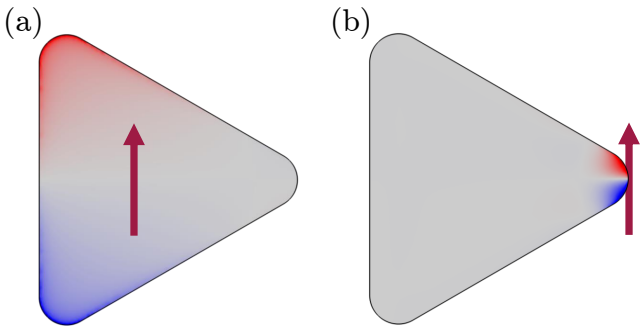


Figure 7.6: Surface charge density on the graphene nanotriangle for an electric dipole oriented along the red arrow. (a) Plasmonic mode corresponding to the parameter set $E_F = 1$ eV and $C = 23.9$ nm (blue dots on Figure 7.5(c - h)), with here the emitter under the center. (b) Localized response corresponding to the parameter set $E_F = 0.31$ eV and $C = 23$ nm (green dots on Figure 7.5(c - h)), with the emitter under a corner.

(see Fig. 7.6(b)) independent of the structure size. Note that for Fermi energies below $E_F = 0.29$ eV, graphene assumes a dielectric behavior, rendering plasmon excitation impossible. However, we keep the notation "pl" to refer to the non-radiative channel.

The previous results were for an emitter below a triangle corner. Now we vary the emitter position, showing that interferences are indeed strongest at the corners. In Figure 7.7, the ph-ph and pl-pl 2ED and 2EQ transition rates, their ratio, and the metric $R$ are plotted for the parameters $E_F = 0.31$ eV and $C = 23$ nm, corresponding to the green dots on Figure 7.5(c - h) (localized

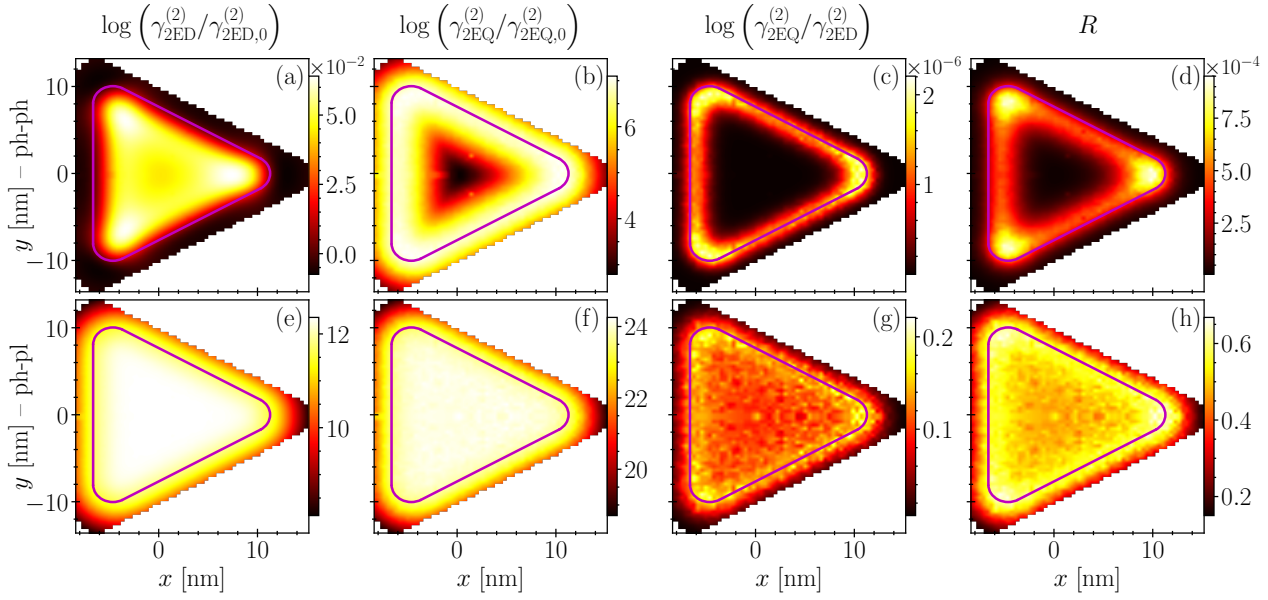


Figure 7.7: Ph-ph (first row) and pl-pl (second row) emission channels of the spectral TPSE rate as a function of the emitter position at $\omega = \omega_{eg}/2$. The graphene Fermi energy and the side length are $E_F = 0.31$ eV and $C = 23$ nm (green dots on Figure 7.5(c - h)). A step size of 0.4 nm is used to discretize the space, leading to the computation over 435 positions on one-sixth of the triangle, since the whole figure can be retrieved using the symmetry of the structure. Note that a bilinear interpolation is used. (a, e) Logarithm of the vacuum normalized spectral TPSE rate for the 2ED transition. (b, f) Logarithm of the vacuum normalized spectral TPSE rate for the 2EQ transition. (c, g) Logarithm of the ratio between the 2EQ and 2ED transition rates. (d, h) Metric $R$.

response, high ratio for the pl-pl channel). When two quanta of the same type are emitted at the same frequency, the tensor $\mathbf{F}^{\mathrm{ED}\cap\mathrm{EQ}}$ appears squared in the interference term given by equation (4.80) and, consequently, the environmental contribution is always positive. Therefore, as the second-order transition moments $\boldsymbol{\mathcal{D}}^{eg}$ and $\boldsymbol{\mathcal{Q}}^{eg}$ involve mostly positive components [Eqs. 5.65], the system will always show a constructive interference.

For the photon-photon emission channel (first row), the 2ED and 2EQ transition rates present different patterns [Figs. 7.7(a, b)]. For the 2ED transition, the rate is weaker than in vacuum and drops away from the structure, while for the 2EQ transition the rate is higher near the borders, especially near the corners, and decreases more slowly away from the structure to reach the vacuum value. Indeed, near the borders and particularly near the corners, there is an increased field gradient, resulting in a greater enhancement of the quadrupole interaction, leading to a higher ratio between the 2EQ and 2ED transitions. Moreover, the metric $R$ [Fig. 7.7(d)] is non-zero only at the borders of the structure and the highest values are at the corners. Due to the 6 orders of magnitude difference between the 2ED and 2EQ transition rates, the $R$ values are low, with a maximum of $3 \times 10^{-3}$.

For the plasmon-plasmon emission channel (second row), the 2ED and 2EQ transition rates are fairly independent of the position below the structure [Figs. 7.7(e, f)]. Moreover, $R$ [Fig. 7.7(h)] is always non-zero under the triangle and is higher at the borders, especially near the corners. For this channel the maximum values are: $\gamma^{(2)}_{2EQ}/\gamma^{(2)}_{2ED} = 0.22$ and $R = 67\,\%$. Therefore, the total transition rate is 2 times higher than the 2ED transition rate, demonstrating a breakdown of the dipole approximation (the 2EQ transition is not negligible) in the TPSE process where interference effects play an important role.

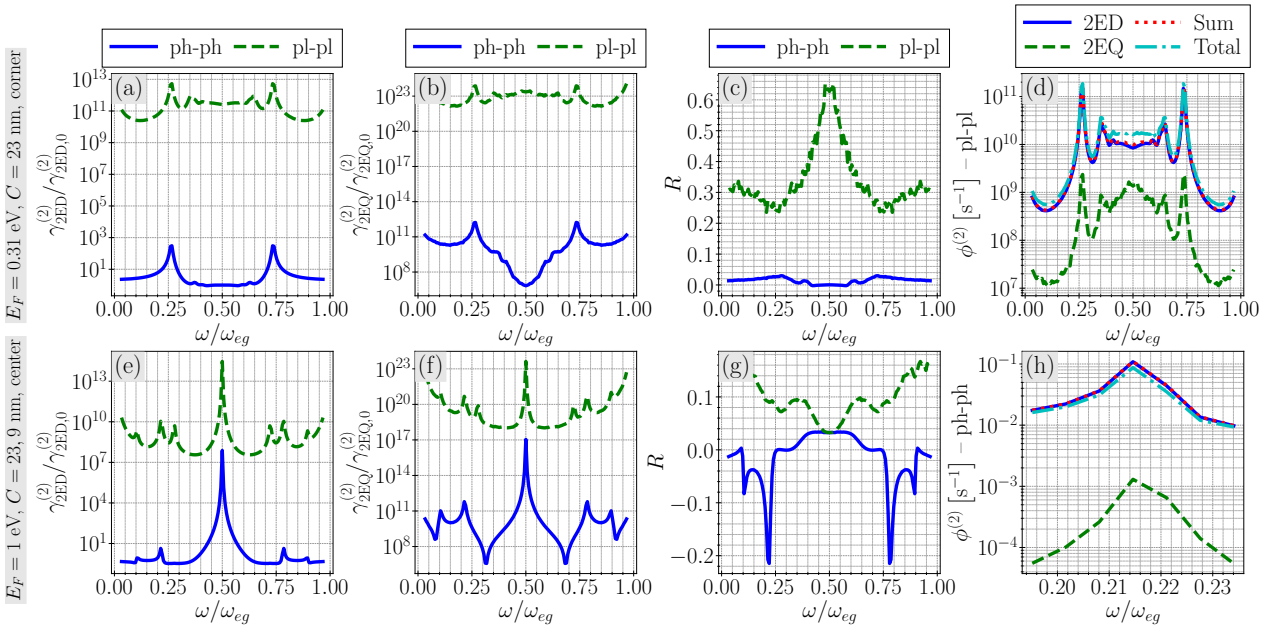


Figure 7.8: Ph-ph and pl-pl emission channels of the spectral TPSE rate. (a - d) The emitter is placed under a corner of the graphene triangle characterized by the parameters $E_F = 0.31$ eV and $C = 23$ nm (green dots on Figure 7.5(c - h)). (e - h) The emitter is positioned below the center of the structure that is characterized by the parameters $E_F = 1$ eV, $C = 23.9$ nm (blue dots on Figure 7.5(c - h)). The spectra were computed over 145 frequencies. (a, e) Vacuum normalized spectral TPSE rate for the 2ED transition. (b, f) Vacuum normalized spectral TPSE rate for the 2EQ transition. (c, g) Metric $R$ for two emission pathways. (d, h) Plot for the pl-pl channel (d) and the ph-ph channel (h) of the 2ED and 2EQ transition rates, the direct sum of these two, and the total transition rate, where the total one includes the interference contribution. The link between the emission profiles $\gamma$ and $\phi$ is given by Eq. (5.43).

The previous results showed the rate of two quanta emitted at the same frequency $\omega = \omega_{eg}/2$. Now we show TPSE spectra where constructive and destructive interferences occur. Figure 7.8 illustrates the spectra related to the ph-ph and pl-pl emission pathways of the 2ED and 2EQ transitions, the metric $R$ as well as the total TPSE rate for one channel (ph-ph or pl-pl). We employ two parameter sets: 1) $E_F = 0.31$ eV, $C = 23$ nm (localized response illustrated in Fig. 7.6(b), green dots on Fig. 7.5(c - h)) with the emitter under a corner; and 2) $E_F = 1$ eV, $C = 23.9$ nm (plasmonic mode illustrated in Fig. 7.6(a), blue dots on Fig. 7.5(c - h)) with the emitter under the center of the structure.

For the first set of parameters (first row), the interferences are always positive [Fig. 7.8(c)], resulting in an increase in the transition rate. For the pl-pl channel [Fig. 7.8(d)] at $\omega = \omega_{eg}/2$, $\phi^{(2)}_{2ED} = 8.4 \times 10^9\,\mathrm{s}^{-1}$, $\phi^{(2)}_{2EQ} = 1.4 \times 10^9\,\mathrm{s}^{-1}$, $R = 63\,\%$, and $\phi^{(2)}_{tot} = 1.6 \times 10^{10}\,\mathrm{s}^{-1}$. Thus, the total transition rate (cyan curve in Fig. 7.8(d)) is 1.9 times higher than the 2ED transition rate (blue curve in Fig. 7.8(d)). For the second set (second row), destructive interference occurs (but not at $\omega = \omega_{eg}/2$[4]) for the ph-ph channel (blue curve in Fig. 7.8(g)). For this channel [Fig. 7.8(h)] at $\omega = 0.22 \times \omega_{eg}$, $\phi^{(2)}_{2ED} = 4.4 \times 10^{-2}\,\mathrm{s}^{-1}$, $\phi^{(2)}_{2EQ} = 6.5 \times 10^{-4}\,\mathrm{s}^{-1}$, $R = -21\,\%$, and $\phi^{(2)}_{tot} = 3.5 \times 10^{-2}\,\mathrm{s}^{-1}$. Thus, the total transition rate (cyan curve in Fig. 7.8(g)) is 20 % lower than the 2ED transition rate (blue curve in Fig. 7.8(g)), demonstrating the destructive interference.

[4]As mentioned earlier, destructive interferences cannot occur at $\omega = \omega_{eg}/2$ in the case of an $s \to s$ transition.

## 7.3 Nanoantennas design for tailoring directivity of two-photon spontaneous emission

As explained in Section 2.2, TPSE is a promising alternative to conventional spontaneous parametric down conversion to create efficient, flexible and integrated entangled photon sources. In addition, the design of nanoantennas provides the degrees of freedom to optimize the quantum efficiency, emission rates, and directivity. In the context of the emission of two photons, we define the quantum efficiency as the ratio between the two-photon emission rate (indicating far-field emission) and the total two-quanta emission rate: $\eta^{(2)}(\omega;\mathbf{R}) := \gamma^{(2)}_{\text{ph-ph}}/\gamma^{(2)}$, with $\gamma^{(2)} = \gamma^{(2)}_{\text{ph-ph}} + \gamma^{(2)}_{\text{ph-pl}} + \gamma^{(2)}_{\text{pl-pl}}$. Moreover, an important challenge for two-photon sources remains the design of systems emitting the photons in separate directions at different frequencies. In this section, we leverage the degrees of freedom provided by the nanoantenna designs to address this issue.

We propose the two designs sketched in Figure 7.9 to spontaneously emit two photons of different energy in different directions, with a quantum efficiency greater than 77 %. First, we combine a dipolar and a quadrupolar mode on a single silver nanorod, with the emitter positioned at the rod extremity, to emit the two photons with different radiation patterns [Fig. 7.9(a)]. Second, we exploit the dipolar modes on two perpendicular nanorods with tailored sizes, with the emitter at the corner, to emit in perpendicular directions [Fig. 7.9(b)]. As proof of concept, we consider again the hydrogen atom as the quantum emitter and we study its two-electric dipole transition [Fig. 7.10] from the excited state $4s$ to the final state $2s$. This transition has been chosen to have a similar transition energy (2.55 eV) as for the hydrogen atom near the silver nanodisks (2.64 eV). Due to the large size of the considered nanostructures compared to the emitter size, it is sufficient to consider only the electric dipole contribution to the TPSE [53], namely the 2ED transition.

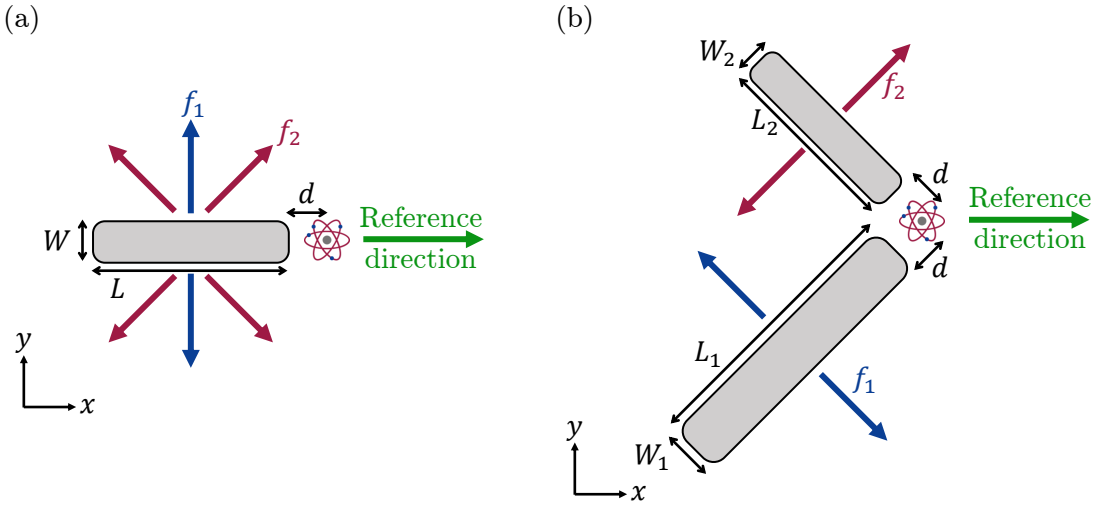


Figure 7.9: Quantum emitter near silver nanorods. The two nanoantennas are designed to radiate two photons of frequencies $f_1$ and $f_2 = 1 - f_1$ with $f_1 \neq f_2$ in different directions. Green arrows denote reference directions for the radiation patterns. (a) Emitter positioned on the axis at a distance $d$ from a rod of length $L$, width $W$, and square cross-section. Dipolar and quadrupolar modes are excited at the frequencies $f_1$ and $f_2$, respectively. (b) Emitter on the axes and at a distance $d$ from two perpendicular rods of square cross-section. A dipolar mode is excited at $f_1$ (resp. $f_2$) on the rod of length $L_1$ ($L_2$) and width $W_1$ ($W_2$).

For the one-nanorod system, it is sufficient to calculate the three following components $F^{\text{ED}}_{xx}$,

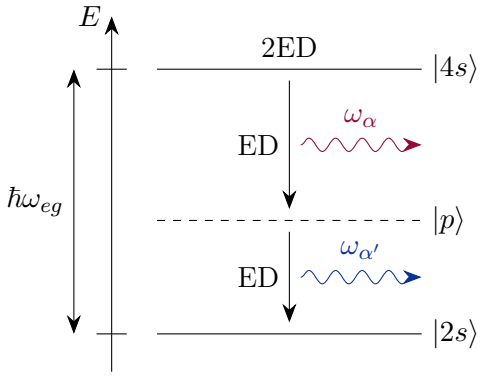


Figure 7.10: Energy representation of a 2ED transition between the $4s$ and $2s$ states of a hydrogen atom. The virtual intermediate states are of type $p$ due to the selection rules [Sec. 2.4]. They are represented between the excited and ground states, even if their energy is greater than the energy of the excited state [Sec. 2.3]. Thus, the energy difference between two levels is equal to the energy of the emitted quanta. The transition energy is $\hbar\omega_{eg} = 2.55$ eV (wavelength of 486 nm) and the two photons have complementary frequencies: $\omega_\alpha + \omega_{\alpha'} = \omega_{eg}$.

$F_{yy}^{\mathrm{ED}}$, and $F_{xy}^{\mathrm{ED}}$ due to the azimuthal symmetry of $x$ axis [Eq. (3.65b)], while the six components [Eq. (3.63)] are required for the two-nanorod system. Concerning the COMSOL models [Sec. 6.3], first, the domain radius is equal to twice the transition wavelength $\lambda_{eg} = 486$ nm, and PMLs are made up of 12 layers. Second, the silver nanorods are modeled with the Drude model [Sec. 6.4]. To avoid unphysically sharp edges, the rods of square cross-section have rounded edges with radius equal to a quarter of their width $W$. Third, the smallest element has a characteristic size of 1 nm on the disk and on the fictional sphere around the emitter used to calculate the emitted power, which have a radius of 5 nm. The computation on 8 cores of one Purcell factor over 95 frequencies for the two-nanorod system (sizes given below) has required 5 hours and 22 GB of RAM.

### Results and discussion

We design a directional emitter using a single nanorod [Fig. 7.9(a)] that emits a photon at the frequency $f_1$ via a dipolar mode of the nanorod, and the second photon at the complementary frequency $f_2 = 1 - f_1$ via a quadrupolar mode of the nanorod, with $f := \omega/\omega_{eg}$ the dimensionless frequency comprised between 0 and 1. We find that this condition is satisfied at $f_1 = 0.34$ ($\lambda = 1.43$ µm) and $f_2 = 0.66$ ($\lambda = 736$ nm) for a 412 nm long and 39 nm wide nanorod. The emission characteristics are presented in Figure 7.11.

The strongest Purcell factor is reached with a dipole oriented along $x$ (the nanorod axis), which is plotted in Figure 7.11(a). The surface charge density and the 3D radiation pattern (for a dipole along $x$) at the frequencies $f_1$ and $f_2$ of the dipolar and quadrupolar modes are illustrated in Figure 7.11(b). In addition to these two modes, $F_{xx}$ exhibits a sextupolar mode (not shown) at $f = 0.94$.

The vacuum normalized spectral TPSE rate is plotted in Figure 7.11(c). Since TPSE involves two quanta emitted at complementary frequencies, the dipolar and quadrupolar modes in Figure 7.11(a) both contribute to the main TPSE peaks at the complementary frequencies $f_1 = 0.34$ and $f_2 = 0.66$. At these frequencies, the term involving the component $F_{xx}$ in the TPSE rate calculation [Eq. (4.58a)] dominates, and the others are negligible (contributing less than 0.01 %). Moreover, at the main TPSE peaks, the emission of a pair of photons is enhanced by a factor $5.4 \times 10^4$ with respect to the vacuum and the quantum efficiency is $\eta^{(2)} = 83\,\%$. As there is no resonance at the complementary frequency

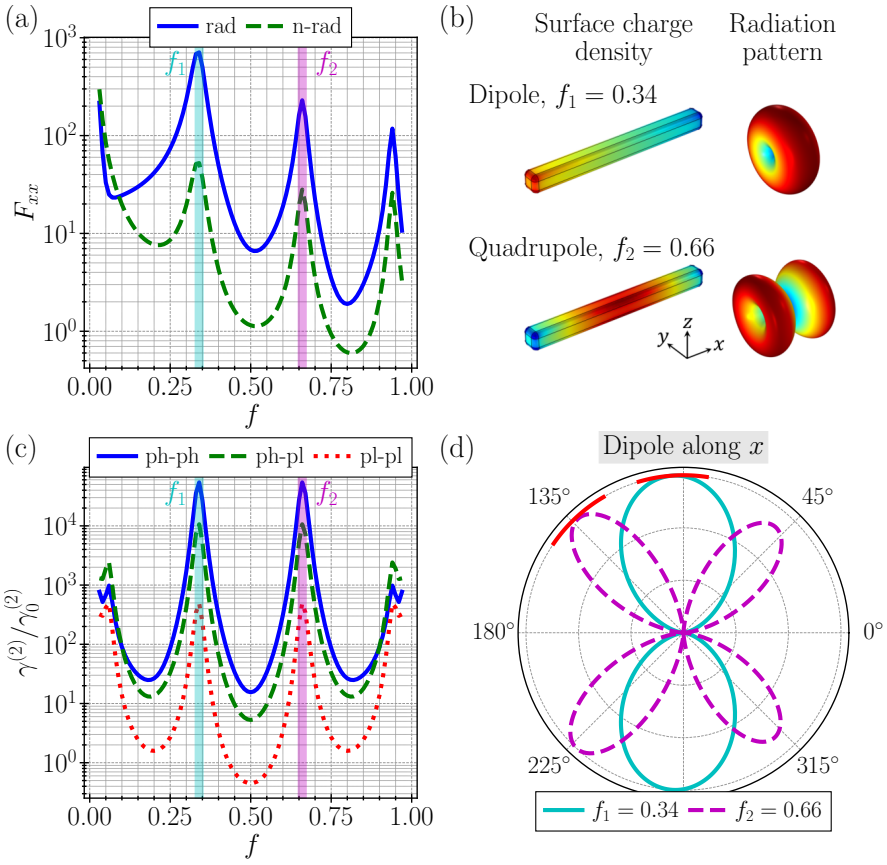


Figure 7.11: Single rod results. (a) Radiative (rad) and non-radiative (n-rad) parts of $F_{xx} = P_x$. (b) Surface charge density on the nanorod and radiation pattern for the complementary frequencies $f_1$ (dipole) and $f_2$ (quadrupole). (c) Ph-ph, ph-pl, and pl-pl emission channels of the vacuum normalized spectral TPSE rate. The first quantum is emitted at $f$, with the second one at the complementary $1 - f$, leading to symmetric spectra with respect to $f = 0.5$. (d) Radiation pattern in the $XY$ plane for a dipole along $x$, identical in the $XZ$ plane, for the complementary frequencies $f_1$ and $f_2$ corresponding to the main TPSE peak. The reference direction and the normal vector are the nanorod axis and the $z$ axis, respectively [Fig. 7.9(a)]. The patterns are calculated using the squared norm of the far-field electric field and are normalized according to their maxima (if a photon is emitted at one frequency, the second one is systematically emitted at the complementary frequency).

$f = 0.06$ of the sextupolar mode at $f = 0.94$, the emitter is 143 times more likely to decay into two photons emitted at the frequencies $f_1$ and $f_2$ than at frequencies $f = 0.06$ and $f = 0.94$. Note also that 65 % of the photons are emitted in the full width at half maximum (FWHM) of the main peaks. The FWHM of a main TPSE peak is equal to $\Delta f = 2.3\,\%$. These values have been calculated by considering the TPSE spectrum which is not normalized with respect to vacuum (not shown).

Since the one-photon Purcell factor $P_x$ is the only non-negligible contribution to the TPSE, the photon pair results mainly from a decay described by two electric dipole transition moments along $x$ [Eq. (4.58a) and Fig. 7.10]. Indeed, as the initial and final states of the quantum emitter are identical, the selection rules require two transition moments with the same orientation. The most likely is to emit two photons at the frequencies $f_1 = 0.34$ and $f_2 = 0.66$ via a dipolar mode and a quadrupolar mode [Fig. 7.11(b)], respectively, so the corresponding radiation patterns are drawn in Figure 7.11(d), with the reference direction being the nanorod axis. Clearly, the two photons are emitted in different patterns, and thus mainly in distinct directions. Note that positioning

the emitter at one extremity of the nanorod results in slightly (left-right) asymmetrical radiation patterns. Quantitatively, we can compute the photon proportion emitted at a given frequency in a cone with an angular width of 25° with axis in the $XY$ plane and forming an angle of $\psi$ with respect to the $x$ axis, corresponding to the maximum of one of the lobes of a radiation pattern. For an isotropic source, this proportion is equal to 1.2 %. In the nanorod system and compared with an isotropic source, 3.0 times more photons are emitted at $f_1$ within a cone at $\psi = 94°$, while 3.7 times more photons are emitted at $f_2$ within a cone positioned at 133° (red curves in Fig. 7.11(d)).

A disadvantage of the single rod is that it is not possible to choose the complementary frequencies of the photons emitted. Indeed, these two frequencies must correspond to the excitation of a dipolar and quadrupolar mode, respectively, which is verified only for one frequency pair. Therefore, we now consider the double-rod design [Fig. 7.9(b)], which employs excitation of dipolar modes on two rods of different sizes. This system does not present the restriction mentioned above since we can freely choose the size of the rods to excite the dipolar modes at complementary frequencies, except that overlap with higher-order modes (e.g., quadrupolar modes) must be avoided. Thus, we employ the following parameters: $L_1 = 289$ nm, $W_1 = 36$ nm, $L_2 = 146$ nm, $W_2 = 21$ nm. As a result, there is radiative enhancement via a dipolar mode at the frequency $f_1 = 0.42$ ($\lambda = 1.16$ µm) on the larger rod, and at the complementary frequency $f_2 = 1 - f_1 = 0.58$ ($\lambda = 838$ nm) on the smaller rod, while preventing a frequency overlap between the dipolar mode of the smaller rod with the quadrupolar mode of the larger one.

The strongest Purcell factors are reached with dipoles oriented in the plane of the rods ($XY$). Thus, the components $F_{xx}$, $F_{yy}$, and $F_{xy}$ dominate and are shown in Figure 7.12(a-c), while the others ($F_{zz}$, $F_{xz}$, and $F_{yz}$) are negligible. The peaks at $f_1 = 0.42$ and $f = 0.84$ correspond to a dipolar and a quadrupolar mode on the larger rod, while the peak at $f_2 = 0.58$ is a dipolar mode on the smaller rod. The vacuum normalized spectral TPSE rate is illustrated in Figure 7.12(d). The dipolar peaks in Figure 7.12(a-c) both contribute to the TPSE peaks at the complementary frequencies $f_1$ and $f_2$. At these frequencies, the terms involving the components $F_{xx}$, $F_{yy}$, and $F_{xy}$ in the TPSE rate calculation [Eq. (4.58a)] dominate, and the others are negligible (contributing less than 0.01 %). Moreover, at the main TPSE peaks, the emission of a pair of photons is enhanced by a factor $7.5 \times 10^4$ with respect to vacuum, and the quantum efficiency is large: $\eta^{(2)} = 77$ %. In addition, the emitter is 120 times more likely to decay into two photons emitted at the frequencies $f_1$ and $f_2$ than at the frequency $f = 0.84$ of the quadrupolar mode. Note also that 61 % of the photons are emitted in the full width at half maximum (FWHM) of the main peaks. The FWHM of a main TPSE peak is equal to $\Delta f = 2.4$ %.

Since there is no enhancement with dipoles oriented perpendicular to the $XY$ plane comprising the system [Fig. 7.9(b)], the photon pair results mainly from a decay described by two electric dipole transition moments in the $XY$ plane [Fig. 7.10]. Moreover, the most likely is to emit two photons at the frequencies $f_1 = 0.42$ and $f_2 = 0.58$ via the dipolar mode on each rod. The corresponding radiation patterns are drawn in Figure 7.12(e,f) for electric dipole transition moments oriented along $x$ and $y$, with the reference direction being the $x$ axis [Fig. 7.9(b)]. Thereby, whatever the orientation (in the $XY$ plane) of the transition moments, the two photons are emitted with asymmetric dipolar radiation patterns rotated about 90 degrees to each other, thus in perpendicular directions. Using the same methodology as for the one-rod system for the comparison with an isotropic source, for a transition moment along $x$ (resp. $y$), 2.9 (3.0) times more photons are emitted at $f_1$ within a cone

at $\psi = 145°$, while 2.3 (2.4) times more photons are emitted at $f_2$ within a cone positioned at 220° (red curves in Fig. 7.12(e,f)).

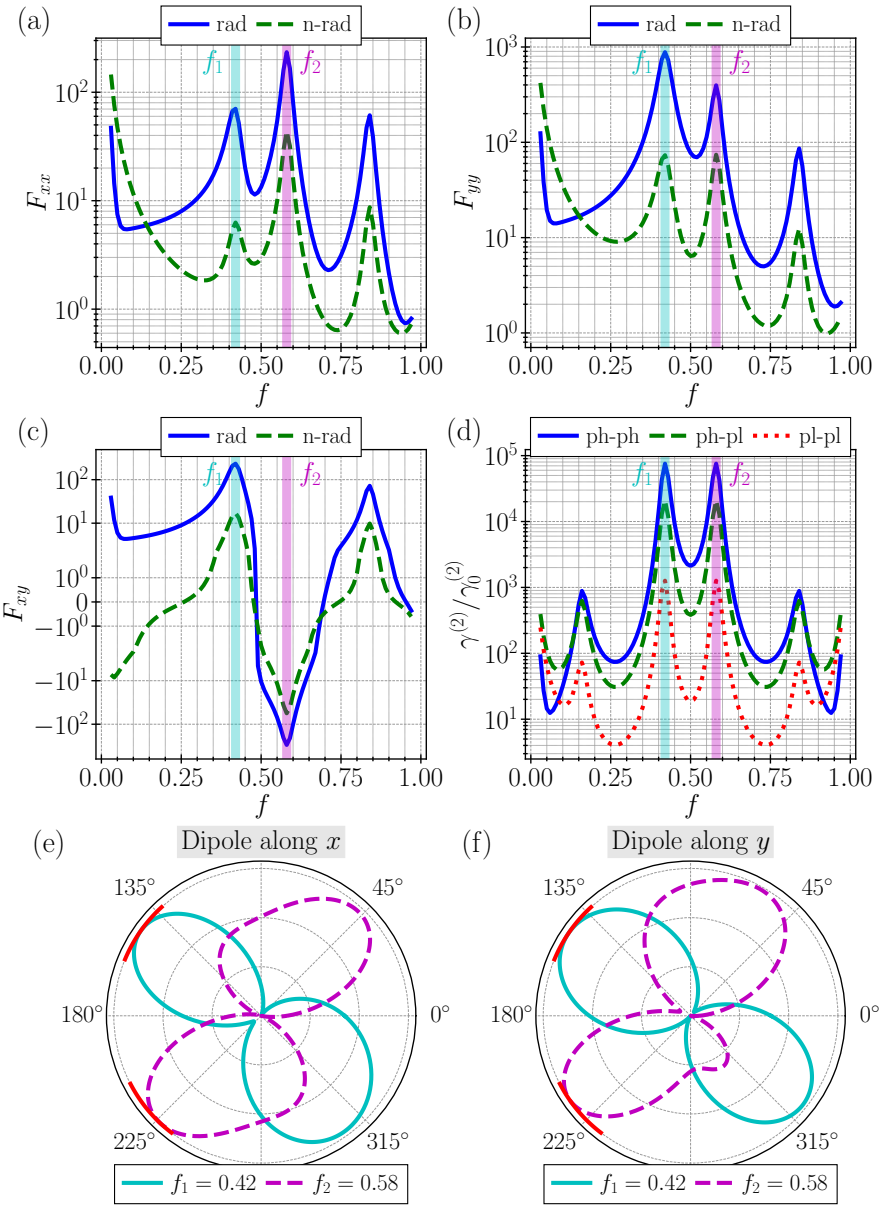


Figure 7.12: Double rod results. Radiative (rad) and non-radiative (n-rad) parts of (a) $F_{xx} = P_x$, (b) $F_{yy} = P_y$, and (c) $F_{xy} = P_{xy} - (P_x + P_y)/2$. (d) Ph-ph, ph-pl, and pl-pl emission channels of the vacuum normalized spectral TPSE rate (all spectra symmetric around 0.5). (e, f) Radiation pattern in the $XY$ plane for a dipole along $x$ and $y$ for the complementary frequencies $f_1$ and $f_2$ corresponding to the main TPSE peak. The reference direction and the normal vector are the $x$ and $z$ axis, respectively [Fig. 7.9(b)]. The patterns are calculated using the squared norm of the far-field and are normalized according to their maxima.

## 7.4 Conclusion

As a validation step of the developed framework, we have shown an enhancement of 5 and 11 orders of magnitude for the 2ED and 2EQ transitions for the emission of two photons for an $s \to s$ transition of a hydrogen-like emitter placed under a plasmonic silver nanodisk. Furthermore, we

have validated the numerical computation of Purcell factors since we obtain the same results as with an analytical calculation of them for the calculation of the 2ED transition rate in the case of an on-axis emitter [26]. We have also demonstrated the flexibility of our framework in the case of an off-axis emitter.

Then, we have studied the interference between the 2ED and 2EQ channels for a $5s \rightarrow 3s$ transition of a hydrogen-like emitter placed 2 nm below a plasmonic graphene nanotriangle. Furthermore, we noted that when two quanta of the same type are emitted at the same frequency, the system is always in a constructive interference configuration if the second-order transition moments involve mostly positive components, as is the case for $s \rightarrow s$ transitions in hydrogen. In addition, interference can lead to a modification greater than 10 % of the total transition rate when the ratio between two multipolar pathways is greater than $2.5 \times 10^{-3}$, highlighting a threshold above which one needs to care about interference effects. Thereby, we have shown a huge enhancement of the 2ED and 2EQ transitions, of 8 and 19 orders of magnitude for the emission of two photons, and of 15 and 26 orders of magnitude for the excitation of two plasmons. For the latter channel, the 2EQ rate reaches 24 % of the 2ED rate, showing a breakdown of the electric dipole approximation in the TPSE process. Moreover, we have found constructive and destructive interference configurations between these two pathways, with for example an increase of 67 % of the total transition rate due to the interference near the triangle corner, leading to a total transition rate being twice as large as the 2ED transition rate. Therefore, it is important to consider higher-order multipolar interactions and interference effects between multipolar two-photon transitions in systems where the field is highly confined.

Finally, we have proposed two subwavelength silver nanorod designs in order to emit the TPSE photons in distinct directions. Indeed, an important challenge for TPSE sources, which are promising alternative to conventional SPDC to create efficient and flexible entangled photon sources, is for systems to exhibit directivity in different directions at different frequencies. The single-rod mechanism exploits a dipolar and quadrupolar mode, while the double-rod employs dipolar modes on perpendicular rods of different size. The double-rod design offers greater freedom in choosing the frequencies. Both structures feature a high quantum efficiency ($> 77$ %) with an enhancement of more than four orders of magnitude of the TPSE rate. For application, one can optimize the radiation patterns to place waveguides, detectors, etc. in the maximum emission directions. We considered a hydrogen-like emitter as a proof of concept, but the findings can be applied to other quantum emitters.

Chapter 8

# Conclusion and outlook

In this thesis, we develop a complete framework to efficiently calculate two-photon spontaneous (TPSE) emission spectra of a quantum emitter in the vicinity of a nanostructure. On the one hand, the second-order transition moments, i.e., the emitter contribution, are calculated analytically using the emitter's wavefunctions. On the other hand, the influence of the environment is formulated in terms of Purcell factors of the one-photon spontaneous emission process, enabling its classical computation by modeling point sources in electromagnetic simulations, giving more flexibility on the model designs than the geometries accessible analytically. Furthermore, our framework takes into account the second-order multipolar interactions, which is relevant for plasmonic nanostructures in which light is highly confined, by deriving equations for the two-electric dipole (2ED), two-magnetic dipole (2MD), and two-electric quadrupole (2EQ) contributions to the TPSE. We also include the calculation of the quantum interferences between the multipolar emission pathways, which is carried out through the calculation of classical interferences between multipolar sources for the two emitted quanta. Indeed, they can lead to a modification greater than 10 % of the total transition rate when the ratio between two multipolar pathways is greater than $2.5 \times 10^{-3}$, highlighting a threshold above which one needs to take care about interference effects. We focus on the interference between the 2ED and 2EQ transitions, but similar equations can be derived for the other interference terms, and also for the mixed transitions that we discarded. Moreover, the formulation with Purcell factors allows the separate calculation of the radiative and non-radiative emission channels, giving access to the quantum efficiency.

Interestingly, there is a decoupling between the emitter and the photonic nanostructure in the framework, due to the assumption that there is a weak coupling between them. Also, the framework is general since it can be applied to an arbitrary emitter near a nanostructure of arbitrary shape. In the case where the emitter contribution cannot be calculated analytically as we did for the hydrogen atom, as for example for molecules, it is possible to use state-of-the-art quantum mechanical methods [106] to calculate the first-order multipolar transition moments involved in the calculation of the second-order multipolar transition moments [Eqs. (4.18)], by considering a sufficient number of bound and free states in the summation over the intermediate states. Similarly, on the environment side, all we need is the geometry and an optical model for the nanostructure to be studied to be able to calculate the Purcell factors. It is therefore possible to design a tailored emitter and choose the nanostructure geometry to suit the desired application. However, the framework is limited to the weak coupling regime and the study of extreme cases of large emitters placed very close to a nanostructure may require the consideration of interactions beyond the electric quadrupolar order.

It is interesting to note that the equations derived for TPSE are also valid for cascades of two single-photon transitions. However in the case of a cascade, there is a divergence due to the

denominators of the second-order transitions moments [Eqs. (4.18)] since the intermediate states are resonant (i.e., the photon energies are equals to the energy difference of the states involved). One approximate solution to this problem is to take into account the lifetime of the intermediate states as a small imaginary contribution to their energy [8], giving rise to an additional term $i\,\Gamma^{(1)}/2$ in the denominators of the second-order transitions moments [Eqs. (4.18)], with $\Gamma^{(1)}$ the one-photon spontaneous emission rate of the emitter in the intermediate resonant state.

Concretely, we study TPSE for a transition between two spherically symmetric states of a hydrogen-like emitter placed near different plasmonic nanostructures. For this purpose, we use the software COMSOL Multiphysics® to calculate the Purcell factors. Firstly, we validate our numerical calculation of Purcell factors by showing an enhancement of 5 orders of magnitude of the 2ED transition rate for the emission of two photons from an emitter positioned along the symmetry axis of a silver nanodisk. In addition, we exploit the flexibility of our framework to study the case of an off-axis emitter and we calculate an enhancement of 11 orders of magnitude for the 2EQ transition rate. Secondly, we design a graphene nanotriangle close to which the 2EQ transition rate is of the same order of magnitude as the 2ED transition rate, thus demonstrating a breakdown of the electric dipole approximation in the TPSE process. We show a huge enhancement of the 2ED and 2EQ transitions, of 8 and 19 orders of magnitude for the emission of two photons, and of 15 and 26 orders of magnitude for the excitation of two plasmons. We also calculate for the first time the interference between two multipolar pathways of the TPSE, where we find both destructive and constructive interferences between the 2ED and 2EQ transitions, with for example an increase of 67 % of the total transition rate near the triangle corner due to the interference. Thirdly, we do a first step towards the design of two-photon nanoantennas, where photons are emitted at different frequencies in separate directions. We propose two subwavelength silver nanorod designs, featuring both a high quantum efficiency ($> 77\,\%$) and an enhancement of more than 4 orders of magnitude of the TPSE rate. The first design exploits a dipolar and quadrupolar mode on a single nanorod, while the second employs dipolar modes on two perpendicular nanorods of different size and offers greater freedom in choosing the frequencies of the emitted photons.

As a first step, we designed proof-of concept geometries to compute TPSE rates, but there are interesting paths to explore. In our calculation of TPSE near plasmonic nanostructures, we studied transitions between two given states, for example the states $4s$ and $2s$ for the system with silver nanorods. However, the emitter in its excited state can decay in other states than the chosen final state, it can decay via different multipolar transitions (e.g., electric dipole and quadrupole transitions), and by transitions of different orders (e.g., one-photon transition, cascade of one-photon transition, and two-photon transition). Therefore, when designing a system (emitter plus environment) for an application, it is necessary to include the calculation and optimization of the internal quantum efficiency, defined as the probability that an emitter will decay with the desired transition and not with the others, e.g., by enhancing the desired TPSE transition while suppressing single-photon transitions [11].

In this thesis, we considered the simplest quantum emitter, namely the hydrogen atom. A logical next step is to explore more complex quantum emitters, such as Rydberg atoms, quantum dots, and molecules. As the contribution of the emitter and of environment are decoupled, studying another emitter requires only to recalculate the second-order transition moments. This can be done analytically for Rydberg atoms [11] and quantum dots [128], whereas state-of-the-art quantum

mechanical methods can be used for molecules [106]. Firstly, the behavior of Rydberg atoms (atoms excited to a state with a high principal quantum number, typically above 50) is similar to the hydrogen atom and they exhibit higher dipole and quadrupole moments due to the large orbit, and thus larger TPSE rates [11]. Moreover, multiple atoms can be used to increase the absorption probability of the probe beam used to excite the atoms [11]. Secondly, in quantum dots the emission wavelength is more tunable, by changing the size, shape, or constitutive material [128]. Thirdly, the multipolar transition moments in molecules can be stronger in a specific direction [60], offering a greater degree of freedom to optimize the emitter, i.e., to ensure that TPSE dominates OPSE.

Concerning the two designs proposed to emit TPSE photons in different directions, they suffer from the low directivity of dipoles and quadrupoles. To improve the design, one can consider for example Yagi-Uda nanoantennas [71] and hybrid metal-dielectric nanostructures [68, 74]. The latter structures combine the advantages of both materials: a large Purcell factor due to the high confinement of the electromagnetic energy in the surroundings of the metal as well as a high scattering directivity with low losses in the dielectric part. In the future, our framework can be used to establish a figure of merit comparing both quantum efficiency and TPSE rate enhancement for different photonic structures, as was done before for one-photon spontaneous emission [58]. For example, gold nanocones lying over a high-index substrate could be a good candidate structure to observe both high quantum efficiency and enhancement [58, 129].

In conclusion, our framework is a complete and flexible tool to design and optimize TPSE nanoantennas, complementing the rich assortment that exists for one-photon spontaneous emission [67]. The interaction is considered up to electric quadrupolar order and the exploitation of interference effects provides an additional degree of freedom in the design. For example, it can be used to tailor entangled two-photon sources, as a more efficient and flexible alternative to the conventional parametric down-conversion sources.

Appendix A

# Spherical harmonics

Spherical harmonics[1] are defined by [100]:

$$Y_L^M(\theta,\varphi) := \sqrt{\frac{2L+1}{4\pi}\frac{(L-M)!}{(L+M)!}}\, P_L^M(\cos\theta)\, e^{iM\varphi}, \tag{A.1}$$

with $P_L^M(\cos\theta)$ the associated Legendre functions, $L \in \mathbb{N}$ and $M \in \mathbb{Z}$ such that $|M| \leq L$. Spherical harmonics are solutions of the equation

$$\Lambda\, Y_L^M(\theta,\varphi) + L(L+1)\, Y_L^M(\theta,\varphi) = 0, \tag{A.2}$$

where

$$\Lambda = \frac{1}{\sin\theta}\frac{\partial}{\partial\theta}\left(\sin\theta\frac{\partial}{\partial\theta}\right) + \frac{1}{\sin^2\theta}\frac{\partial^2}{\partial\varphi^2}, \tag{A.3}$$

is the angular part of the Laplacian expressed in spherical coordinates. This type of equation appears, for example, when considering a central potential in the Schrödinger equation [45, 100]. Spherical harmonics satisfy several properties, including:

1. Complex conjugate
$$\left(Y_L^M(\theta,\varphi)\right)^* = (-1)^M\, Y_L^{-M}(\theta,\varphi)\,; \tag{A.4}$$

2. Parity
$$Y_L^M(\pi-\theta,\pi+\varphi) = (-1)^L\, Y_L^M(\theta,\varphi)\,; \tag{A.5}$$

3. Orthonormality
$$\int_{4\pi}\left(Y_L^M(\theta,\varphi)\right)^*\, Y_{L'}^{M'}(\theta,\varphi)\,\mathrm{d}\Omega = \delta_{LL'}\,\delta_{MM'}, \tag{A.6}$$

where $\mathrm{d}\Omega = \sin\theta\,\mathrm{d}\theta\,\mathrm{d}\varphi$ denotes the solid angle element.

[1] These functions defined on the surface of a sphere are derived from the angular part of harmonic functions, i.e., functions satisfying Laplace's equation, hence their name spherical harmonics [100].

| Spherical harmonics |
|---|
| $Y_0^0 = \frac{1}{\sqrt{4\pi}}$ |
| $Y_1^0(\theta) = \sqrt{\frac{3}{4\pi}}\,\cos\theta$ |
| $Y_1^{\pm 1}(\theta,\varphi) = \mp\sqrt{\frac{3}{8\pi}}\,\sin\theta\, e^{\pm i\varphi}$ |
| $Y_2^0(\theta) = \sqrt{\frac{5}{16\pi}}\,(3\cos^2\theta - 1)$ |
| $Y_2^{\pm 1}(\theta,\varphi) = \mp\sqrt{\frac{15}{8\pi}}\,\sin\theta\,\cos\theta\, e^{\pm i\varphi}$ |
| $Y_2^{\pm 2}(\theta,\varphi) = \sqrt{\frac{15}{32\pi}}\,\sin^2\theta\, e^{\pm 2i\varphi}$ |

Table A.1: Some values of the spherical harmonics $Y_L^M(\theta,\varphi)$ [100].

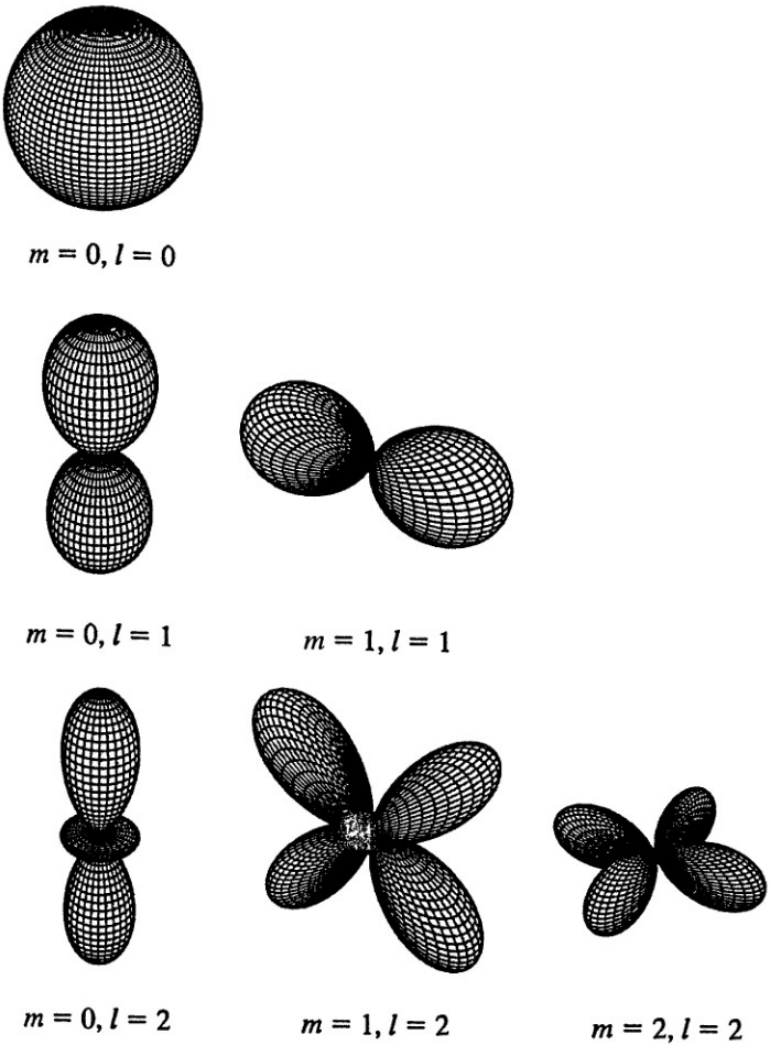


Figure A.1: Three-dimensional representation of $\left(\mathrm{Re}\, Y_L^M(\theta,\varphi)\right)^2$ for $L = 0, 1, 2$ and $0 \leq M \leq L$. These functions correspond to the angular dependence of the stationary wavefunctions of the hydrogen atom. For $L = 0$, the surface described is a sphere. Figure taken from Ref. 100.

# Bibliography


[1] M. Göppert-Mayer, Über elementarakte mit zwei quantensprüngen, *Annalen der Physik* **401**, 273–294 (1931).

[2] D. P. Craig and T. Thirunamachandran, *Molecular quantum electrodynamics: an introduction to radiation-molecule interactions* (Academic Press, London ; Orlando, 1984).

[3] G. Breit and E. Teller, Metastability of hydrogen and helium levels. *The Astrophysical Journal* **91**, 215 (1940).

[4] L. J. Spitzer and J. L. Greenstein, Continuous emission from planetary nebulae, *The Astrophysical Journal* **114**, 407 (1951).

[5] S. P. Goldman and G. W. F. Drake, Relativistic two-photon decay rates of $2\,s_{1/2}$ hydrogenic ions, *Physical Review A* **24**, 183–191 (1981).

[6] P. J. E. Peebles, Recombination of the primeval plasma, *The Astrophysical Journal* **153**, 1 (1968).

[7] J. Chluba and R. A. Sunyaev, Free-bound emission from cosmological hydrogen recombination, *Astronomy & Astrophysics* **458**, L29–L32 (2006).

[8] J. Chluba and R. A. Sunyaev, Two-photon transitions in hydrogen and cosmological recombination, *Astronomy & Astrophysics* **480**, 629–645 (2008).

[9] H. Krüger and A. Oed, Measurement of the decay-probability of metastable hydrogen by two-photon emission, *Physics Letters A* **54**, 251–253 (1975).

[10] M. Lipeles, R. Novick, and N. Tolk, Direct detection of two-photon emission from the metastable state of singly ionized helium, *Physical Review Letters* **15**, 690–693 (1965).

[11] S. Ghosh, N. Rivera, G. Eisenstein, and I. Kaminer, Creating heralded hyper-entangled photons using Rydberg atoms, *Light: Science & Applications* **10**, 100 (2021).

[12] W. M. McClain, Two-photon molecular spectroscopy, *Accounts of Chemical Research* **7**, Publisher: American Chemical Society, 129–135 (1974).

[13] A. Hayat, P. Ginzburg, and M. Orenstein, High-rate entanglement source via two-photon emission from semiconductor quantum wells, *Physical Review B* **76**, 035339 (2007).

[14] A. Hayat, P. Ginzburg, and M. Orenstein, Observation of two-photon emission from semiconductors, *Nature Photonics* **2**, 238–241 (2008).

[15] H. M. van Driel, On the path to entanglement, *Nature Photonics* **2**, 212–213 (2008).

[16] A. Nevet, N. Berkovitch, A. Hayat, P. Ginzburg, S. Ginzach, O. Sorias, and M. Orenstein, Plasmonic nanoantennas for broad-band enhancement of two-photon emission from semiconductors, *Nano Letters* **10**, 1848–1852 (2010).

[17] Y. Ota, S. Iwamoto, N. Kumagai, and Y. Arakawa, Spontaneous two-photon emission from a single quantum dot, *Physical Review Letters* **107**, 233602 (2011).

[18] D. Dovzhenko, V. Krivenkov, I. Kriukova, P. Samokhvalov, A. Karaulov, and I. Nabiev, Enhanced spontaneous emission from two-photon-pumped quantum dots in a porous silicon microcavity, *Optics Letters* **45**, 5364 (2020).

[19] C.-F. Wang, A. B. C. Mantilla, Y. Gu, and P. Z. El-Khoury, Ambient tip-enhanced two photon photoluminescence from CdSe/ZnS quantum dots, *The Journal of Physical Chemistry A* **127**, 1081–1084 (2023).

[20] A. Hayat, A. Nevet, P. Ginzburg, and M. Orenstein, Applications of two-photon processes in semiconductor photonic devices: invited review, *Semiconductor Science and Technology* **26**, 083001 (2011).

[21] A. N. Poddubny, P. Ginzburg, P. A. Belov, A. V. Zayats, and Y. S. Kivshar, Tailoring and enhancing spontaneous two-photon emission using resonant plasmonic nanostructures, *Physical Review A* **86**, 033826 (2012).

[22] N. Rivera, I. Kaminer, B. Zhen, J. D. Joannopoulos, and M. Soljačić, Shrinking light to allow forbidden transitions on the atomic scale, *Science* **353**, 263–269 (2016).

[23] V. V. Klimov, Control of the emission of elementary quantum systems using metamaterials and nanometaparticles, *Physics-Uspekhi* **64**, 990–1020 (2021).

[24] C. Couteau, Spontaneous parametric down-conversion, *Contemporary Physics* **59**, 291–304 (2018).

[25] E. M. Purcell, H. C. Torrey, and R. V. Pound, Resonance absorption by nuclear magnetic moments in a solid, *Physical Review* **69**, 37–38 (1946).

[26] Y. Muniz, A. Manjavacas, C. Farina, D. A. R. Dalvit, and W. J. M. Kort-Kamp, Two-photon spontaneous emission in atomically thin plasmonic nanostructures, *Physical Review Letters* **125**, 033601 (2020).

[27] C. Whisler, G. Holdman, D. D. Yavuz, and V. W. Brar, Enhancing two-photon spontaneous emission in rare earths using graphene and graphene nanoribbons, *Physical Review B* **107**, 195420 (2023).

[28] N. Rivera and I. Kaminer, Light-matter interactions with photonic quasiparticles, *Nature Reviews Physics* **2**, 538–561 (2020).

[29] G. Rosolen and B. Maes, Strong multipolar transition enhancement with graphene nanoislands, *APL Photonics* **6**, 086103 (2021).

[30] L. Novotny and B. Hecht, *Principles of nano-optics*, 2nd ed. (Cambridge University Press, Cambridge, 2012).

[31] Y. Muniz, F. S. S. da Rosa, C. Farina, D. Szilard, and W. J. M. Kort-Kamp, Quantum two-photon emission in a photonic cavity, *Physical Review A* **100**, 023818 (2019).

[32] P. W. Milonni, Why spontaneous emission?, *American Journal of Physics* **52**, 340–343 (1984).

[33] R. Loudon, *The quantum theory of light*, 3rd ed, Oxford science publications (Oxford University Press, Oxford ; New York, 2000).

[34] J. Qiu, Y. Li, and Y. Jia, *Persistent phosphors: from fundamentals to applications*, Woodhead publishing series in electronic and optical materials (Woodhead Publishing, an imprint of Elsevier, Duxford Cambridge, MA Kidlington, 2021).

[35] W. H. He, *Maldives – blue sand*, https://www.flickr.com/photos/78546112@N00/11269034823, (2013) (visited on 05/28/2024).

[36] NASA, Goddard, and SDO, *Sun Emits a Solstice CME*, https://science.nasa.gov/image-detail/amf-gsfc_20171208_archive_e001435, (2017) (visited on 05/28/2024).

[37] Wikimedia Commons, *File:rbg-led.jpg – Wikimedia Commons, the free media repository*, https://commons.wikimedia.org/w/index.php?title=File:RBG-LED.jpg&oldid=792680478, (2023) (visited on 05/28/2024).

[38] Wikimedia Commons, *File:phosphorescence.jpg – Wikimedia Commons, the free media repository*, https://commons.wikimedia.org/w/index.php?title=File:Phosphorescence.jpg&oldid=655902501, (2022) (visited on 05/28/2024).

[39] *Illustration abstraite de faisceau laser rouge*, https://fr.freepik.com/vecteurs-premium/illustration-abstraite-faisceau-laser-rouge_11179930.htm, (visited on 05/28/2024).

[40] P. Dirac, The quantum theory of the emission and absorption of radiation, *Proc. R. Soc. Lond. A* **114**, 243–265 (1927).

[41] E. Jaynes and F. Cummings, Comparison of quantum and semiclassical radiation theories with application to the beam maser, *Proceedings of the IEEE* **51**, 89–109 (1963).

[42] P. W. Milonni, *The quantum vacuum: an introduction to quantum electrodynamics* (Academic Press, Boston, 1994).

[43] W. Demtröder, *Atoms, molecules and photons*, Graduate Texts in Physics (Springer Berlin Heidelberg, Berlin, Heidelberg, 2010).

[44] M. Born and E. Wolf, *Principles of optics: electromagnetic theory of propagation, interference and diffraction of light*, 7th expanded ed (Cambridge University Press, Cambridge ; New York, 1999).

[45] C. Cohen-Tannoudji, B. Diu, and F. Laloë, *Quantum mechanics. Volume 1: Basic concepts, tools, and applications*, trans. by S. Reid Hemley, N. Ostrowsky, and D. Ostrowsky, Second edition (Wiley-VCH Verlag GmbH & Co. KGaA, Weinheim, 2020).

[46] L. D. Barron and C. G. Gray, The multipole interaction Hamiltonian for time dependent fields, *Journal of Physics A: Mathematical, Nuclear and General* **6**, 59–61 (1973).

[47] R. D. Cowan, *The theory of atomic structure and spectra*, Los Alamos series in basic and applied sciences 3 (University of California Press, Berkeley, 1981).

[48] N. Rivera, G. Rosolen, J. D. Joannopoulos, I. Kaminer, and M. Soljačić, Making two-photon processes dominate one-photon processes using mid-IR phonon polaritons, *Proceedings of the National Academy of Sciences* **114**, 13607–13612 (2017).

[49] J. W. V. Storey, M. C. B. Ashley, M. Naray, and J. P. Lloyd, 21 cm line of atomic hydrogen, *American Journal of Physics* **62**, 1077–1081 (1994).

[50] M. L. Andersen, S. Stobbe, A. S. Sørensen, and P. Lodahl, Strongly modified plasmon-matter interaction with mesoscopic quantum emitters, *Nature Physics* **7**, 215–218 (2011).

[51] P. Tighineanu, M. L. Andersen, A. S. Sørensen, S. Stobbe, and P. Lodahl, Probing electric and magnetic vacuum fluctuations with quantum dots, *Physical Review Letters* **113**, 043601 (2014).

[52] P. Tighineanu, A. S. Sørensen, S. Stobbe, and P. Lodahl, Unraveling the mesoscopic character of quantum dots in nanophotonics, *Physical Review Letters* **114**, 247401 (2015).

[53] Y. Zhang, Z.-C. Dong, and J. Aizpurua, Influence of the chemical structure on molecular light emission in strongly localized plasmonic fields, *The Journal of Physical Chemistry C* **124**, 4674–4683 (2020).

[54] M. Soljačić and J. D. Joannopoulos, Enhancement of nonlinear effects using photonic crystals, *Nature Materials* **3**, 211–219 (2004).

[55] P. K. Jain, D. Ghosh, R. Baer, E. Rabani, and A. P. Alivisatos, Near-field manipulation of spectroscopic selection rules on the nanoscale, *Proceedings of the National Academy of Sciences* **109**, 8016–8019 (2012).

[56] A. M. Kern and O. J. F. Martin, Strong enhancement of forbidden atomic transitions using plasmonic nanostructures, *Physical Review A* **85**, 022501 (2012).

[57] V. Yannopapas and E. Paspalakis, Giant enhancement of dipole-forbidden transitions via lattices of plasmonic nanoparticles, *Journal of Modern Optics* **62**, 1435–1441 (2015).

[58] F. Marquier, C. Sauvan, and J.-J. Greffet, Revisiting quantum optics with surface plasmons and plasmonic resonators, *ACS Photonics* **4**, 2091–2101 (2017).

[59] S. Sanders, A. May, A. Alabastri, and A. Manjavacas, Extraordinary enhancement of quadrupolar transitions using nanostructured graphene, *ACS Photonics* **5**, 3282–3290 (2018).

[60] T. Neuman, R. Esteban, D. Casanova, F. J. García-Vidal, and J. Aizpurua, Coupling of molecular emitters and plasmonic cavities beyond the point-dipole approximation, *Nano Letters* **18**, 2358–2364 (2018).

[61] M. Kosik, O. Burlayenko, C. Rockstuhl, I. Fernandez-Corbaton, and K. Słowik, Interaction of atomic systems with quantum vacuum beyond electric dipole approximation, *Scientific Reports* **10**, 5879 (2020).

[62] E. Rusak, J. Straubel, P. Gładysz, M. Göddel, A. Kędziorski, M. Kühn, F. Weigend, C. Rockstuhl, and K. Słowik, Enhancement of and interference among higher order multipole transitions in molecules near a plasmonic nanoantenna, *Nature Communications* **10**, 5775 (2019).

[63] J. Sloan, N. Rivera, J. D. Joannopoulos, I. Kaminer, and M. Soljačić, Controlling spins with surface magnon polaritons, *Physical Review B* **100**, 235453 (2019).

[64] D. S. Wang, T. Neuman, and P. Narang, Spin emitters beyond the point dipole approximation in nanomagnonic cavities, *The Journal of Physical Chemistry C* **125**, 6222–6228 (2021).

[65] N. Rivera, T. Christensen, and P. Narang, Phonon polaritonics in two-dimensional materials, *Nano Letters* **19**, 2653–2660 (2019).

[66] S. A. Maier, *Plasmonics: fundamentals and applications* (Springer, New York, 2007).

[67] A. F. Koenderink, Single-photon nanoantennas, *ACS Photonics* **4**, 710–722 (2017).

[68] A. Barreda, F. Vitale, A. E. Minovich, C. Ronning, and I. Staude, Applications of hybrid metal-dielectric nanostructures: state of the art, *Advanced Photonics Research* **3**, 2100286 (2022).

[69] G. P. Agrawal, *Nonlinear fiber optics*, 4th ed, Quantum electronics–principles and applications (Elsevier / Academic Press, Amsterdam ; Boston, 2007).

[70] H. F. Hofmann, T. Kosako, and Y. Kadoya, Design parameters for a nano-optical Yagi–Uda antenna, *New Journal of Physics* **9**, 217–217 (2007).

[71] A. F. Koenderink, Plasmon nanoparticle array waveguides for single photon and single plasmon sources, *Nano Letters* **9**, 4228–4233 (2009).

[72] H. A. Abudayyeh and R. Rapaport, Quantum emitters coupled to circular nanoantennas for high-brightness quantum light sources, *Quantum Science and Technology* **2**, 034004 (2017).

[73] H. Aouani, O. Mahboub, E. Devaux, H. Rigneault, T. W. Ebbesen, and J. Wenger, Plasmonic antennas for directional sorting of fluorescence emission, *Nano Letters* **11**, 2400–2406 (2011).

[74] E. Rusak, I. Staude, M. Decker, J. Sautter, A. E. Miroshnichenko, D. A. Powell, D. N. Neshev, and Y. S. Kivshar, Hybrid nanoantennas for directional emission enhancement, *Applied Physics Letters* **105**, 221109 (2014).

[75] A. Lewis, J. Weller, and R. Battye, The cosmic microwave background and the ionization history of the Universe, *Monthly Notices of the Royal Astronomical Society* **373**, 561–570 (2006).

[76] C. L. Cesar, D. G. Fried, T. C. Killian, A. D. Polcyn, J. C. Sandberg, I. A. Yu, T. J. Greytak, D. Kleppner, and J. M. Doyle, Two-photon spectroscopy of trapped atomic hydrogen, *Physical Review Letters* **77**, 255–258 (1996).

[77] F. Hu, L. Li, Y. Liu, Y. Meng, M. Gong, and Y. Yang, Two-plasmon spontaneous emission from a nonlocal epsilon-near-zero material, *Communications Physics* **4**, 84 (2021).

[78] L. Weitzel, Y. Muniz, C. Farina, and C. A. D. Zarro, Two-photon spontaneous emission of an atom in a cosmic string background, *Physical Review D* **106**, 045020 (2022).

[79] NASA, ESA, and C. R. O'Dell, *Hubble image of the Ring Nebula (Messier 57)*, https://esahubble.org/images/heic1310a, (2013) (visited on 05/28/2024).

[80] J. E. Ehrlich, X. L. Wu, I.-Y. S. Lee, Z.-Y. Hu, H. Röckel, S. R. Marder, and J. W. Perry, Two-photon absorption and broadband optical limiting with bis-donor stilbenes, *Optics Letters* **22**, 1843 (1997).

[81] P. Shadbolt, J. C. F. Mathews, A. Laing, and J. L. O'Brien, Testing foundations of quantum mechanics with photons, *Nature Physics* **10**, 278–286 (2014).

[82] Y. Wang, S. Pandey, C. H. Greene, and N. Shivaram, Attosecond entangled photons from two-photon decay of metastable atoms: a source for attosecond experiments and beyond, *Physical Review Research* **4**, L032038 (2022).

[83] G. New, *Introduction to nonlinear optics* (Cambridge Univ. Press, Cambridge, 2011).

[84] R. W. Boyd, *Nonlinear optics*, 2nd ed (Academic press, San Diego, 2003).

[85] Y. Zeng, Y. Fu, X. Chen, W. Lu, and H. Ågren, Highly efficient generation of entangled photon pair by spontaneous parametric downconversion in defective photonic crystals, *Journal of the Optical Society of America B* **24**, 1365 (2007).

[86] A. Dousse, J. Suffczyński, A. Beveratos, O. Krebs, A. Lemaître, I. Sagnes, J. Bloch, P. Voisin, and P. Senellart, Ultrabright source of entangled photon pairs, *Nature* **466**, 217–220 (2010).

[87] P. G. Kwiat, K. Mattle, H. Weinfurter, A. Zeilinger, A. V. Sergienko, and Y. Shih, New high-intensity source of polarization-entangled photon pairs, *Physical Review Letters* **75**, 4337–4341 (1995).

[88] N. Zettili, *Quantum mechanics: concepts and applications*, 2. ed., reprint (Wiley, Chichester, 2010).

[89] C. Cohen-Tannoudji, J. Dupont-Roc, and G. Grynberg, *Atom—photon interactions: Basic process and appilcations*, 1st ed. (Wiley, Apr. 1998).

[90] C. Cohen-Tannoudji, B. Diu, and F. Laloë, *Quantum mechanics. Volume 2: Angular momentum, spin, and approximation methods*, trans. by S. Reid Hemley, N. Ostrowsky, and D. Ostrowsky, Second edition (Wiley-VCH Verlag GmbH & Co. KGaA, Weinheim, 2020).

[91] V. B. Beresteckij, E. M. Lifšic, and L. P. Pitaevskij, *Quantum electrodynamics*, 2. ed., reprint, Course of theoretical physics 4 (Butterworth-Heinemann, Oxford, 2008).

[92] M. C. Bottorff, G. J. Ferland, and J. P. Straley, Two-photon transitions and continuous emission from hydrogenic species, *Publications of the Astronomical Society of the Pacific* **118**, 1176–1179 (2006).

[93] O. Jitrik and C. F. Bunge, Transition probabilities for hydrogen-like atoms, *Journal of Physical and Chemical Reference Data* **33**, 1059–1070 (2004).

[94] J. D. Jackson, *Classical electrodynamics*, 3rd ed (Wiley, New York, 1999).

[95] A. Zangwill, *Modern electrodynamics* (Cambridge University Press, Cambridge, 2013).

[96] D. Kleppner, Inhibited spontaneous emission, *Physical Review Letters* **47**, 233–236 (1981).

[97] P. Goy, J. M. Raimond, M. Gross, and S. Haroche, Observation of cavity-enhanced single-atom spontaneous emission, *Physical Review Letters* **50**, 1903–1906 (1983).

[98] E. Yablonovitch, Inhibited spontaneous emission in solid-state physics and electronics, *Physical Review Letters* **58**, 2059–2062 (1987).

[99] C. Cohen-Tannoudji, B. Diu, and F. Laloë, *Quantum mechanics. Volume 3: Fermions, bosons, photons, correlations and entanglement*, trans. by S. Reid Hemley, N. Ostrowsky, and D. Ostrowsky, First edition (Wiley-VCH GmbH & Co. KGaA, Weinheim, 2020).

[100] G. B. Arfken, H.-J. Weber, and F. E. Harris, *Mathematical methods for physicists: a comprehensive guide*, 7th ed (Elsevier, Amsterdam ; Boston, 2013).

[101] A. Matsumoto, Multipole matrix elements for hydrogen atom, *Physica Scripta* **44**, 154–157 (1991).

[102] H. A. Bethe and E. E. Salpeter, *Quantum mechanics of one- and two-electron atoms* (Springer Berlin Heidelberg, Berlin, Heidelberg, 1957).

[103] N. I. of Standards and Technology, *NIST handbook of mathematical functions* (Cambridge University Press, Cambridge New York Melbourne, 2010).

[104] The mpmath development team, *Mpmath: a Python library for arbitrary-precision floating-point arithmetic (version 1.3.0)*, http://mpmath.org (2023).

[105] SciPy 1.0 Contributors, SciPy 1.0: Fundamental Algorithms for Scientific Computing in Python, *Nature Methods* **17**, 261–272 (2020).

[106] R. G. Parr and Y. Weitao, *Density-functional theory of atoms and molecules* (Oxford University Press, Jan. 1995).

[107] *COMSOL Multiphysics cyclopedia*, https://www.comsol.com/multiphysics/ (COMSOL Multiphysics® COMSOL AB, Stockholm, Sweden, 2024).

[108] J.-M. Jin, *The finite element method in electromagnetics*, 2nd ed (John Wiley & Sons, New York, 2002).

[109] B. M. A. Rahman and A. Agrawal, *Finite element modeling methods for photonics* (Artech house, Boston, 2013).

[110] L. Chien, *COMSOL Blog: discretizing the weak form equations*, https://www.comsol.com/blogs/discretizing-the-weak-form-equations, (2015) (visited on 07/03/2024).

[111] D. W. Pepper and J. C. Heinrich, *The finite element method: basic concepts and applications*, 2nd ed, Series in computational and physical processes in mechanics and thermal sciences (Taylor & Francis, New York, 2006).

[112] F. Walter, *COMSOL Blog: solutions to linear systems of equations: direct and iterative solvers*, https://www.comsol.com/blogs/solutions-linear-systems-equations-direct-iterative-solvers, (2013) (visited on 07/03/2024).

[113] W. H. Press, ed., *Numerical recipes: the art of scientific computing*, 3rd ed (Cambridge University Press, Cambridge, UK ; New York, 2007).

[114] L. Chien, *COMSOL Blog: a brief introduction to the weak form*, https://www.comsol.com/blogs/brief-introduction-weak-form, (2014) (visited on 07/03/2024).

[115] *Wave optics module user's guide* (COMSOL Multiphysics® v. 6.2. COMSOL AB, Stockholm, Sweden, 2024).

[116] S. Bettina, *COMSOL Blog: the strength of the weak form*, https://www.comsol.com/blogs/strength-weak-form, (2014) (visited on 07/03/2024).

[117] V. Namias, Application of the Dirac delta function to electric charge and multipole distributions, *American Journal of Physics* **45**, 624–630 (1977).

[118] T. C. Xinzhong, *COMSOL Blog: Modeling graphene in high-frequency electromagnetics*, https://www.comsol.com/blogs/modeling-graphene-in-high-frequency-electromagnetics/, (2022) (visited on 10/10/2023).

[119] G. Yang, L. Li, W. B. Lee, and M. C. Ng, Structure of graphene and its disorders: a review, *Science and Technology of Advanced Materials* **19**, 613–648 (2018).

[120] L. A. Falkovsky and A. A. Varlamov, Space-time dispersion of graphene conductivity, *The European Physical Journal B* **56**, 281–284 (2007).

[121] L. A. Falkovsky, Optical properties of graphene, *Journal of Physics: Conference Series* **129**, 012004 (2008).

[122] K. S. Novoselov, A. K. Geim, S. V. Morozov, D. Jiang, Y. Zhang, S. V. Dubonos, I. V. Grigorieva, and A. A. Firsov, Electric field effect in atomically thin carbon films, *Science* **306**, 666–669 (2004).

[123] J. Christensen, A. Manjavacas, S. Thongrattanasiri, F. H. L. Koppens, and F. J. García De Abajo, Graphene plasmon waveguiding and hybridization in individual and paired nanoribbons, *ACS Nano* **6**, 431–440 (2012).

[124] F. H. L. Koppens, D. E. Chang, and F. J. García de Abajo, Graphene plasmonics: a platform for strong light-matter interactions, *Nano Letters* **11**, 3370–3377 (2011).

[125] S. Smeets, B. Maes, and G. Rosolen, General framework for two-photon spontaneous emission near plasmonic nanostructures, *Physical Review A* **107**, 063516 (2023).

[126] S. Smeets, B. Maes, and G. Rosolen, Interference between multipolar two-photon transitions in quantum emitters near plasmonic nanostructures, *Discover Nano* **19**, 155 (2024).

[127] B. Diaconescu, K. Pohl, L. Vattuone, L. Savio, P. Hofmann, V. M. Silkin, J. M. Pitarke, E. V. Chulkov, P. M. Echenique, D. Farías, and M. Rocca, Low-energy acoustic plasmons at metal surfaces, *Nature* **448**, 57–59 (2007).

[128] J. R. Zurita-Sánchez and L. Novotny, Multipolar interband absorption in a semiconductor quantum dot. I. Electric quadrupole enhancement, *Journal of the Optical Society of America B* **19**, 1355 (2002).

[129] X.-W. Chen, M. Agio, and V. Sandoghdar, Metallodielectric hybrid antennas for ultrastrong enhancement of spontaneous emission, *Physical Review Letters* **108**, 233001 (2012).